The Reactivity of Chemical Warfare Agent Simulants on Carbamate Functionalized Monolayers and Ordered Silsesquioxane Films

Melinda K. M^{c}Pherson

A dissertation submitted to the faculty of the
Virginia Polytechnic Institute and State University
in partial fulfillment of the requirements for the degree of

DOCTOR OF PHILOSOPHY
in
Chemistry

John R. Morris, Chair
Mark R. Anderson
Karen J. Brewer
Larry T. Taylor
Brian M. Tissue

April 6, 2005
Blacksburg, Virginia

Keywords: self-assembled monolayers, carbamate, Langmuir-Blodgett film, trisilanolphenyl-polyhedral oligomeric silsesquioxane, organophosphonate, chemical warfare agent simulant

Copyright 2005, Melinda K. M^{c}Pherson

The Reactivity of Chemical Warfare Agent Simulants on Carbamate Functionalized Monolayers and Ordered Silsesquioxane Films

Melinda K. M^{c}Pherson

ABSTRACT

The reactivity of chemical warfare agents (CWAs) and CWA simulants on organic and oxide surfaces is not currently well understood, but is of substantial importance to the development of effective sensors, filters and sorbent materials. Polyurethane coatings are used by the armed forces as chemical agent resistive paints to limit the uptake of CWAs on surfaces, while the use of metal oxides has been explored for decontamination and protection purposes. To better understand the chemical nature of the interactions of organophosphonate simulants with these surfaces, an ultra-high vacuum environment was used to isolate the target interactions from environmental gaseous interferences. The use of highly-characterized surfaces, coupled with molecular beam and dosing capabilities, allows for the elucidation of adsorption, desorption, and reaction mechanisms of CWA simulants on a variety of materials.

Model urethane-containing organic coatings were designed and applied toward the creation of well-ordered thin films containing carbamate linkages. In addition, novel trisilanolphenyl-polyhedral oligomeric silsesquioxane (POSS) molecules were used to create Langmuir-Blodgett films containing reactive silanol groups that have potential use as sensors and coatings. The uptake and reactivity of organophosphonates and chlorophosphates on these surfaces is the focus of this study.

Surfaces were characterized before and after exposure to the phosphates using a number of surface sensitive techniques including: contact angle goniometry, reflection-absorption infrared spectroscopy (RAIRS), X-ray photoelectron spectroscopy (XPS) and temperature-programmed desorption (TPD) measurements. In conjunction with surface probes, uptake coefficients were monitored according to the King and Wells direct reflection technique. The integration of these analytical techniques provides insight and direction towards the design of more effective chemical agent resistant coatings and aids in the development of more functional strategies for chemical warfare agent decontamination and sensing.

Acknowledgements

I would like to offer my sincere thanks and gratitude to Dr. John R. Morris for his guidance, support, and patience through-out my graduate career at Virginia Tech. In addition, I am thankful to my committee members and various faculty instructors for their contributions to my education in chemistry.

Since arriving at Michigan State University as a freshman in the fall of 1996, Dr. Jay A. Siegel has been my teacher and mentor. I value his friendship, advice, and encouragement to take my scholarship to the next level.

Members of the Morris Research Group, both past and present, deserve mention, as they have made the daily grind of graduate school bearable and even enjoyable. In particular, I would like to acknowledge Gwen M. Davis, B. Scott Day, Larry R. Fiegland, James R. Lohr, and Emily R. Low.

I would like to thank the members of the Esker Research Group for sharing their knowledge of POSS technology and further allowing me to use their laboratory space and equipment to make Langmuir-Blodgett films.

My thanks go to Mr. Frank Cromer and Mr. William Bebout for their analytical expertise and to Mr. Melvin Shaver, Mr. John Miller and Mr. Scott Allen for their talents.

Aside from the science crowd, I would like to thank my family and friends for their steadfast support during this somewhat demanding phase of life: my parents, Jack and Kathleen Ferguson; my sister, Sarah Ferguson; and countless dear friends in Michigan, Virginia, and places beyond. I am most indebted to my husband, Joshua, for his love, support, and friendship during this crazy interlude in our lives.

Table of Contents

Chapter 1……..1
Introduction and Motivation…… 1
Thesis Statement……..1
1.1. Background……..……..…… 1
1.1.1. Condensed Phase Chemistry of CWAs……..3
1.1.2. CWA Simulant Molecules…….…… 4
1.1.3. Interfacial Chemistry…… 5
1.2. Interactions between Organic Surfaces and Organophosphonates……. 8
1.2.1. Background…… 8
1.2.2. Interactions of CWA Simulants with Model Organic Surfaces……9
1.2.3. Modeling Polyurethane Surfaces……...… 13
1.3. Interactions between Metal Oxides and CWAs or CWA Simulants……..… 17
1.3.1. Background…… 17
1.3.2. Magnesium Oxide……...……...… 17
1.3.2.1 CWA Simulant Interactions with Magnesium Oxide…… 17
1.3.2.2 Interactions of CWA Simulants with Magnesium Oxide Nanoparticles…… 23
1.3.2.3 Interactions of CWAs with Magnesium Oxide…… 29
1.3.2.4 The Role of Co-Adsorbed Water on Magnesium Oxide..…… 32
1.3.3. Iron Oxide……..…… 32
1.3.3.1 CWA Simulant Interactions with Iron Oxide…… 32
1.3.3.2 The Role of Co-Adsorbed Water on Iron Oxide..…… 35
1.3.4. Aluminum Oxide……...…… 35
1.3.4.1 CWA Simulant Interactions with Aluminum Oxide…….…… 35
1.3.4.2. Interactions of CWAs with Aluminum Oxide……..…… 37
1.3.5. Tungsten Oxide: CWA Simulant Interactions with Tungsten Oxide….. 37
1.3.6. Titanium Oxide: CWA Simulant Interactions with Titanium Oxide……38
1.3.7. Silicon Oxide: CWA Simulant Interactions with Silicon Oxide…….. 40
1.4. Summary and Implications……..… 43

Chapter 2……..46
Experimental Approach……... 46
2.1. Background……46
2.2. Surface Characterization Techniques and Experimental Details……47
2.2.1. Ultra-high Vacuum Surface Analytical Techniques……..47
2.2.1.1. Sample Introduction System and Alignment Procedures…… 48
2.2.1.2. Sticking Probability Measurement and Molecular Beam Production……51
2.2.1.3. Quadrupole Mass Spectrometer Detector……55
2.2.1.4. Temperature Programmed Desorption Spectroscopy……... 56
2.2.2. Reflection Absorption Infrared Spectroscopy……... 58
2.2.2.1. Experimental Considerations……63
2.2.3. Contact Angle Goniometry……66
2.2.4. X-ray Photoelectron Spectroscopy…… 68

Table of Contents continued

2.3. Gas-Surface Exposure Studies……70
2.4. Instrumental Design: Variable Temperature Sample Holder……71
2.5. Summary……73

Chapter 3…… 74
Preparation and Characterization of a Model Hydrogen-Bonding Organic Self-Assembled Monolayer…… 74
3.1. Introduction…… 74
3.1.1. Chemical Agent Resistive Coating……... 74
3.1.2. Model Surfaces…….…… 75
3.1.3. Model-Hydrogen Bonding Surfaces…….. 79
3.2. Experimental Details……...81
3.2.1. Materials…… 81
3.2.2. Preparation of Self-Assembled Monolayers…….. 82
3.2.3. Preparation of Carbamate-Containing Self-Assembled Monolayers…….83
3.2.3.1. 1,4-Phenylene Diisocyanate Experiments…… 83
3.2.3.2. Solution-Phase Preparation Routes…….. 84
3.2.3.3. Vapor-Phase Isocyanate Reactions…….. 86
3.2.4. Characterization of SAMs and Interactions with CWA Simulants……... 88
3.2.4.1. Reflection Absorption Infrared Spectroscopy……. 88
3.2.4.2. Contact Angle Goniometry…….. 88
3.2.4.3. X-ray Photoelectron Spectroscopy…….. 88
3.2.5. CWA Simulant Exposure Studies…… 89
3.3. Results and Discussion……89
3.3.1. Reflection Absorption Infrared Spectroscopy……...…… 89
3.3.1.1. CH_3-terminated Self-Assembled Monolayer…… 89
3.3.1.2. OH-terminated Self-Assembled Monolayer……. 91
3.3.1.3. Mixed ω-Functionalized Self-Assembled Monolayers…… 93
3.3.1.4 Intra-chain Carbamate Self-Assembled Monolayers.…… 94
3.3.1.4.1. 1,4-Phenylene Diisocyanate SAMs……...…….. 94
3.3.1.4.2. Solution-Phase Chemistry ……...……98
3.3.1.4.3. Vapor-Phase Chemistry …….. 100
3.3.1.4.3.a. High-Frequency Modes…….. 100
3.3.1.4.3.b. Difference Spectrum…….. 104
3.3.1.4.3.c. Low-Frequency Modes…….. 106
3.3.1.4.3.d. Mixed Monolayers: Disrupting the Hydrogen-Bonding Network……..…… 108
3.3.2. Contact Angle Goniometry……112
3.3.3. X-ray Photoelectron Spectroscopy…… 114
3.3.4. Exposure of SAMs to CWA Simulants…….…… 118
3.4. Summary……119

Table of Contents continued

Chapter 4……..121
POSS Langmuir-Blodgett Films: Preparation, Characterization, and Exposure to Dimethyl Methylphosphonate and Trimethylphosphate……121
4.1. Introduction……..……...…121
4.1.1. Langmuir-Blodgett Films……..…… 123
4.1.2. Trisilanol-Phenyl Polyhedral Oligomeric Silsesquioxane LB-Films…… 125
4.2. Experimental Details…….……..……129
4.2.1. Materials……..…….. 129
4.2.2. Langmuir-Blodgett Film Deposition……. 130
4.2.3. Solution-Phase Preparation Methods……131
4.2.4. Characterization of LB-Films and Interactions with CWA Simulants….. 132
4.2.4.1. Reflection Absorption Infrared Spectroscopy…….. 132
4.2.4.2. X-ray Photoelectron Spectroscopy……... 132
4.2.4.3. Temperature Programmed Desorption Measurements……. 132
4.2.4.4. Uptake Coefficient Measurements……133
4.2.5. CWA Simulant Exposure Studies……..134
4.2.5.1. High-Vacuum Organophosphonate Vapor Exposure……... 134
4.2.5.2. Saturated Organophosphonate Vapor Sorption…… 134
4.3. Results and Discussion……... 135
4.3.1. Film Structure…… 135
4.3.1.1. Reflection Absorption Infrared Spectroscopy……. 135
4.3.1.1.1. Ordered POSS LB-Films……. 135
4.3.1.1.2. POSS LB-Films Prepared on Mixed Monolayer Templates…140
4.3.1.1.3. POSS and TEP Films Prepared via Solution-Phase Routes… 141
4.3.1.2. X-ray Photoelectron Spectroscopy……... 144
4.3.2. Exposure of Films to Non-Chlorinated CWA Simulant Molecules…….. 146
4.3.2.1. Uptake of DMMP within POSS Films……. 146
4.3.2.2. Adsorption Energy of DMMP and TMP within POSS Films…….. 152
4.3.2.3. RAIRS Characterization of DMMP-saturated POSS Films……. 155
4.3.2.4. RAIRS Characterization of TMP-saturated POSS Films……. 160
4.3.2.5. XPS Characterization of DMMP- and TMP-saturated POSS Films……. 163
4.3.2.6. Exposure of Solution-Phase POSS Films to DMMP……165
4.3.2.7. Exposure of Solution-Phase TEP Films to DMMP…….. 165
4.4. Conclusion…….. 166

Chapter 5……..168
POSS Langmuir-Blodgett Films: Exposure to Methyl Dichlorophosphate and Trichlorophosphate……..... 168
5.1. Introduction…… 168
5.2. Experimental Details…….. 172
5.2.1. Materials…… 172
5.2.2. Langmuir-Blodgett Film Deposition……..172

Table of Contents continued

5.2.3. Solution-Phase Preparation Methods…… 173
5.2.4. Characterization of LB-Films and Interactions with CWA Simulants….. 174
5.2.4.1. Reflection Absorption Infrared Spectroscopy…….. 174
5.2.4.2. X-ray Photoelectron Spectroscopy……... 174
5.2.4.3. Uptake Coefficient Measurements……174
5.2.4.4. Temperature Programmed Desorption Measurements……. 175
5.2.4.5. Fast Atom Bombardment Mass Spectrometry (FAB-MS)……... 176
5.2.5. CWA Simulant Exposure Studies: Saturated Organophosphonate Vapor Sorption……..……177
5.3. Results and Discussion……... 177
5.3.1. Exposure of Films to Chlorinated CWA Simulant Molecules……...177
5.3.1.1. Uptake of MDCP within POSS Films…….. 177
5.3.1.2. RAIRS Characterization of MDCP- and TCP-saturated POSS Films …….. 178
5.3.1.3. XPS Characterization of MDCP- and TCP-saturated POSS Films.. 183
5.3.1.4. Temperature Programmed Desorption Studies…….186
5.3.1.5. FAB-MS Characterization of Bulk POSS and MDCP-exposed Bulk POSS……186
5.3.2. Hydrolysis of Chlorinated Phosphates within POSS Films……...188
5.3.3. The Role of Water Co-Absorbed within POSS Films……... 190
5.4. Conclusions……195

Chapter 6……..197
Conclusions and Future Work……. 197
6.1. Conclusions……197
6.2. Future Work…… 199

References……202

List of Figures

Figure 1.1 Structures of VX, GB, GF, GD, and GA……...1

Figure 1.2 Structures of CWA simulant molecules……5

Figure 1.3 The adsorption of organophosphonates on a hydrogen-bonded surface..…. 13

Figure 1.4 The Suter et al. procedure to generate SAMs containing urethane linkages…….…...……. 16

Figure 1.5 The decomposition of triethylphosphate on MgO……...…….…….20

Figure 1.6 Chemisorption at Lewis acid sites……...……...……..23

Figure 1.7 Adsorption and formation of bridging species and methanol…...……... 24

Figure 1.8 Oxygen exchange, upon DMMP adsorption……...…….……. 28

Figure 1.9 Surface hydroxyl groups and the formation of volatile products...…….. 28

Figure 1.10 The Mars and Van Krevelen mechanism……...…….……...…. 34

Figure 1.11 DMMP adsorption on aluminum oxide……...36

Figure 1.12 Hydrolysis of MDCP…….……..……... 38

Figure 1.13 Adsorption complexes and a hydrolysis product of DMMP on TiO_2…..... 39

Figure 1.14 Adsorption of TMP, DMMP, MDCP, and TCP on silica surfaces…….... 41

Figure 2.1 Ultra-high vacuum analytical chamber…….……..... 50

Figure 2.2 Specular scattering of a molecular beam…….…...……...51

Figure 2.3 Glass bubbling apparatus…….……..53

Figure 2.4 TPD experimental design…….…...…….. 57

Figure 2.5 Infrared radiation impinging on a substrate…….…...……..58

Figure 2.6 Bruker IFS66v/S infrared spectrometer…….…..……. 60

Figure 2.7 RAIR spectra exhibiting “icing” of the MCT detector…….…….65

List of Figures continued

Figure 2.8 Contact angle goniometer……..……67

Figure 2.9 Contact angle measurement…….……...……..68

Figure 2.10 X-ray photoemission experiment…….……...…… 69

Figure 2.11 Energy diagram for XPS…….……...……..... 70

Figure 2.12 Variable temperature sample mounting device…….……..…….... 72

Figure 2.13 Sample mount and transfer device…….……...…….. 73

Figure 3.1 Self-assembled monolayers…….…….……76

Figure 3.2 The structure of *n*-alkanethiol SAMs on Au …….……..…….. 78

Figure 3.3 The overlayer structure formed by alkanethiolate SAMs on Au ……...…...79

Figure 3.4 Mixed monolayers containing multiple functional groups at the terminal position…….…..……..….83

Figure 3.5 The reaction between a hydroxyl-terminated monolayer template and diisocyanate molecules…...…...…….……..... 85

Figure 3.6 The vapor-phase method used to create alkanethiolates with intralayer carbamate functional groups…… 87

Figure 3.7 RAIR spectra of *n*-alkanethiol SAMs on Au …….….. 90

Figure 3.8 RAIR spectra of hydroxyl-terminated alkanethiol SAMs…….…… 92

Figure 3.9 RAIR spectra of SAMs prepared from mixed ethanolic solutions of 16-mercapto-1-hexadecanol and 1-hexadecanethiol…….…..94

Figure 3.10 RAIR spectra of 1,4-phenylene carbamate bearing SAMs……...….. 95

Figure 3.11 The RAIR spectrum of a phenylene carbamate containing SAM with terminal amine groups……...…..……..…..97

Figure 3.12 RAIR spectra of SAMs containing intrachain carbamate groups prepared via solution-phase alkyl-isocyanate chemistry……...…… 99

Figure 3.13 RAIR spectra of Au/S$(CH_2)_{16}$-O(C=O)NH$(CH_2)_{n-1}CH_3$ prepared via vapor-phase routes……..…….. 101

List of Figures continued

Figure 3.14 Difference spectrum……..……... 105

Figure 3.15 Carbamate modes of Au/S$(CH_2)_{16}$-O(C=O)NH$(CH_2)_{n-1}CH_3$……..……. 107

Figure 3.16 Carbamate modes of Au/S$(CH_2)_{16}$-O(C=O)NHCH_3 and a Au/S$(CH_2)_{16}$-O(C=O)NDCH_3 (B)……...…….……. 108

Figure 3.17 RAIR spectra of carbamate SAMs prepared on mixed template monolayers…….…..109

Figure 3.18 RAIR spectra of carbamate SAMs prepared on mixed template monolayers…….…..111

Figure 3.19 Static contact angles of water on carbamate SAMs…….……...…….. 113

Figure 3.20 XP survey spectra ……...…….……114

Figure 3.21 High resolution XP spectra of the O (1s), N (1s) and C (1s) regions of a Au/S$(CH_2)_{16}$-OH SAM……...…….…… 115

Figure 3.22 High resolution XP spectra of the O (1s), N (1s) and C (1s) regions of a Au/S$(CH_2)_{16}$-O(C=O)NHCH_3 SAM……..…….…… 116

Figure 3.23 High resolution XP spectra of the C (1s) region of Au/S$(CH_2)_{16}$-O(C=O)NHCH_3 and Au/S$(CH_2)_{16}$-COOH SAMs……...……... 117

Figure 4.1 Schematic of POSS molecules...…….…….. 122

Figure 4.2 Y-type Langmuir-Blodgett film preparation…….…… 124

Figure 4.3 Π-A isotherm…….……...126

Figure 4.4 RAIR spectra of 20 layer POSS films…….……... 127

Figure 4.5 XRF studies of POSS LB-films…….……128

Figure 4.6 A plot of the number of POSS layers versus the film thickness...…….…. 129

Figure 4.7 RAIR spectra of POSS films…….…… 136

Figure 4.8 RAIR spectra of POSS films…….……... 137

Figure 4.9 RAIRS peak integrations for major modes of the POSS films…….…… 139

List of Figures continued

Figure 4.10 RAIR spectra of heated POSS films……..……..140

Figure 4.11 RAIR spectra of POSS films prepared on mixed monolayer templates.....141

Figure 4.12 RAIR spectra of solution deposited POSS films……..…..….142

Figure 4.13 The RAIR spectrum of a solution deposited TEP film……...…… 143

Figure 4.14 XP survey spectrum of a freshly-prepared 40 layer POSS LB-film…..... 144

Figure 4.15 High resolution O (1s), C (1s) and Si (2p) regions of the XP spectrum ….145

Figure 4.16 Uptake coefficient of DMMP on POSS LB-films……...146

Figure 4.17 Timed study of POSS films saturating with DMMP……...….... 148

Figure 4.18 RAIR spectra of a 40-layer clean POSS film and a 40-layer DMMP-exposed film .....……...…..…149

Figure 4.19 Integrated area of the δ_s (P-CH_3) vibrational mode……..…..….150

Figure 4.20 Desorption of organophosphonate molecules from POSS films…….… 151

Figure 4.21 TPD of DMMP from a 40 layer POSS film…….….... 152

Figure 4.22 TPD of TMP from a 40 layer POSS film…….……... 154

Figure 4.23 RAIR spectra of a 40-layer clean film, a 40-layer DMMP-exposed film, and gas-phase DMMP…….…….……155

Figure 4.24 Low-frequency modes of the RAIR spectra of a 40-layer clean film , a 40-layer DMMP-exposed film, and gas-phase DMMP…….…….……. 156

Figure 4.25 DMMP hydrogen bonds with the silanol groups of POSS molecules..159

Figure 4.26 RAIR spectra of a 40-layer clean film, a 40-layer TMP-exposed film, and gas-phase TMP…….……161

Figure 4.27 Low-frequency modes of the RAIR spectra of a 40-layer clean film , a 40-layer TMP-exposed film, and gas-phase TMP……..... 162

Figure 4.28 High resolution XP spectra of the O (1s), C (1s) and P (2p) regions of a POSS LB film, a DMMP-saturated POSS LB-film and a TMP-saturated POSS LB-film…….…….....164

List of Figures continued

Figure 5.1 Possible DMMP decomposition pathways…… 169

Figure 5.2 Multilayer POSS films created using Langmuir- Blodgett techniques ..…….…… 171

Figure 5.3 Representation of a fast atom bombardment (FAB) source…….…..…… 176

Figure 5.4 The high frequency region of the RAIR spectrum of a freshly-prepared POSS LB-film and the spectra of POSS LB-films saturated with DMMP, MDCP, and TCP ……...…….…….. 179

Figure 5.5 The low frequency region of the RAIR spectrum of a freshly-prepared POSS LB-film and the spectra of POSS LB-films saturated with DMMP, MDCP, and TCP……..…….…… 181

Figure 5.6 High resolution XP spectra of the O (1s), Cl (2p), and P (2p) regions…..... 184

Figure 5.7 FAB-MS results…….…….. 187

Figure 5.8 The RAIR spectrum of a freshly-prepared POSS LB-film and the spectra of a POSS LB-film exposed sequentially to D_2O, then DMMP, and finally MDCP……...…...…….…… 191

Figure 5.9 The low frequency region of the RAIR spectra of a freshly-prepared POSS LB-film exposed sequentially to D_2O, then DMMP, and finally MDCP……..…….…… 192

List of Tables

Table 1.1 Nerve agent chemical properties……2

Table 1.2 Toxicological Data……2

Table 1.3 Chemical warfare agent simulant chemical properties……5

Table 1.4 Spectral changes due to adsorption of phosphorous containing species…… 19

Table 1.5 Summary of previously reported experimental results MgO……..31

Table 3.1 Infrared frequencies and assignments of 1,4-phenylene carbamate containing SAMs……..…….... 96

Table 3.2 Infrared frequencies and assignments of phenylene carbamate containing SAMs with terminal amine groups……...…… 97

Table 3.3 Solution-phase reaction parameters of the spectra in Figure 3.12……. 100

Table 3.4 Spectral frequencies and assignments for a $Au/S(CH_2)_{16}$-$O(C=O)NH(CH_2)_{n-1}CH_3$ SAM……..……... 102

Table 3.5 Peak width values (FWHM)…….…….. 103

Index of Acronyms

CARC	Chemical agent resistive coating
CWA	Chemical warfare agent
DIMP	Diisopropylmethylphosphonate
DMMP	Dimethylmethylphosphonate
FAB	Fast atom bombardment
GA	Ethyl N,N-dimethylphosphoro-amidocyanidate (Tabun)
GB	2-Propyl methylphosphonofluoridate (Sarin)
GD	3,3-Dimethyl-2-butyl methyl phosphonofluoridate (Soman)
HD	Bis(2-chloroethyl) sulphide
LB	Langmuir Blodgett
MDCP	Methyldichlorophosphate
MS	Mass spectrometry
POSS	Trisilanolphenyl polyhedral oligomeric silsesquioxane
RAIRS	Reflection Absorption Infrared Spectroscopy
SAM	Self assembled monolayer
TCP	Trichlorophosphate
TEP	Trisilanolethyl polyhedral oligomeric silsesquioxane
TMP	Trimethylphosphate
TPD	Temperature programmed desorption
UHV	Ultra-high vacuum
VX	O-Ethyl S-2-(diisopropylamino)ethyl methylphosphonothiolate
XPS	X-ray photoelectron spectroscopy

Chapter 1
Introduction and Motivation

Thesis Statement

The goal of the research presented here is to understand the fundamental interfacial reactions between chemical warfare agent simulants and both urethane-containing and ordered silsesquioxane thin films.

1.1. Background

A chemical agent is a substance that is intentionally used by military or terrorist forces to seriously harm, incapacitate, or kill people as a result of its damaging physiological effects. Chemical warfare agents (CWAs) include nerve agents, blister agents and choking agents. Nerve agents, depicted in Figure 1.1, are exceedingly toxic, inhibiting the acetylcholinesterase enzyme[1] and causing respiratory failure and death within minutes (see Tables 1.1 and 1.2).

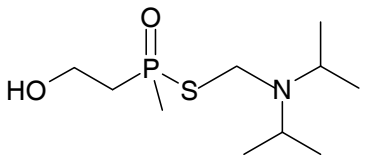

O-Ethyl S-2-(diisopropylamino)ethyl methylphosphonothiolate (VX)

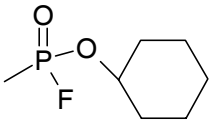

O-cyclohexyl-methylfluorophosphonate (GF, Cyclosarin)

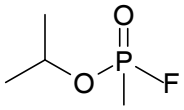

2-Propyl methylphosphonofluoridate (GB, Sarin)

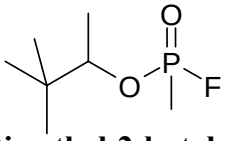

3,3-Dimethyl-2-butyl methyl phosphonofluoridate (GD, Soman)

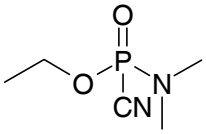

Ethyl N,N-dimethylphosphoro-amidocyanidate (GA, Tabun)

Figure 1.1 Structures of VX, GB, GF, GD, and GA.

Nerve agents were first developed just prior to and during World War II. Dr. Gerhart Schrader, a German chemist, first introduced an organophosphorus insecticide as

a potential chemical weapon.[2] The substance Schrader exposed was called *tabun*, but was renamed GA, or "German" agent "A" after World War II by the Chemical Weapons Section of the German military.[2] Further research lead to the production of a series of agents, including sarin, which was much more toxic than GA. By the 1950's a new class of chemical weapons, the V-series, was in development by the United States of America and Great Britain.[2] This "venomous" class of weapons was more persistent in nature than previous CWAs.

Table 1.1 Nerve agent chemical properties.

Name	Molecular Weight	Melting Point (°C)	Boiling Point (°C)	Vapor Pressure (Torr)	Decomposition Temperature (°C)
VX	267.38	Below -51	240	0.0007 @ 20°C	Half life of 36 hrs. at 150
GB	140.1	-56	158	2.9 @ 25°C 2.1 @ 20°C	150
GF	180.2	-30	239	0.044 @ 20°C	---
GD	182.178	-42	198	0.4 @ 25°C	130
GA	162.3	-5	240	0.037 @ 20°C	150

Table 1.2 Toxicological Data.

Route	Form	Effect	Type	GA	GB	GD	VX	Dosage
ocular	vapor	miosis	ECt50	--	<2	<2	<0.09	mg-min/m^3
inhalation	vapor	runny nose	ECt50	--	<2	<2	<0.09	mg-min/m^3
inhalation (15 l/min)	vapor	incapacitation	ICt50	--	35	35	25	mg-min/m^3
inhalation (15 l/min)	vapor	death	LCt50	135	70	70	30	mg-min/m^3
percutaneous	liquid	death	LD50	4,000	1,700	350	10	mg/70 kg man

The demand to better understand the chemical reactivity and environmental fate of CWAs has recently received a great deal of attention. The importance of this body of research stems from the long-term practical goals of protection, decontamination and detection of CWAs. Presently, a polyurethane-based paint is used by the military in an effort to limit the uptake of chemical warfare agents by the surfaces of heavy equipment. Studying the fundamental interfacial reactions between urethane functional groups and CWA simulants may offer insight into new materials that may be used to effectively

protect not only heavy equipment but also personnel from exposure to CWAs. Investigating the decomposition of CWA simulants by oxide materials may lead to the development of new reactive materials and coatings capable of decontaminating heavy and sensitive equipment, as well as personnel, exposed to CWAs. Furthermore, studies examining fundamental interfacial interactions of CWA simulants may lead to more selective and sensitive sensing devices than those currently in use. An improved insight into the uptake and reactivity mechanisms of CWA simulants may ultimately lead to the creation of more efficient, effective strategies for decontamination of surfaces exposed to actual CWAs and the development of advantageous sensors, filters, and sorbent materials.

1.1.1. Condensed Phase Chemistry of CWAs

Although little is known about the gas-surface chemistry of CWAs, the condensed phase has been explored by numerous groups. Yang has presented a review of CWA decontamination systems, focusing on the condensed phase chemistry of the less persistent G-nerve agents and VX.[3] Hydrolysis was examined as a possible decontamination mechanism, as these agents are known to react with water under certain conditions. At pH levels near 10, GB and GD hydrolyze relatively quickly to form their respective phosphonic acids and fluoride anions.[3] Furthermore, copper(II) has been shown to catalyze the hydrolysis of these G-agents.[4] VX dissolves to yield a basic solution and subsequently undergoes hydrolysis only to generate highly toxic products.[3] For this reason, base-catalyzed hydrolysis is not a viable decontamination reaction for VX. Oxidation of the P-S bond of VX was explored and found to be successful using a commercially available product with a $KHSO_5$ active ingredient.[5] However, this reaction

was ineffective with GB and GD. Catalytic oxidation of VX was accomplished on irradiated TiO_2 surfaces in acetonitrile and in the presence of water to yield phosphonic acid and sulfonic acids.[3] Basic solutions of Na_2CO_3 and NaOH have also been shown to eliminate GD and bis(2-chloroethyl) sulphide (HD) from soil samples.[6] Along the same lines, $NaBO_3$ has been used to accelerate the hydrolysis of industrial organophosphonates in water and soil.[7] Based upon these collected works, the body of knowledge regarding the bulk phase chemistry of CWAs is quite broad, yet relatively little is known about the surface chemistry of these species.

1.1.2. CWA Simulant Molecules

A majority of work, including field exercises by the army, has examined CWA simulants, such as those shown in Figure 1.2. Crooks and Klabunde, among others, have begun to explore the surface interactions of CWA simulants on a range of surfaces.[8-16] G-agent simulant molecules are somewhat less toxic than CWAs and are therefore utilized not only as a means of isolating the chemical reactivity of certain functional groups, but also for safety reasons. Systematically studying the interfacial chemistry of simulant molecules will aid in the determination of the role that particular functional groups play in the reactions of CWAs. Comparison of agent and agent simulant chemistries will aid in the determination of the environmental fate of organophosphonates, as well as in the development of chemical sensors and decontamination strategies. Chemical properties of these simulant molecules are listed in Table 1.3. It is expected that halogenated simulant molecules (i.e. MDCP and TCP) may more closely mimic the chemical reactivity of nerve agents, such as GB and GD, than non-halogenated simulants, such as DIMP and DMMP.

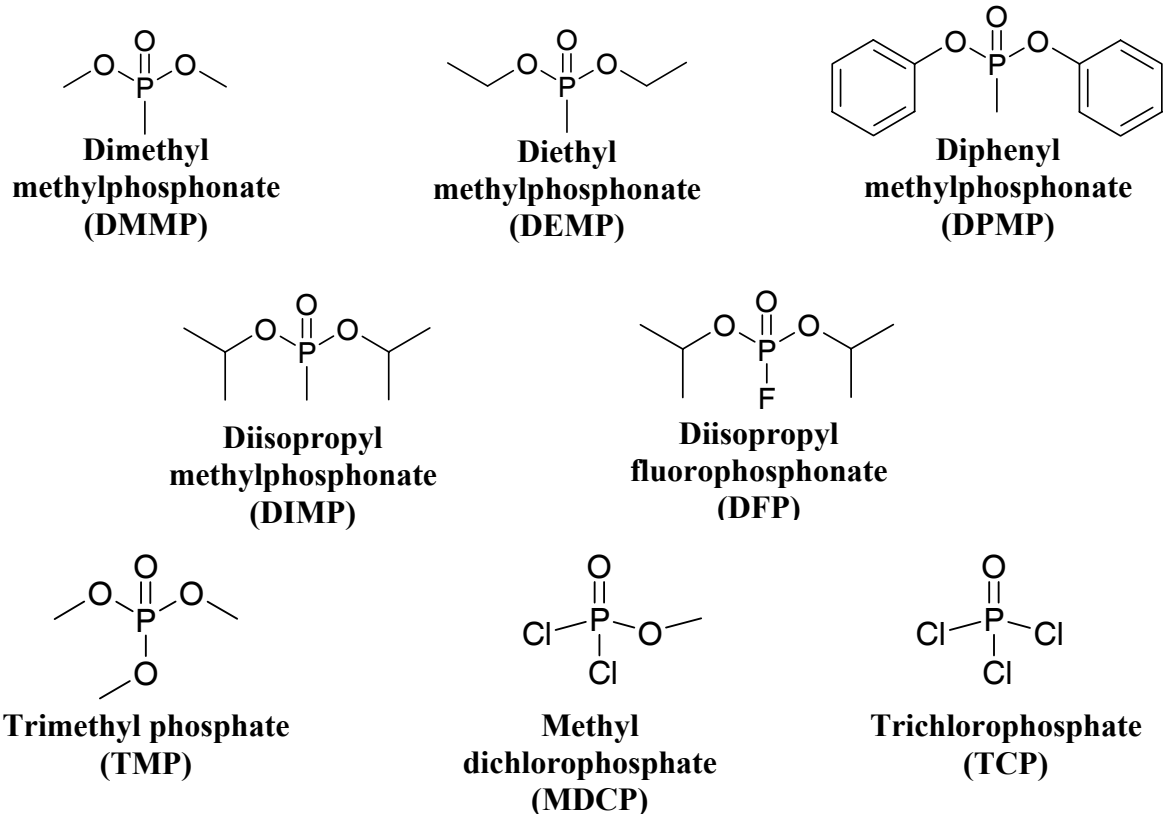

Figure 1.2 Structures of CWA simulant molecules.

1.1.3. Interfacial Chemistry

Research has demonstrated that organophosphonate species can interact with polar functional groups within organic thin films.[14,17-22] Bertilsson et al. have examined the uptake of DMMP by methyl-, hydroxyl-, and carboxylic acid-terminated organic self-assembled monolayer (SAM) systems.[17,19] Preferential hydrogen-bonding between the

Table 1.3 Chemical warfare agent simulant chemical properties.

Name	Molecular Weight	Melting Point (°C)	Boiling Point (°C)	Vapor Pressure (Torr)
DMMP	124.08	---	181.1	0.962
DEMP	152.13	---	194	5.2 at 70 (°C)
DPMP	248	35	205	---
DIMP	180.18	25	---	0.277
DFP	184.15	-82	62 at 9 Torr	---
TMP	140.08	-46	197	---
MDCP	148.91	---	63	---
TCP	153.33	1.25	105.8	---

phosphoryl groups of DMMP in the first monolayer disrupted the lateral hydrogen-bonding network of the neighboring terminal groups of the SAMs and multilayer adsorption followed under higher doses of DMMP. In contrast to the hydroxyl- and carboxylic acid-terminated SAMs, methylated SAMs showed only weak van der Waals interactions with DMMP and no significant uptake.[14,17,19] Crooks et al. exposed SAMs with methyl, hydroxyl, carboxylic acid, and metal-ion functionalized carboxylic acid terminal groups to diisopropyl methylphosphonate (DIMP)[14] and observed results in agreement with Bertilsson's work with DMMP. These studies established a better understanding of the adsorption mechanism between phosphoryl groups of adsorbates and surface species. Furthermore, the role of humidity in these adsorption channels has also been explored.[23] Initial findings have encouraged further investigation of organophosphonate chemistry on organic surfaces containing other functional groups, such as urethane (or carbamate) linkages.

Metal oxides have been investigated for use in the decontamination of environments containing CWAs and/or pesticides[10,11,15,16,24-36] and have been extensively studied as a strategy for sensing organophosphorus compounds.[9,37-41] Single crystal and powder metal-oxide surfaces offer acidic sites through which organophosphonate species can adsorb and subsequently undergo decomposition via hydrolysis reactions. Research efforts have focused on the uptake and reactivity of organophosphonate species on WO_3,[39,40] Al_2O_3,[25,28,29,32,33] MgO,[9,10,15,28,29] TiO_2,[28,31,40] and Fe_2O_3.[24,29,30,42,43] High surface area WO_3 powder has been shown to adsorb DMMP at room temperature through hydrogen-bonding interactions between hydroxyl groups of the surface and the phosphoryl oxygen atoms of DMMP.[39,40] Subsequent decomposition at elevated

temperatures between 478 and 578 K blocked available adsorption sites, limiting further uptake.[40] Sheinker et al. observed similar results in their studies of DMMP decomposition on Al_2O_3 particulate surfaces.[32] In addition, extensive research has examined the uptake and reactivity of organophosphonates on MgO.[9,15,28,29] Initial chemisorption of DMMP on MgO was attributed to the interaction of the phosphoryl functional group with surface Lewis acid sites and was followed by decomposition that involved the stepwise elimination of methoxy groups through hydrolysis reactions.[9,10] Similar decomposition reactions on TiO_2 have been observed at temperatures near 200 K,[31] as well as at and above room temperature.[40] Tesfai et al. reported the dissociative adsorption of DMMP on alumina supported-iron oxide at room temperature through cleavage of the P-C bond.[30] Others have monitored similar decomposition reactions on Fe_2O_3 at elevated temperatures.[24,29]

Though a significant body of research has examined the reactivity of organophosphonates on metal-oxide surfaces, much less is known about interactions on silica surfaces. Henderson et al. and Kanan et al. have explored the adsorption of organophosphonate CWA simulants on silica surfaces.[24,37,41] Results indicated that DMMP adsorbed molecularly through hydrogen-bonding forces at cold temperatures (170 K).[24] Desorption of the phosphonate species also occurred below room temperature. Whereas decomposition reactions of CWA simulants have been reported on oxide surfaces, such as MgO,[9,10,15,28,29] Fe_2O_3[24,29,30,42,43] Al_2O_3,[25,28,29,32,33] WO_3,[39,40] and TiO_2,[28,31,40] no indication of decomposition has been reported on silica.[24,37]

The following review focuses on two key aspects of organophosphonate surface chemistry: 1) interactions between organic surfaces and organophosphonates (Section

1.2.) and 2) interactions between oxides and organophosphonates (Section 1.3.).

1.2. Interactions between Organic Surfaces and Organophosphonates

1.2.1. Background

A chemical agent resistive coating (CARC) is used by the military to limit the uptake of chemical agents by vehicles and equipment. This coating is comprised of polyester and hexamethylene diisocyanate, which polymerize to generate a polyurethane coating that possesses –[CONH-R'-NHCOO-R-O]– repeating units.[44-47] Despite the ubiquitous use of CARC through-out the military, few studies actually focus on elucidating the uptake of CWAs or CWA simulants on CARC. Coatings, such as this, are difficult to study because the exact density and structure of the film is unknown. Moreover, the concentration and depth of urethane groups relative to the air interface is also unspecified. The poorly defined, uncontrolled surface structure leads to numerous uptake and potential decomposition pathways of CWAs. It is difficult to determine where the initial uptake and subsequent reactions are occurring and even more difficult to build systems that are reproducible on the molecular level.[48-50]

The complicated nature of polyurethane paint and subsequently the complex analyses of experimental results, provide the necessary motivation to use well-defined model organic surfaces. Controlled, reproducible surfaces can be used to examine the reactions that take place with surface molecules and organophosphonate CWA simulants. Self-assembled monolayers (SAMs) have been used to create well-ordered, highly-characterized organic surfaces.[19,23,51-58] For example, the placement of carbamate linkages within a SAM can be precisely controlled, as can the overall packing density of the functional groups and the atomic scale structure at the interface. Several studies have

explored organophosphonate uptake on model surfaces constructed from ω-substituted alkanethiols ($SH - (CH_2)_n - X$) on gold.[14,17,19,23] These studies lay the groundwork for extending the use of SAMs to more complicated monolayers that model the CARC polyurethane coating. By incorporating urethane functional groups at varied positions and concentrations, a more detailed understanding of how structural variation in CARC can impact the reactivity.

1.2.2. Interactions of CWA Simulants with Model Organic Surfaces

Crooks et al.[14] used self-assembled monolayers of alkanethiols on gold with $-CH_3$, $-OH$, $-CO_2H$, and $-(CO_2^-)_2Cu^{2+}$ terminations to create model surfaces that were subsequently exposed to varying concentrations of the simulant diisopropyl methylphosphonate (DIMP). Organophosphonate saturated N_2 vapor, at a pressure of 0.7 ±0.3 mmHg, was combined with pure N_2, to yield varying organophosphonate vapor concentrations. Surface acoustic wave (SAW) devices, ellipsometry and polarization modulation-Fourier transform infrared (PM-FTIR) spectroscopy were combined to probe the vapor-surface interactions. DIMP, like acetone, isooctane, n-propanol, trichloroethylene, toluene and water, was found not to adsorb preferentially on the methyl-terminated surface. In contrast, adsorption of DIMP on hydroxyl-terminated surfaces produced strong peaks in the PM-FTIR spectrum at 1230 cm^{-1} and 1249 cm^{-1}, indicating adsorption of two different phases of the organophosphonate. The lower energy peak is representative of the first layer of adsorbed DIMP that is strongly hydrogen bonded through the phosphoryl oxygen to the hydroxyl group of the SAM.[14,17] The higher energy peak is due to subsequent layers of DIMP that are more weakly hydrogen bonded, forming a pure liquid phase. The same type of behavior is seen with

the carboxylic acid-terminated SAM. In this case, PM-FTIR spectra suggested that the hydrogen bonding of the initial monolayer is much stronger than that observed in subsequent layers. There is also spectral evidence of a decrease in lateral hydrogen bonding among the surface moieties and a simultaneous increase in hydrogen bonding between surface molecules and DIMP. Additionally, the copper ion-terminated monolayer was found to adsorb more than sixteen monolayer equivalents of DIMP, which were partially removed with a nitrogen purge. This result suggests a reversible orientational change of the P=O dipole or a change in the absorption coefficient of the vibration band. Accordingly, this system has potential chemical sensor applications.

Liedberg and co-workers explored using SAMs as a chemical sensing medium by exposing alkanethiol monolayers to the CWA simulant DMMP.[17] Using reflection absorption infrared spectroscopy (RAIRS) and temperature-programmed desorption (TPD) in an ultra-high vacuum (UHV) environment, results, in agreement to those obtained by Crooks, were observed. Gas exposure levels of ~1, ~4, and ~14 langmuirs were used; one langmuir is equivalent to 10^{-6} Torr · s. At 100 K, two distinct phases of DMMP adsorbed to a hydroxyl-terminated surface: an initial hydrogen-bonded layer followed by subsequent layers of solid-like DMMP. After the same doses of DMMP at 100 K, only the solid-like phase was observed for a methyl-terminated monolayer. Moreover, an OH-T/CH_3-T mixed surface exposed to DMMP generated an IR spectrum sharing characteristics with both of the pure monolayers after DMMP exposure.

Liedberg used the spectral information to propose probable surface interactions of DMMP. The P=O peak shifts, from 1245 cm^{-1} in a liquid phase to 1228 cm^{-1} once DMMP was adsorbed to the hydroxyl-terminated surface, purportedly indicating that the

adsorption process favored the phosphoryl oxygen oriented towards the surface. Liedberg further postulated that it is more favorable for the methyl groups of DMMP to be pointed toward the methyl-terminated SAM, thereby increasing the energy of interaction by van der Waals forces and allowing for additional dipole-dipole interactions with other DMMP molecules.

In a later study, Liess and Liedberg[19] investigated the interactions of DMMP on a carboxylic acid-terminated SAM, as well as the effects of humidity on the adsorption of DMMP by organic thin films. As expected, the acid-terminated surface formed stronger bonds with the organophosphonate than the hydroxyl-terminated surface. Using SAW devices to measure adsorption isotherms, adsorptive capabilities of the surfaces were studied at relatively low concentration exposure levels, 1-4 langmuirs, of the organophosphonate. Equilibrium of the system was reached after a "few" minutes and the cell was purged with N_2 after each pulse of DMMP. When the flow cell concentration of vapor phase DMMP in nitrogen was 26 ppm, methyl-terminated SAMs adsorbed less than 0.1 monolayer of DMMP, while the hydroxyl-terminated SAMs and acid-terminated SAMs retained 0.6 and ~0.7 monolayers, respectively. Liquid cell measurements of DMMP and decanol in hexadecane or octanoic acid, were taken and compared to the vapor phase measurements of the hydrogen bonded surfaces. Shifts in the OH stretching region of the SAM surfaces supported the findings of Crooks in that there is a reordering of the hydrogen bonds of the SAM; specifically, upon adsorption of the organophosphonate the lateral hydrogen bonds on the surface are broken or perturbed and replaced by hydrogen bonds between the SAM and DMMP molecules. This reorientation allows for the hydrocarbon backbone to relax into a more favorable, less-

strained geometry.

Liess and Liedberg[23] went on to detail the influence of humidity in the interactions of DMMP with organic surfaces. Water vapor was introduced in the DMMP/nitrogen stream and changes in surface mass were measured with a SAW device, while molecular vibrational modes were monitored with RAIRS. The studies revealed that the presence of water causes DMMP to interact more strongly with a hydroxyl-terminated SAM through the reorganized surface molecules and free hydroxyl groups present in the water layer. Adsorbed DMMP may induce structural changes in the adsorbed water, leading to the formation of hydrogen bonds with different strengths and a broadening of the ~3400 cm^{-1} band. Furthermore, the decrease in the 3707 cm^{-1} band is indicative of a decrease in free OH modes of water as DMMP is adsorbed. These findings point to the formation of a complex network of hydrogen bonding among free water molecules, surface hydroxyl groups, and the organophosphonate molecules. Further evidence of the strength of these interactions is seen in the change in the vibrations of the outermost methylene group at 2878 cm^{-1}. An increasing negative peak seemingly indicates that the SAM is affected by the DMMP adsorption in the presence of water. Finally, as the humidity was increased, spectra showed a red-shift in the phosphoryl peak of DMMP adsorbed to the hydroxyl-terminated SAM.

In comparison to the hydroxyl-terminated surface, the prominent Lewis acid characteristics of the acid-terminated SAM resulted in dissimilar interactions. When low levels, near ~10% relative humidity, of water were introduced to the system, DMMP adsorption was increased. However, as the level of humidity was increased, the amount of adsorbed DMMP actually decreased. The carboxylic acid groups interact very

strongly with the water, limiting the number of available, non-hydrogen bonded, hydroxyl groups with which the DMMP can bond, thus limiting the overall coverage of DMMP on the surface.

In conjunction the works of Crooks and Liedberg have generated preliminary information concerning the interactions of organophosphonates on organic thin films. Hydrogen-bonding surfaces were shown to adsorb monolayers of the phosphorous containing species through the P=O bond and subsequent layers were more weakly held through van der Waals forces, as depicted in Figure 1.3. Moreover, the role of humidity was examined and it was found that the concentration of free, that is non-hydrogen bonded, hydroxyl groups plays a part in determining extent of adsorption.

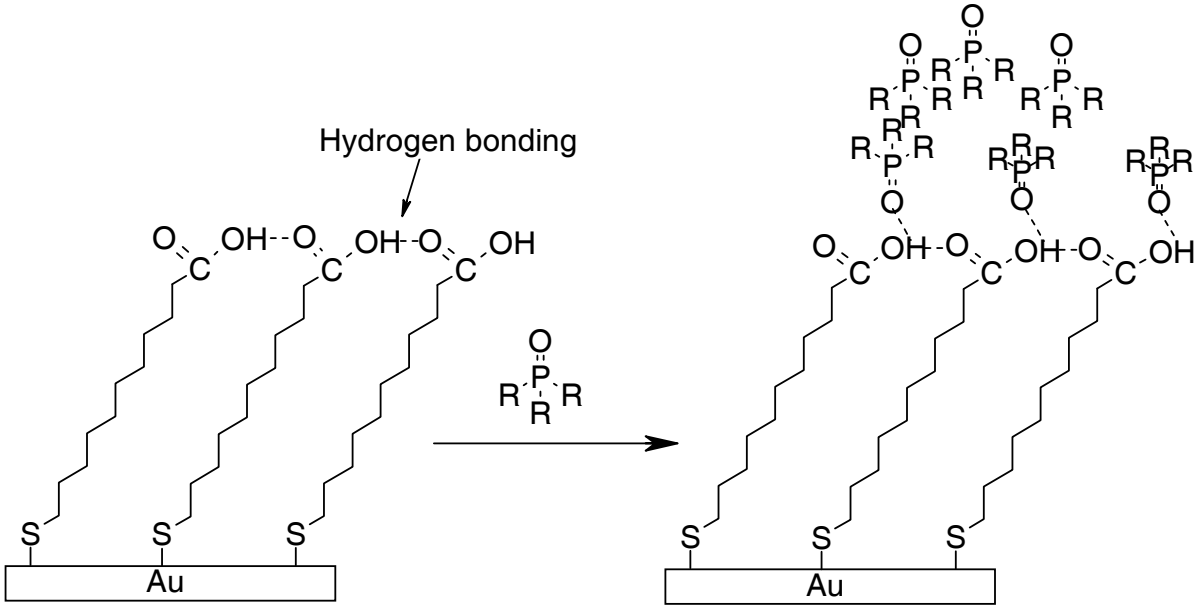

Figure 1.3 The adsorption of organophosphonates on a hydrogen-bonded surface.

1.2.3. Modeling Polyurethane Surfaces

Although the previous investigations using SAMs provide good insight into terminal functional group interactions with organophosphonates, there remain many

questions about uptake and reactivity on organic surfaces, especially urethane-containing materials. The uptake probabilities, bonding energies, reactivity, and residence times of CWA simulants on well-characterized organic surfaces remain unexplored. Objectives in the Morris group include using model SAM surfaces to explore the quantitative uptake, bonding energies, reactivity, and structure of CWA simulant surface chemistry on polyurethane surfaces.

A growing body of work exists in which SAMs have been used to create model polymeric surfaces. Applying isocyanate chemistry, several studies have examined urethane containing mono- and multilayers. Ratner et al.[59] utilized dodecyl isocyanate to modify polymer surfaces to mimic lipid cell-wall structures. In addition, Blanchard and coworkers[60] have used 4,4'-methylene diphenylisocyanate to create multilayers with urea linkages.

Of significance is the work by Suter in which novel monolayers were created using molecules containing isocyanate functionalities.[61] Monolayers with buried urethane linkages offer a substantially better model for CARC than straight alkyl chain SAMs. In accordance with established procedures in the literature, 1-mercapto-11-undecanol was used to prepare an OH-terminated alkanethiol monolayer on gold.[51] The surface hydroxyl groups of the SAM were then reacted with 1,4-phenylene diisocyanate, as seen in Figure 1.4. Only one of the isocyanate groups reacts with the surface, leaving a free isocyanate group that can in turn react with a variety of substances, including water to form an amine or an alcohol to yield a urethane linking group. X-ray photoelectron spectroscopy (XPS), IR, and ellipsometry were used to characterize the surfaces. Hydroxyl group conversion with an isocyanate group was found to be 90 ± 10%

effective, while the free isocyanate group functionalization was found to be complete with neat water after only 5 minutes and with neat hexanol after five hours.

Here, the strategies presented by Suter are extended to create CARC-like monolayers. There are numerous straight, as well as functionalized, isocyanate chains available commercially that can be used in SAM synthesis. Though a number of these chemicals offer significant health risks, there is potential for removing the phenylene ring and creating monolayers that are well-ordered, highly-characterized, and reproducible models for urethane paints. The model SAMs offer a surface from which to study fundamental interactions of hydrogen-bonding carbamate functional groups with CWA simulants. Chapter 3 details the creation and characterization of urethane-containing SAMs.

The creation of these monolayers will afford great control over the placement and concentration of the urethane linkages within an organic film. Adsorption probability and diffusion propensity of organophosphonates into the surface can be examined as a function of the number of carbon atoms between the urethane group and the interface. Moreover, bonding energies and residence times can be determined using TPD and pulsed-beam techniques. These properties will generate answers to questions regarding adsorption energies between organophosphonates and hydrogen bonding groups within an organic film as compared to like groups on the surface. The tendency of humidity to catalyze hydrolysis of CWA simulants will also be addressed.

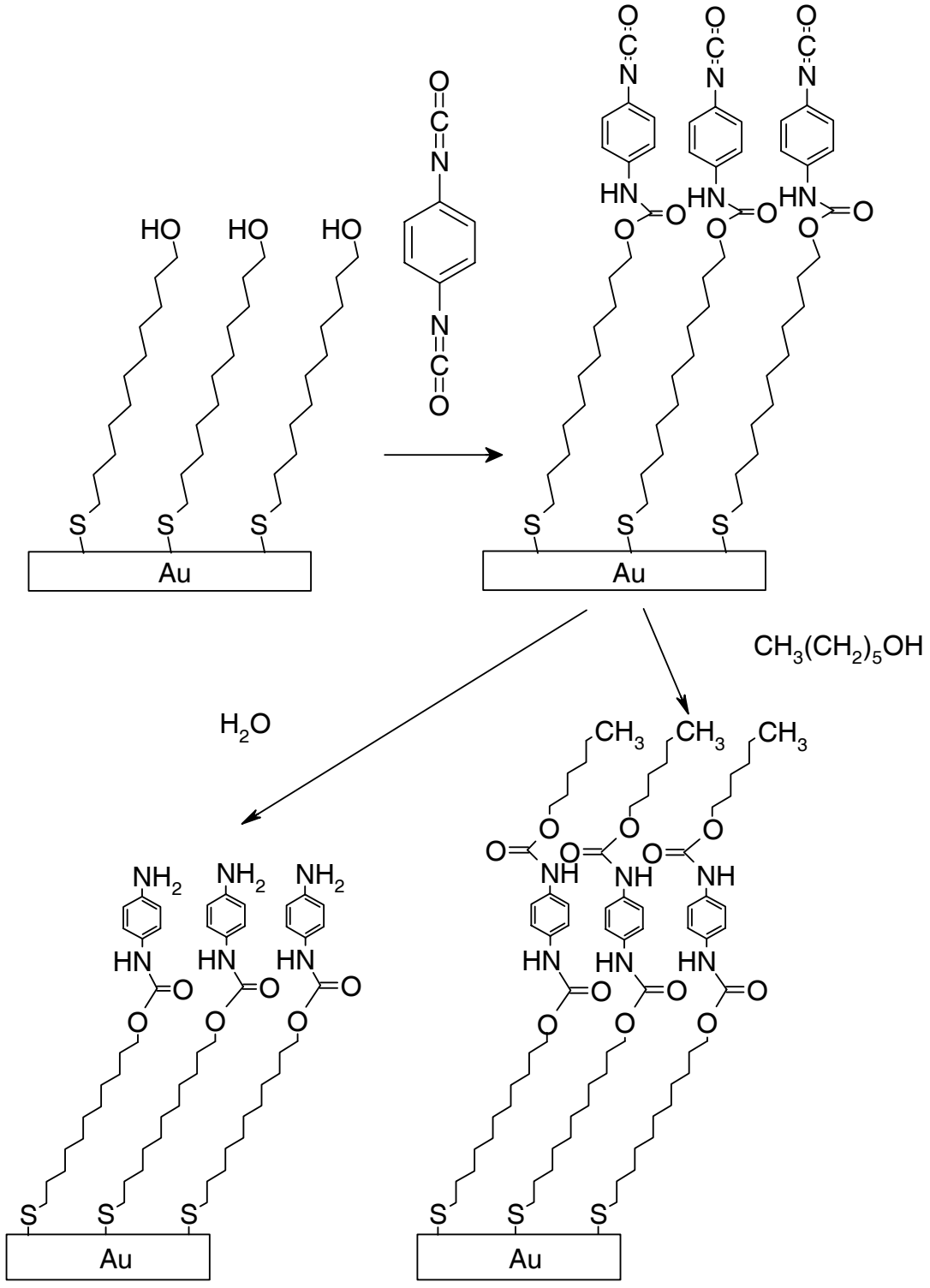

Figure 1.4 The Suter et al. procedure used to generate SAMs containing urethane linkages.

1.3. Interactions between Metal Oxides and CWAs or CWA Simulants

1.3.1. Background

In addition to CWA chemistry on organic coatings, significant amounts of research have been carried out on the surface chemistry of metal oxides and CWA simulants. Metal oxides have been studied extensively because of their ability to adsorb and decompose organophosphonates, whereas pure elemental surfaces were not found to be entirely effective.[26,27,62,63] Work performed on actual CWAs[16], in conjunction with data on CWA simulants, provides useful comparison, as well as insight to functional group reactivity. In addition to pristine crystalline surfaces, nanosized particles have also been used to study organophosphonate chemistry. The high-surface area, metal oxides offer reactive sites where adsorption and decomposition can readily occur. Research efforts have focused on the interactions of agents and simulants primarily on MgO,[9,10,15,28,29] however, several studies have examined organophosphonate chemistry on Fe_2O_3,[24,29,30,43] Al_2O_3,[25,28,29,32,33] WO_3,[28,39,40] TiO_2,[28,31,40] and SiO_2.[24,37,41]

1.3.2. Magnesium Oxide

1.3.2.1. CWA Simulant Interactions with Magnesium Oxide

Magnesium-oxide surfaces are relatively easy to prepare, use, and characterize, and the simple crystal structure and basic character supply an interesting setting for organophosphonate surface chemistry.[64-66] Furthermore, structural (edge, point, step, substitution and dislocation) and electronic (electron excess or deficient) defect sites present in MgO may be responsible for its considerable adsorptive and catalytic activities.

Studies, conducted primarily by the Kenneth Klabunde group at Kansas State

University and scientists at the Army Research Laboratories at the Aberdeen Proving Ground in Maryland, indicate that organophosphonates are initially sorbed on MgO through the phosphoryl oxygen by means of hydrogen bonding.[9,10] Decomposition occurs at elevated temperatures and involves the stepwise elimination of methoxy groups. In addition to crystalline MgO, Klabunde researched the sorbent nature of MgO nanoparticles[8,11] and applied the knowledge that MgO can destructively adsorb CWAs to the area of personnel protection/decontamination systems.

Not only is the military interested in decontamination strategies, but the determination of interaction and destruction pathways of CWAs is also of interest. If CWA/CWA simulant decomposition channels are known and product formation is accurately monitored, there is potential for the development of better chemical sensing devices. With the many studies characterizing MgO surfaces and examining organophosphonate surface chemistry on MgO, this surface seems to provide a model environment for the exploration of CWA chemistry.

Lin and Klabunde[9] examined the adsorption and subsequent decomposition of organophosphites $(RO)_3P$, organophosphates $(RO)_3P{=}O$, and organophosphines R_3P on MgO, that was thermally activated at 700 °C for 14 h. Surfaces were exposed to "several Torr" of the phosphorous compounds for "several minutes," at which time the chamber was evacuated to pressures near 10^{-2} Torr. Working in the vacuum environment, the temperature of the MgO pellets was raised to 25, 75, 125 and 175 °C. At the various temperatures, it was found that phosphites adsorb more readily than phosphates and that phosphines are least likely to adsorb on the surface. Overall, decreasing amounts of all were adsorbed as the temperature was increased. This is indicative of multiple surface

Table 1.4 Spectral changes due to adsorption of phosphorous containing species.

Phosphorous Species	Vibrational Mode	Gas (cm^{-1})	Adsorbed (cm^{-1})
$(CH_3CH_2O)_3P$	CH_3 bend	1382	1370
	CH_2 bend	1440	1430
	νP-OC	1160, 1030	1080
		915	885
$(CH_3CH_2O)_3P$ after baking, T=220°C	δCH_3CH_2		
	νP=O		Grows in at 1285
	??		1200-900
$(CH_3CH_2O)_3P=O$	P=O	1245	-
	$\nu P\text{-}O\text{-}CH_2$	1145	1150
	νP-O-(C)	810	850
		790	835
	ν (P)-O-C	1010, 960	1030
$(CH_3CH_2O)_3P=O$ after baking, T=220°C	νP=O		Grows in at 1320
	$\nu P\text{-}O\text{-}CH_2$		Grows in at 1145
	?? P-O-P ??		1140, 1020, 840
$(CH_3)_3P$	νP-C	1190	1220
	δCH_3CH_2	1400-1300	1460-1300
$(CH_3)_3P$ after baking, T=220°C	??		1275

interactions; some adsorbed molecules are chemisorbed and others are more weakly bound.

Lin et al.[9] found that steric effects and basicity of impinging molecules have considerable effects on adsorption. $(CH_3CH_2O)_3P$ was used as a standard; when Cl or CF_3 were substituted on the side branches, adsorption decreased due to a decrease in basicity. Moreover, when larger or smaller R groups were used, adsorption decreased even further, likely as a result of increasing steric hindrance.

To determine the nature of the adsorbed species, IR spectra were taken of vapor-phase triethyl-phosphite, -phosphate, and -phosphine, as well as activated MgO and adsorbed organic species prior to and after baking at 220 °C. Peak shifts are shown in Table 1.4. A schematic representation of the decomposition mechanism of triethylphosphate is depicted in Figure 1.5.[12] Lin determined that the phosphite adsorbs through the phosphorous atom and, when heated, the organic branches are lost to decomposition yielding an ether. A P=O species is left chemisorbed to the surface and

slight shifts of C-H peaks to lower energy and the red-shifting and broadening of P-OC bands indicated a net gain in electron density. The mechanism involves a nucleophilic substitution at the phosphorous atom and a nucleophilic substitution at a carbon atom with an oxygen neighbor. Similarly, the phosphate was determined to adsorb through the P=O group, but large peak shifts in the spectrum to higher energy suggested a net loss in

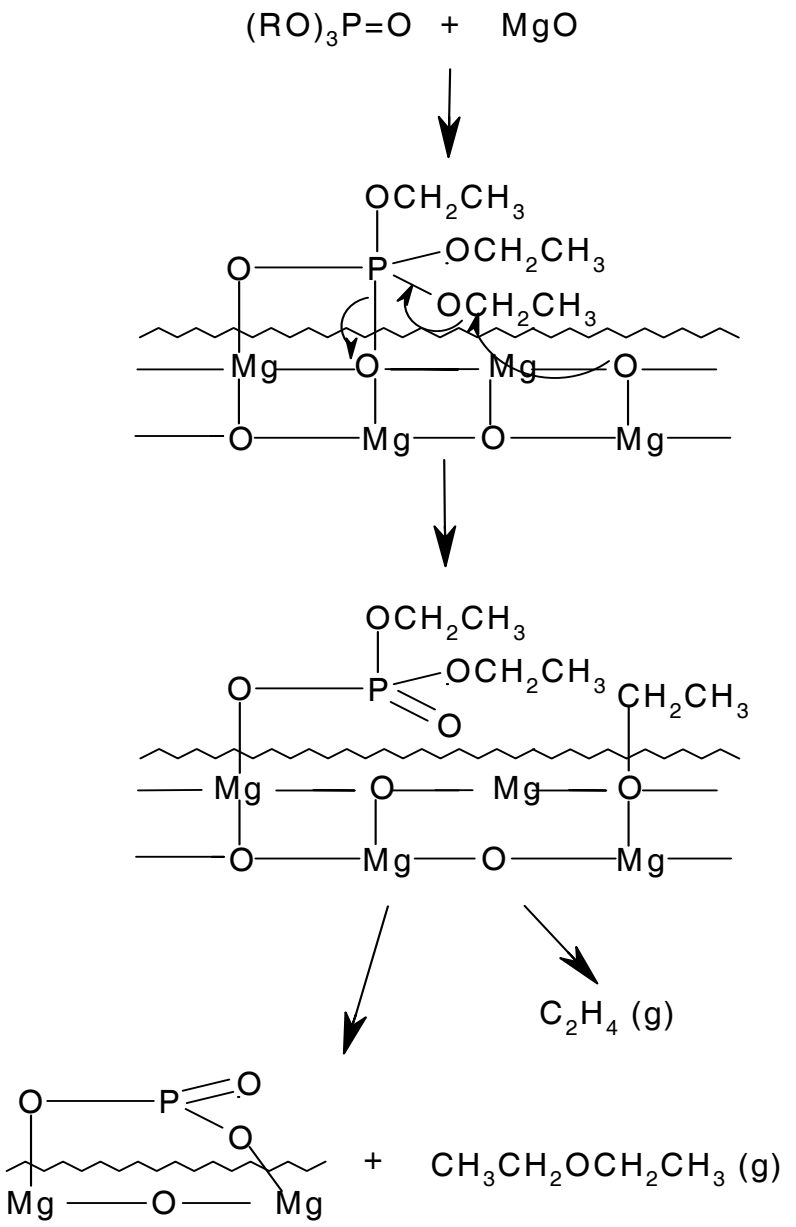

Figure 1.5 The decomposition of triethylphosphate on MgO.

electron density. No evidence of ether production was observed, suggesting an electrophilic attack on the oxygen bound to the R-group. Lastly, it was speculated that the few slight spectral changes indicated that the phosphine did not adsorb as strongly as the other species.

Aurian-Blajeni and Boucher[28] studied the interaction of DMMP on metal-oxide powders using diffuse reflectance-FTIR (DRIFTS). Surface areas of the various metal oxides, including MgO, ranged from 2-162 m^2g^{-1}. The surfaces were exposed to DMMP vapor over a range of temperatures, 25-102 °C, and over a range exposure times, 0.5 h-multiple days. Liquid DMMP was applied to the powders and spectra taken were evaluated against those obtained from the vapor exposed samples. The phosphoryl peak shifted from the bulk liquid value of 1240 cm^{-1} to higher wavenumbers in each instance. This peak shift was determined to correlate with the isoelectric point of the oxide, which can be used to measure the surface acidity. Adsorption was further found to be related to powder surface area; as surface area increased the fractional peak height of the CH_3-O deformation peak, at 1468 cm^{-1}, increased in a nonlinear fashion. The effects of varying exposure time yielded similar results. Longer exposure times correlated with increases in fractional peak height. Changes in adsorption due to temperature, however, were correlated with changes in vapor pressure and activated chemisorption. The relationship was found to be Arrhenius-like, where the amount of DMMP adsorbed after one hour, $q_{t=1h}$, can be described by equation 1:

$$q_{t=1h} = cT^{-1/2}e^{(-E/RT)} \quad (1)$$

where c is proportional to the pressure of DMMP and E is the activation energy.

Li et al.[10] extended the work of Aurian-Blajeni and Boucher and examined the

adsorption of DMMP, triethylphosphate (TEP), and trimethylphosphate (TMP) on heat-treated MgO with surface areas of 10-390 m^2g^{-1}. MgO was chosen for its simple basic crystal structure and its excellent capacity to adsorb CWA simulants. Metal oxides, with greater surface area, have more adsorption sites and possess greater catalytic activity. With this in mind, Li evaluated the effectiveness of different processes to create adsorbent MgO nanoparticles. The analytical technique used to inspect the powders was FTIR-photoacoustic spectroscopy (FTIR-PAS). In this method, a modulated infrared beam is absorbed by a sample in a closed cell. A high-sensitivity microphone is then used to record the sample's spectrum by monitoring pressure fluctuations.

Powder samples were exposed to phosphate vapors in one of two ways. The static exposure method involved exposing 0.10 g of MgO to concentrated phosphate vapor for 1 h followed by evacuation of the chamber with a vacuum system. The second method placed the powder in a U-tube and helium containing phosphate was flowed over the powder and into a gas chromatograph. In this way, adsorbed species and adsorption techniques were both studied.

Spectra for each of the neat organophosphates were dominated by the P=O and P-O-C stretches. Upon adsorption to MgO, all peaks were broadened, but the only major shift in the spectra was that of the phosphoryl band to lower energies. To pinpoint the adsorption mechanism, powder samples were heat treated at 500 and 700 °C. Because it is exceedingly difficult to make "dry" MgO in low vacuum or under ambient conditions, surfaces contain adsorbed water and dissociated hydroxyl groups.[13] At 700 °C, the MgO surface contains 30 percent fewer "background" hydroxyl groups, than at 500 °C. The spectra of adsorbed DMMP at both 500 and 700 °C were found to be identical. As seen

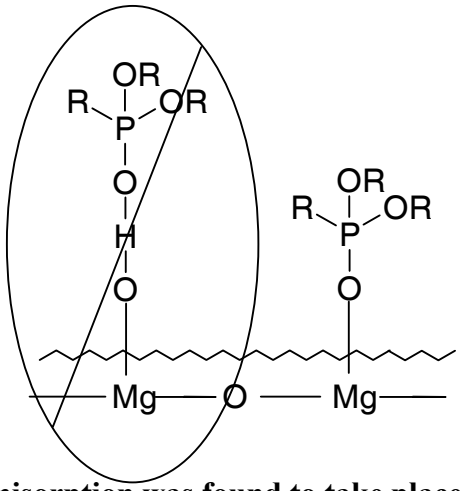

Figure 1.6 Chemisorption was found to take place at Lewis acid sites.

in Figure 1.6, it was speculated that participation of the hydroxyl groups in the adsorption process is unlikely. However, the water on the surface was never quantitatively measured. Moreover, IR spectra confirmed that hydroxyl groups were generated by decomposition of the organophosphate species.

The two adsorption techniques illustrated that initially a strongly chemisorbed layer of organophosphate is present. Once the surface becomes saturated a secondary physisorbed layer forms that is readily removed upon evacuation of the chamber at room temperature or purging with helium at 190 °C. As the temperature was raised and the phosphates began to decompose, evidence was seen for the formation of an O-P-O bridging species on the surface.

1.3.2.2. Interactions of CWA Simulants with Magnesium Oxide Nanoparticles

In the interest of exploring solid reagents that are able to adsorb and decompose organophosphonates, Klabunde[8] narrowed the scope of this research and focused on the dissociative adsorption and decomposition of DMMP on MgO nanoparticles. A pulse-microreactor GC system, followed by FTIR-PAS, was used to detect the volatile products, as well as those nonvolatile species remaining on the surface.

The number of MgO groups on the surface was calculated based on the powder surface area and the MgO(100) unit cell. Analysis of their experimental results indicated that it takes approximately two MgO moieties to decompose one molecule of DMMP. Therefore, the sample with the smallest particles, and thus the largest surface area, proves most effective at decomposition of the organophosphonates. X-ray diffraction revealed that DMMP decomposition products, such as the bridging species seen in Figure 1.7, are not crystalline and are not focused on structural or electronic defect sites. Rather, these

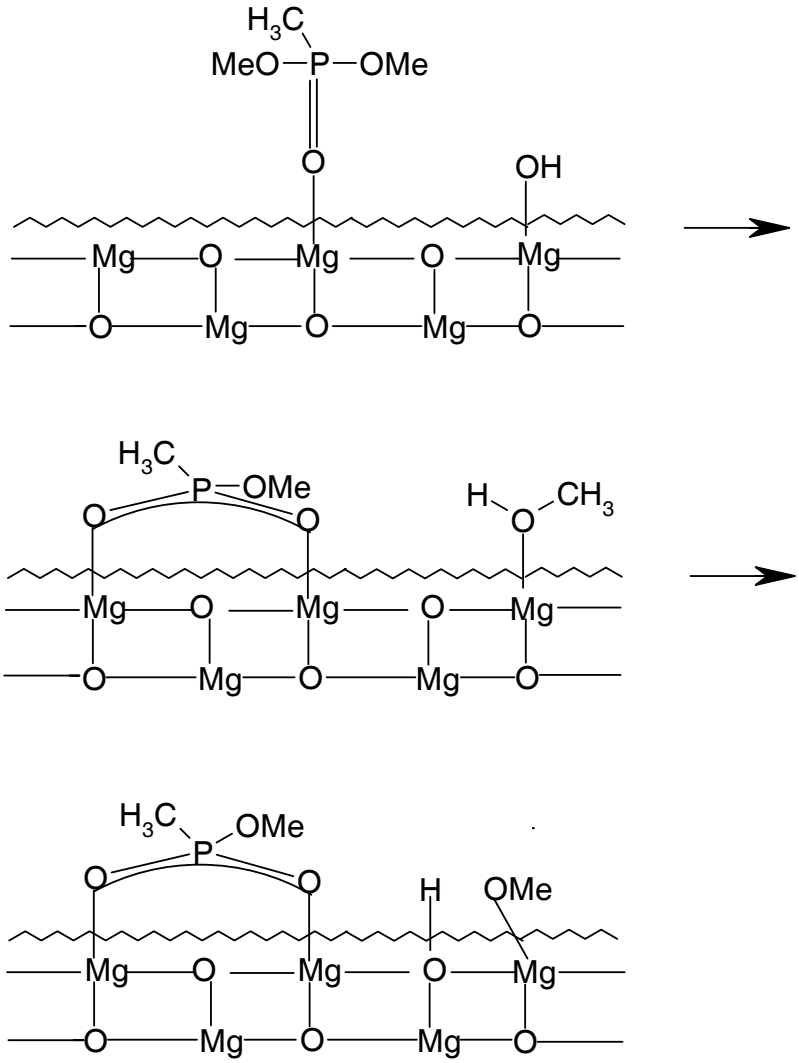

Figure 1.7 Adsorption and formation of bridging species and methanol.

products were found to extend across the surface. This lead Klabunde to conclude that organophosphate surface reactions are stoichiometric and not catalytic.

As indicated by GC, formic acid and methanol were the major volatile products formed. In agreement with previous results, a $C_2H_6PO_3$ bridged species was found to be held to the MgO surface. The study was performed at 200, 300, 400 and 500 °C. At the lower temperatures, volatile products were adsorbed to the surface, in effect blocking further adsorption of DMMP molecules. Klabunde presented several different surface reaction mechanisms to explain these results. It was suggested that the most likely pathway involves the formation of an O-P-O bridge, as well as methanol dissociation on the surface via interaction with a surface hydroxyl group, present in ambient MgO. This is depicted in Figure 1.7. The new surface bound $-OCH_3$ group was then assumed to be oxidized by additional DMMP to yield a surface bound $-OCH_2OH$ group. A new hydroxyl group on the surface would then be present and available for further DMMP decomposition.

Li et al.[11] extended this work further to probe surface reactions, product formation and the effects of water. A GC-MS pulsed microreactor was used and similar experimental conditions as those detailed in previous studies were employed. The effectiveness of MgO as a destructive adsorbent material was assessed by flowing DMMP, trimethylphosphate (TMP), trimethylphosphine, triethylphosphate (TEP), and triethylphosphite through a reactor cell, in the absence of MgO. When the temperature was raised to around 400 °C, TEP and triethylphosphite underwent dealkylation reactions, releasing C_2H_4 and small amounts of phosphorous oxides, PO_2OH and P_2O_3. Decomposition products from other species were not observed until the temperature had

been raised to 750 °C, at which time CH_3, OCH_3, and CH_3PO_3 fragments were detected. Furthermore, at 850 °C, additional fragmentation yielded H_2O and C_2H_4, and possibly a P_4 cluster. The presence of water, in the empty reactor cell, lowered the decomposition temperature of DMMP and TMP; methanol and phosphorus oxides were detected at 500 °C. Water, however, had little effect on trimethylphosphine and the ethoxy-substituted compounds.

Despite the non-catalytic nature proposed by Klabunde, previous studies indicated that particles with high surface area are most effective at breaking up the organophosphorus molecules. In this work, particles with surface areas of 130 and 390 m^2g^{-1} were compared.[11] MgO was placed in the reactor cell and the organophosphorus compounds were carried over the nanoparticle bed by means of a helium stream. The presence of MgO correlated with substantially lower decomposition temperatures, as compared to empty cell trials. Near 170 °C, DMMP and TMP began to decompose to produce formic acid and by 200 °C the decomposition was complete. Higher temperatures correlated with the detection of: methane, water, carbon monoxide, carbon dioxide and some formic acid. However, no phosphorus-containing products were seen, indicating that all of these species remained adsorbed to the surface. In addition to DMMP and TMP, the ethoxy species also began to show signs of decomposition at 170 °C, with ethanol as the primary product. At 300 °C, ethane was detected and by 600 °C the phosphine broke down to produce methane.

When water was introduced into the reactor cell containing MgO nanoparticles, methanol replaced formic acid as the principle product of DMMP and TEP at lower temperatures (170-500 °C) and at higher temperatures, secondary products remained the

same with the exception of formic acid. Water lowered the decomposition temperature of triethylphosphine to 500 °C, but did not effect the decomposition of the ethoxy-containing adsorbents.

Not only was water effectively used to lower decomposition temperatures, it was also used to regenerate the solid nanoparticles. When the MgO beds were completely exhausted with sorbents, 2-μL injections of water were used to release additional amounts of methanol and formic acid. At 500 °C, the adsorptive capacity of the MgO was regenerated by about 30 percent, leading to the possibility of reusable surfaces for CWA destruction. Decomposition products and relative amounts of the products did not change with the change in powder surface area. The MgO(390) was, as expected, capable of decomposing greater amounts of the adsorbed species.

The previous studies elucidated DMMP decomposition mechanisms on MgO under certain conditions, but questions remained regarding the oxidation of the $–OCH_3$ group held on the surface and where the additional oxygen atom originated. Using ^{18}O-surface labeling experiments and DMMP as the adsorbate, Li determined that though the oxidation power may be initially supplied by the surface oxygen, it is mainly driven by the phosphoryl oxygen.[11] An $Mg^{18}O$ surface was prepared, as in Figure 1.8, and rapid exchange of the surface and phosphoryl oxygens yielded formic acid containing one ^{18}O atom as a product. Thus, a key decomposition process is the oxidation of the methyl group to create a methoxy group that can subsequently be released as methanol.

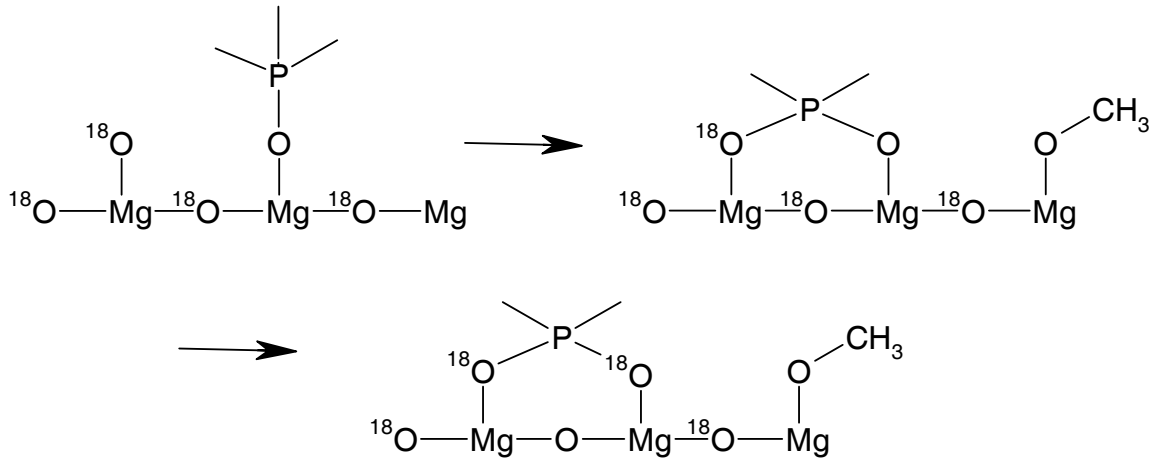

Figure 1.8 Oxygen exchange, upon DMMP adsorption.

In a theoretical study, Yudanov teamed with Klabunde[15] to explore the interaction channels of DMMP on single crystal MgO(001). As depicted in Figure 1.9, experimental data lead researchers to believe that bridging species are formed and methanol was released after O-CH_3 interactions with surface hydroxyl groups. Using the MINDO/3 method, calculations, in agreement with the hypothesis put forth by Klabunde, were generated. However, there was a slight difference in the findings: DMMP was found to adsorb molecularly and dissociate at higher temperatures. Surface hydroxyl groups were

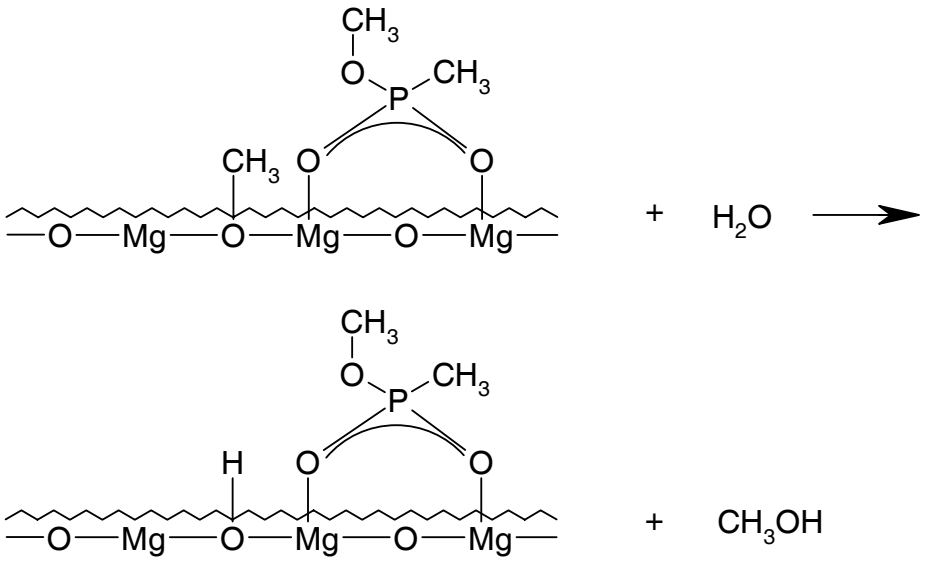

Figure 1.9 The presence of surface hydroxyl groups may not be necessary for volatile formation.

found to be unnecessary for methanol formation. Rather, methanol could be created by reaction of water with a surface bound methyl group. This mechanism appears to offer a 40 kJ/mol gain in energy. Methanol may then go on to be oxidized to formic acid, while the $(CH_3O)_2PCH_3$ is strongly dissociatively held on the surface. This dissociation would offer a 155 kJ/mol gain in energy.

1.3.2.3. Interactions of CWAs with Magnesium Oxide

Wagner, Bartram, and Klabunde[16] widened the scope of organophosphorus surface chemistry to include reactions of the chemical warfare agents VX, GD, and HD on aerogel-prepared MgO nanoparticles. This distinctive work is one of the few reports in which data regarding actual CWAs, rather than simulants, is presented. Solid-state MAS NMR was used to probe in situ reactions of the CWAs with MgO particles having a 344 m^2g^{-1} surface area. Samples were exposed to air; thus, the degree of surface hydration and presence of other contaminants was unknown in this work.

Liquid samples of the CWAs were combined with nanoparticles and the subsequent reactions were observed using ^{31}P MAS NMR. A 6 μL aliquot of 3,3-dimethyl-2-butyl methylphosphonofluoridate (GD) was added to 106 mg of MgO. A spectrum taken 9.5 minutes after the experiment commenced, showed a doublet at 28.5 ppm due to GD. As expected, comparable to simulant molecules, GD was hydrolyzed by surface hydroxyl groups and/or any water present in the system. As this process occurred (at t = 1 h), broad peaks representing GD-acid (pinacolyl methylphosphonic acid) and methylphosphonic acid (MPA) grew in at 25.7 and 18.5 ppm, respectively. A steady state was rapidly achieved and the first-order half-life was determined to be 28 minutes.

Similar parameters were used to investigate the interactions of O-ethyl S-2-

(diisopropylamino)ethyl methylphosphonothiolate (VX) with MgO. Upon hydrolyzation, VX yielded ethyl methylphosphonic acid and MPA. Unexpectedly, no S-(2-diisopropylamino)ethyl methylphosphonothioate, a toxic hydrolysis by-product, was detected. The first-order half-life was found to be 68 h.

The hydrolysis of these CWAs is triggered by the basicity of the MgO surface. This conclusion has also been described by Yang in her work on the solution-state chemistry of CWAs.[3,67,68] Here, the broad peaks seen in the spectra of VX and GD are indicative of magnesium phosphonate complexes held to the surface. Thus, the orientation of the MgO crystal lattice may encourage product formation. The geometry of the (100) plane can accommodate a bidentate bridged species, such as GD-acid or EMPA, while a (111) face, edge or corner site may be necessary to accommodate the tridentate MPA.

In addition to surface hydrolysis reactions, Klabunde examined the kinetic behavior of the surface reactions. Each of the CWAs exhibited a fast initial reaction before steady state conditions were reached. GD reached a steady state after 10 minutes, while VX took 1 hour. The rapid initial rate is attributed to the abundance of available MgO active sites. Adsorbates with lower surface tension and viscosity were able to spread and react the fastest, as seen with GD. Once the liquid has extended over available surface sites, it must evaporate and diffuse through the gas phase. Thus, continued reactions, after the fast initial reactions, appear to be a function of the reactants vapor pressure. GD, with a vapor pressure of 0.4 Torr, exhibits a faster steady state reaction than does VX. The relationships of surface tension and vapor pressure with the steady state half-life offer a method to predict the pervasiveness of other CWAs on MgO.

Table 1.5 Summary of previously reported experimental results MgO.

Adsorbate	Surface	Decomposition Products	Characteristics
$(CH_3CH_2O)_3P=O$	Empty cell	C_2H_4, PO_3H, P_2O_3, @↑T P_4	Dealkylation reaction ~400°C
$(CH_3CH_2O)_3P=O$	MgO	CH_3CH_2OH, C_2H_4, alkenes	P left on surface, which passivates over time
$(CH_3CH_2O)_3P$	Empty cell	C_2H_4, PO_3H, P_2O_3, @↑T: P_4	Dealkylation reaction ~400°C
$(CH_3CH_2O)_3P$	MgO	C_2H_4, $(CH_3CH_2)_2O$, alkenes	P left on surface, which passivates over time
$(CH_3)_3P$	Empty cell	CH_3, OCH_3, CH_3PO_3, H_2O, C_2H_4	High T needed for decomposition
$(CH_3)_3P$	MgO	C_2H_4, alkenes	H_2O lowered decomposition T, surface passivation
DMMP	Empty cell	$(CH_3)PO_3$, PO_3, P_4, H_2O, C_2H_4	High T needed for decomposition, H_2O lowered decomposition T
DMMP	MgO (100) powder, nanoparticles	CH_2O_2, CH_4O, @↑T: CH_4, H_2O, CO_2, CO, CH_3CH_2OH	O-P-O bridging residue left on the surface, which passivates
$(CH_3O)_3P$	Empty cell	$(CH_3)PO_3$, PO_3, P_4, H_2O, C_2H_4	H_2O lowered decomposition T
$(CH_3O)_3P$	MgO (130)	CH_2O_2, CH_4	P left on surface, which passivates over time
GD	MgO nanoparticles	GD-acid, $CH_3PO_3^{2-}$	Analogous to solution chemistry
VX	MgO nanoparticles	$C_3H_8PO_3^-$, $CH_3PO_3^{2-}$	Analogous to solution chemistry

In summary, Klabunde and co-workers' pioneering efforts, in the area of organophosphonate simulant and agent chemistry on metal oxide surfaces, have generated a better understanding of adsorption and decomposition mechanisms. Properties, such as steric hindrance and basicity, were shown to influence the extent of dissociative versus molecular adsorption. Comparable to adsorption on organic films, initial interactions were through the phosphoryl oxygen. Decomposition reactions were concentrated at highly active edge and corner sites; Table 1.5 summarizes products identified in the many studies carried out on magnesium-oxide surfaces. These results provide a foundation for examining uptake probabilities and product branching ratios of CWA simulants on clean and water-exposed MgO.

1.3.2.4. The Role of Co-Adsorbed Water on Magnesium Oxide

Studies indicate that the presence co-adsorbed water enhances the propensity of metal-oxide surfaces to adsorb and decompose organophosphonates, however there is a need for more detailed work in this area. There is an existing body of research regarding the adsorption of water on single crystal MgO(100).[50,69-71] This work can lend insight into the effects that surface-bound water has on subsequent adsorption and decomposition of other species, particularly CWA simulants.

Kay and co-workers[72] used molecular beam reflection and TPD to examine the adsorption and decomposition on single crystal MgO(100). It was shown that the sticking coefficient was near unity over a range of temperatures (150-250 K), until the temperature-dependent saturation coverage level was reached. Below 150 K, the sticking probability seems to be independent of coverage.

Researchers have attempted to investigate the pathway of water adsorption on MgO surfaces. Results vary, with some indicating a molecular adsorption and others favoring a dissociative mechanism. Regardless, with water trapped on a MgO surface, hydroxyl groups likely interact with organophosphonates through hydrogen bonding. Surface migration may then lead to stronger bonds with exposed surface sites. These two adsorption channels may be responsible for unidentified IR vibrational modes seen in work done by Mintz and Klabunde.[9,29] Nonetheless, more detailed work is needed to determine how humidity levels influence the adsorption of organophosphonates.

1.3.3. Iron Oxide

1.3.3.1. CWA Simulant Interactions with Iron Oxide

Mitchell and co-workers,[29,30] as well as White and co-workers,[24,42,43] have studied

the interactions between iron-oxide surfaces and organophosphorus molecules. The variable oxidation states of Fe_2O_3 may provide unique pathways through which CWA simulant molecules, such as DMMP and DIMP, may adsorb and subsequently react. Oxidation of the organophosphorus compounds may follow the Mars and Van Krevelen route and occur as a result of oxide ions becoming available due to the change in oxidation state of the metal.[73]

Mitchell et al. demonstrated that a very strong interaction occurs between the P=O group of DMMP molecules and Fe_2O_3 surfaces.[29] Infrared spectroscopy studies revealed that the P=O stretching mode shifted from 1208 cm^{-1} at 30 °C to 1077 cm^{-1} at 100 °C, indicating the formation of a strong complex. Results indicated that a second complex may have formed through nucleophilic attack of surface hydroxyl groups by the phosphorus atom of DMMP. No significant loss of CH_3 groups was observed even at 100 °C, but more significant decomposition was observed near temperatures of 200 °C.

To better understand the interactions between DMMP and Fe_2O_3 surfaces, Mitchell and co-workers studied the surface chemistry of organophosphonates on alumina-supported Fe_2O_3.[30] Al_2O_3 was chosen because of its well-defined surface chemistry and the relative ease by which its activity could be differentiated from that of iron oxide. The catalytic surfaces were prepared by sequential impregnation using nonaqueous methods and a Fe(III) complex. Diffuse reflectance infrared Fourier transform infrared spectroscopy (DRIFTS) was used to follow the DMMP decomposition reactions on the supported Fe_2O_3 surface.

Upon prolonged exposure to DMMP at room temperature, the Fe_2O_3 surface bound methyl and methoxy infrared bands increased in a disproportionate manner. This

result suggested that DMMP readily decomposes on Fe_2O_3 through a cleavage of the phosphorus-carbon linkages. The adsorption of organophosphonates on Fe_2O_3 surfaces is a not molecular, but rather a dissociative process. This system is in contrast to other metal-oxide systems, such as Al_2O_3, MgO and La_2O_3,[29] in which the methoxy groups are typically the first species cleaved from the parent phosphate molecules. This somewhat unusual behavior may be a result of the Fe(II)/Fe(III) redox couple, as depicted in Figure 1.10.

$$Fe_2O_3 + 2e^- \longrightarrow 2FeO + O^{2-}$$
$$(H_3CO)_2P(O)\text{-}CH_3 + O^{2-} \longrightarrow (H_3CO)_2P(O)_{ads}^- + H_3CO_{ads}^-$$
$$2FeO + \tfrac{1}{2}\, O_2 \longrightarrow Fe_2O_3$$

Figure 1.10 The Mars and Van Krevelen mechanism.

White and co-workers used TPD and Auger electron spectroscopies (AES) to study the interactions of DMMP with Fe_2O_3.[24,42] At 200 K, a single TPD peak associated with multilayers of DMMP was observed. Despite varying surface exposures to DMMP from 2.5 L to 30 L, no desorption peak was observed for the initial monolayer of adsorbed DMMP. Rather, CH_3OH (600 K), CO_2 (586 K), CO (586 K), H_2 (595 K), H_2O (>600 K), HCOOH (550 K), and surface-bound phosphorus residues (>600 K) were observed. These products were the result of the decomposition of the first monolayer of adsorbed DMMP.

AES was used to study the chemical nature of the surface-bound phosphorus residues, both prior to and after desorption of the DMMP decomposition products at elevated temperatures. A fully oxygen-coordinated phosphorus species was observed after heating to 247 K, as evidenced by peaks at 96 and 114 eV, which suggested that the P-CH_3 bond was oxidized by lattice oxygen and the phosphorus subsequently diffused

into the bulk Fe_2O_3. The migration of phosphorus into the oxide film allowed for decomposition of additional DMMP molecules, but decomposition only occurred at elevated temperatures.

1.3.3.2. The Role of Co-Adsorbed Water on Iron Oxide

Hegde and White also used TPD and AES to study the effects of co-adsorbed water on the interaction of DMMP with oxidized iron. Results indicated that pre-exposure to water lead to an increase in the extent of DMMP decomposition.[43] TPD spectra revealed decomposition products, such as H_2O, CH_3OH, CO and CO_2, desorbing from the surface below 200 K. These results indicated that DMMP decomposes at low temperatures on Fe_2O_3.

1.3.4. Aluminum Oxide

1.3.4.1. CWA Simulant Interactions with Aluminum Oxide

Templeton and Weinberg used inelastic electron tunneling spectroscopy (IETS) to examine organophosphorus interactions with Al_2O_3 surfaces.[25,74] UHV experiments were conducted over a range of surface temperatures (200-673 K) and CWA simulant exposure levels (3×10^{-4}-10 Torr · s). These studies were aimed at more accurately describing Al_2O_3 surface chemistry, as well as determining if organophosphorus adsorption was molecular or dissociative.

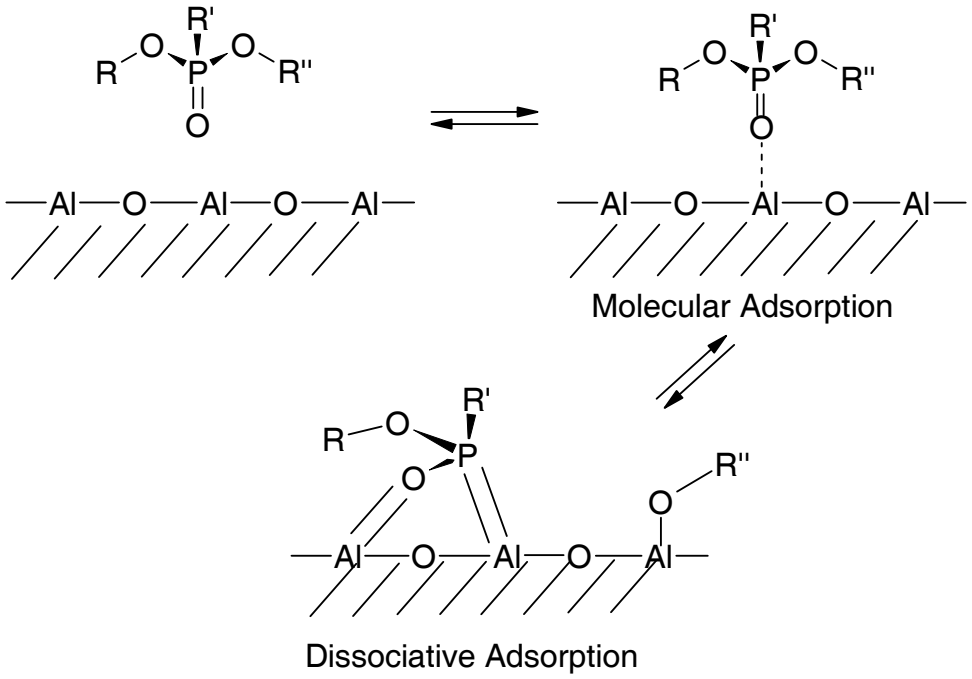

Figure 1.11 DMMP adsorption on aluminum oxide.

IET spectra indicated that, at 200 K and exposures as low as 300 L, DMMP adsorbed molecularly via a Lewis base/Lewis acid complex between DMMP and surface hydroxyl groups, as seen in Figure 1.11. At higher temperatures (295-473 K), the adsorption mechanism became dissociative. A phosphorus-oxygen bond was cleaved and yielded surface bound methyl methylphosphonate (MMP), which decomposed at 573 K. This sequential decomposition reaction produced a tridentate methylphosphonate species.

The interfacial behavior of DIMP and DPMP on aluminum oxide was somewhat similar to that of DMMP.[25] IET spectra revealed molecular adsorption of DIMP and dissociative adsorption of DPMP at 295 K, while dissociative adsorption of DIMP was observed at 373 K. The decomposition reactions of DIMP and DPMP were like that of DMMP. The reaction was initiated by a cleavage of the phosphorus-oxygen bond and at elevated temperatures cleavage of carbon-oxygen bonds was noted.

Mitchell and co-workers investigated the interactions of DMMP on Al_2O_3 with

infrared spectroscopy.[29,32] Results indicated that the absorption pathways of DMMP on Al_2O_3 are very similar to those of DMMP interacting with an MgO system. The first interaction channel was a coordination of the phosphoryl group to acidic surface sites. Subsequent decomposition through cleavage of the methoxy groups from the parent molecule likely resulted in evolution of methanol from the surface. Further decomposition was not observed until temperatures reached nearly 400 °C.

1.3.4.2. Interactions of CWAs with Aluminum Oxide

Wagner et al. employed ^{31}P, ^{13}C, and ^{27}Al magic angle spinning (MAS) nuclear magnetic resonance (NMR) spectroscopy to investigate the room-temperature reactions of VX, GB, and GD with nanosize Al_2O_3.[34] The CWAs were determined to readily hydrolyze and produce surface-bound phosphonate species. High exposure levels of the nerve agents induced the formation of aluminophosphonate complexes. This result indicated that the reactions are not only interfacial, but occur within the Al_2O_3 particle. The relative ease at which CWAs are decomposed by Al_2O_3 bodes well for the future of such materials as field decontamination agents or filtration materials.

1.3.5. Tungsten Oxide: CWA Simulant Interactions with Tungsten Oxide

The Tripp Research Group at the University of Maine has characterized the interaction of organophosphorus compounds on high surface area tungsten-oxide powders.[39,40] The focus of these studies was to investigate the usefulness of WO_3 sensing materials. Infrared studies confirmed DMMP, dimethyl hydrogen phosphonate (DMHP), and trimethylphosphate (TMP) adsorption on WO_3 powders occurred through the phosphoryl functional group. DMMP decomposition occurred at elevated temperatures with the stepwise loss of methoxy groups near 200 and 300 °C. This resulted in the

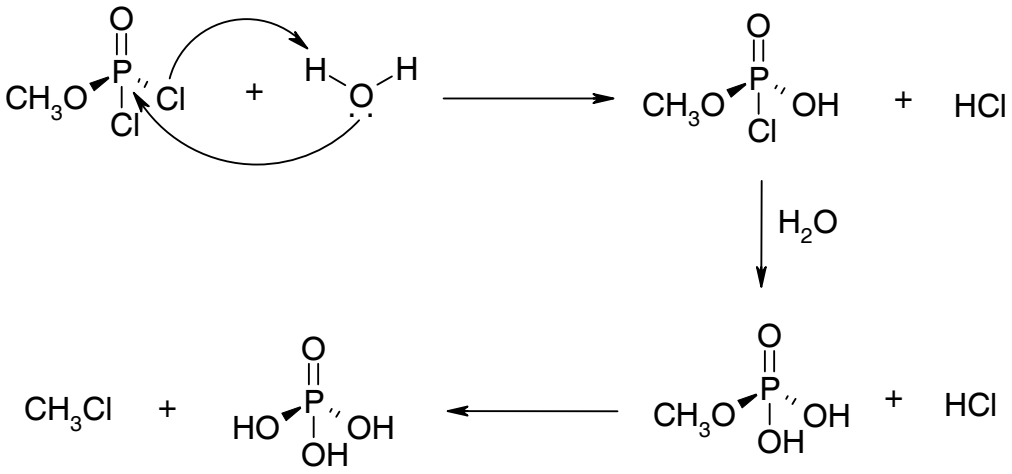

Figure 1.12 Hydrolysis of MDCP.

formation of a stable phosphate surface complex, which was responsible for a loss of sensor response above room temperature.

Kanan, Lu, and Tripp then went on to study the interactions of chlorinated phosphate molecules with WO_3 powders.[39] Kanan suggests that MDCP is a better simulant molecule for studying the behavior of CWAs owing to the presence of chlorine, which likely is a good model for the fluorine atoms present in sarin and soman. In agreement with the behavior of DMMP and TMP, MDCP adsorbed on WO_3 through the phosphoryl group. Lewis acid, Brønsted acid and water adlayers provided available adsorption sites. The presence of water adlayers or water vapor induced a rapid hydrolysis of MDCP molecules. The reaction products HCl and CH_3Cl, as seen in Figure 1.12, were observed by GC-MS.

1.3.6. Titanium Oxide: CWA Simulant Interactions with Titanium Oxide

Rusu et al. have monitored the adsorption and decomposition of DMMP on powdered titanium-oxide surfaces.[31] Transmission-FTIR spectra indicated that at cold temperatures (<166 K) DMMP condensed on the TiO_2 surface as an ice layer. Warming the surface to temperatures between 166 and 200 K caused diffusion of the

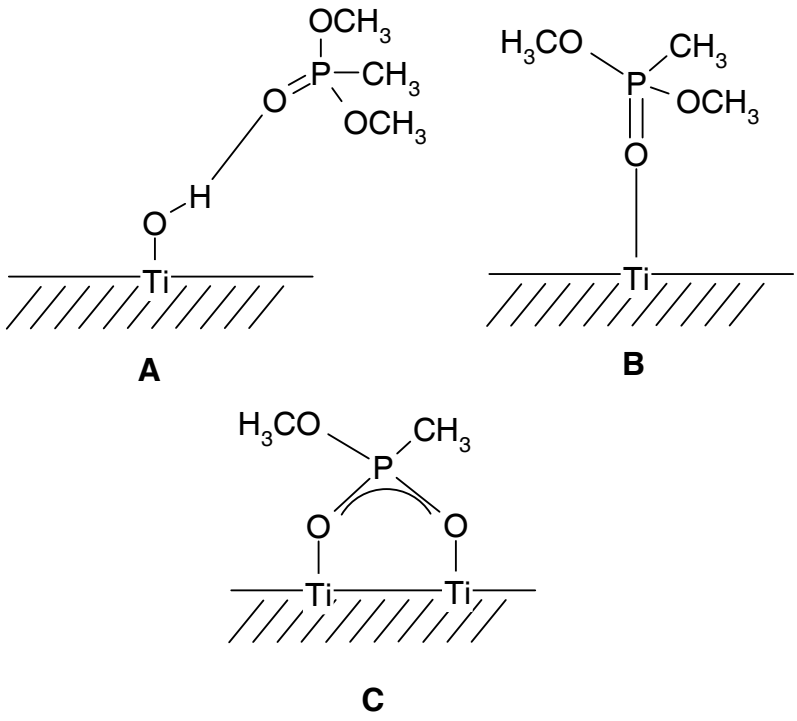

Figure 1.13 Adsorption complexes (A, B) and a hydrolysis product (C) of DMMP on TiO_2.

organophosphonate molecules into the film. Hydrogen bonds formed between surface TiOH groups and DMMP. Additional interactions occurred at surface Lewis acid sites. (see Figure 1.13). Above 214 K, sequential decomposition of DMMP took place through cleavage of the methoxy groups from the phosphoryl core of the molecule. These reactions resulted in the formation of surface Ti-OCH_3 groups and complete consumption of surface hydroxyl groups. Further decomposition resulted in the formation of adsorbed phosphate derivatives, as seen in Figure 1.13. Kim et al. have investigated the interactions of organophosphorus compounds on TiO_2 at temperatures higher than those reported by Rusu and reported similar reactions.[31,40]

Chen and co-workers observed the decomposition of DMMP on TiO_2 with XPS and TPD.[75] Application of principal component analysis to the C (1s) and P (2p) XPS channels established two linearly independent phosphorus-containing species and two

linearly independent carbon-containing species on the surface between room temperature and 700 K. At room temperature, however, molecular DMMP was the primary adsorbate. TPD spectra confirm that molecular DMMP desorbed from the titania surface at about 550 K. Carbon-containing decomposition residues were driven from the surface by 800 K and only at 1000 K were phosphorus containing species detected. Chen went on to study the variable chemical reactivity of titania-supported nickel and copper clusters and films.[76,77] The carbon and phosphorus decomposition residues of DMMP effectively poisoned the catalytic decomposition of additional DMMP on the TiO_2-supported Ni clusters. Thus, TiO_2(110) surfaces provided a more effective decomposition strategy for organophosphonate species.

1.3.7. Silicon Oxide: CWA Simulant Interactions with Silicon Oxide

The adsorption of DMMP on silica surfaces has been previously investigated by Henderson et al.[24,37,41] Dehydrated SiO_2 surfaces were placed in a UHV instrument operating at a base pressure of 5×10^{-9} Torr. A leak valve system was used to introduce DMMP into the dosing chamber and a pressure of 5×10^{-7} Torr was maintained during surface exposure. The organophosphonate molecules were determined to adsorb to silica at 170 K.[24] Subsequent desorption during TPD studies occurred molecularly at 200 to 210 K and 275 K for multilayer and monolayer states, respectively.[24] Assuming first order desorption kinetics, an activation energy of desorption of ~16.9 kcal/mol (81.8 kJ/mol) was determined for the monolayer state. Furthermore, the monolayer state was found to saturate at a DMMP exposure of 30 L. No indication of DMMP decomposition was observed in the TPD experiments and AES confirmed the lack of organophosphonate reaction.

Further experiments by Henderson and co-workers examined DMMP interactions with hydrated SiO_2 surfaces. TPD results were nearly identical to those obtained from the dehydrated SiO_2 surfaces. However, at elevated temperatures (~650 K), small amounts of methanol and methylphosphonate evolved, suggesting a hydrolysis reaction between weakly sorbed water and DMMP. A decrease in the DMMP peak area by 8-10% indicated only a small effect of co-adsorbed water. The significant lack of enhancement or poisoning of DMMP adsorption in the presence of water implies that adsorption must involve either exchange with weakly adsorbed water or interaction at sites not influenced by hydration.

Similar experiments conducted by Kanan et al. used FTIR to study the exposure of high surface area, dehydrated silica thin films to DMMP, trimethylphospate (TMP),

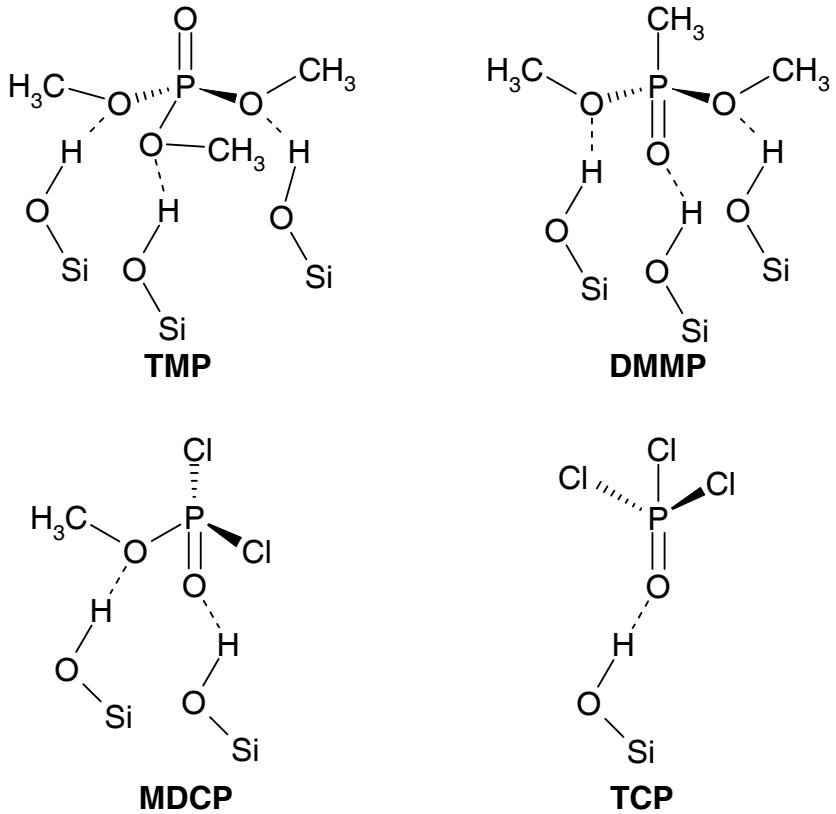

Figure 1.14 Adsorption of TMP, DMMP, MDCP, and TCP on silica surfaces.

methyl dichlorophosphate (MDCP) and trichlorophosphate (TCP).[24] Figure 1.14 depicts the interactions between the CWA simulant molecules and the silica surfaces. Upon exposure to saturated organophosphonate vapor for two minutes at room temperature, Kanan and co-workers observed molecular DMMP and TMP adsorption. Loss of the initial Si-OH mode at 3747 cm^{-1} and the appearance of a broad Si-OH mode at 3223 cm^{-1}, in addition to the red-shift of the Si-OH bending mode from 863/768 cm^{-1} to 900-1050 cm^{-1}, confirmed formation of new hydrogen bonds. Spectral modes assigned to surface bound methoxy and phosphoryl functional groups indicated weak interactions between free surface silanol groups and the oxygen containing functional groups of the adsorbates. Thermal studies revealed that DMMP completely desorbed by ~300 °C. The additional methoxy moiety of TMP held the molecules more strongly on the surface and subsequently led to a desorption temperature of ~400 °C.[37] In agreement with Henderson et al., no sign of decomposition was observed.

IR spectra of chlorinated phosphate species adsorbed on thin films of high surface area silica revealed interactions similar to those observed for DMMP and TMP.[37] The primary interactions between MDCP and the substrate were hydrogen bonds between the methoxy and phosphoryl groups of the adsorbates and the free silanols of the surface. Having no methoxy groups, TCP was found to interact with the silica films exclusively through very weak interactions between the phosphoryl group and surface silanols. The P-Cl vibrational modes, in the case of both MDCP and TCP, had no frequency shift upon adsorption. Thus, no measurable interaction through the halogen atoms was reported. Temperatures near 150 °C were required to desorb MDCP molecules from the surface, whereas removal of the TCP molecules from the surface by evacuation at room

temperature further characterized the very weak interactions. As with DMMP and TMP, no indication of phosphate decomposition was observed.

1.4. Summary and Implications

Pioneering studies have demonstrated that organophosphorus compounds readily adsorb on various organic and metal-oxide surfaces. DIMP and DMMP have been shown to weakly adsorb on well-ordered organic surfaces possessing –OH, $–CO_2H$, and $–(CO_2^-)_2Cu^{2+}$ terminations. Although weak hydrogen bonding interactions were observed in each system, the metal ion-functionalized films seeded the growth of multilayers of organophosphonate species. Despite these preferential interactions, no study has reported the decomposition of organophosphorus CWA simulants on organic thin films. Furthermore, no studies have examined the interactions between organophosphorus compounds and urethane-containing films.

In order to more accurately model the militarily relevant organic coatings, this study presents new urethane-containing monolayers. The adsorption characteristics of CWA simulants on these surfaces are evaluated. The detailed knowledge of simulant chemistry on urethane-containing surfaces will aid in the understanding of the environmental fate of CWAs and in the development of more effective resistant coatings. The literature is rich with studies detailing the chemical interactions between organophosphonate molecules and metal oxide surfaces. Magnesium-, iron-, aluminum-, tungsten-, titanium-, and silicon- oxide films exposed to CWA simulant molecules have been characterized with IR, AES, TPD, NMR, and XPS. Generally, DMMP adsorbed on most oxides, such as MgO, Fe_2O_3, Al_2O_3, WO_3, and TiO_2, through the phosphoryl functionality. Subsequent decomposition occurred through elimination of the methoxy

groups at elevated temperatures. This reaction resulted in surface bound, stable phosphonate residues. DMMP interactions with silicon oxide, however, were primarily comprised of hydrogen bonding interactions between methoxy moieties and surface silanol sites. Even at elevated temperatures, no direct evidence of DMMP decomposition was observed.

Though much research has been performed on metal oxides, the combination of oxides and organic species within a single thin film has not been previously investigated as a potential surface for the decomposition of organophosphonates. This type of film provides a high degree of control over chemical properties and may allow for the design of coatings that interact strongly with organophosphonate molecules. Novel trisilanol-phenyl polyhedral oligomeric silsesquioxane (POSS) molecules combine a core silicon-oxide inorganic structure with peripheral organic substituents. Langmuir-Blodgett (LB) films of POSS molecules provide the opportunity to explore how DMMP uptake and reactivity depend on the molecular-level structure and chemical functionality of a novel set of thin films.

The present work utilizes vacuum technology and surface spectroscopies to study the interactions between CWA simulants and both urethane-containing thin films and hybrid organic-inorganic POSS LB-films. The encompassing focus of this research is to better understand the fundamental interactions and reactions of halogenated and non-halogenated organophosphonate CWA simulants with carbamate functional groups present in well-ordered thin films. In addition, the interactions and reactions occurring between CWA simulants and the slightly acidic silanol groups of POSS films are targeted. The target species and surfaces are isolated from gaseous interferents by

probing chemical interactions in an ultra-high vacuum environment. Molecular beam and dosing devices will offer complete control of incident molecules' energy and approach geometry. Mass spectroscopy, RAIRS, XPS, and TPD will identify any desorbed or surface-bound products and lead to a better understanding of CWA simulant chemistry. This insight will lead to better decontamination strategies, as well as new possibilities for the development of CWA sensors and CWA resistive coatings.

Chapter 2
Experimental Approach

2.1. Background

Real-world materials, such as polyurethane-based chemical agent resistive coatings (CARC)[44-47] or metal-oxide slurries, employed by the military as protective barriers or decontamination strategies are difficult to study because the exact chemical properties, including physical structure and chemical composition, are unknown. Moreover, the concentration and depth of reactive groups relative to the air interface is also unspecified. The poorly defined, uncontrolled surface structure leads to numerous interaction/reaction pathways with CWAs and simulant molecules. It is difficult to determine where interfacial reactions are occurring and even more difficult to build systems that are reproducible on the molecular level.

The complicated nature of CARC paint and oxide creams and the subsequent complex analyses, gives the necessary motivation to use well-defined model organic and inorganic surfaces to effectively discern interfacial reaction pathways and characteristics. Controlled, reproducible surfaces can be used to examine the reactions that take place with surface molecules and organophosphonate CWA simulants. Self-assembled monolayers (SAMs) provide well-ordered, highly-characterized organic surfaces[51] and here, were applied toward the creation of well-ordered organic thin films containing urethane linkages. In addition, trisilanolphenyl polyhedral oligomeric silsesquioxane (POSS) LB-films are highly-characterized surfaces that were utilized to explore reaction pathways of organophosphonates with inorganic-organic hybrid materials.[78,79] A full description of these model surfaces is found in subsequent chapters.

Effective characterization of model SAM and LB-film surfaces and accurate description of organophosphonate interfacial interactions require analytical capabilities that are both sensitive and selective. The chemistry of the interfacial region of a coating or film will dictate environmental interactions. Studies of these interactions and potential reactions must focus only on surface chemical and physical properties and omit contributions from the bulk phase.

The work presented here combines several surface analytical tools in an effort to thoroughly describe the properties of SAMs and LB-films, not only during and after interfacial reactions with organophosphates, but prior to CWA simulant exposure. To better study the chemical nature of the interactions of organophosphonate CWA simulants with target surfaces, an ultra-high vacuum environment was used to isolate the interactions from environmental gaseous interferences. The use of highly-characterized surfaces coupled with molecular beam and dosing capabilities allowed for the elucidation of adsorption and desorption characteristics of CWA simulants on a variety of materials through TPD and sticking probability studies. The principal techniques used to characterize freshly prepared surfaces and surfaces exposed to organophosphonates include: RAIRS, contact angle goniometry, and XPS.

2.2. Surface Characterization Techniques and Experimental Details

2.2.1. Ultra-high Vacuum Surface Analytical Techniques

Ultra-high vacuum (UHV) conditions are often necessary for successful function of surface analytical techniques. It becomes critical to perform studies, such as temperature programmed desorption (TPD) and sticking probability measurements, in environments that have a base of pressure of ~1 x 10^{-9} mbar. These conditions limit the

number of background atoms and molecules that make contact with the surface substrate and may potentially stick to the interface. Eliminating interferents that may change the sample properties is crucial to maintaining a clean, well-characterized substrate for the duration of experiments. The TPD and sticking probability studies conducted here were performed in a UHV instrument (Figure 2.1) equipped with a load lock system, high-vacuum differentially pumped source chambers, and an Extrel mass spectrometer. The cylindrical central chamber, which has a base pressure ~5 x 10^{-10} Torr, is equipped with multiple viewing and through ports for mating of various flanged components. The UHV instrument employed in these studies is a two-stage chamber. The upper stage, where the load lock system is mated on an 8" flanged feed-through, houses the Cryo-Plex 8 UHV Cryopump (Austin Scientific Company Inc., pumping speed 1000 Ls^{-1}) and will have future analytical capabilities including XPS and Auger spectroscopies. The current lower stage accommodates the molecular beam source and mass spectrometer detector chambers, as well as an SRS RGA mass spectrometer (Stanford Research Systems Residual Gas Analyzer). At the base of the main UHV chamber, a large turbomolecular pump (Pfeiffer TMP1601P, pumping speed 1500 Ls^{-1}) assists the cryopump in achieving and maintaining UHV conditions in the central chamber. Pressure values, turbomolecular pumps, gate valves and foreline valves are controlled using an Interlock program.[80] A Labview® based software program, along with FieldPoint relay modules, ensures that the integrity of the UHV instrument will not be compromised through unexpected pressure bursts or power losses.[80,81]

2.2.1.1. Sample Introduction System and Alignment Procedures

The load lock system (MDC Vacuum Products Corp.) allows sample transfer to

the main UHV analysis chamber without compromising the ultra-high vacuum. This sample introduction system consists of a rotating translation arm, introduction chamber, a gate valve isolating the main UHV chamber and a gate valve isolating the turbomolecular pump used to evacuate the load lock chamber. Sample installation requires venting the load lock chamber with ultra-pure N_2. Sample surfaces, either SAMs on Au-coated glass or LB-films on Au-coated glass (1 cm x 1 cm), are mounted on the stainless steel sample holder with securing tabs. The sample holder is then locked securely on the transfer arm with a lock and grove mechanism. Prior to sample introduction, the load lock chamber is first evacuated with a liquid-N_2 cooled sorption pump and then a turbomolecular pump (Pfeiffer TMU071P, pumping speed 50 Ls^{-1}) evacuates the chamber to pressures near 10^{-6} mbar. Upon isolation of the turbomolecular pump, the 6" manual gate valve is opened and the transfer arm is gently introduced to the main analysis chamber. The sample holder is mated to a Cu block, which is affixed to a rod and manipulator that has x, y, z translation, rotation and tilt capabilities, as well as electrical and cryogenic feedthroughs (McAllister Technical Services). A channel locking mechanism detaches the stainless steel mount from the transfer arm and the arm can then be withdrawn from the UHV chamber and the manual gate valve closed. The Cu block mounting contains a liquid-N_2 reservoir and a button heater which are used to control surface temperature. Furthermore, a thermocouple wire positioned at the face of the sample mount is used to monitor the surface temperature.

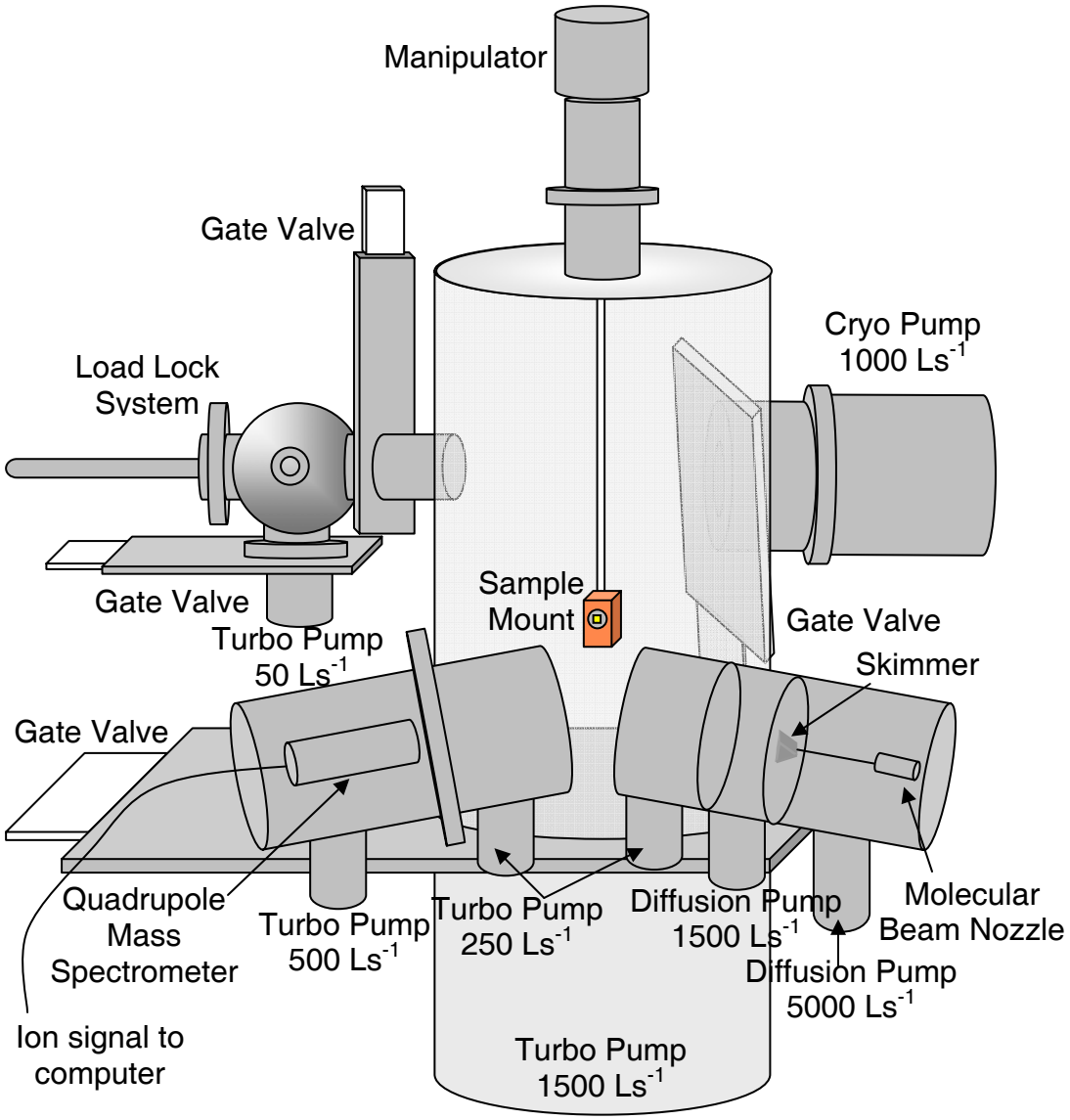

Figure 2.1 Custom designed ultra-high vacuum surface analysis instrument.

Sample alignment is critical to performing accurate, reproducible experiments. Molecular beam studies require knowledge of incident/exit beam angles for proper sample exposure and product detection. TPD studies are conducted with the sample surface normal to the detector aperture to maximize the ion signal in the quadrupole mass spectrometer. Precise alignment of the sample surface is accomplished with manipulator

adjustments and assured using a HeNe laser for accurate positioning. To align the sample substrate for molecular beam and TPD experiments, the manipulator rod is lowered to the source/detector stage and the surface is positioned normal to the detector aperture with the aid of the HeNe laser shining through the rear viewing port of the detector chamber. When the laser beam reflects through the view port, the sample position is acceptable for TPD studies. Sticking probability measurements require the use of molecular beams, and thus a different surface position. The geometry of the UHV apparatus is such that the source and beam orifices are positioned 60° from one another. This requires precise substrate alignment for molecular beam studies and is achieved by rotating the top hat mounted rotation stage 30°, such that the incident molecular beam strikes the surface at an angle of 30° and is specularly reflected to the mass spectrometer (Figure 2.2).

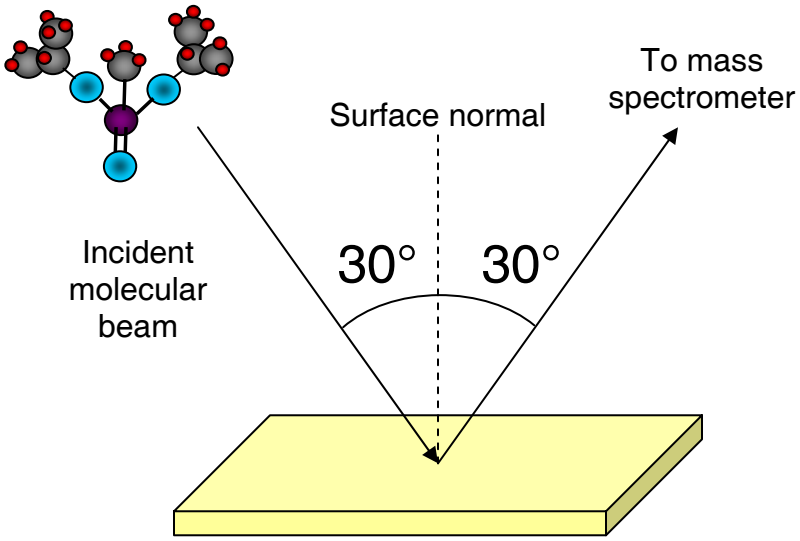

Figure 2.2 Specular scattering of the molecular beam at 30° is employed for sticking probability studies.

2.2.1.2. Sticking Probability Measurement and Molecular Beam Production

The sticking probability, or uptake coefficient, measurements of organophosphonates on POSS surfaces presented in Sections 4.3.2.1 and 5.3.1.1. were

examined according to the King and Wells technique.[82] This method necessitates first measuring the background pressure in the central UHV chamber. A molecular beam of the desired vapor is created and a Teflon® flag is placed in the main UHV chamber to block the beam's path. A clean sample substrate is aligned and the partial pressure of analyte vapor in the main chamber is measured with the mass spectrometer. When desired, the Teflon® flag is rotated out of position and the fraction of the incident beam that adsorbs on the surface is determined from the decrease in the partial pressure (mass spectrometer signal) of the analyte vapor as the beam is allowed to strike the surface. The sticking coefficient (S) is a function of surface coverage ($f(\theta)$) and any energy barriers (E_a) that must be overcome for adsorption to take place:

$$S = f(\theta)^{(-E_a / RT)} \tag{1}$$

S can be calculated from the pressure drop, beam flux (F), and pumping speed in the chamber and is always a value in the range $0 < S < 1$. In general, S is related to the rate of adsorption (R_{ads}) and flux according to equation 2:

$$R_{ads} = S \cdot F \tag{2}$$

where the R_{ads} behaves Arrheniusly and F is described by:

$$F = \frac{P}{(2\pi mkT)^{1/2}} \tag{3}$$

where P is the gas pressure (Nm^{-2}), m is the mass of one molecule (kg), and T is the temperature (K).

Typical molecular beams can be created with pressurized cylinders of the desired gas.[83] At room temperature, however, a majority of CWA simulants are liquids. At 303 K, for example, DMMP is a liquid with a vapor pressure of 1.06 Torr. Therefore, to create molecular beams of the desired organophosphonates, N_2 (~750 Torr) was bubbled through a reservoir containing the liquid simulant held at elevated temperatures (353 K). This glass bubbling system is depicted in Figure 2.3. Several milliliters of the desired liquid are placed in the bottom of the vessel. The two pieces of the apparatus are clamped together with an o-ring seal and the lower portion of the unit is confined in a temperature bath/circulator (VWR 1160A) held at the preferred temperature. The end of

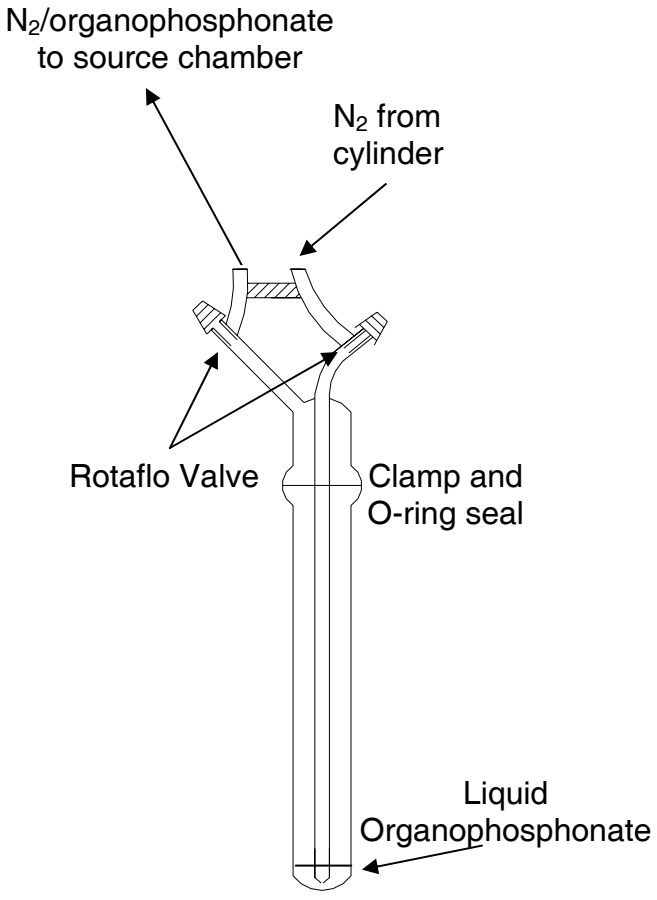

Figure 2.3 The glass bubbling apparatus to create molecular beams of CWA simulants.

the straw-like glass tube is secured by an Ultratorr fitting (Dibert) to a short length of Teflon® tubing that attaches to a N_2-cylinder and a Swagelok® valve and tubing connect the bubbler to a mechanical vacuum pump. This allows for evacuation of the headspace in the straw-like tube. The second tube on the apex of the apparatus is connected to the source chamber of the UHV instrument. Swagelok® valves are also incorporated into this plumbing, such that the volume of the bubbling apparatus can be evacuated prior to beam creation and the source chambers can be isolated until desired. Once the glass system has been evacuated, the N_2 (~750 Torr) is allowed to slowly bubble through the liquid. The resulting organophosphonate/N_2 vapor is first pulled through the Teflon® lines with the mechanical pump. Isolation of the pump and opening of the specified valve allow the pumps associated with the source chamber to pull the organophosphonate/N_2 vapor through the system. Saturation of the Teflon® lines with the organophosphonate/N_2 vapor requires several hours. If experiments are to be conducted on an on-going basis, the vapor delivery system is stable and does not need to be completely evacuated from day-to-day. Simply isolating the system from the N_2 source, pumps and molecular beam source chamber is sufficient. The lines remain saturated and molecular beams can be created in a short time for subsequent studies. Once the delivery system and associated tubing lines have become saturated, the organophosphonate/N_2 vapor enters the source chambers.

Thermal molecular beams are used in surface studies because they provide a well-collimated, stable source of gaseous species. The organophosphonate/N_2 vapor from the bubbling apparatus is collimated into a beam in the differentially pumped source chambers. The vapor enters the first source chamber (2.6×10^{-5} Torr) through a 0.05 mm

diameter nozzle (General Valve). This chamber is evacuated with a robust oil diffusion pump (VHS 10 Diffusion Pump, pumping speed 5000 Ls^{-1}). A 0.40 mm diameter conical skimmer located 6 mm from the nozzle collimates the beam before it enters the second differential pumping stage (Diffstak® Mk2 diffusion pump, pumping speed 1000 Ls^{-1}). The organophosphonate/N_2 beam then passes through a 1.5 mm collimating aperture, located in a third differentially-pumped chamber (Pfeiffer TMU261P, pumping speed 250Ls^{-1}), before passing into the main UHV chamber through a 2.2 mm aperture. The beam strikes the surface with a spot size of 1 cm^2. Uptake measurements were recorded for a range of surface temperatures from 138 K to room temperature.

2.2.1.3. Quadrupole Mass Spectrometer Detector

Gas-phase species that are reflected from the surface at the specular angle of 30° or desorbed from the surface during TPD studies (described below) are monitored with an ABB Extrel (MEXM 1000 model) mass spectrometer (MS). The MS is equipped with a pulse counting electron multiplier/preamplifier, RF filter and Tungsten filaments, which serve as electron impact axial analyzers. The electron multiplier was set at 1900 V and the dynode at 4000 V for the experiments described here. A 1 amu mass resolution is attained over the range of 2 to 1000 amus. An 8" flange on the lower stage of the main chamber couples the doubly differentially pumped detector chambers to the body of the instrument. The aperture in the first differentially pumped chamber is 4.3 mm in diameter and the aperture in the second differentially pumped chamber, leading to the quadrupole mass spectrometer, is 4.7 mm. Baseline pressures of ~10^{-10} mbar are achieved in the detector chambers with two turbomolecular pumps (Pfeiffer TMU261P, pumping speed 210 Ls^{-1}, and Pfeiffer TMU521P, pumping speed 500 Ls^{-1}). The ionizer

of the mass spectrometer is positioned 29 cm from the surface and views a 1 cm^2 spot size on the surface.

2.2.1.4. Temperature Programmed Desorption Spectroscopy

A host of information with respect to adsorbate-surface interactions can be determined using TPD.[84,85] In this technique, a clean sample substrate is exposed to a gas-phase species. In some cases exposure is done at cold temperatures to promote adsorption. The sample is then heated in a controlled fashion and using a mass spectrometer, desorbing species are monitored, as depicted in Figure 2.4. Based upon the ion fragments detected, the profile and area of the spectral traces, the peak temperature position, and the heating rate, a great deal of information regarding adsorbent/adsorbate interactions can be obtained. The heat of adsorption, quantitative coverage information, and kinetic and energetic information can all potentially be obtained through TPD studies.

The probability of a molecule desorbing at one temperature, to produce an equilibrium vapor pressure, is based upon Boltzmann statistics. Thus, TPD spectral traces have Boltzmann characteristics. Desorption of molecules from a surface follows Arrhenius-like behavior and is described by the Polyani-Wigner equation:

$$I(T) \propto \frac{dM}{dt} = -\frac{d\theta_M}{dt} = \nu(\theta_M{}^n) \cdot \theta_M{}^n \cdot \exp\left(\frac{-E_{des}(\theta_M)}{R \cdot T}\right) \qquad (4)$$

where $I(T)$ is the mass spectrometer signal, $\frac{dM}{dt}$ is the rate of desorption of the adsorbate, $-\frac{d\theta_M}{dt}$ is coverage loss rate, $\nu(\theta_M{}^n)$ is a frequency factor, θ_M is the instantaneous coverage, n is the kinetic order of desorption, $E_{des}(\theta_M)$ is the desorption activation energy, R is the gas constant and T is the surface temperature. The heating

rate β can be factored into equation (4) to give:

$$-\frac{d\theta_M}{dt} = \frac{\nu \cdot \theta_M{}^n}{\beta} \cdot \exp\left(\frac{-E_{des}}{R \cdot T}\right) \tag{5}$$

where coverage and energy are both expressed.

TPD measurements were performed in the aforementioned UHV instrument. Samples were installed via the load lock chamber and laser-aligned to place the normal of the substrate in-line with the two collimating apertures of the Extrel mass spectrometer. A linear heating ramp of ~0.1 K s^{-1} was employed and substrates were heated to a temperature of ~300 °C. Species desorbing from the surface in the path of the mass spectrometer are detected and resulting ion signals are sent to a computer for further analysis.

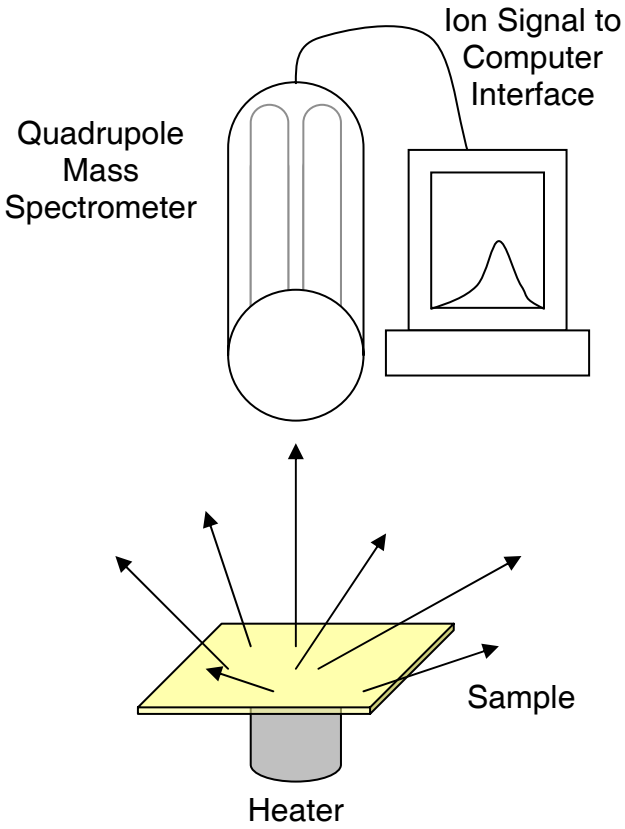

Figure 2.4 TPD experimental design.

2.2.2. Reflection Absorption Infrared Spectroscopy

The use of vibrational spectroscopy to study surface bound species, as well as interfacial reactions, is well established.[86,87] The primary tool used here in the study of organophosphonate interactions with SAMs and LB-films was reflection absorption infrared spectroscopy. The well-ordered model surfaces were prepared on gold substrates and thus, the reflective nature of the metal interface permitted reflectance methods to be utilized in the analysis of surface bound species. The molecular geometry and chemical environment, as well as identity, of adsorbates on surfaces can be determined from this powerful spectroscopic technique.

Reflective techniques are useful in the analysis of opaque samples and ordered surface coatings or films, such as those presented in the following studies. In RAIRS experiments, a beam of infrared radiation is directed towards a sample, the impinging photons excite vibrations in analyte species and Fourier transform techniques are used to generate spectra. In the course of spectral generation, an interferogram of sample signal

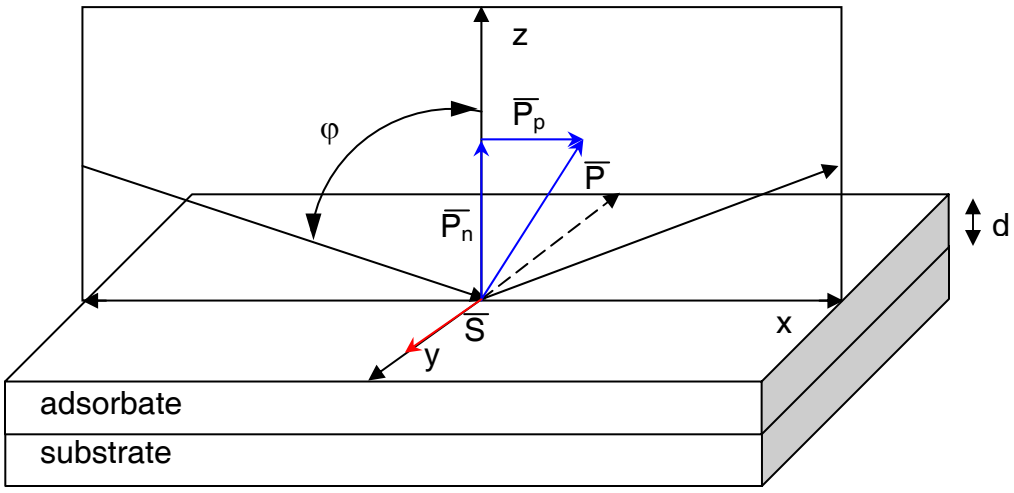

Figure 2.5 Infrared radiation impinging on a substrate can be resolved into two components.

is collected using an interferometer, which measures all of the infrared frequencies simultaneously. The spectrometer acquires and digitizes the interferogram and performs a mathematical function known as a Fourier transform. This function deconvolutes all individual cosine waves that contribute to the interferogram. The result of the transformation is a plot of intensity versus wavelength or frequency. The primary distinctions between RAIRS and typical transmission IR experiments were described by Greenler and comprise a set of surface selection rules.[86,87] Figure 2.5 summarizes Greenler's findings. The electric field of the impinging IR beam can be resolved into two components: parallel (s-polarized) and normal (p-polarized) to the incident plane. The s-polarized light only has a component parallel to the surface in the y direction (S), but the p-polarized radiation has components that are parallel (Pp) and perpendicular (Pn) to the substrate. The electric field vector of the impinging IR beam, that is normal to the surface, excites dipole-active vibrational modes of surface bound molecules. The perpendicularly polarized radiation, when reflected from the surface, results in a net doubling of the electric field vector amplitude, whereas the parallel polarized radiation (s-polarized) has a net amplitude of zero, due to the 180° phase shift upon reflection. Therefore, only surface bound molecules with active IR modes that have a portion of their transition dipole moment perpendicular to the surface will be observed in RAIR spectra. In addition to this surface selection rule, Greenler, using Maxwell's equations, determined that the p-polarized component of electromagnetic radiation that is perpendicular to the surface reaches a maximum at grazing angles of incidence (φ).[87] Therefore, RAIRS experiments are performed using IR radiation at or near an incident angle of 86°.

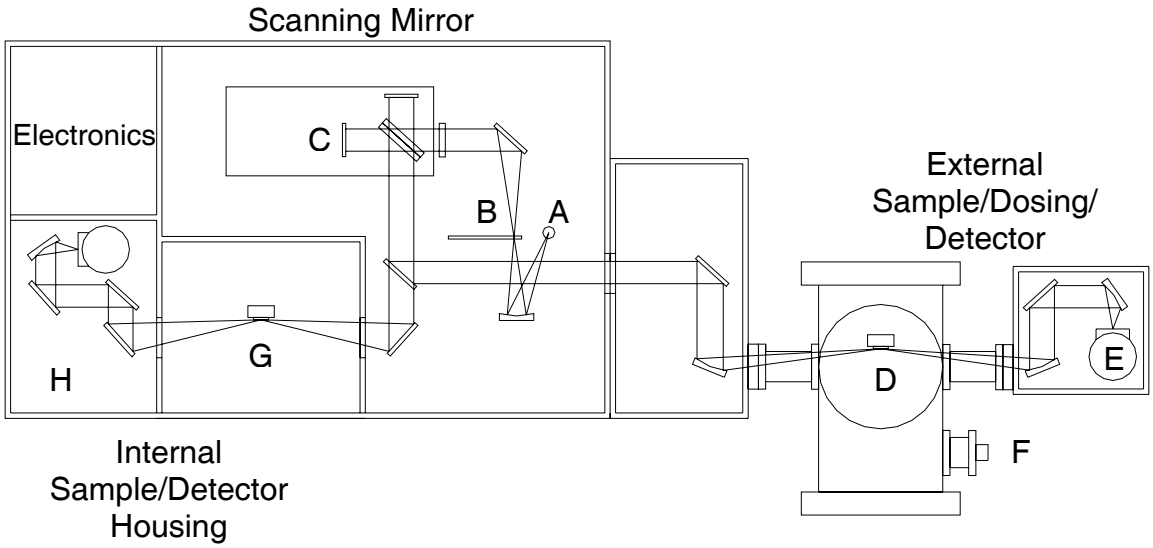

Figure 2.6 A schematic representation of the Bruker IFS66v/S Infrared spectrometer: (A) IR or UV/Vis source position, (B) Aperture wheel, (C) Interferometer (beam splitter, moving mirror, polarizer), (D) External high-vacuum exposure chamber, (E) External detector position, (F) Dosing system, (G) Internal vacuum chamber, (H) Internal detector position.

In the following work, RAIRS was performed using a Bruker IFS 66v/S spectrometer, depicted in Figure 2.6. Spectra were collected using p-polarized IR light from an SiC glowbar MIR source (A) at an incident angle of 86° and either a liquid N_2 cooled MCT (mercury-cadmium-telluride) or DTGS (deuterated-triglycine-sulphate) detector (E, H). A wire grid polarizer was used to further enhance the signal-to-noise of the RAIR set-up. Clean gold substrates were used as background references, unless otherwise noted. Each spectrum was collected using a resolution of 2 cm^{-1} and is the average of 100 scans.

Using this instrument, RAIR studies can be conducted in the internal sample/detector housing for traditional routine surface analysis or *in situ* experiments can be accomplished using the external sample/dosing high vacuum chamber. The commercial Bruker IFS66v/S instrument operates under vacuum conditions. A

Vacuubrand diaphragm pump (MD4, pumping speed 1.04 Ls^{-1}) maintains a pressure of approximately 18 mbar in the internal sample and interferometer housings when the N_2, which serves as an air-bearing for the moving mirror, is flowing. Vacuum conditions help to eliminate unwanted background interferences such as water and carbon dioxide and also preserve the quality of the hygroscopic KBr windows. The IR radiation from the glowbar is reflected from a gold coated parabolic mirror (focal length 180 mm) and through an aperture (0.7 mm x 4 mm slit for *in situ* studies with MCT detector, Ø1 mm for internal MCT experiments, and Ø9 mm for internal DTGS studies). The aperture spatially filters the beam of IR radiation and must be chosen such that the detector element is not saturated with light. The collimated beam then passes through a Zn-Se wire-grid polarizer, where the p-polarized light is selected. The p-polarized IR radiation is directed through the interferometer and can be selectively sent to either the internal or external sample compartments through KBr windows.

The internal sample housing is isolated by two KBr windows and is differentially pumped with the diaphragm pump that also evacuates the source, interferometer and internal detector chambers. Vacuum isolation of this sample cell allows for ease in sample transfer and protection of sensitive optical and electronic components. Samples are introduced to this chamber by forcep and positioned on an aluminum block affixed to an optical mount that serves as the sample holder. Positioning of the last mirror (focal length 250 mm) in the source chamber allows the IR radiation to be directed onto the sample, positioned in the internal sample housing, at an angle of approximately 86°. Upon reflection from either a background or sample substrate, the IR radiation passes through the second KBr window and into the internal detector compartment. The light is

reflected from a series of flat, gold coated mirrors onto a parabolic mirror (focal length 43 mm) and finally is directed into either a MCT or DTGS detector.

For *in situ* gas-phase exposure experiments in the external high vacuum chamber, the optical components of the RAIRS set-up are very similar to those in the internal housing. To direct the IR radiation to the external chamber, it is first directed from the interferometer to an auxiliary chamber where a parabolic mirror (focal length 250 mm) is located. This mirror directs the light to the sample positioned in the external chamber where it reflects from the surface at a glancing angle of approximately 86°. Samples are introduced to the cylinder shaped high vacuum chamber by forceps, through an 8" flange-mounted door. The substrate is positioned on an aluminum mount that is suspended from an aluminum optical post affixed to a manipulator (PHI model 10-504), which is mated to the chamber on a 6" Conflat® flange. The manipulator allows for x, y, z translation, rotation and tilt, which refine and adjust the sample position to maximize the amount of reflected light that reaches the detector aperture. The sample mount is stabilized from outside vibrations with an o-ring gently pushing on the unit from the rear. As the IR light is reflected from the substrate, it is directed to the external detector housing chamber, which is held at ~5 mbar by a Vacuubrand diaphragm pump (MD1, pumping speed 0.32 Ls^{-1}), and a series of mirrors guide the light into an MCT detector.

The external high vacuum chamber is isolated from the main bench of the IR spectrometer and external detector housing by KBr windows (55 mm ϕ x 5 mm, wedged 0.33°) positioned in flanges that allow for differential pumping if desired (McAllister). Because this vacuum chamber operates under high vacuum conditions, differential pumping of the salt windows was not required to reach desired pressure levels. O-ring

seals were used to mate the 2 ¾" window flanges to the spectrometer and detector box. Flexible bellows on Conflat® flanges were bolted to the KBr window flanges and main external vacuum chamber. This extension ensured that the sample was positioned at the appropriate focal length from the parabolic focusing mirrors.

The vacuum chamber was roughed out from atmosphere to ~1 x 10^{-3} Torr with a liquid N_2 cooled sorption pump. High vacuum conditions (~ 1 x 10^{-7} Torr) were reached by first isolating the sorption pump with a 2 3/4" manual gate valve and allowing a Varian turbo molecular pump (Varian Model 969-9008, pumping speed 250 Ls^{-1}) to evacuate the chamber. Vacuum levels in the external chamber were monitored with a precision fullrange cold cathode/pirani gauge (Pfeiffer Vacuum, Compact FullRange Gauge, PKR 251). Vapor-phase organophosphonate exposures were controlled with a precision leak valve (MDC 315012) coupled with the bubbling apparatus described above (Section 2.2.1.2.). Because of the base pressure of the vacuum chamber and accuracy of the leak valve and vacuum gauge, the smallest notable incremental pressure increases were on the order of ~10^{-7} Torr.

2.2.2.1. Experimental Considerations

Proper function and performance of this highly sensitive spectrophotometer is dependant upon routine maintenance and great care in daily use. Precise alignment of optical components, as well as careful installation of sample surfaces is required to obtain artifact-free spectra. As an illustration, if sample slides are not positioned such that the plane characterized by the sample interface is perpendicular to the incident beam of IR radiation, artifacts, such as a sine wave-containing baseline may be present in the final spectrum.[80] This problem is corrected by ensuring that both the clean background slide

and sample slide are positioned appropriately. If more dramatic misalignment of optics is observed through loss of amplitude intensity on the OPUS® control software program, the glowbar source may be exchanged with a NIR/Vis Tungsten filament source (position A in Figure 2.6). Utilizing this auxiliary light source allows visualization of the light-beam path. The spectrometer can be vented to atmospheric pressure and with the use of an opaque card, the beam position on each of the optical components can be assessed. It is important that during alignment procedures, only one mirror be adjusted at a time. This limits the number of parameters involved in re-positioning the light path at any given time.

Maintenance of the MCT and DTGS detectors is also critical to proper function of the Bruker IFS66v/S instrument. The MCT detector is a semiconductor and operates on the principle of electron promotion to conduction bands from valence bands when the detector element absorbs infrared photons. Electrons in the conduction band respond to an applied voltage to produce to an electrical current. This current is a measure of promoted electrons and is directly proportional to the number of infrared photons striking the detector element. The signal-to-noise (S/N) and spectral response of an MCT detector change with temperature. As the temperature increases, the S/N decreases due to an increase in background photon count arising from heat given off by the detector element. The spectral response also shifts to shorter wavelengths. To overcome this hindrance, an MCT detector is equipped with a liquid-N_2 dewar and can be easily cooled. The detector also houses a vacuum jacket that surrounds the liquid-N_2 dewar and helps to maintain the cold-shield surrounding the photoconductive detector. Periodically (6 months), this vacuum shield must be re-evacuated to avoid “icing” issues. As the

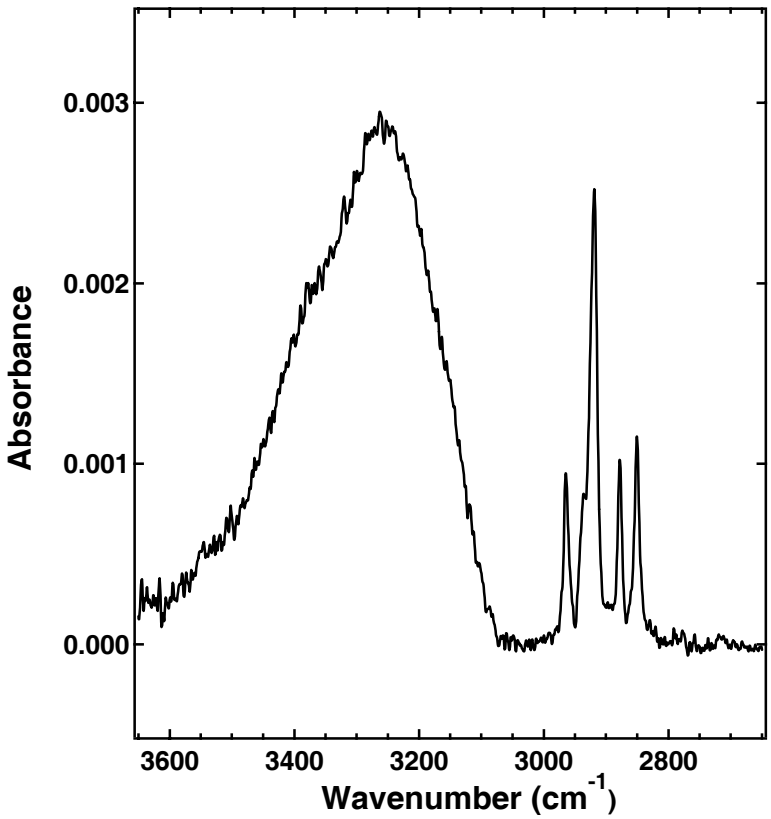

Figure 2.7 RAIR spectrum of a hexadecanethiol SAM on gold. The large feature from ~3100-3600 cm^{-1} is due to "icing" in the MCT detector.

vacuum is lost and the partial pressure of water in the shield increases, large spectral artifacts in the region of 3000-3600 cm^{-1} may be observed, as shown in Figure 2.7. This is a direct result of water condensing and freezing on the detector element and can be corrected by evacuating the vacuum jacket. This procedure requires the use of an adapter valve (InfraRed Associates) and a turbomolecular pump (Varian Model 969-9008, pumping speed 250 Ls^{-1}). Pumping on the vacuum shield for several days can typically bring the pressure to ~10^{-6} or10^{-7} Torr and subsequently the detector is in useful condition for several months.

The second type of detector utilized in the Bruker IFS66v/S is known as a pyroelectric bolometer and can operate at room temperature. When DTGS detectors

absorb infrared photons, the temperature of the detector element changes. Furthermore, the dielectric constant of the sulfate material is also affected. This results in a change in capacitance that can be measured as a voltage across the detector element. The advantage of using a DTGS detector is the broad coverage range (400 to 4000 cm^{-1}) of the mid-infrared region of the electromagnetic spectrum. The DTGS detector is equipped with KBr windows and must therefore be stored under vacuum when not in use. The Bruker IFS66v/S has multiple detector positions where this supplementary detector can be safely stored.

2.2.3. Contact Angle Goniometry

Efforts to measure and characterize surface tension and surface free energy are accomplished through the use of contact angle goniometry. This technique requires placing a drop of solvent on a surface and measuring the angles formed between the liquid-gas, solid-gas, and solid-liquid interfaces, as depicted in Figure 2.8. From this measurement, wetting and adhesion properties of the solid surface can be determined. Moreover, contact angle measurements are useful in the description of properties, such as surface roughness, hydrophobicity/hydrophilicity and chemical homogeneity of a thin film or surface.

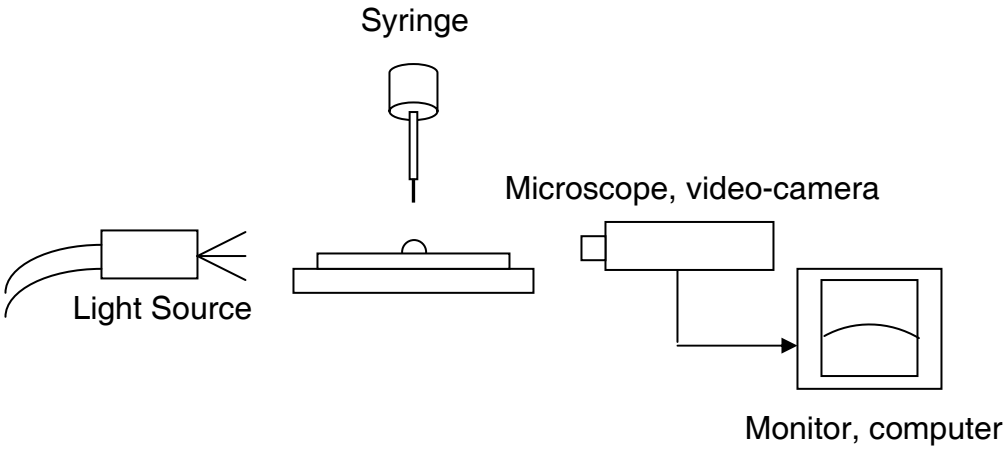

Figure 2.8 A schematic of the experimental design of a contact angle goniometer.

As a droplet of liquid interacts with a non-absorbent surface, it comes to rest in an equilibrium shape. The contact angle of the liquid on the surface is defined as the angle (Θ) where the solid, liquid and gas phases intersect and is related to the interfacial tensions according to equation 6, where γ_{SL} is the surface free energy of the solid covered with the liquid, γ_{SG} is the surface free energy of the solid in contact with the gas, and γ_{LG} is the surface free energy of the liquid- gas interface.

$$\cos(\theta)_{SLG} = (\gamma_{SL} - \gamma_{SG}) / \gamma_{LG} \quad (6)$$

A hydrophobic surface results in a water contact angle greater than 90° and the droplet is said not to wet the surface. Alternatively, a hydrophilic surface yields a water contact angle of less than 90° and the surface is said to be wet by the liquid. Figure 2.9 illustrates the latter scenario. Contact angle measurements can be used to correlate polarity to the interfacial chemical structure of a surface.

In this work, static contact angle measurements were recorded using a FTA125 Contact Angle Analyzer (First Ten Angstroms). All data was collected at room temperature under ambient humidity. The static contact angles of deionized water on a given monolayer were measured. A minimum of five different points on each sample

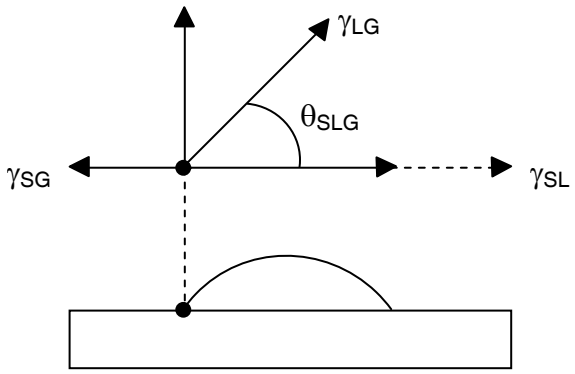

Figure 2.9 Interfacial tensions determine the contact angle of a liquid droplet on a surface.

were recorded and averaged. The contact angles were found to be highly reproducible for different samples.

2.2.4. X-ray Photoelectron Spectroscopy (XPS)

A detailed chemical analysis of a surface, including composition, formal oxidation state of the atom, and the local chemical and physical environment of an atom, can be obtained using XPS or electron spectroscopy for chemical analysis (ESCA). XP experiments require placing the surface of interest in a vacuum environment and irradiating it with photons in the range of 200 to 2000 eV (Figure 2.10). The technique relies on the exchange of energy from the impinging photon beam and core level electrons present in the interfacial region of a sample. The x-ray photon can impart sufficient energy to the surface to cause core level electrons to be ejected, as represented in Figure 2.11. Determination of the kinetic energy (E_k) of these escaping photoelectrons is calculated using the energy of the x-ray radiation ($h\nu$) and the electron binding energy (E_b), as given in equation 7, where E_w is the work function of the spectrometer:

$$E_k = h\nu - E_b - E_w \tag{7}$$

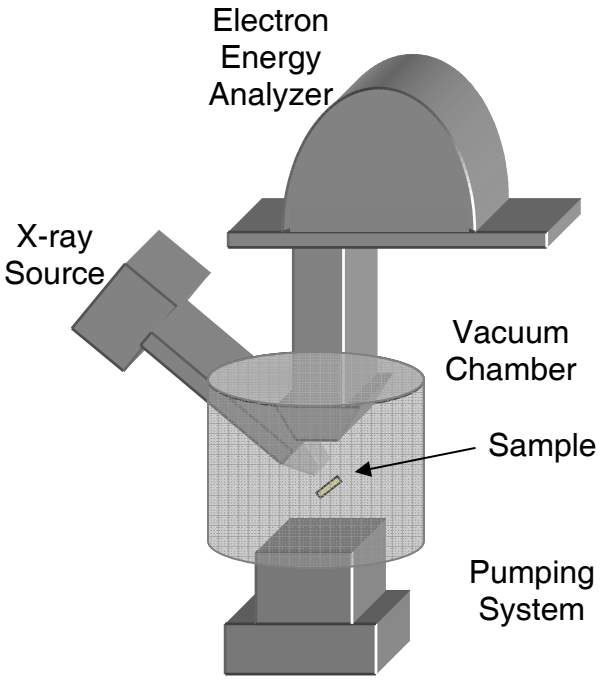

Figure 2.10 The design of an x-ray photoemission experiment.

The chemical environment of the atom in the target system dictates the binding energy of the ejected photoelectrons and is therefore a useful tool in the description of oxidation states of surface species.

In the experiments described here, XPS was performed on a Perkin Elmer 5400 X-ray Photoelectron Spectrometer equipped with a monochromatized Mg(Kα) radiation source (1253.6 eV) and a position sensitive, multi-channel plate detector. Measurements were taken at a pressure of ~10^{-7} mbar and a take-off angle of 15° with respect to the surface normal. Binding energies are referenced to C (1s) at 284.8 eV. Survey spectra were collected for 5 minutes using a pass energy of 44.75 eV, a 1 mm x 3.5 mm spot size and 300 W electron beam power. High resolution multiplex spectra were collected with an acquisition time of 8 minutes per region.

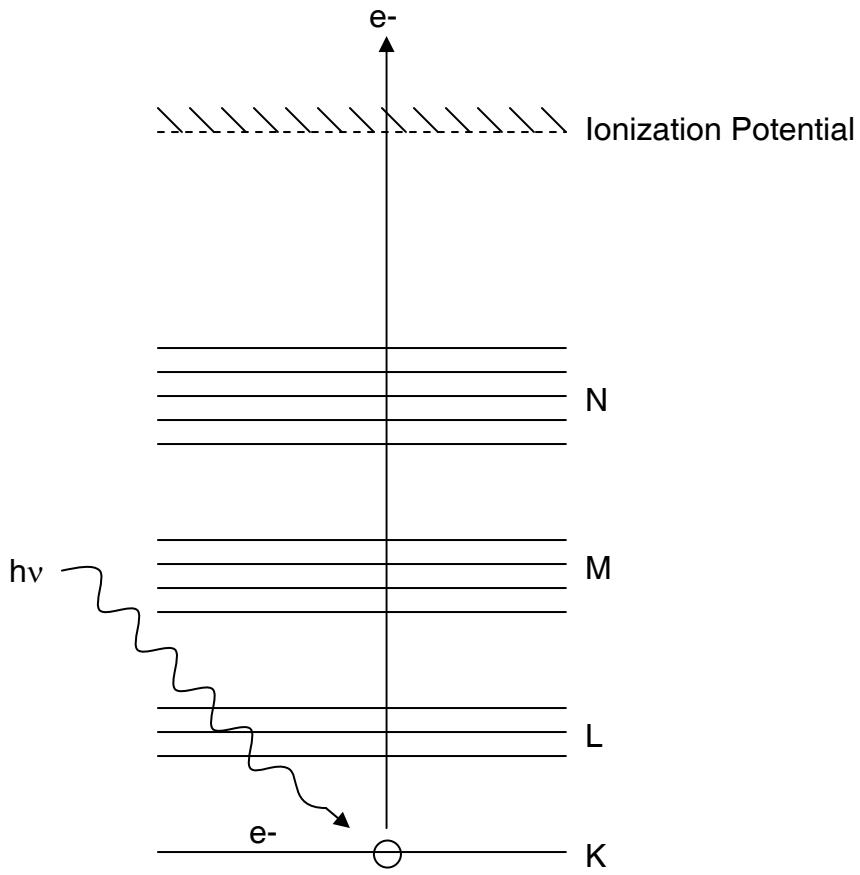

Figure 2.11 An example energy diagram for XPS. E_k is the kinetic energy of escaping photoelectrons, E_b is the electron binding energy, and E_w is the work function of the spectrometer.

2.3. Gas-Surface Exposure Studies

Complete saturation of POSS films with organophosphonates was accomplished by placing the film in an atmosphere saturated with CWA simulant vapor. POSS films were placed in a 60 cm^3 vapor deposition chamber initially purged with N_2 and approximately 5 μL of the organophosphonate was introduced via pipette. The gas-phase concentration of the molecules was kept high by heating the chamber mildly to 308 K.

POSS films were also exposed to CWA simulants in the molecular beam and *in situ* RAIR studies described above. It is noteworthy that due to the toxic nature of organophosphonate molecules, liquid N_2 cooled traps (MDC, SP150) are employed as

collection devices on the external vacuum chamber coupled to the RAIR spectrometer and also on the molecular beam source chambers. The traps are placed between either the turbomolecular (RAIRS set-up) or diffusion pump (UHV instrument) and the backing mechanical pump. As experiments are completed, the trap is removed and allowed to warm to room temperature in a functional chemical fumehood.

2.4. Instrumental Design: Variable Temperature Sample Holder

The abilities to transfer samples with ease, efficiently conduct thermal studies, and accurately monitor surface temperatures are highly desired in UHV surface science experiments. The UHV instrument detailed above is outfitted with a commercially available manipulator/sample unit that provides these capabilities. In ongoing efforts to further the available surface analytical resources, the variable temperature sample mount, depicted in Figure 2.12, has been designed to be integrated with the external vacuum chamber coupled to the RAIR spectrometer. The general design of this sample mount is based upon the work of Schmidt et al.[88]

The sample mounting device consists of a liquid N_2 reservoir and a button heater (HeatWave Labs, Inc., 1251-03) that can be utilized in thermal studies. Sample cooling is accomplished by pumping liquid N_2 through the cryogenic feedthroughs (not shown), flexible tubing, and into the reservoir. The copper reservoir ensures effective cooling, while sapphire plates are used as a thermal switch between the reservoir and sample receiver. Optimal thermal contact between the sample stub and receiver is accomplished by a series of machined threads, which also secure the sample during analysis. A small button heater permits sample heating to 1200 °C. Face mounted thermocouple connections provide an accurate record of surface temperatures. The sample transfer

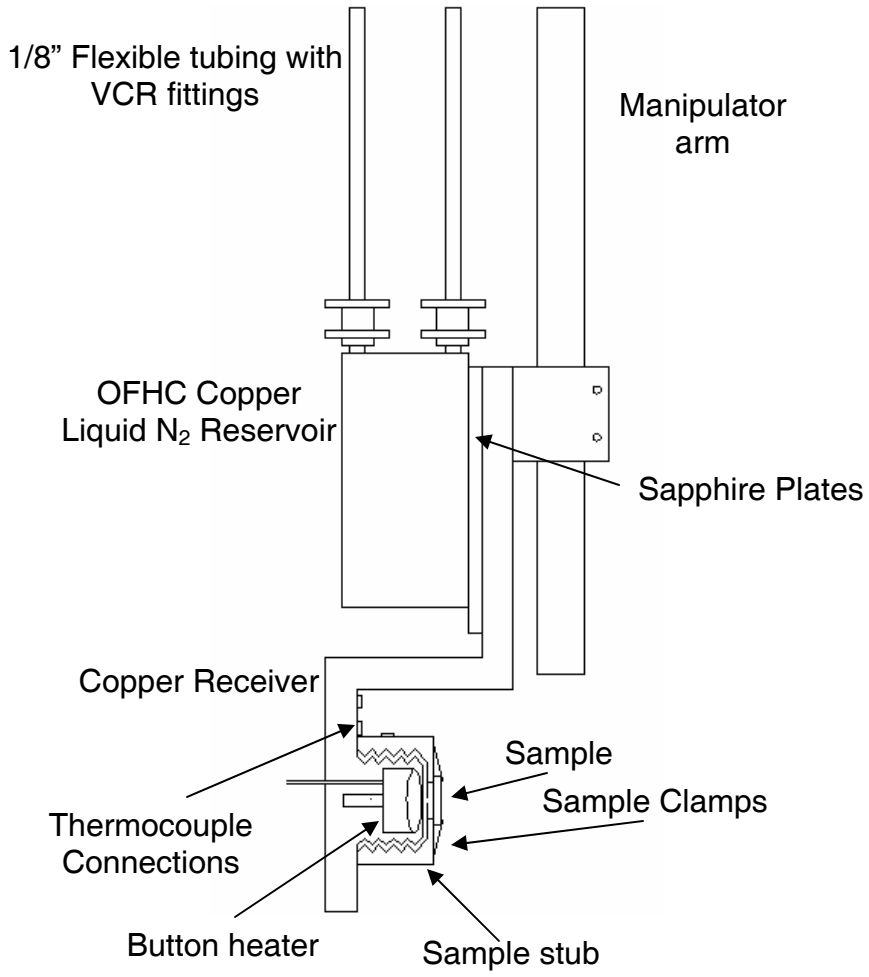

Figure 2.12 A variable temperature sample mounting device that will be used for *in situ* RAIRS studies.

device can be mated to standard load lock components, such as a rotatable arm that permits sample insertion to a central vacuum chamber. A set screw on the transfer mount secures it to the transfer arm. The sample stub can be transferred from a load lock arm to the mounting unit, located in the main analytical vacuum chamber, with lock and grove mechanisms. The locking devices on the transfer arm and on the internal unit are necessary to ensure that instrumental vibrations or human error do not result in loss of a sample stub or damage to vacuum chambers or pumps. These precautionary safety features are depicted in Figure 2.13.

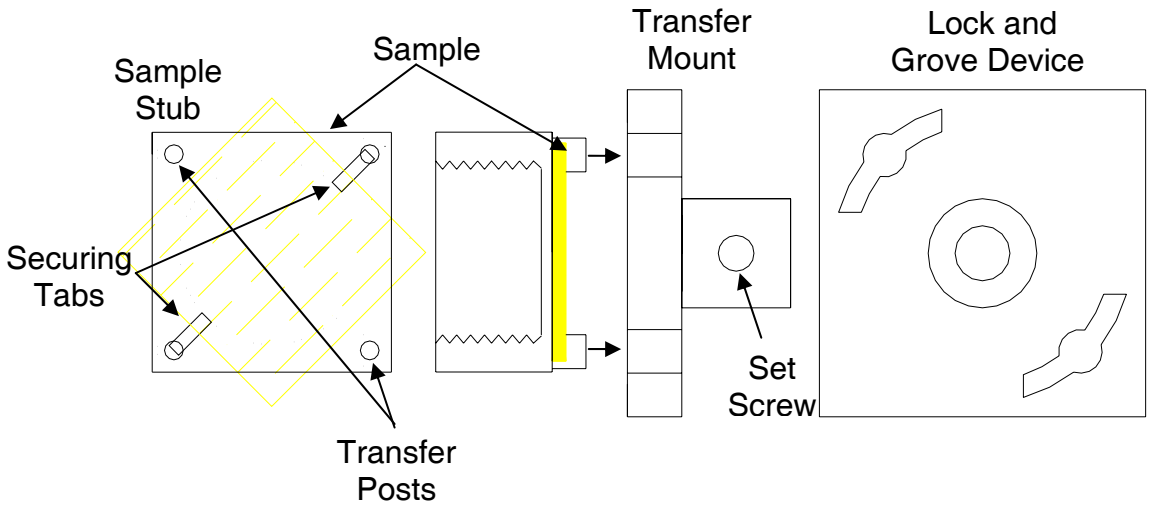

Figure 2.13 Custom designed sample mount and transfer device, each equipped with a locking mechanism.

2.5. Summary

A great deal of interesting chemistry may occur at the boundary of two phases. Study of chemical interactions and reactions at a surface requires not only pristine surface substrates, but also techniques capable of probing only the interfacial boundary region of interest. The techniques outlined here were utilized in studies characterizing surfaces that model CARC and films containing hybrid inorganic-organic POSS molecules. UHV studies using molecular beam techniques offer insight into the uptake and reactivity of organophosphonates on the silsesquioxane coatings. The simultaneous use of molecular beam studies, TPD, RAIRS, contact angle goniometry, and XPS provide a thorough description of nearly every aspect of organophosphonate interaction with militarily relevant surfaces.

Chapter 3
Preparation and Characterization of a Model Hydrogen-Bonding Organic Self-Assembled Monolayer

3.1. Introduction

Elucidating mechanistic channels of surface reactions can often be complicated. Disordered or random surfaces can hinder determination of reaction sites, as well as reaction pathways. Well-ordered thin films clarify the structure of interfacial surface reactants, which greatly assists in the evaluation of reaction mechanisms. Self-assembled monolayers (SAMs), such as functionalized alkanethiols on gold, present an ordered structure upon which to examine various surface reactions. The use of SAMs to control surface structure and subsequent properties has generated extensive interest. By varying the functional groups present within a SAM or at the terminus of a monolayer, control over properties such as wettability,[89-92] electron transfer,[93] and corrosion resistance,[94] can be achieved. This control can be harnessed to specifically tailor SAMs for use in a number of disciplines including non-linear optics,[95] biosystems, sensors,[96-98] and coating technologies.[99] SAMs are also developed as model surfaces to gain a better understanding of interfacial reactions, including enzyme function[100] and the role of atmospheric pollutants in surface chemistry.[80,101] Here, well-ordered monolayers containing urethane, or carbamate, linkages are characterized.[102] These surfaces can be used to model polyurethane films, which are used in a variety of applications, including chemical agent resistive coatings (CARC).[103]

3.1.1. Chemical Agent Resistive Coating

The widespread use of chemical agent resistive paints by the United States military as a coating for vehicles, aircraft, support equipment etc. began in 1983, when

the urethane-based coating replaced standard alkyl and acrylic paints.[103] The standard paints were found to absorb up to 25% of liquid CWAs applied at the interface within thirty minutes.[104] Desorbing residual agents and degradation products could then create a hazard over time. To avoid this occurrence, the military implemented the widespread use of polyurethane CARC.

The CARC used by the United States military is comprised of polyester and hexamethylene diisocyanate, which polymerize to generate a polyurethane coating that possesses –[CONH-R'-NHCOO-R-O]– repeating units.[105] CARC is used for a number of esthetic and mechanical purposes. The matte finish coating can be formulated with a variety of pigments to give colors such as tan and green, which are used as coatings for camouflage and unit identification. On a more fundamental scientific level, however, CARC paints are thought to resist the absorption of chemical warfare agents and thus, ease the burden of decontamination. If equipment is exposed to CWAs, any adsorbed harmful substances can be removed with either a sodium hydroxide and diethlenetriamine solution or with a hypochlorous acid based solution.[105] The general effectiveness of CARC paint is unclear and a better understanding of structure and composition as they relate to the function of CARC paints is needed. The disordered array of potentially reactive hydrogen-bonded urethane groups makes a comprehensive study of CWA uptake characteristics difficult. Model surfaces must therefore be used as a means to study the interfacial characteristics of urethane surfaces, as well as the uptake and reactivity of CWA simulants on CARC-like materials.

3.1.2. Model Surfaces

Self-assembled monolayers (SAMs) have been studied extensively over the past

decade as model systems.[19,23,51-56,58] A SAM is a two-dimensional film that is formed when surfactant-like molecules spontaneously assemble at an interface in a monomolecular layer. Examples of molecular chemisorption resulting in the formation of a SAM include the ionic interactions between fatty acids and metal oxides[106,107] and the covalent attachment of organosulfurs on metals.[53,90,108,109] Adsorbates offer control over head and tail groups, as well as the overall thickness (i.e. length of the alkyl chain) of the SAM, as depicted in Figure 3.1. Coupled with surface sensitive techniques, SAMs offer the potential to discern a great deal of information about interfacial properties, reaction mechanisms, self organization and solvent-molecule interactions.

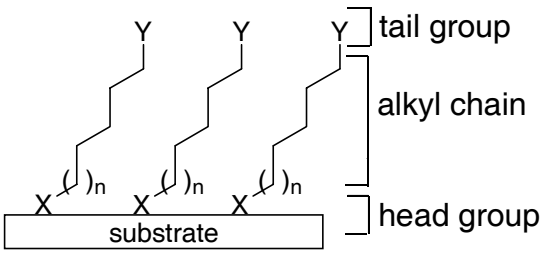

Figure 3.1 Self-assembled monolayers are comprised of molecules having variable head and tail groups, as well as intramolecular structure, i. e. alkyl chain length.

An abundance of research has explored the formation of thin films on metal, metal-oxide and silica surfaces to produce monolayers with a range of surface structures and properties. Nuzzo and Allara reported creating SAMs via chemisorption of organic disulfides on gold substrates.[91,110] In addition to disulfides, an array of head-groups including: -SH, -COOH, SiO_x, and PO_x have been utilized to form monolayers. A wide range of functional groups have been placed at the terminal interface: $-CH_3$, -OH, -COOH, $-(C=O)OCH_3$, $-O(C=O)CH_3$, $-O(C=O)CF_3$, $-O(C=O)C_6H_5$, $-O(SO_3)H$, -C=C, $-NH_2$, etc. More recent work has examined the placement of sub-terminal functional groups, such as amides, along the SAM backbone.[59,60,111-120] One of the most commonly

used SAM systems is formed from the spontaneous adsorption of organosulfur compounds on metallic substrates.[51] The gold-thiol system is easily prepared and has been shown to be highly-stable under a variety of conditions.[109]

n-Alkanethiols on Au substrates have been characterized extensively using a number of surface analytical tools. Techniques, such as RAIRS, ellipsometry, XPS, contact angle goniometry, electrochemistry, and force microscopy measurements, have clearly demonstrated that alkanethiols ($n \geq 12$) form well-ordered, densely packed monolayers. RAIR spectroscopy is a powerful technique for monolayer characterization. The fundamental principles of transmission infrared spectroscopy apply to RAIRS; however, this technique is particularly sensitive to surface adsorbed species. If the adsorbate molecules have a component of their dipole oriented perpendicular to the plane of the surface, the vibrational modes can be detected and recorded in a spectrum. The RAIR spectra in Figure 3.2 show the spectral disparities between a disordered hydrocarbon film and that of a 1-hexadecanethiol SAM on Au. The SAM spectrum has sharp well-defined vibrational modes, whereas the disordered hydrocarbon surface has broad bands that, in comparison, are shifted to higher wavenumbers. Because SAMs are an ordered geometric arrangement of molecules, the IR absorptions of an individual molecule are nearly identical to those of other molecules in the arrangement. This leads to the narrow bands that are typically red-shifted in comparison to absorptions resulting from more disordered systems.[121]

N-Alkanethiol SAMs on gold are formed when the sulfur atom binds to the three-fold hollow site on the substrate, forming an all-trans $\sqrt{3} \times \sqrt{3}$, R30° overlayer, shown in Figure 3.3. Hydrogen gas is lost during this exothermic process, which results in a strong

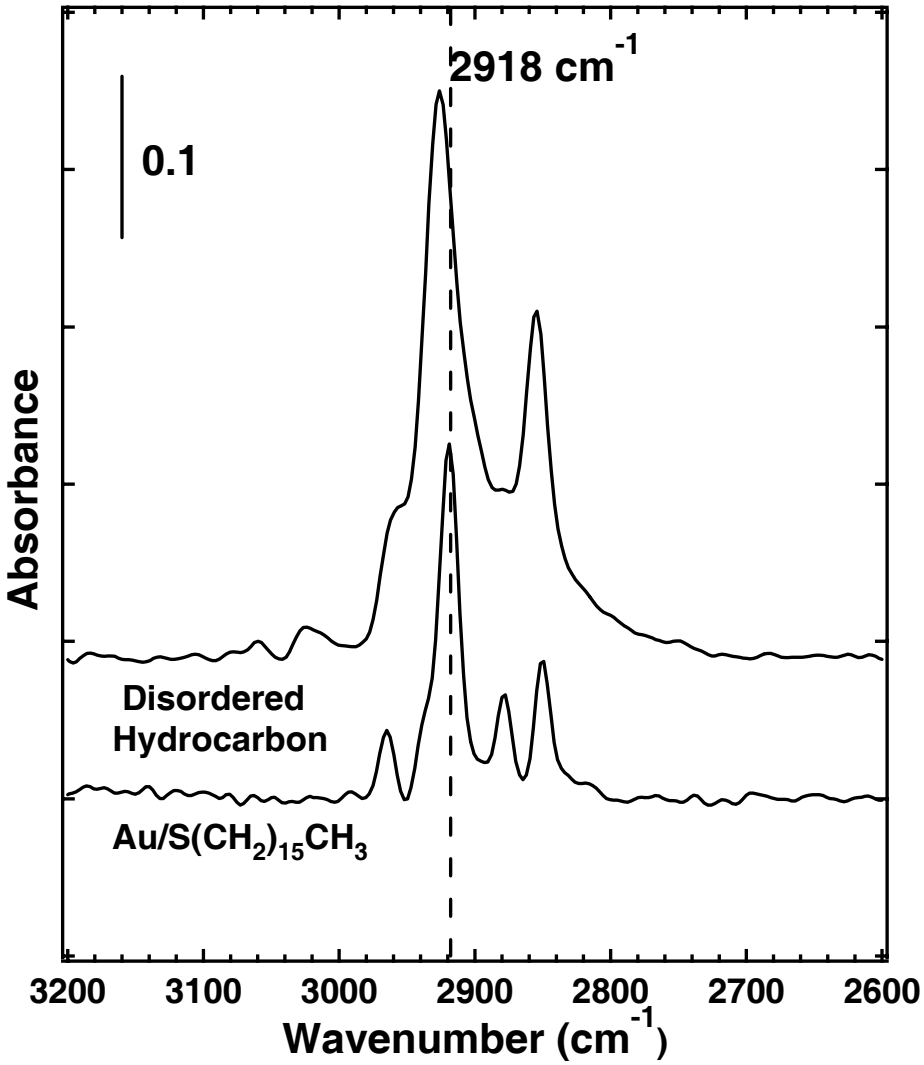

Figure 3.2 The structure of *n*-alkanethiol SAMs on Au (111) is well-ordered compared to that of a hydrocarbon film.

bond between the gold and sulfur atoms (44 kcal/mol).[51] Lateral, interchain van der Waals interactions are responsible for vertical chain alignment. The alkane chains are not bulky enough, however, to occupy the 5 Å available between the binding sites on the gold substrate. Therefore, a chain tilt angle of approximately 30° to the surface normal is observed, which results in an occupied area of ~21.4 $Å^2$.

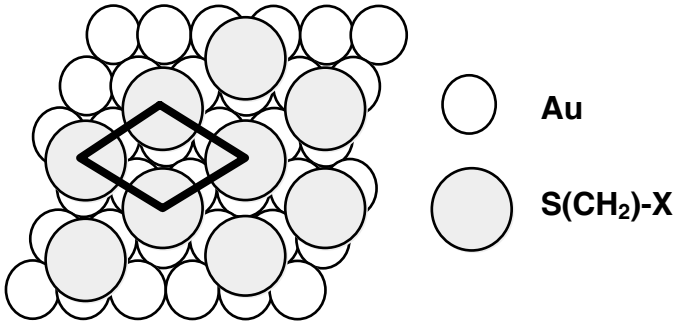

Figure 3.3 The overlayer structure formed by alkanethiolate SAMs on Au (111).

The van der Waals interactions present between long chain ($n \geq 12$) alkanethiolates on Au results in highly-ordered structures, exhibiting only very few gauche defects. Shorter chain alkanethiolates on gold generate somewhat less well-ordered structures. The interchain forces between short chains are insufficient to align the backbone of the alkyl chains in a highly-ordered fashion. As described by Porter, this results in lower packing densities and smaller than expected film thicknesses.[108] In addition to chain length, the presence of bulky terminal or intra-chain functional groups may also affect order in SAMs. Moreover, mixed monolayers formed from molecules with varied chain lengths or terminal functional groups may exhibit varied packing structures and degrees of order.

3.1.3. Model Hydrogen-Bonding Surfaces

The use of self-assembled monolayers (SAMs) to tailor surface structure and subsequent interfacial characteristics has been studied at length. Functional groups, located at the terminal position of a monolayer, offer control over properties such as wettability and corrosion resistance, as well as structure and packing arrangement. Numerous studies have demonstrated the ability to create ordered SAMs with hydrogen-bonding groups (-OH, -COOH, $-NH_2$) at the termini of monolayers. Relatively few

studies, however, have explored the structural and chemical effects of sub-terminal functional groups in organic monolayers.[59,60,111-120]

Previous investigations that have focused on functional groups within SAMs revealed that steric effects and hydrogen-bonding interactions often disrupt monolayer order and packing efficiency. For example, Hutchison et al. examined SAMs made from alkanethiols containing secondary amide groups.[116,120] They found the two-carbon layer between the amide and the gold to be well-ordered, but that overlayers only ordered well when ***fifteen or more*** carbon atoms were present in the terminal chains. Their work suggests that functional group spacing, bond geometry, and electronic effects play important competing roles in determining the order of intralayer-functionalized SAMs. Conclusions drawn by Whitesides, Nuzzo, and co-workers in studies of SAMs containing buried amide groups support these findings.[115] Their work revealed that, though providing some stability against thermal decomposition, amide linkers significantly disrupt the order of the alkane chains. Furthermore, Sprik and co-workers used scanning tunneling microscopy and molecular dynamics simulations to evaluate the structure of hydrophilic SAMs.[122] They determined that hydrogen bonding interactions of terminal hydroxyl groups can disrupt the order of the SAM. Chain ends must orient in such a way that interactions with neighboring molecules are favorable for hydrogen-bonding. The directional nature of these interactions disrupts the symmetry of individual chains and leads to an overall disordering of the SAM structure. In contrast, the microscopy studies of Weiss and co-workers found evidence that long-range ordering of monolayer chains was driven in part by buried hydrogen-bonding groups.[117,118] Likewise, studies by Ratner et al. suggest that ordered monolayers may form when surface hydroxyl groups react with

long-chain isocyanates to yield intrachain carbamates.[59]

Suter and co-workers recently described a highly versatile method for creating SAMs with buried functional groups. Their strategy involved reacting an OH-terminated SAM with 1,4-phenylene diisocyanate to create a monolayer terminated with highly-reactive isocyanate groups. The isocyanate-terminated SAM readily reacts with alcohols or amines to form a variety of monolayers with potentially useful structures and functionalities. These highly-ordered systems offer a unique approach for selective placement of carbamate functional groups and subsequent isolation of carbamate-organophosphonate interactions. Here, isocyanate chemistry provides a means to create carbamate-containing thin films. It was hypothesized that use of a well-ordered hydroxyl-terminated template monolayer would seed the growth of intrachain carbamate functional groups and order alkyl tail groups. Solution chemistry produced rather disordered films, however, RAIRS, contact angle goniometry and XPS measurements confirm that vapor phase reactions generated well-ordered carbamate containing SAMs. The isocyanate reactions appear to convert nearly all hydroxyl groups to carbamate functional groups and the terminal alkyl chains appear well-ordered when the total number of carbon atoms in the terminal chain exceeds five.

3.2. Experimental Details

3.2.1. Materials

Absolute ethanol was obtained from Aaper Alcohol. 16-mercapto-1-hexadecanol was obtained from Frontier Scientific Inc. and 11-mercapto-1-undecanol (97%), 16-mercapto-1-hexadecanoic acid (90%), 2-hydroxyethyldisulfide (85%), 1-hexadecanethiol (92%), 1-pentadecanethiol (98%), 1-tetradecanethiol (98+%), 1-dodecanethiol (98+%), 1-

undecanethiol (98%), 1-decanethiol (96%), 1-nonanethiol (95%), 1-octanethiol (98.5+%), 1-heptanethiol (95%), 1-hexanethiol (95%), 1-pentanethiol (98%), 1-butanethiol (99+%), 1-propanethiol (99%), and 1-ethanethiol (97%), were obtained from Aldrich. Methyl isocyanate (98%) was purchased from Chem Service and ethyl isocyanate (98%), propyl isocyanate (99%), isopropyl isocyanate (99%), butyl isocyanate (98%), pentyl isocyanate (98%), hexyl isocyanate (97%), heptyl isocyanate (97%), octyl isocyanate (97%), undecyl isocyanate (98%), dodecyl isocyanate (90%), 1,6, hexamethylene diisocyanate (99+%), 1,12 diisocyanatododecane (%) and 1,4 phenylene diisocyanate (96%) were purchased from Aldrich. HPLC grade toluene and hexane were obtained from Aldrich and were degassed and dried with alumina columns prior to use. Deuterium oxide (99.9%) was purchased from Cambridge Isotope Laboratories, Inc. Anhydrous butanol (99+%), anhydrous hexanol (99%), undecanol (99%), and dodecanol (98+%), were purchased from Aldrich. The alcohols were used neat except in the case of dodecanol which was made into a 1 M solution in hexane. The 1,4 phenylene diisocyanate was further purified by melting (to control static), cooling to room temperature and sublimation at a pressure ~10^{-2} mbar. All other chemicals were used as received, without additional purification.

3.2.2. Preparation of Self-Assembled Monolayers

Gold substrates were prepared by evaporation of a 50 Å chromium adhesion layer onto a silica surface, 1" x 1" x 0.62" or 1 cm x 1 cm x 1 mm, followed by a coating of 1000 Å of gold (Evaporated Metal Films). The substrates were cleaned in a 3:7 mixture of H_2O_2 (30%)/H_2SO_4 (concentrated) (*"piranha solution" is an oxidizing mixture that can be explosive when in contact with organic materials*) at room temperature for 1 hour,

rinsed with copious amounts of deionized water (Millipore Purification Systems, 18.2 MΩ), and placed in a 1 mM ethanolic solution of the thiol or disulfide precursor for approximately 18 hours. Prior to analysis, the SAMs were removed from the ethanolic solution, rinsed with absolute ethanol and dried in a stream of ultra-pure N_2.

Mixed monolayers, or SAMs made up of more than one type of molecule, as depicted in Figure 3.4, were prepared using the same procedures outlined for the creation of pure monolayers. Stock solutions of the desired thiols were created and combined in such a way that the final total concentration of thiols in solution was 1 mM. It is important to note that the final concentration of each of the thiols adsorbed on the gold substrate is not the same as the concentration of the molecules in solution.[81] Thermodynamics and solubilities play critical roles in the determination of SAM composition.[109,123]

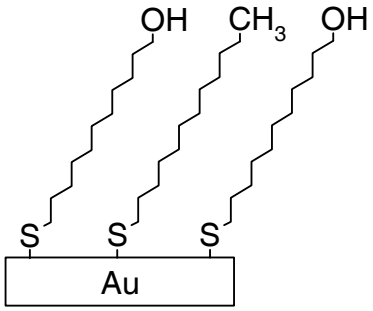

Figure 3.4 Mixed monolayers contain multiple functional groups at the terminal position.

3.2.3. Preparation of Carbamate-Containing Self-Assembled Monolayers

3.2.3.1. 1,4-Phenylene Diisocyanate Experiments

Following procedures outlined by Persson et al. and illustrated in Figure 1.4,[61] isocyanate chemistry was used here to create carbamate-containing SAMs. The synthetic route is relatively straightforward and highly versatile in that a number of different functional groups can be placed at the terminal position. Clean gold slides were

immersed in a 1mM solution of 11-mercapto-1-undecanol in ethanol for ~18 hours at room temperature. Upon the formation of a hydroxyl-terminated monolayer template, each slide was rinsed with ethanol and subsequently dried in a stream of ultra-pure N_2. The slides were transferred into a N_2-atmosphere glovebox where they were immersed in a 0.1 M solution of 1,4-phenylene diisocyanate in water-free toluene for ~24 hours at room temperature. After functionalization with the 1,4-phenylene diisocyanate, the terminal isocyanate group remains very water sensitive. Therefore, after the substrates were rinsed with a series of toluene and dichloromethane washes, they were carefully placed in Erlenmeyer flasks, capped with septum style lids, and only then removed from the glovebox. To terminate the chains with the desired endgroup, water or a straight chain alcohol was introduced to the flask via syringe. This step was performed outside of the N_2-atmosphere glovebox to eliminate the possibility of unwanted reactions occurring between the alcohol or water and other hygroscopic substances being stored in the dry atmosphere. The isocyanate-functionalized slide remained immersed in either water for 5 minutes to 18 hours or an alcohol for 5 hours at room temperature. Prior to analysis, the amine and carbamate-functionalized surfaces were rinse with absolute ethanol and dried in a stream of ultra-pure N_2.

3.2.3.2. Solution-Phase Preparation Routes

An assortment of solution-phase preparatory methods was investigated for the synthesis of carbamate groups within thiol-terminated molecules for use in SAM formation on gold substrates. Initial studies used 1 mM solutions of 11-mercapto-1-undecanol in ethanol to produce template hydroxyl-terminated monolayers. In a dry N_2-atmosphere, these surfaces were immersed in solutions (1 μM – 1 M) of 1,4-phenylene

diisocyanate, 1,6, hexamethylene diisocyanate or 1,12 dodecyl diisocyanate in dry toluene or hexane. Isocyanate reaction times ranged from 2 to 48 hours and experiments were conducted between room temperature and 62 °C. Upon the initial reaction with the diisocyanate molecules, the newly functionalized monolayer substrates were rinsed several times with dry solvent (toluene or hexane) and conversion of the secondary isocyanate group at the terminal position was attempted by immersing the surface in an alcohol for 5 hours at room temperature, as depicted in Figure 3.5. Prior to analyses the surfaces were rinsed with dry solvent and dried in a stream of ultra-pure N_2.

In conjunction with monolayer-template based reactions, solution-phase reaction of the diisocyanate molecules with the alcohols was attempted prior to the interfacial

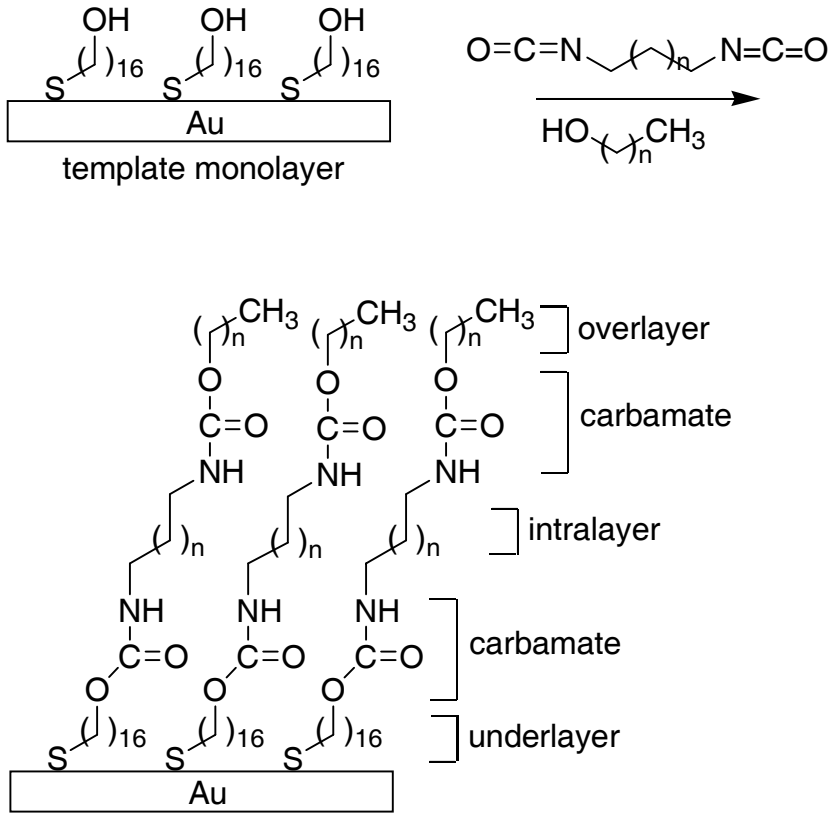

Figure 3.5 An idealized representation of the reaction between a hydroxyl-terminated monolayer template and diisocyanate molecules.

reaction of the isocyanate moieties with the terminal hydroxyl groups of the SAM. Solutions of 1,4-phenylene diisocyanate, 1,6, hexamethylene diisocyanate or 1,12 dodecyl diisocyanate in toluene or hexane were reacted with neat alcohols in varying proportions (1:1-1:3) for 5 hours over a range of temperatures (25 – 62 °C). The resulting mono-isocyanate, mono-carbamate molecules were then introduced to a hydroxyl terminated monolayer template for 5 hours at room and elevated temperatures. Prior to analyses the surfaces were rinsed with dry solvent and dried in a stream of ultra-pure N_2.

Solution-phase preparation methods using alkyl-isocyanate molecules, were also investigated in attempt to create carbamate-containing SAMs. Again, in an N_2-atmosphere, several different solvents (dry toluene and dry hexane) were used to prepare isocyanate solutions of varying concentration (1 μM – 1 M). Initial studies focused on reacting the mono-isocyanate molecules with hydroxyl-terminated SAM templates. Templates were created from 11-mercapto-1-undecanol, 16-mercapto-1-hexadecanol, or 2-hydroxyethyldisulfide. Varying reaction parameters including reaction time and temperature were explored. Analogous to the diisocyanate studies, reactions between the alkyl isocyanates and 11-mercapto-1-undecanol or 16-mercapto-1-hexadecanol were also attempted prior to monolayer formation. Deposition of these reacted, thiol-terminated molecules on the Au substrates was done at room temperature. The prepared SAM surfaces were rinsed with dry solvent and dried prior to analyses.

3.2.3.3. Vapor-Phase Isocyanate Reactions

Solution-phase reactions between isocyanate molecules and hydroxyl-terminated alkanethiols generated SAMs with substandard order. Therefore, in attempt to create

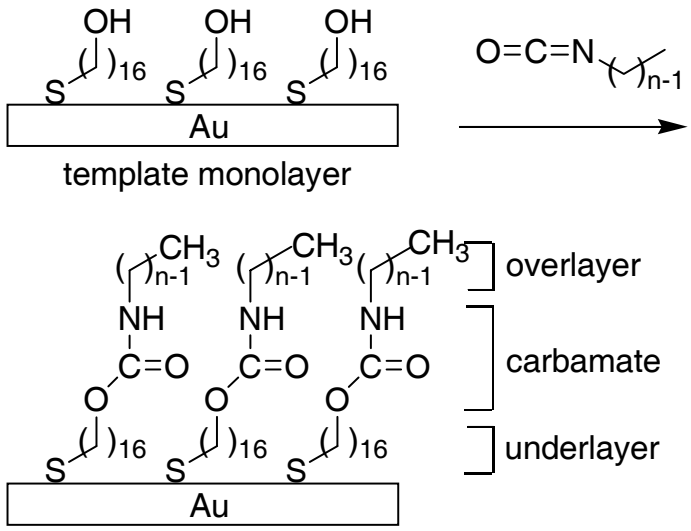

Figure 3.6 An illustration of the vapor-phase method used to create alkanethiolates with intralayer carbamate functional groups.

more ordered films, isocyanate reactions with hydroxyl-terminated SAMs were carried out at the gas-surface interface. To prepare a monolayer containing carbamate linkages using vapor-phase chemistry, the template hydroxyl-terminated SAMs were removed from 1 mM ethanolic solutions of 11-mercapto-1-undecanol or 16-mercapto-1-hexadecanol, rinsed repeatedly with absolute ethanol and dried in a stream of ultra-pure N_2. Monolayers were then placed in a 60 cm^3 vapor deposition chamber that was purged with N_2 and the system was then confined to a N_2-atmosphere. Approximately 100 μL of the desired alkyl isocyanate were introduced to the chamber via pipette. The length and structure of the overlayer chains were varied by reacting the initial SAM with a range of alkyl isocyanates, as shown schematically in Figure 3.6. The vapor-phase concentration of the isocyanate molecules present in the deposition chamber was kept as high as possible by heating the chamber to 40 °C during deposition. Under these conditions, it was determined that the reaction reached completion after approximately 18 hours, even for the longest-chain isocyanate studied. The modified surfaces were removed from the

deposition chamber, and rinsed with absolute ethanol and dried in a stream of ultra-pure N_2.

3.2.4. Characterization of SAMs and Interactions with CWA Simulants

3.2.4.1. Reflection Absorption Infrared Spectroscopy

RAIR spectra were collected using a Bruker IFS 66v/S spectrometer equipped with a liquid N_2 cooled MCT (mercury-cadmium-telluride) detector. The infrared radiation was p-polarized and a grazing incidence angle of 86° to the surface normal was used. Clean gold substrates were used as background references, unless otherwise noted. Each spectrum was collected using a minimum resolution of 2 cm^{-1} and is the average of 100 scans.

3.2.4.2. Contact Angle Goniometry

The static contact angle of deionized water on SAM surfaces was measured using a FTA125 Contact Angle Analyzer (First Ten Angstroms). All measurements were made at room temperature under ambient humidity. A minimum of five different points on each sample were recorded and averaged and the results were highly reproducible for different samples and sample sets.

3.2.4.3. X-ray Photoelectron Spectroscopy

XP spectra were collected on a Perkin Elmer 5400 X-ray Photoelectron Spectrometer. A monochromatized Mg(Kα) radiation source (1253.6 eV) and a position sensitive, multi-channel plate detector were used to make the measurements. The vacuum chamber maintained a background pressure of ~10^{-7} mbar during data collection. Surface sensitivity was ensured by using a take-off angle of 15° with respect to the surface normal. Binding energies are referenced to C (1s) at 284.8 eV. Survey spectra

were collected for 5 minutes using a pass energy of 44.75 eV, a 1 mm x 3.5 mm spot size and 300 W electron beam power. High resolution multiplex spectra were collected with an acquisition time of 8 minutes per region.

3.2.5. CWA Simulant Exposure Studies

Exposure of the SAMs to CWA simulants was accomplished by placing the film in an atmosphere saturated with organophosphonate vapor. SAMs were placed in a 60 cm^3 vapor deposition chamber initially purged with N_2 and approximately 5 μL of the simulant was introduced via pipette. The gas-phase concentration of the phosphate molecules was kept high by heating the chamber mildly to 308 K.

3.3. Results and Discussion

3.3.1. Reflection Absorption Infrared Spectroscopy

3.3.1.1. CH_3-terminated Self-Assembled Monolayer

Infrared spectroscopy is an invaluable tool in the assessment of monolayer structure. Evaluation of order and average orientation of the adsorbate molecules can be accomplished through careful inspection of vibrational peak positions and shapes. The infrared spectra displayed in Figure 3.7 are those collected from a series of *n*-alkanethiols adsorbed on Au ($HS(CH_2)_{n-1}CH_3$), where n is equal to the total number of carbon atoms in the alkyl backbone. This well-characterized system serves as a comparison for the other SAM systems described here.[108]

Long chain alkanethiols form densely packed structures with the alkyl chains fully extended at a tilt angle of ~30° to the surface normal, while the shorter chains are more sparsely covered, less well-ordered, and loosely packed.[108] The carbon-hydrogen vibrational modes serve as indicators of these structural descriptions. The positioning of

the asymmetric stretching vibration (d^-) of the methylene units at 2918 cm^{-1} is representative of a well-ordered system, possessing few defect sites.[90] Comparison with the infrared spectrum of $CH_3(CH_2)_{21}SH$ crystals (ν_{as} CH_2 at 2918 cm^{-1}), reported by Porter and co-workers, reveals that the 2918 cm^{-1} peak position observed for the SAM system is consistent with a crystalline-like environment.[108] This benchmark peak may be further red-shifted by 1-2 cm^{-1} in exceptionally ordered films.[108] The infrared spectrum of liquid $CH_3(CH_2)_7SH$ (ν_{as} CH_2 at 2924 cm^{-1}) confirms that the SAM system is not

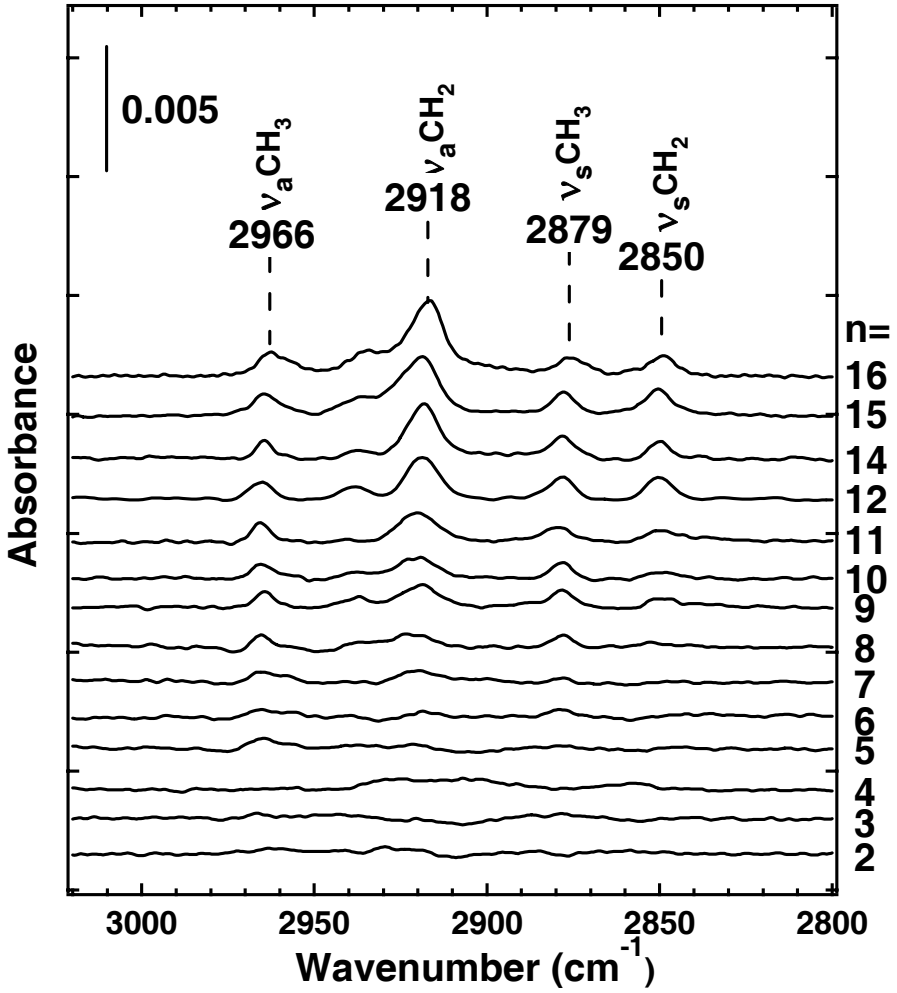

Figure 3.7 RAIR spectra of *n*-alkanethiol SAMs on Au (111); n is the number of carbon atoms in the alkyl chain.

"liquid-like," as in the case of disordered hydrocarbon films where the asymmetric methylene vibrational mode may be blue-shifted by ~6 cm^{-1}.[108] In addition to the asymmetric methylene stretch, the asymmetric vibration of the methyl groups (r_a^- at 2966 cm^{-1}, r_b^- at 2958 cm^{-1} (shoulder)), the symmetric vibrations of the methyl (r^+ at 2879 cm^{-1}, Fermi resonance at 2937 cm^{-1} (shoulder)) and methylene (d^+ at 2850 cm^{-1}) groups and the scissoring vibration of the methylene groups (d^+ at 1468 cm^{-1}), reveal structural information about the thin films.[90] The C-H peak positions of the longer alkyl chains in Figure 3.7 are indicative of an all-trans conformation and crystalline packing arrangement. The spectra of the shorter chain SAMs reveal a system that is liquid-like or illustrative of a bulk disordered phase. In addition, the fewer C-H units present in the shorter-chain systems result in a decrease in peak intensity. The slight shifts in peak position and shape as chain length decreases suggest a loss of film organization and a decrease in packing density.[108]

3.3.1.2. OH-terminated Self-Assembled Monolayer

In addition to *n*-alkanethiols, *ω*-functionalized thiol SAMs on Au have received a good deal of attention. These highly-organized films can serve as a templates for subsequent surface functionalization, as reported by Crooks and others.[102,112,124] Numerous literature reports detail the structural implications of hydroxyl, carboxylic acid, amine, amide, and fluorinated functional groups at the terminal position. Analogous to the *n*-alkanethiol SAMs, the van der Waals interactions between the longer chain ($n \geq 12$) thiols drive the ordered assembly of the monolayers with non-bulky functional groups at the terminus. The dense chain packing and subsequent crystallinity of the SAM are not compromised by the presence of terminal hydroxyl groups (i.e. $HS(CH_2)_{16}OH$).

Therefore, the methylene vibrational modes of long-chain OH-terminated SAMs are nearly identical to those of *n*-alkanethiol SAMs. RAIR spectra of ω-hydroxyl SAMs with eleven and sixteen carbon atoms in the alkyl chains are reported in Figure 3.8. The asymmetric stretching mode (d^-) is present at 2918 cm^{-1} and the symmetric stretching mode (d^+) is present at 2850 cm^{-1}. In addition to these modes, a third methylene stretching vibration, attributed to the perturbation of the methylene group adjacent to the hydroxyl moiety, appears as a peak at 2878 cm^{-1}. This is an example of how hydrogen-bonding disrupts the highly-ordered nature of simple methyl-terminated SAMs. The

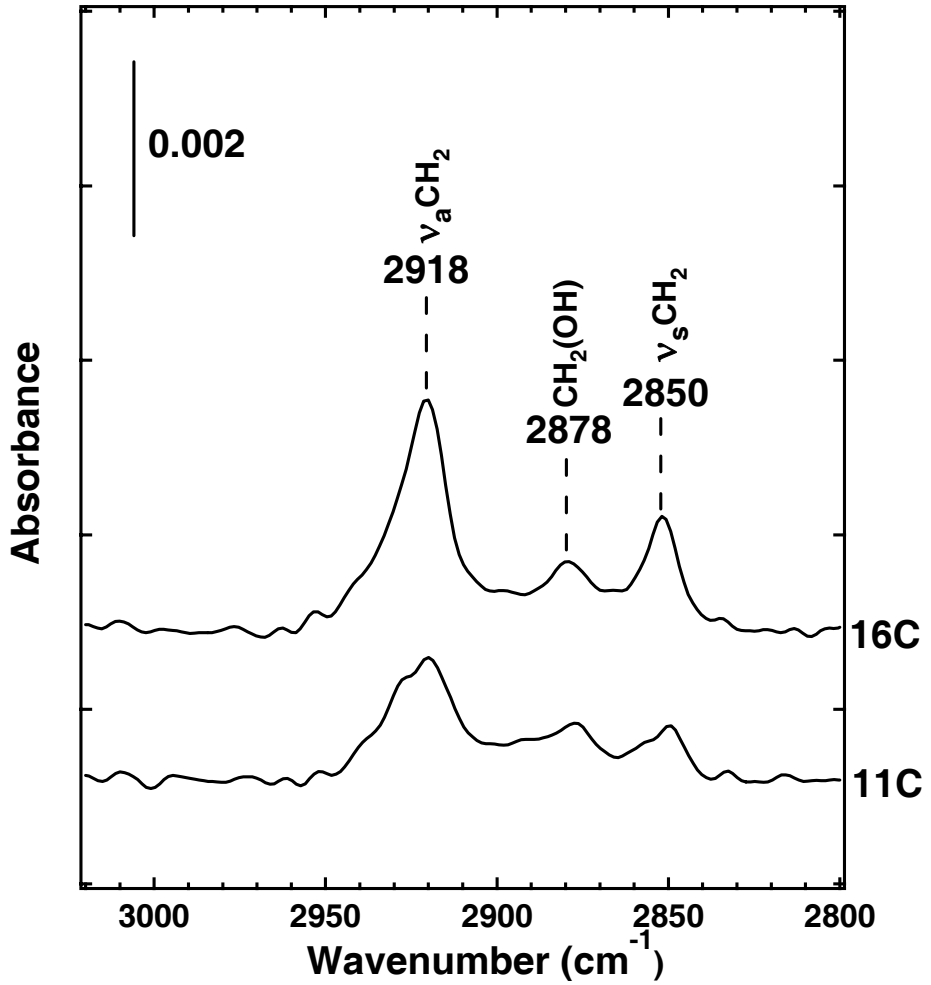

Figure 3.8 RAIR spectra of hydroxyl-terminated alkanethiol SAMs on Au (111); 16C and 11C represent the number of carbon atoms in the alkyl chain.

lower frequency region of the spectrum contains a vibrational mode attributed to a scissoring motion of the methylene units (d^+ at 1468 cm^{-1}). Bertilsson and Liedberg report a hydrogen-bonded OH mode in the region of 3100 to 3500 cm^{-1},[123] however this mode is not visible in the above spectra. The lack of signal in this high frequency portion of the RAIR spectra is attributed to the orientation of the O-H dipole with respect to the surface. Transition dipoles oriented parallel to the surface are, according to the surface selection rules, not visible in a RAIR spectra.[86,87] Of s- and p-polarized infrared radiation incident upon the surface, only p-polarized light interacts with adsorbed species because of phase-shifting upon reflection. Consequently, active vibrations must have part of their dipole oriented perpendicular to the surface plane in order to be detected. Thus, regardless of the number carbon atoms in the alkyl chain, the orientation of the terminal hydroxyl groups appears to be parallel to the surface, likely a result of hydrogen bonding interactions between adjacent molecules.

3.3.1.3. Mixed *ω*-Functionalized Self-Assembled Monolayers

Bertilsson et al. and Bain et al. have characterized SAMs prepared from thiols with terminal hydroxyl and methyl functional groups.[123,125-127] Surfaces, such as these, may have applications in sensing or biotechnologies and have been utilized, like pure hydroxyl-terminated films, as templates for subsequent reactions. Aggregations of like-molecules have been reported to be minimal, while a high degree of order is maintained for surfaces with a range of composisitons.[125-127] Figure 3.9 contains RAIR spectra of mixed monolayers formed from 1 mM ethanolic solutions of 1-hexadecanethiol and 16-mercapto-1-hexadecanol. The mole fraction of hydroxyl-terminated chains in the solution is indicated by the vertical scale. The spectra clearly reveal well-ordered

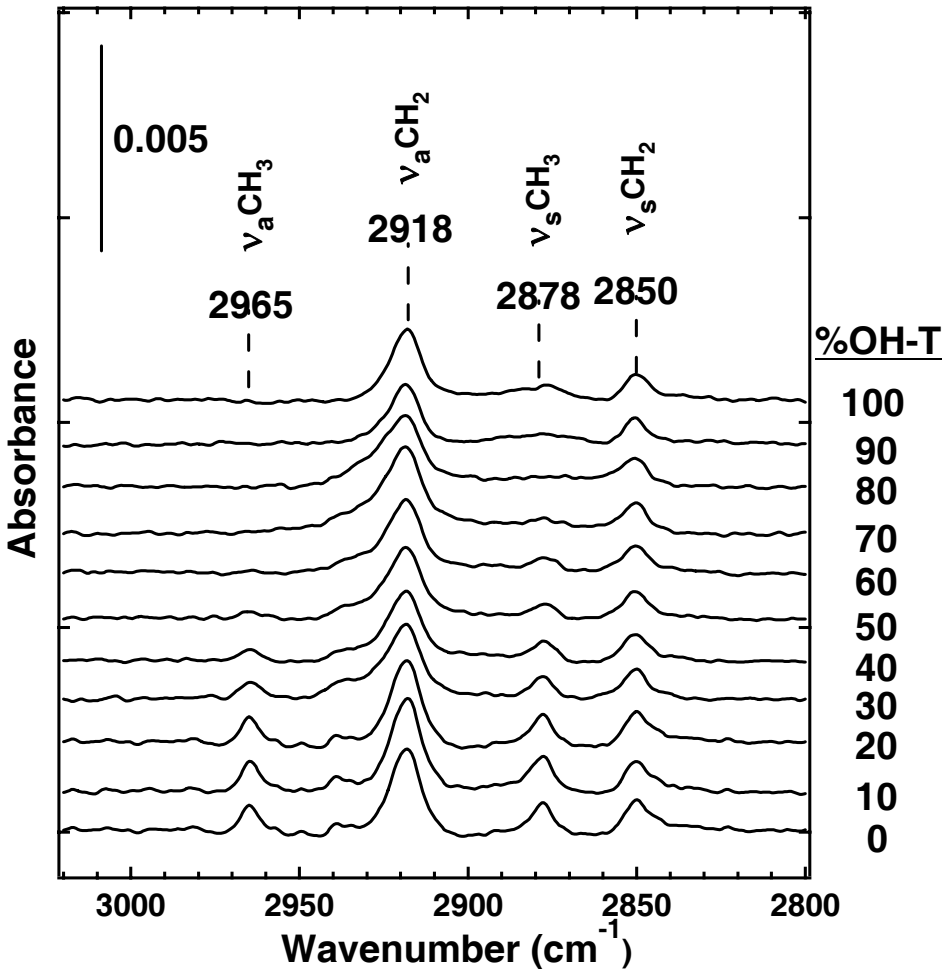

Figure 3.9 RAIR spectra of SAMs on Au (111) prepared from mixed ethanolic solutions of 16-mercapto-1-hexadecanol and 1-hexadecanethiol.

systems. A loss of methyl group asymmetric and symmetric vibrational mode intensity is evident as the mole fraction of hydroxyl-terminated chains in the solution increases.

3.3.1.4 Intra-chain Carbamate Self-Assembled Monolayers

3.3.1.4.1. 1,4-Phenylene Diisocyanate SAMs

The procedures outlined by Persson et al. were used to create thin films that contain carbamate linkages.[61] Figure 3.10 presents RAIR spectra of hydroxyl-terminated SAMs on Au, prepared from 11-mercapto-1-undecanol, that have been modified in sequence with 1,4-phenylene diisocyanate and butanol (A) or dodecanol (B) (assignments are given in Table 3.1). In general, the peak positions are blue-shifted compared to the

values reported for a well-ordered system.[61] Furthermore, broad peaks and the presence of several additional modes suggest the formation of unwanted side-products, such as allophanates.[128]

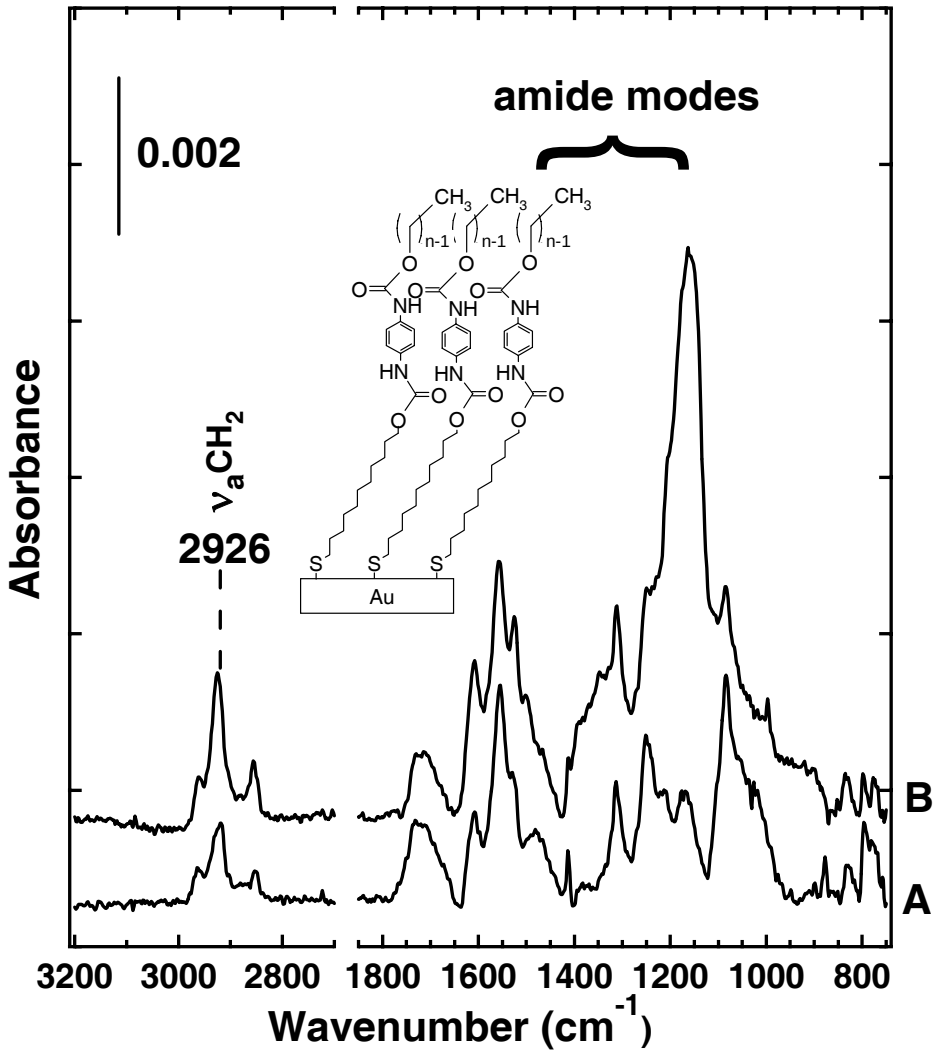

Figure 3.10 RAIR spectra of 1,4-phenylene carbamate bearing SAMs on Au (111) prepared according to Persson et al. The terminal chains are comprised of 4 carbons (A) and 12 carbons (B).

Table 3.1 Infrared frequencies and assignments of 1,4-phenylene carbamate containing SAMs. Peak positions reported by Persson et al. are given for reference.

freq, cm^{-1}	Persson et al. freq, cm^{-1}	assignment
2960	2965	$\nu_{as}(CH_3)$, r_a^-
2926	2919	$\nu_{as}(CH_2)$, d^-
2883	2878	$\nu_s(CH_3)$, r^+
2856	2852	$\nu_s(CH_2)$, d^+
1718	1653	ν(C=O), amide I
1608	1601	$\nu(C_{ar}\text{-}C_{ar})$
1558	1548	ν(C-N), N-H bend, amide II
1525	1514	ν(C-N)
1471	1414	$\delta(CH_2)$
1412		?
1311, 1250	1315, 1236	ν(C-N), N-H bend, amide III
1161		ν (O=)C-O-C
1088	1082	ν(C-O)

The spectrum presented in Figure 3.11 is that of a 1,4-phenylene diisocyanate functionalized hydroxyl-terminated SAM that has been subsequently reacted with water to yield terminal amine groups. Modes of interest are reported in Table 3.2. Unlike the surfaces that were reacted with an alcohol to yield terminal alkyl chains, the reaction between water and terminal isocyanate groups did not go to completion. The presence of a strong isocyanate stretching vibration at 2276 cm^{-1} and a strong amine stretching vibration at 3300 cm^{-1} indicate that though a large fraction of reactive isocyanate groups were converted to amines, complete conversion was not achieved (even after 18 hours). Furthermore, the SAM structure appears disordered and, as with the alcohol reacted films, appears to contain unwanted side products.[128]

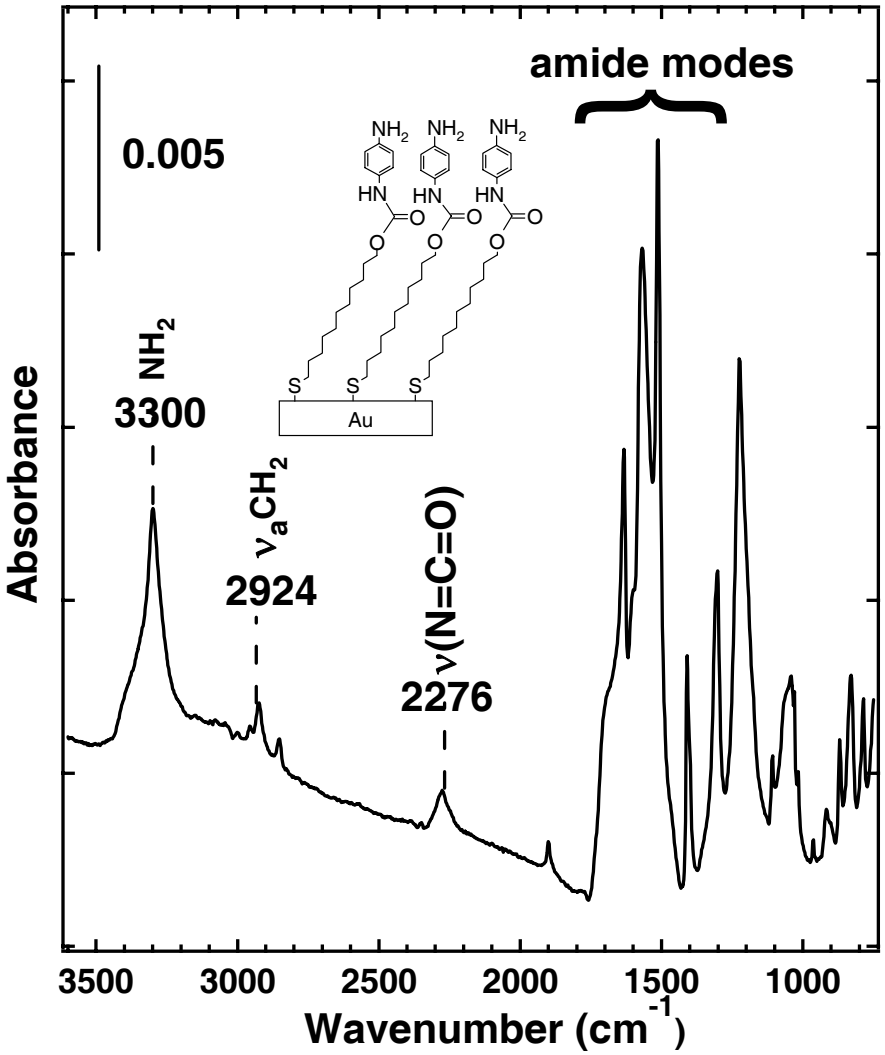

Figure 3.11 The RAIR spectrum of phenylene carbamate bearing SAMs on Au (111) with terminal amine groups, prepared according to Persson et al.

Table 3.2 Infrared frequencies and assignments of phenylene carbamate containing SAMs with terminal amine groups. Peak positions reported by Persson et al. are given for reference.

freq, cm^{-1}	Persson et al. freq, cm^{-1}	assignment
3300	3296	$\nu_{as}(CH_3)$, r_a^-
2924	2919	$\nu_{as}(CH_2)$, d^-
2276	2278	ν(N=C=O)
1900	-	?

The results of the solution-phase SAM preparation, using 1,4-phenylene diisocyanate as a linking group, are unsatisfactory. Similar unacceptable results were obtained for experiments using 1,6, hexamethylene diisocyanate or 1,12 dodecyl diisocyanate as the linking group. The surface structure appeared disordered and in some cases it was evident that both terminal isocyanate groups reacted with surface hydroxyl groups to yield an alkyl "loop" at the interface. The indeterminate structure of the films prevents study of interfacial reactions between organophosphate CWA simulants and the carbamate groups. Moreover, the presence of bulky phenyl groups in the Persson et al. synthesis does not produce a SAM system that is a suitable model for CARC paints. The isocyanate chemistry attempted in the preparation of di-carbamate layers can, however, be extended to the preparation of monolayers containing intrachain carbamate linkers lacking bulky ring structures.

3.3.1.4.2. Solution-Phase Chemistry

Figure 3.12 presents RAIR spectra resulting from SAMs prepared using the parameters outlined in Table 3.3. These spectra are representative of the most ordered films attained using solution-phase, isocyanate chemistry.

The high-frequency region of the IR spectra reveals that in each preparatory method, the resulting monolayer structure is somewhat disordered, relative to an *n*-alkanethiol SAM. The asymmetric methylene vibrational modes are blue-shifted from 2918 cm^{-1}, the peak position expected for well-ordered thin films. It is expected that the orientation and tilt angle of the terminal alkyl chains is slightly different than that of the underlayer chains. Nonetheless, the characteristic hydrocarbon vibrational modes are broad and in some cases, unresolved, suggesting a heterogeneous arrangement of

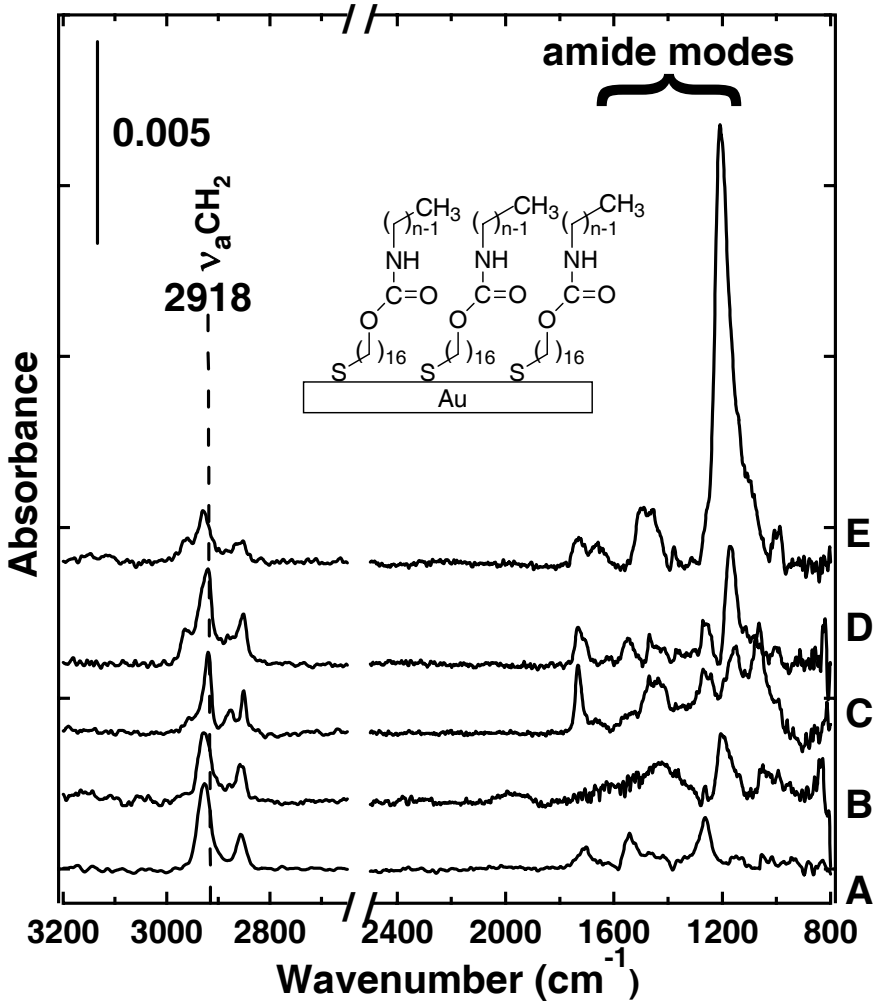

Figure 3.12 RAIR spectra of SAMs on Au (111) containing intrachain carbamate groups. The films were prepared using solution-phase alkyl-isocyanate chemistry.

adsorbate molecules. Furthermore, the peak positions and intensities of the amide bands in the lower frequency region of the spectrum are not consistent with reported values.[61] The presence of intrachain carbamate groups undoubtedly affects the SAM structure. However, uncharacterizable carbamate position and orientation, as well as irreproducible results, render the solution-phase preparatory scheme undesirable. Effective study of interfacial properties and reactions requires a well-ordered structure with specific knowledge of functional group location and spatial arrangement.

Table 3.3 Solution-phase reaction parameters of the spectra in Figure 3.12.

Spectrum	Reactants	Solvent	Reaction Time (hours)	Temperature (°C)
A	undecyl isocyanate (.1 M), 11C OH-T SAM	toluene	2	40
B	undecyl isocyanate (.02 M), 11-mercapto-1-undecanol (1 mM) (1:1)	hexane	22 (reacted in presence of clean Au slide)	33
C	octyl isocyanate (5x10-7 M), 11C OH-T SAM	toluene	168	40
D	heptyl isocyanate (33 mM), 11C OH-T SAM	toluene	264	40
E	butyl isocyanate (.3M), 16-mercapto-1-hexadecanol (1 mM) (1:30)	toluene	264 (solution reaction time); 18 (in presence of clean Au substrate)	62

3.3.1.4.3. Vapor-Phase Chemistry

Results demonstrate that vapor-phase reactions for incorporating hydrogen-bonding functional groups within SAMs may produce more organized structures than analogous solution-phase preparation routes. Insights into the molecular structure and order of the vapor-phase synthesized monolayers are revealed by the infrared spectra of Figures 3.13 and 3.15. Table 3.4 lists the peak positions and the mode assignments of the primary transitions for the carbamate functionalized SAMs.[59,61,90,91,108,115,129,130] In general, the peak intensities and positions are found to be similar for the entire range of monolayers studied, indicating that the extent of the vapor-phase reaction in the synthesis of the monolayer is independent of isocyanate chain length. However, detailed analysis of the high- and low-frequency modes reveals modest structural and hydrogen-bonding differences between the short-chain ($n < 5$) and long-chain ($n \geq 5$) carbamate SAMs.

3.3.1.4.3.a. High-Frequency Modes

Figure 3.13 shows the RAIR spectra of the carbamate SAMs in the C-H stretching region. One of the most notable trends in the IR data is that the asymmetric CH_3

stretching mode shifts to lower wavenumbers as n increases from n=1 to n=5. This effect is likely due to increased order of the overlayers as methylene groups are added. The additional CH_2 groups contribute to the van der Waals forces that drive the all-trans configuration of densely packed monolayers. For $n \geq 5$, the peak position for this mode

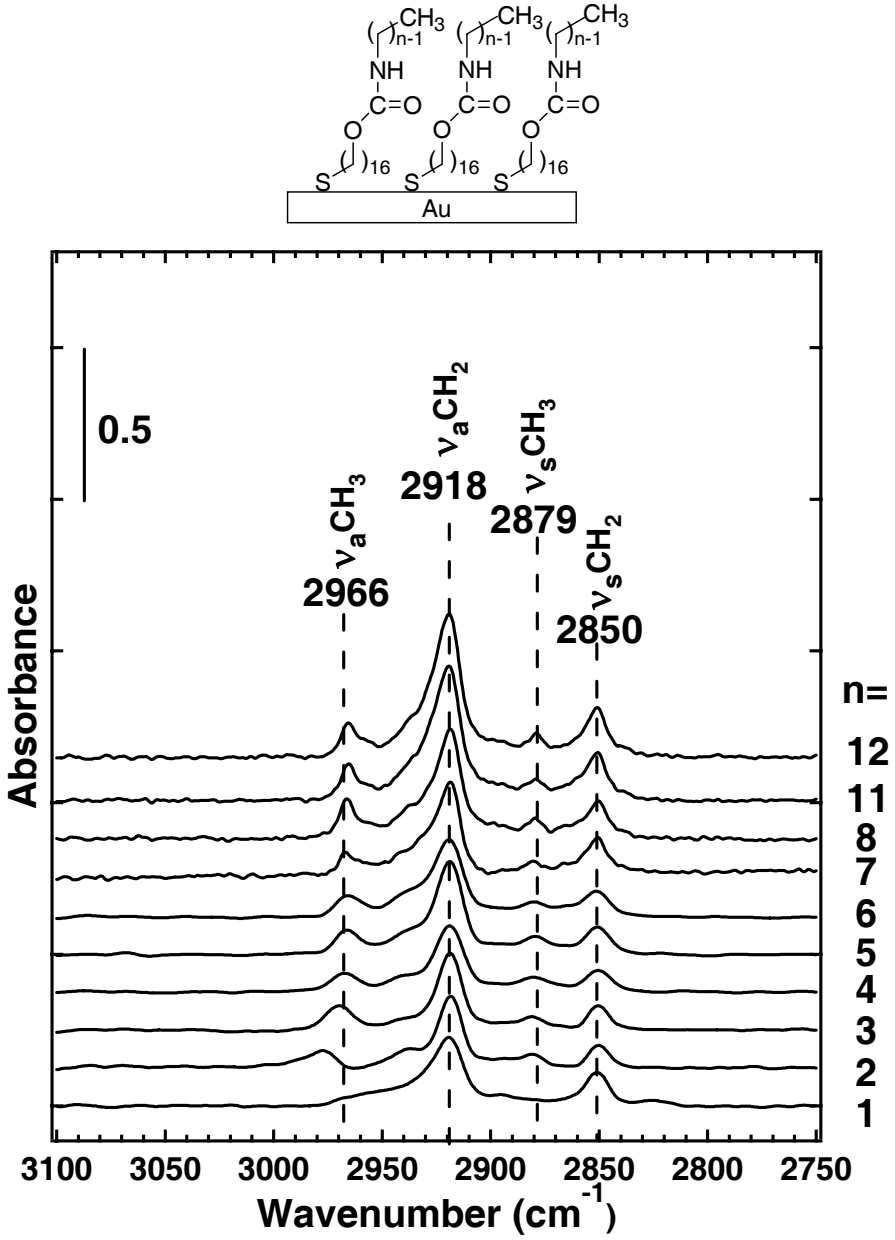

Figure 3.13 RAIR spectra of $Au/S(CH_2)_{16}$-$O(C=O)NH(CH_2)_{n-1}CH_3$. The degree of order increases with terminal chain length.

is identical to that observed for a well-ordered *n*-alkanethiol SAM (2966 cm^{-1}). The diminished intensity of the CH_3 stretching modes for the n = 1 and n = 2 SAMs may also be attributed to the tendency of the short-chain monolayers toward disordered structures. This interpretation agrees with the contact angle measurements discussed below to provide further evidence that well-ordered monolayers form for n > 5.

Table 3.4 Spectral frequencies and assignments for a $Au/S(CH_2)_{16}$-$O(C=O)NH(CH_2)_{n-1}CH_3$ SAM.

freq, cm^{-1}	assignment[a]
2966	$\nu_{as}(CH_3)$, r_a^-
2958	$\nu_{as}(CH_3)$, r_b^- (sh)
2937	$\nu_s(CH_3)$, FR
2918	$\nu_{as}(CH_2)$, d^-
2879	$\nu_s(CH_3)$, r^+
2850	$\nu_s(CH_2)$, d^+
1704	ν(C=O), amide I
1548	ν(C-N), N-H bend, amide II
1471	$\delta(CH_2)$
1304, 1277, ~1255	ν(C-N), N-H bend, amide III
1152	ν (O=)C-O-C
1061	ν(C-O)

In addition to the CH_3 stretching modes, the peak positions, intensities, and widths of the CH_2 modes have been used extensively to assess the order and orientation of SAMs. As discussed above, well-ordered monolayers are evidenced by narrow peaks at 2918 cm^{-1} (FWHM = 13) for the d^- mode and 2851 cm^{-1} for the d^+ mode. The spectra in Figure 3.13 show that these key spectral features are observed for every monolayer studied and the intensities scale with the number of methylene groups in the monolayer. The asymmetric CH_2 peak widths, shown in Table 3.5, indicate that the carbamate SAMs are nearly as well-ordered as a dodecanethiolate SAM on Au. For the short-chain carbamate SAMs, the peak intensity at 2918 cm^{-1} is comprised almost entirely of signal from the relatively large number of methylene groups in the underlayer. The position of this peak implies that the order of the underlayer changes little upon functionalization of the original OH-terminated template monolayer with the isocyanate reactants. The slight broadening of the d^- peak is attributed to a Fermi resonance of the CH_3 bending mode present on the carbamate functionalized SAMs. The steady increase in d^- peak intensity at 2918 cm^{-1} as a function of chain length provides a strong indication that the structure

Table 3.5 Peak width values (FWHM) for the RAIR data of carbamate SAMs and a dodecanthiolate monolayer on Au.

SAM Structure	$\nu_{as}CH_2$ width (cm^{-1})
$Au/S(CH_2)_{16}$-O(C=O)$NHCH_3$	18
$Au/S(CH_2)_{16}$-O(C=O)$NH(CH_2)CH_3$	13
$Au/S(CH_2)_{16}$-O(C=O)$NH(CH_2)_2CH_3$	13
$Au/S(CH_2)_{16}$-O(C=O)$NH(CH_2)_3CH_3$	17
$Au/S(CH_2)_{16}$-O(C=O)$NH(CH_2)_4CH_3$	14
$Au/S(CH_2)_{16}$-O(C=O)$NH(CH_2)_5CH_3$	14
$Au/S(CH_2)_{16}$-O(C=O)$NH(CH_2)_6CH_3$	15
$Au/S(CH_2)_{16}$-O(C=O)$NH(CH_2)_7CH_3$	16
$Au/S(CH_2)_{16}$-O(C=O)$NH(CH_2)_{10}CH_3$	16
$Au/S(CH_2)_{16}$-O(C=O)$NH(CH_2)_{11}CH_3$	16
$Au/S(CH_2)_{11}CH_3$	13

of the long-chain overlayers mirrors that of the well-ordered underlayers. The relative intensities of the asymmetric and symmetric CH_2 stretching modes may be characteristic of an orientation of the overlayer chains that differs slightly from that of the underlayer. This ratio suggests that the presence and position of the carbamate groups affect the overall monolayer structure. However, it is difficult to distinguish the contributions of the overlayer from those of the underlayer in the IR measurements of Figure 3.13.

3.3.1.4.3.b. Difference Spectrum

Use of deuterated over- or underlayer alkyl chains to better assess the relative order of the methylene chains was cost prohibitive. Thus, a spectrum of an n = 6 carbamate monolayer was collected using the initial OH-terminated template monolayer as the background. The difference spectrum, labeled (C) in Figure 3.14, consists of contributions from the carbamate group, the CH_2 and CH_3 stretches above the carbamate group, and any slight changes in the underlayer structure. For reference, the RAIR spectra of the original OH-terminated monolayer (B) and the n = 6 carbamate monolayer (A), both recorded with clean gold as the background, are shown.

Features of the n = 6 difference spectrum include the CH_3 modes (r_a^- at 2965 cm^{-1}, a broad Fermi resonance at 2937 cm^{-1}, and a less intense r^+ stretch at 2880 cm^{-1}) and the two characteristic CH_2 stretches positioned at 2918 cm^{-1} for the d^- mode and centered at 2856 cm^{-1} for the d^+ mode. The position and intensity of these peaks, along with evidence from contact angle measurements (Section 3.3.2.), indicate that the alkyl overlayer for n = 6 may be nearly as well ordered as a typical ω-functionalized SAM. These results suggest that the use of vapor-phase reactions for functionalizing SAMs with buried hydrogen-bonding groups yield more organized monolayers than solution-phase

routes. The primary difference of the two approaches for assembling monolayers may be that the vapor-phase strategy begins with a highly-ordered template that effectively seeds the growth of the overlayer chains. In contrast, solution-phase preparation of SAMs with functionalized alkanethiols requires what may be a competition between the gold-sulfur bond formation and hydrogen-bonding interactions among the chains as they diffuse to the surface and assemble into the lowest energy configuration available.

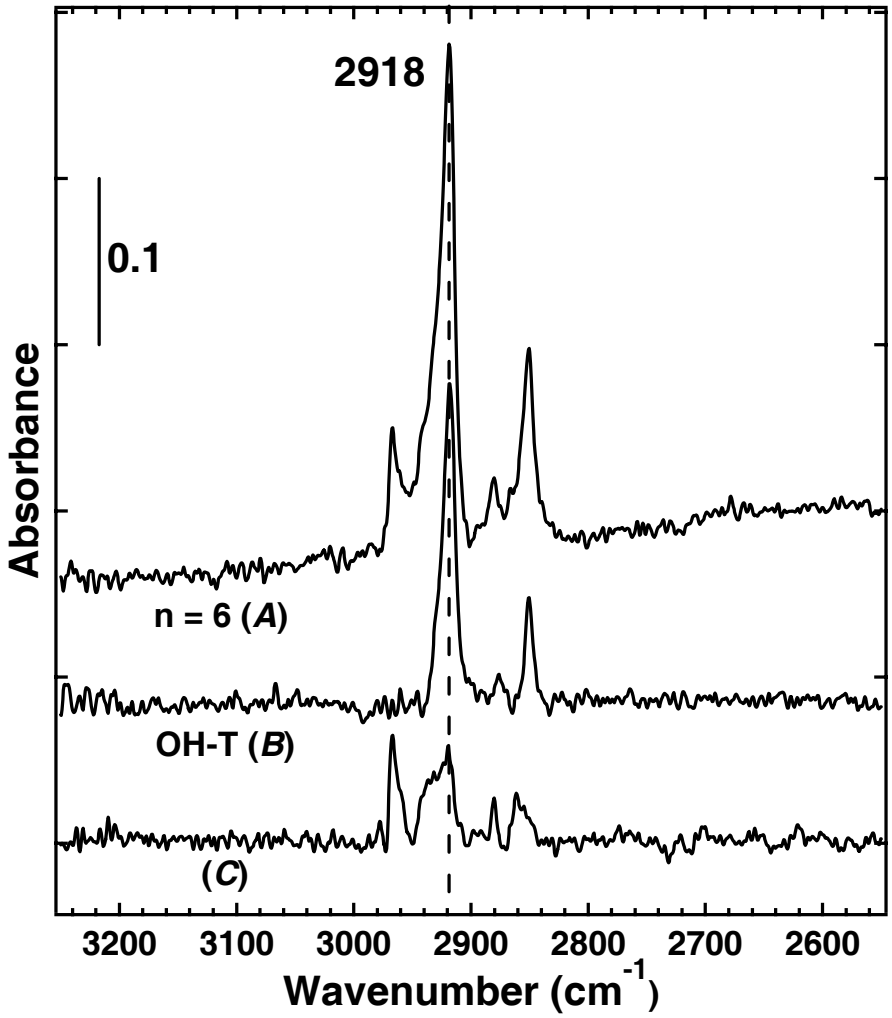

Figure 3.14 Spectra of (*A*) Au/S$(CH_2)_{16}$-O(C=O)NH$(CH_2)_{n-1}CH_3$ (n = 6), (*B*) Au/S$(CH_2)_{16}$-OH and (*C*) the difference spectrum ((*A*) – (*B*)).

3.3.1.4.3.c. Low-Frequency Modes

RAIR spectra of the low-energy modes associated with the carbamate vibrations are shown in Figure 3.15. The lowest frequency modes at 1152 cm^{-1} and 1060 cm^{-1} are attributed to the (O=)C-O-C stretch and the C-O-C stretch respectively. The amide II peak, a C-N stretch coupled with an N-H bend, is located at 1548 cm^{-1} and the amide III stretch is positioned at 1277 cm^{-1}. The amide III mode exhibits shoulders at ~1304 cm^{-1} and ~1255 cm^{-1}, likely due to multiple environments of the buried carbamate groups. Hydrogen-deuterium exchange of the amide proton confirms the carbamate mode assignments.

Figure 3.16 contains the RAIR spectra of an ethyl-carbamate SAM (A) and an ethyl-carbamate SAM that has been immersed in D_2O at room temperature for ~18 hours (B). The most dramatic differences between the spectra are the decrease in intensity of the amide II mode at 1548 cm^{-1} and the amide III mode at 1277 cm^{-1}. Concomitantly, there is an increase in signal at 1464 and 1191 cm^{-1}. The spectral shifts are consistent with literature reports of H-D exchange within amide functional groups.[131,132] The amide I peak associated with the C=O stretch is centered at 1704 cm^{-1} for the long-chain SAMs. The weak, broad nature of this transition and the absence of an N-H stretch in the high frequency region (not shown) are attributed to the presence of hydrogen bonding between adjacent carbamate groups. However, the amide I peak is slightly higher in energy (~1710 cm^{-1}) for the shorter chain carbamates, suggesting that the hydrogen-bonding interactions may be weaker for the less well-ordered monolayers. To further explore the effect of hydrogen bonding on the amide I peak position, the carbamate vibrational modes as a function of surface carbamate concentration were examined.

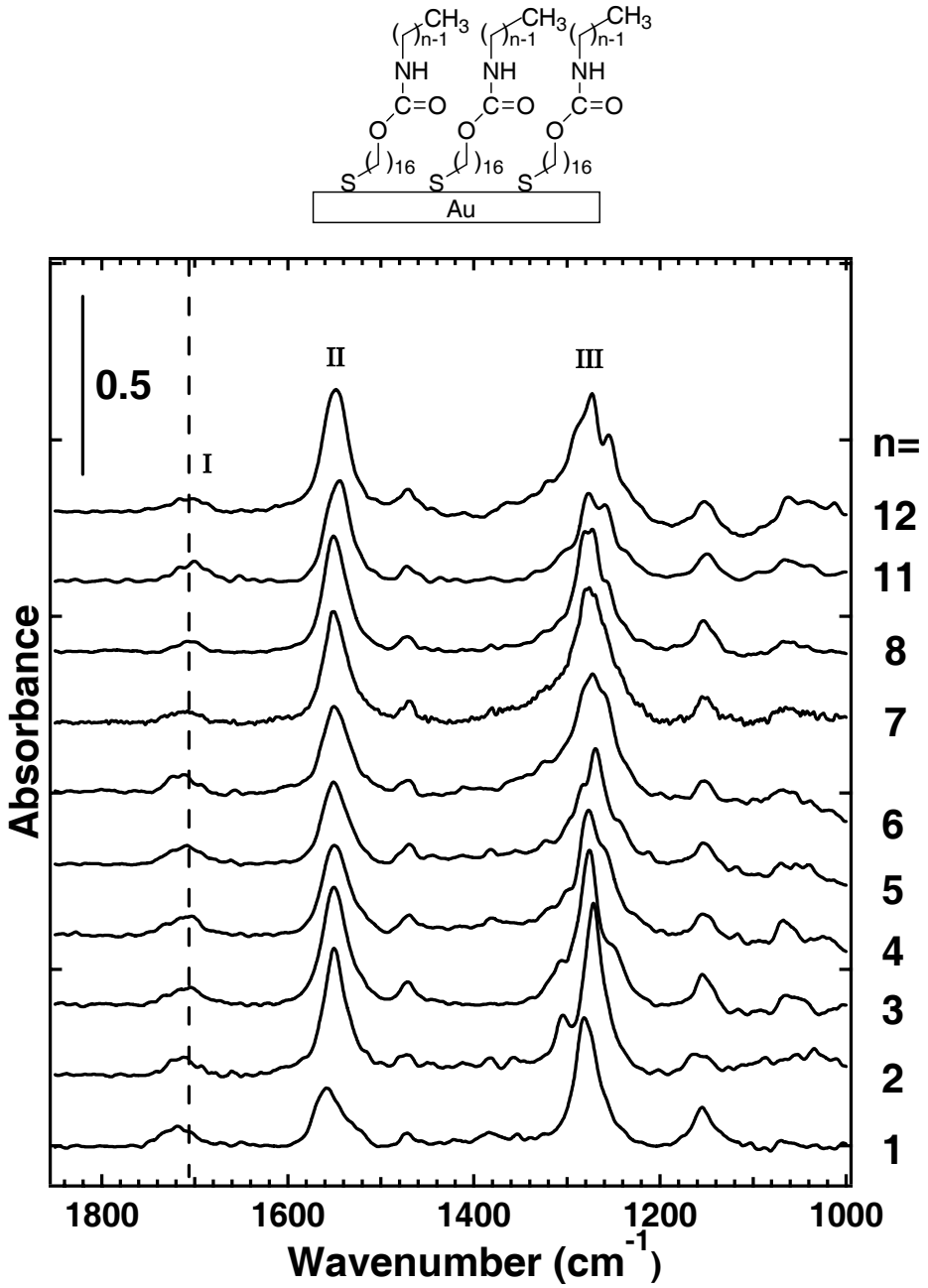

Figure 3.15 Characteristic carbamate modes of Au/S$(CH_2)_{16}$-O(C=O)NH$(CH_2)_{n-1}CH_3$ surface. The numerals indicate the respective amide vibrational modes.

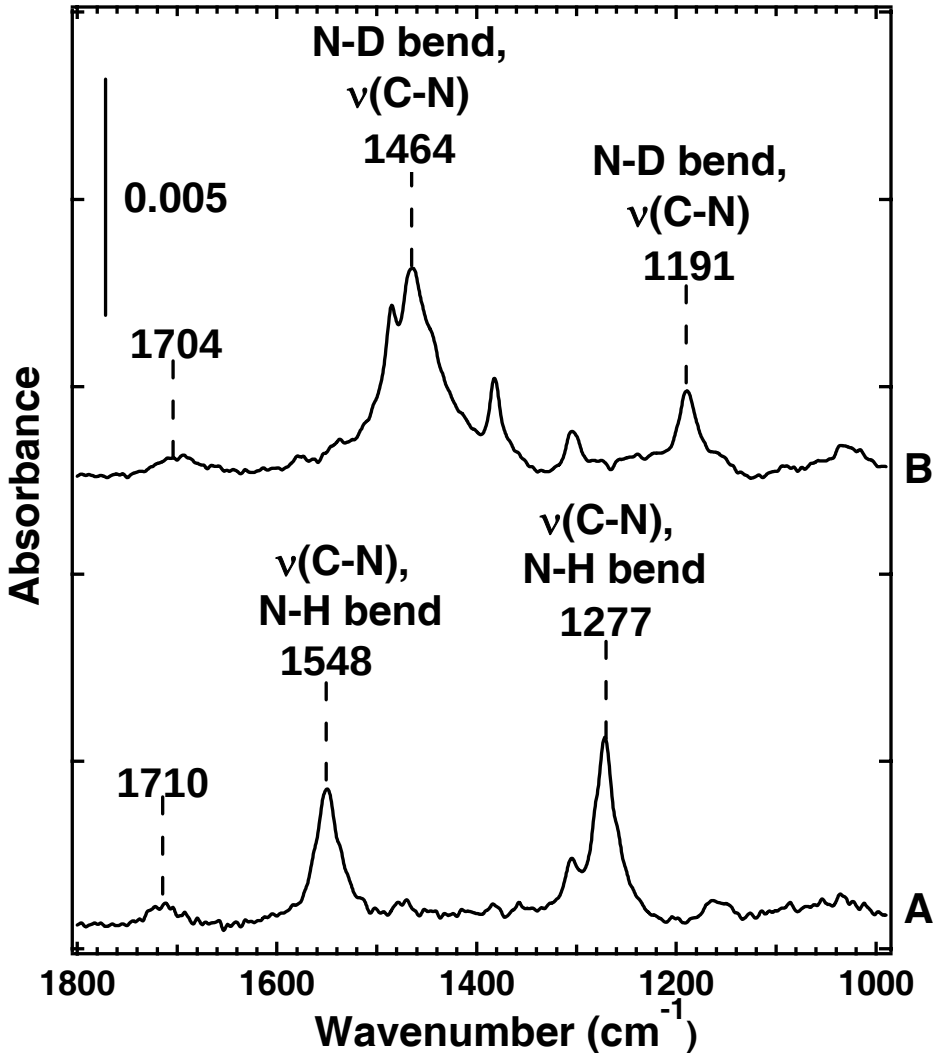

Figure 3.16 Characteristic carbamate modes of a Au/S$(CH_2)_{16}$-O(C=O)NHCH$_3$ (A) surface and a Au/S$(CH_2)_{16}$-O(C=O)NDCH$_3$ (B).

3.3.1.4.3.d. Mixed Monolayers: Disrupting the Hydrogen-Bonding Network

Previous RAIRS work has demonstrated that mixed solutions of OH- and CH_3-terminated alkanethiols yield SAMs with disrupted hydrogen-bonding interactions relative to the pure OH-terminated system. This strategy has been applied to the investigation of the extent of lateral hydrogen bonding in the carbamate SAMs.

As expected, the use of mixed template monolayers affects the structure of the carbamate SAMs. Figure 3.9 demonstrates that mixed monolayer templates of OH-

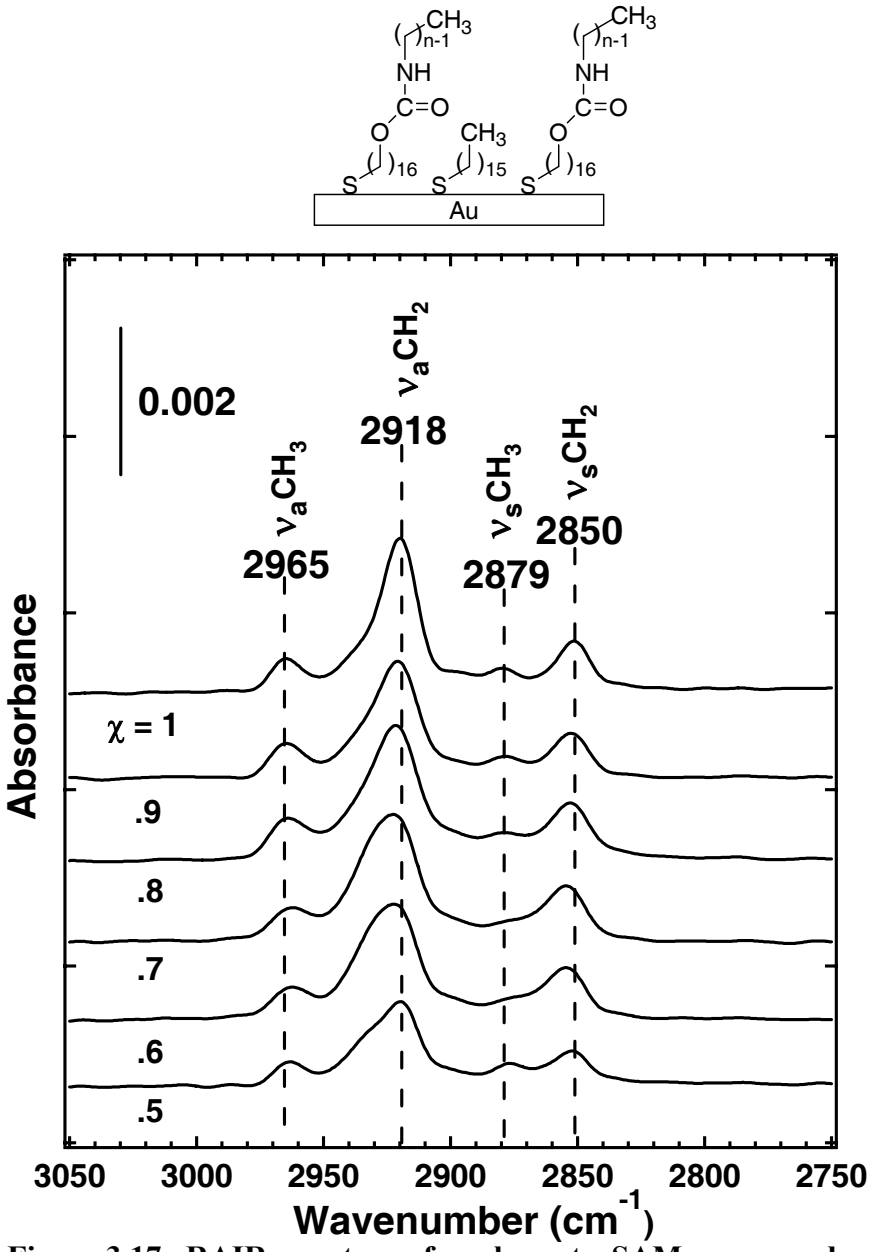

Figure 3.17 RAIR spectra of carbamate SAMs prepared on a hydroxyl-terminated and mixed CH_3:OH terminated template monolayers. χ is the mole fraction of OH-terminated molecules in the 1 mM ethanolic solution used to create the template monolayer.

terminated ($HS(CH_2)_{16}OH$) and CH_3-terminated ($HS(CH_2)_{15}CH_3$) alkanethiols maintain a high degree of order. However, in comparison to the ordered carbamate SAMs discussed above, the spectra of Figure 3.17 and Figure 3.18 indicate that less well-ordered overlayers are formed when carbamate SAMs are prepared from mixed template

monolayers. As χ, the mole fraction of $HS(CH_2)_{16}OH$ used to create the template monolayer, decreases, the peaks associated with methylene functional group vibrations blue-shift from well-order *n*-alkanethiol systems. Furthermore, the peak widths of the C-H vibrational bands in the spectra in Figure 3.17 suggest a disruption of overlayer order. The peak width (FWHM) of the film prepared with a $\chi = 0.5$ template is 25 cm^{-1}, nearly double the width of the asymmetric methylene stretching vibration of a dodecanethiolate monolayer on Au. The order of the terminal chains is compromised by the spacing of reactive hydroxyl groups of the template. It is likely that the spacing between adjacent terminal alkyl chains is greater than that of an *n*-alkanethiol SAM, resulting in a more disordered structure due to the diminished van der Waals interactions between chains.

Figure 3.18 compares the low frequency region of RAIR spectra of carbamate functionalized SAMs prepared using template monolayers created from mixed solutions of OH-terminated ($HS(CH_2)_{16}OH$) and CH_3-terminated ($HS(CH_2)_{15}CH_3$) alkanethiols. The spectra show that the characteristic carbamate peaks decrease in intensity as χ, the mole fraction of $HS(CH_2)_{16}OH$ used to create the template monolayer, decreases. This effect is simply the result of fewer carbamate groups on the surface as the concentration of the limiting reagent (the surface OH groups) is reduced. In addition, the C=O peak shifts from 1704 cm^{-1} to 1722 cm^{-1} as χ decreases and the hydrogen-bonding carbamate network is disrupted. The change in the C=O peak position for the carbamate SAMs prepared with mixed templates is similar to that observed for small n in the carbamate SAMs prepared with the pure OH-terminated monolayer templates (See Figure 3.15). This similarity suggests that the van der Waals forces of the long-chain carbamate SAMs may not only aid the organization of the overlayer methylene chains, but also help

reorient the carbamate groups into more favorable alignment for effective C=O---HN hydrogen bonding. Control experiments with pure methyl-terminated SAMs resulted in a complete absence of carbamate and isocyanate signal.

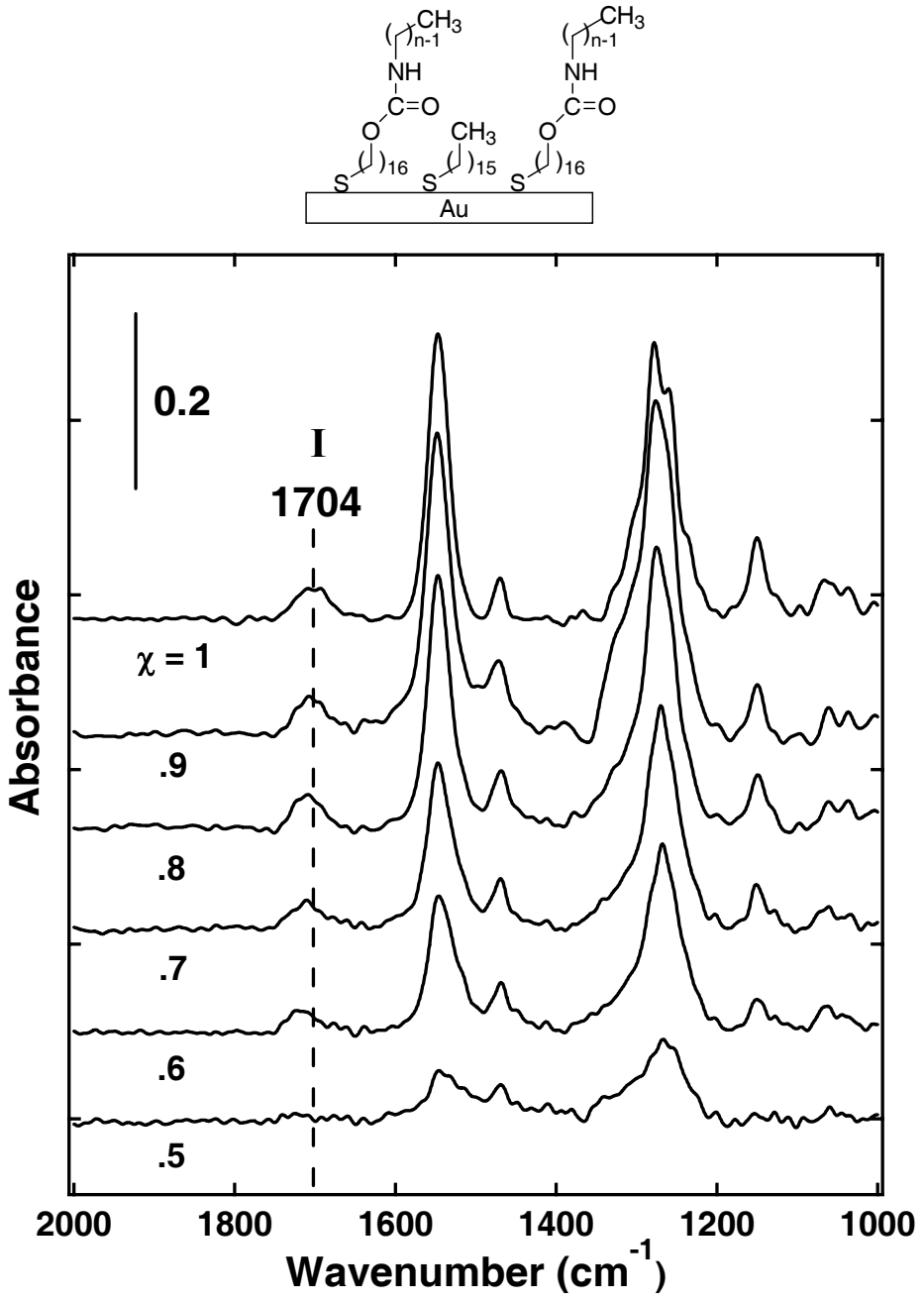

Figure 3.18 RAIR spectra of carbamate SAMs prepared on a hydroxyl-terminated and mixed CH_3:OH terminated template monolayers.

3.3.2. Contact Angle Goniometry

Contact angle measurements are sensitive to both the hydrophilic nature of a surface and the molecular structure of the SAM.[109,133] Figure 3.19 shows the static contact angles of water on the carbamate SAMs as a function of the isocyanate chain length used to create the monolayers. Also shown are the contact angles for the original well-ordered OH-terminated template SAM and a 16-carbon CH_3-terminated SAM.

The data of Figure 3.19 shows that the contact angle increases from 22° to 52° upon reaction of the OH-terminated SAM with methyl isocyanate. The contact angle is significantly lower than that expected for a well-ordered *n*-alkanethiol monolayer. This result is similar to that observed by Liedberg et al. who measured the advancing contact angle of water on a methyl ester-terminated SAM to be only 64°.[134] The small contact angles for these systems likely reflect the fact that the surfaces contain polar functional groups close to the interface where they are able to interact with the water droplet.[134]

The carbamate SAMs become more hydrophobic as the chain length above the carbamate increases and the functional groups are buried further below the interface. However, the contact angles remain lower than that measured for the CH_3-terminated SAM until the overlayer chain length is greater than 5 carbon atoms. The slow assent to a highly hydrophobic surface as chain length increases is similar to the results of Bain et al. who measured the contact angles of water on *n*-alkanethiol SAMs.[109] They found that at least five methylene groups were required to form monolayers that exhibit contact angles equal to those of long-chain *n*-alkanethiol monolayers on gold. Their study demonstrated that van der Waals interactions among the alkane chains are critical to the formation of highly-ordered SAMs. Likewise, for $n > 5$, the contact angles of the

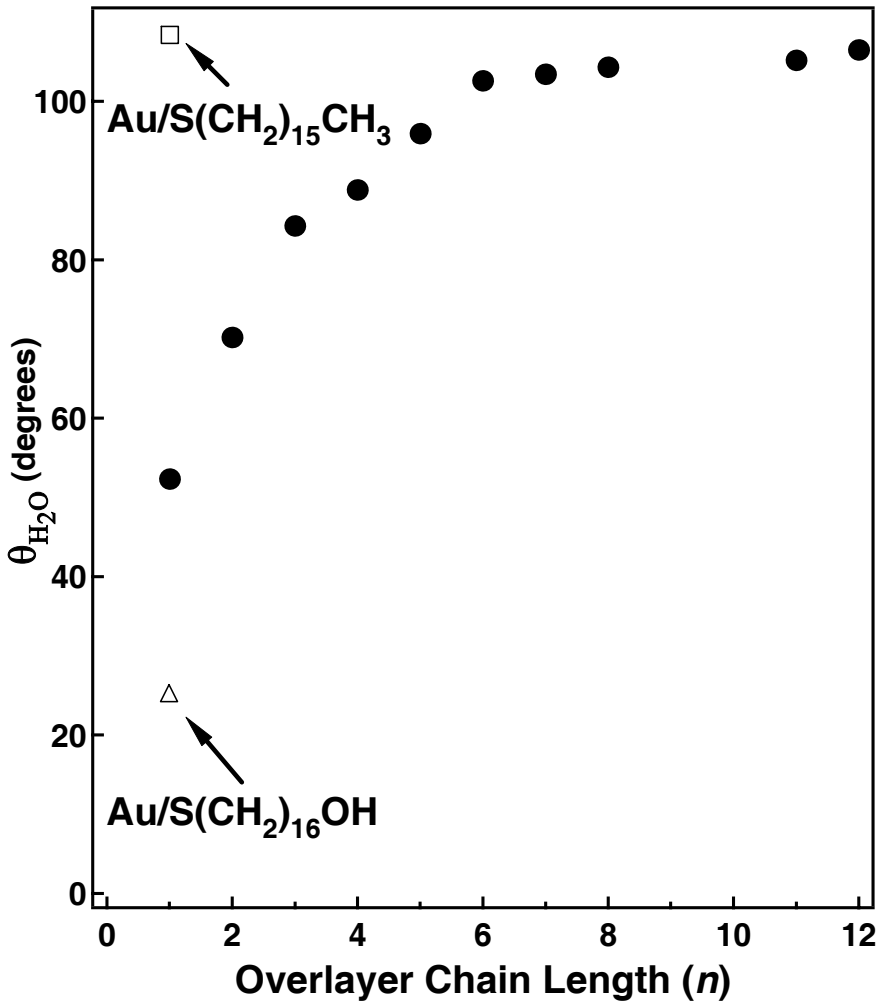

Figure 3.19 Static contact angles of water on carbamate SAMs as a function of the number of carbon atoms, n, in the overlayer (•). Also shown for reference are SAMs of $Au/S(CH_2)_{16}$-OH (Δ) and $Au/S(CH_2)_{15}CH_3$ (□), created via the typical solution-phase deposition method. Error bars are within the diameter of the symbols.

carbamate functionalized SAMs are similar to a long-chain CH_3-terminated monolayer (open square in Figure 3.19). In agreement with RAIR data, it appears that the carbamate groups within the monolayers disrupt the overlayer packing efficiency enough to require van der Waals interactions, involving at least four methylene groups, to recover the type of structure found in simple ω-functionalized alkanethiol SAMs.

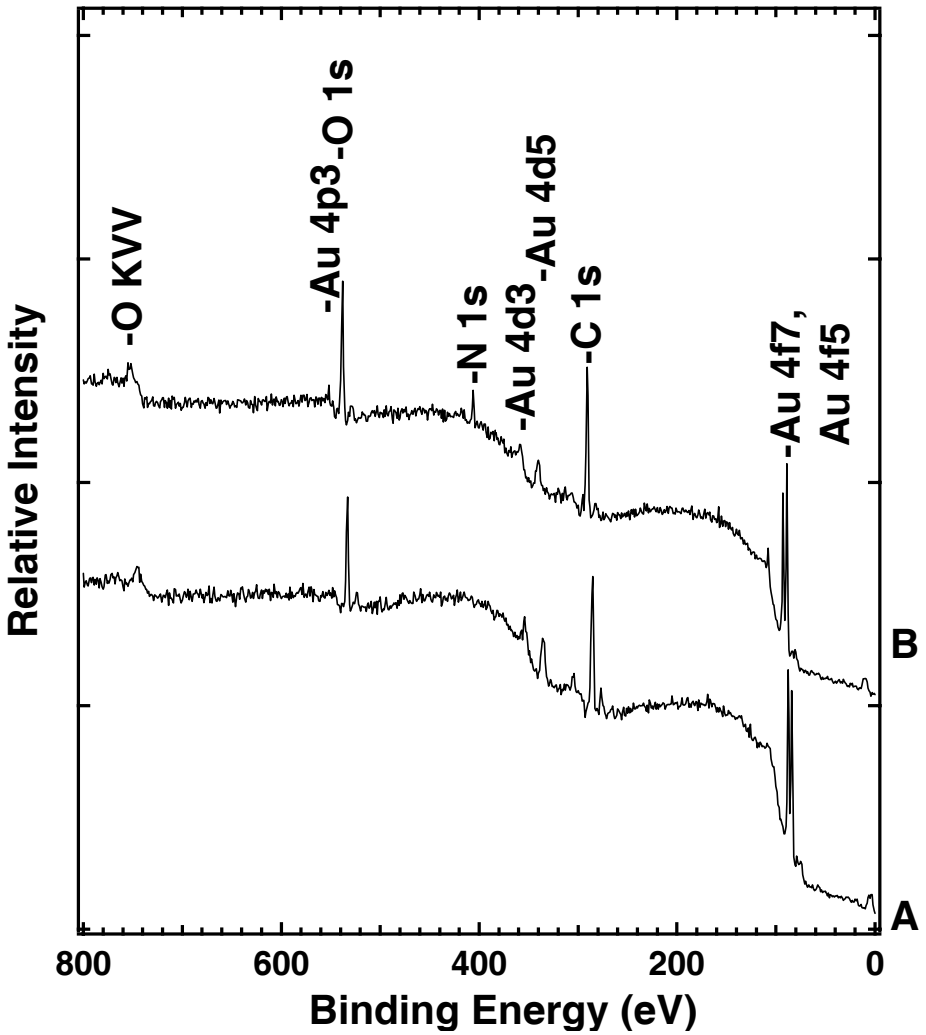

Figure 3.20 XP survey spectra of a hydroxyl-terminated SAM on Au (111) created via the typical solution deposition method (A) and a methyl-carbamate terminated SAM prepared with vapor deposition techniques (B).

3.3.3. X-ray Photoelectron Spectroscopy

XPS provides both a qualitative and quantitative analyses of monolayers or thin films with sensitivity to both elemental composition and bonding environment. Figure 3.20 illustrates survey XP spectra of hydroxyl-terminated and carbamate-functionalized monolayers. The hydroxyl-functionalized SAM was prepared in the traditional solution-phase route, while the carbamate-SAM was created via the vapor-phase reaction of an OH-terminated SAM with methyl isocyanate molecules, and thus has a terminal alkyl

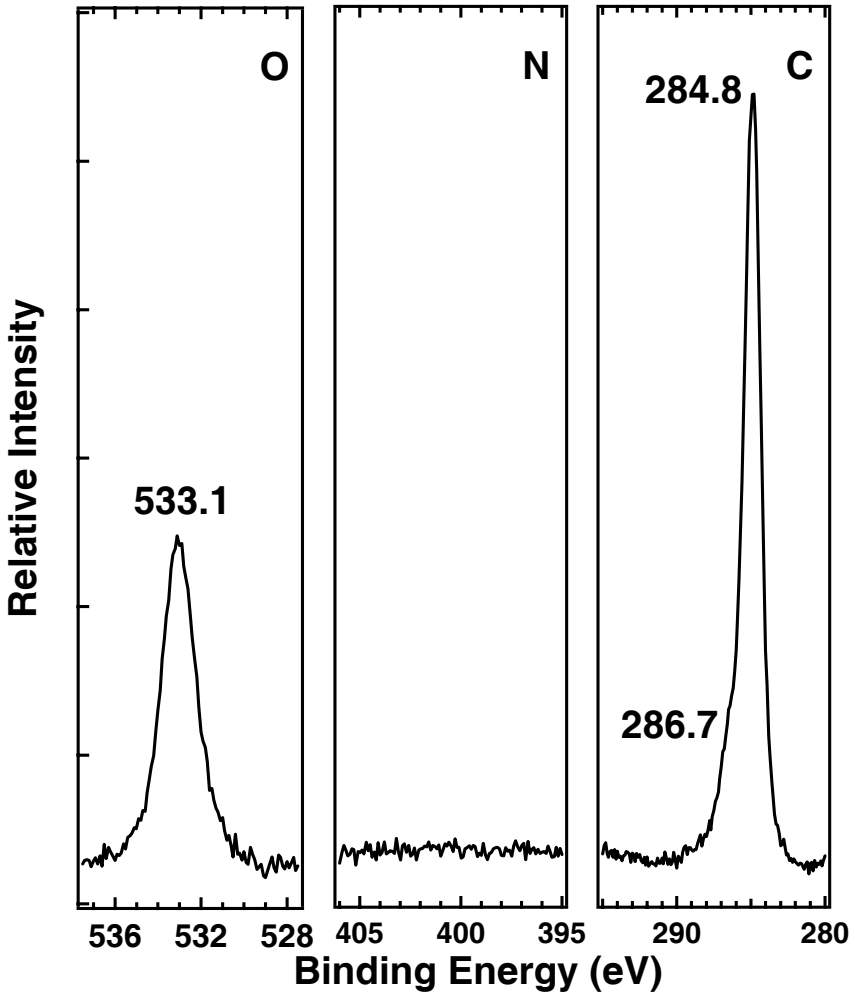

Figure 3.21 High resolution XP spectra of the O (1s), N (1s) and C (1s) regions of a Au/S$(CH_2)_{16}$-OH SAM.

chain length of one carbon atom. The primary features of the survey spectra include signal from O (1s), N (1s), and C (1s) electrons, indicating the presence of the carbamate functional groups. The O KVV Auger peak was not used in the present analysis and the Au photoelectron peaks (4p3, 4f7,4f5) are a result of the substrate.

Closer inspection of these characteristic peaks reveals important information about bonding environment. Figure 3.21 contains high resolution spectra of the O (1s), N (1s) and C (1s) regions of a hydroxyl-terminated monolayer. The O (1s) peak of the SAM is present at 533.1 eV and is consistent with literature values.[135-137] Not unexpectedly, there is an absence of N (1s) signal. The major C (1s) peak, at 284.8 eV, is

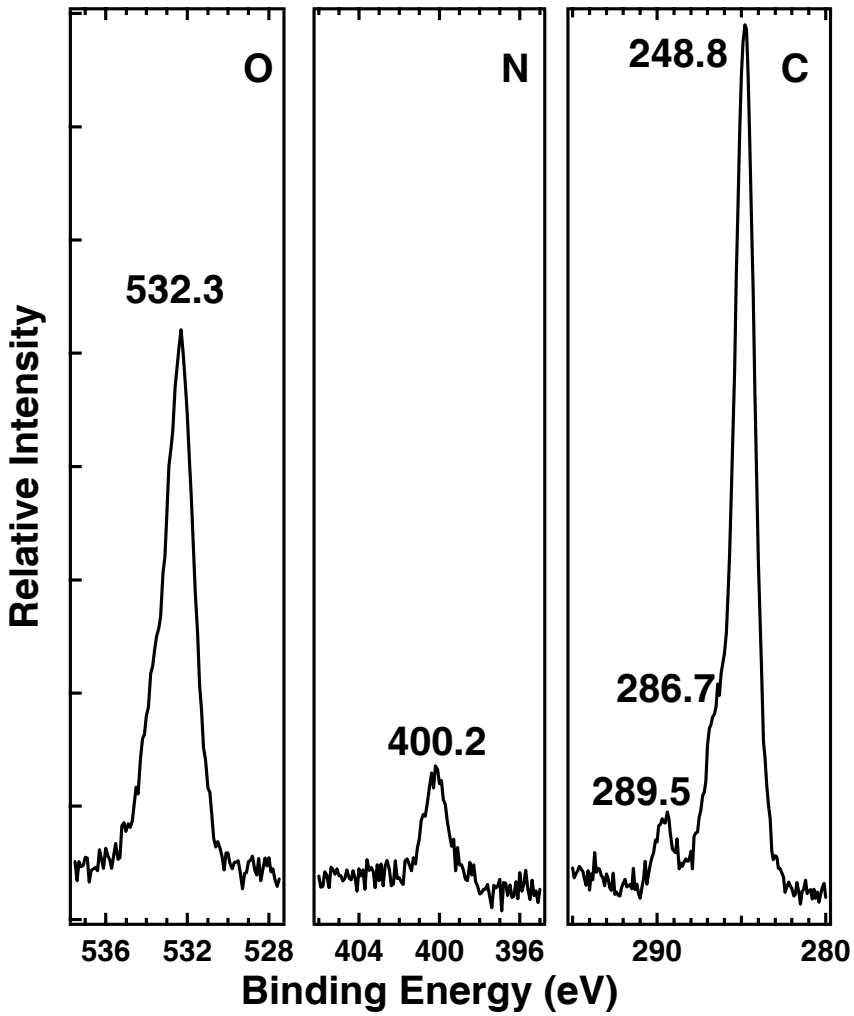

Figure 3.22 High resolution XP spectra of the O (1s), N (1s) and C (1s) regions of a Au/S$(CH_2)_{16}$-O(C=O)NHCH$_3$ SAM.

assigned to the long-chain alkyl backbone of the monolayer, while the shoulder, 286.7 eV, arises from the carbon atom that is adjacent to the terminal heteroatom.[109] The higher binding energy corresponds to the more positive oxidation state of this atom. The high resolution XP spectra in Figure 3.22 are obtained from a methyl-carbamate terminated SAM. Upon reaction with methyl isocyanate, the hydroxyl groups of the template monolayer are converted to carbamate groups. The O (1s) photoelectron peak is present at 532.3 eV. The shift to slightly lower binding energies, relative to the hydroxyl-

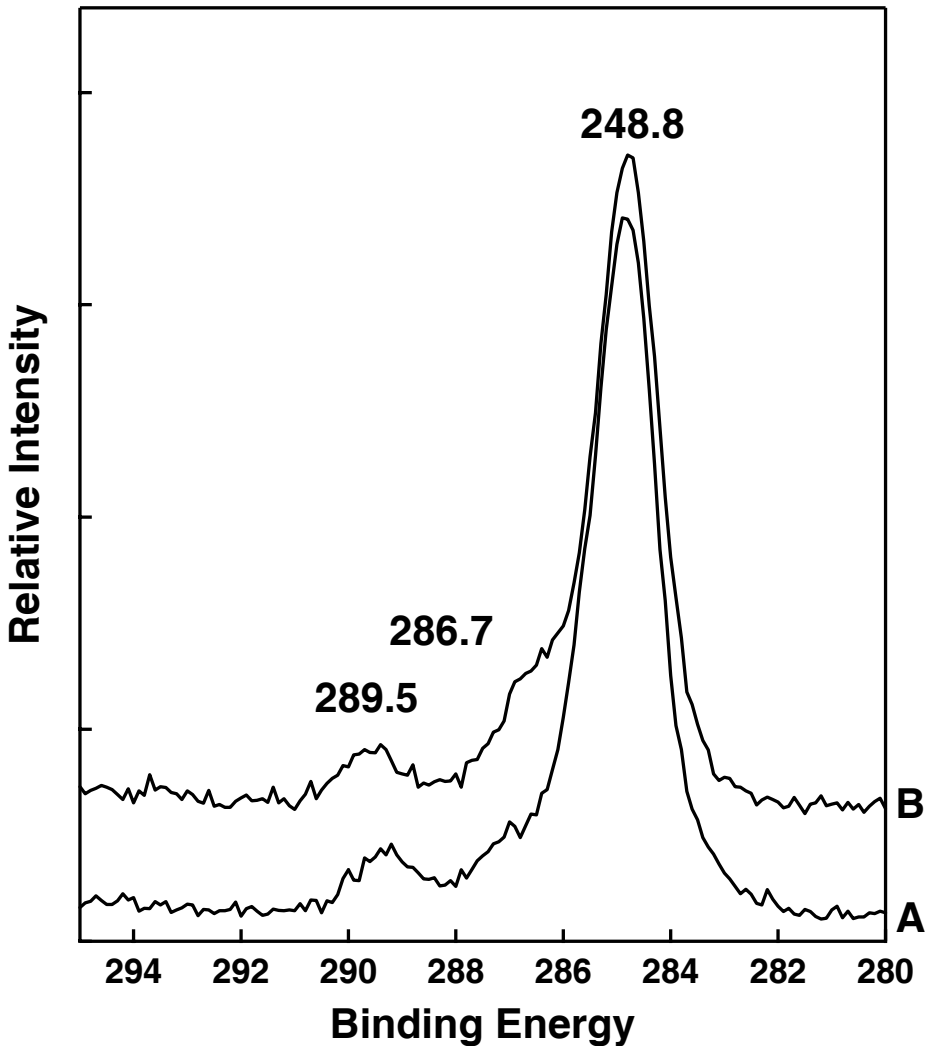

Figure 3.23 High resolution XP spectra of the C (1s) region of $Au/S(CH_2)_{16}$-COOH (A) and $Au/S(CH_2)_{16}$-$O(C=O)NHCH_3$ (B) SAMs.

terminated SAM, is representative of an increased electron density on the oxygen atoms. The nitrogen binding energy of 400.2 eV is consistent with the presence of carbamate functional groups, as is the presence of a multi-component carbon peak.[61]

Figure 3.23 shows a high-resolution spectrum of the C (1s) region of the methyl-carbamate SAM compared to that of an $Au/S(CH_2)_{16}COOH$ monolayer created via the typical solution-deposition method. The C (1s) peak of the carbamate functionalized SAM is split into three components. The most intense peak at 284.8 eV is attributed to

the carbon along the alkane chains, the shoulder at 286.7 eV derives from carbon bound to an electronegative atom such as oxygen or nitrogen, and the small peak at 289.5 eV arises from the carbonyl carbon.[61] The carbonyl signal in the spectrum of the COOH-terminated SAM, also at 289.5 eV, provides an indication of the peak intensity expected for a typical alkanethiol monolayer on gold that contains one C=O for every alkyl chain. Integration of the carbonyl peaks in Figure 3.23 shows that the intensity of the carbonyl peak for the carbamate functionalized SAM is nearly identical to the corresponding peak of the COOH-terminated SAM. This comparison suggests that the OH groups on the template surface react with the vapor-phase isocyanates to yield a monolayer completely or nearly completely converted to carbamate functional groups.

3.3.4. Exposure of SAMs to CWA Simulants

Exposure of methyl- and hydroxyl-terminated SAMs and carbamate-functionalized monolayers to CWA simulants was done in an environment saturated with dimethyl methylphosphonate (DMMP) vapor. The vapor deposition chamber used for high-flux exposure was heated slightly to promote the number of simulant molecules in the vapor-phase. RAIR spectra revealed that no long-term adsorption occurred on any of the three types of surfaces. A low persistence of DMMP on the thin films is not surprising. Hydrogen bonds formed between DMMP and surface hydroxyls or carbamates would have very short residence times, $\sim 10^{-7}$ s. Weak van der Waals interactions would result in even shorter residence times on methyl-terminated SAMs ($\sim 10^{-12}$ s). In both cases observation in the current system is unfeasible. Interestingly, similar studies with the trichlorophosphate and methyl dichlorophosphate reveal similar results. The chlorophosphates are purportedly more reactive than DMMP and still did

not react with the methyl-terminated, hydroxyl-terminated and carbamate-containing SAMs. It is likely that the hydrophobic nature of the well-ordered SAMs prevent diffusion to the carbamate functional groups. Future studies will examine interactions of CWA simulants on carbamate SAMs, prepared with mixed monolayer templates. The more open structure of the SAM on a mixed template may bring about uptake or interfacial reactions between the organophosphonate molecules and the carbamate moieties.

3.4. Conclusions

This study presents a procedure for creating well-ordered self-assembled monolayers (SAMs) that contain laterally hydrogen-bonded carbamate groups located at varying positions below a terminal methyl group. The monolayer chains have the overall form: $Au/S(CH_2)_{16}$-$O(C=O)NH(CH_2)_{n-1}CH_3$. Reflection absorption infrared spectroscopy demonstrates that the alkyl underlayer remains well ordered after reacting with vapor-phase isocyanates. The alkyl overlayer appears well ordered when the total number of carbon atoms in the terminal chain exceeds five. These results demonstrate that vapor-phase reactions for incorporating hydrogen-bonding functional groups within SAMs may produce more organized structures than analogous solution-phase preparation routes.

Carbamate-functionalized SAMs offer a model for CARC materials used by the military. CWA simulant exposure studies suggest that films containing carbamate moieties may have resistance to uptake and reactivity of organophosphonates at room and slightly elevated temperatures. Future studies will investigate the relationship between surface carbamate concentration and positioning with respect to adjacent chains and CWA simulant uptake and reactivity. Thermal studies, in which the SAM is cooled, may

offer insight into the adsorption mechanisms and how surface structure is affected by impinging CWA simulants.

Chapter 4
POSS Langmuir-Blodgett Films: Preparation, Characterization, and Exposure to Dimethyl Methylphosphonate and Trimethylphosphate

4.1. Introduction

The development of efficient decontamination and sensing strategies for organophosphorus compounds has recently received much attention. Previous work highlights the need to develop a fundamental understanding of organophosphonate chemistry on surfaces and within thin films.[27,50] The objective of this study is to continue the development and understanding of interaction pathways of the chemical warfare agent (CWA) simulants dimethyl methylphosphonate (DMMP) and trimethylphosphate (TMP) on surfaces designed to sequester and possibly decompose organophosphonates. The uptake and sorption characteristics of DMMP and TMP on Langmuir-Blodgett (LB) films of trisilanolphenyl-polyhedral oligomeric silsesquioxane (POSS) have been studied.

As illustrated in the idealized schematic of Figure 4.1, the POSS films examined in the present study combine a silica core with hydrogen-bonding silanol groups and organic peripheral substituents. These films provide the opportunity to explore how organophosphonate uptake and reactivity depend on the molecular-level structure and chemical functionality of a novel set of thin films. The combination of oxides and organic species within a single thin film has not been previously investigated as a potential surface for the decomposition of organophosphonates. This type of film provides a high degree of control over chemical properties and may allow for the design of coatings that interact strongly with organophosphonate molecules. Modification of the physical and chemical properties of a given surface can alter molecular interactions and lead to an increase in the specificity and selectivity of the surface.

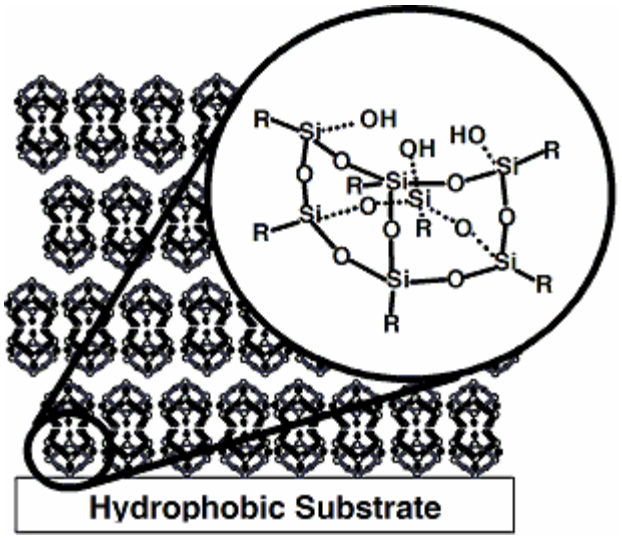

Figure 4.1 Using LB-film deposition techniques, POSS molecules are used to create well-ordered multilayer films that combine a silicon-oxide core with organic ring substituents and silanol groups. In this idealized schematic, R represents phenyl groups.

Silica tetrahedra can be readily assembled into a number of structures including branched networks, ladder-like polymers and eight-cornered cages known as cubic silsesquioxanes. The corners of these ~.5 nm^3 cubes can be functionalized with reactive organic groups (~1.5 nm^3) and incorporated into organic polymers and thin films.[138-142] A large number of silsesquioxane monomers and polymers are available and offer numerous structural frameworks for macromolecular systems.

The interactions of silsesquioxane molecules with adsorbates are not well studied. The reactions of trisilanol cyclohexyl functionalized silsesquioxanes with trifunctional monomers such as $RSiCl_3$, $MeGeCl_3$, $MeSnCl_3$, and $(C_5Me_5)ZrCl_3$ have been reported.[143] Corner capping reactions were shown to readily occur, resulting in completely condensed products.[143] The suitability of polyhedral oligomeric silsesquioxane macromers has also been studied for resistance to fire[144] and atomic oxygen.[145,146] The ability to tailor silicon-oxide structures to meet preferred specifications makes the hybrid inorganic-

organic system highly desirable. In the work described below, the interactions of organophosphonate CWA simulants within POSS LB-films are explored.

4.1.1. Langmuir-Blodgett Films

In addition to traditional solution-phase preparation methods of ordered monolayers (i.e. SAMs, see Section 3.1.2.), Langmuir and Langmuir-Blodgett techniques are widely used in the preparation of thin films. These adaptable techniques have been thoroughly investigated for the creation of films that may be useful in a number of device applications, including sensors, solar cells and insulating/resistive layers. Films prepared from alcohols,[147] esters,[148] amines,[149] substituted aromatic compounds,[150-152] dyes,[153,154] and polymers[155-157] have been reported in the literature. In addition, LB films prepared from amphiphilic molecules, such as phospholipids, pigments, proteins and peptides, can serve as models for biological systems.[158-161]

Langmuir-films, pioneered by Irving Langmuir in the 1910's and 1920's, are prepared by spreading a thin film of amphiphilic molecules at the air-water boundary. The amphiphilic nature of the molecules drives the orientation of the monolayer such that the polar head group is immersed in the water sub-phase, while the more hydrophobic portions of the molecules are directed towards the air. Mechanical controls are used to compress the film, such that a tightly packed array is formed and a uniform surface pressure is maintained through out film deposition. Katherine Blodgett reported the first sequential transfer of Langmuir films to solid substrates in 1934. Figure 4.2 depicts how y-type transfer is used to form the multilayer films, termed Langmuir-Blodgett (LB) films. A hydrophobized substrate is lowered into and through the Langmuir film and the van der Waals interactions between the hydrophobic substrate and amphiphilic molecules

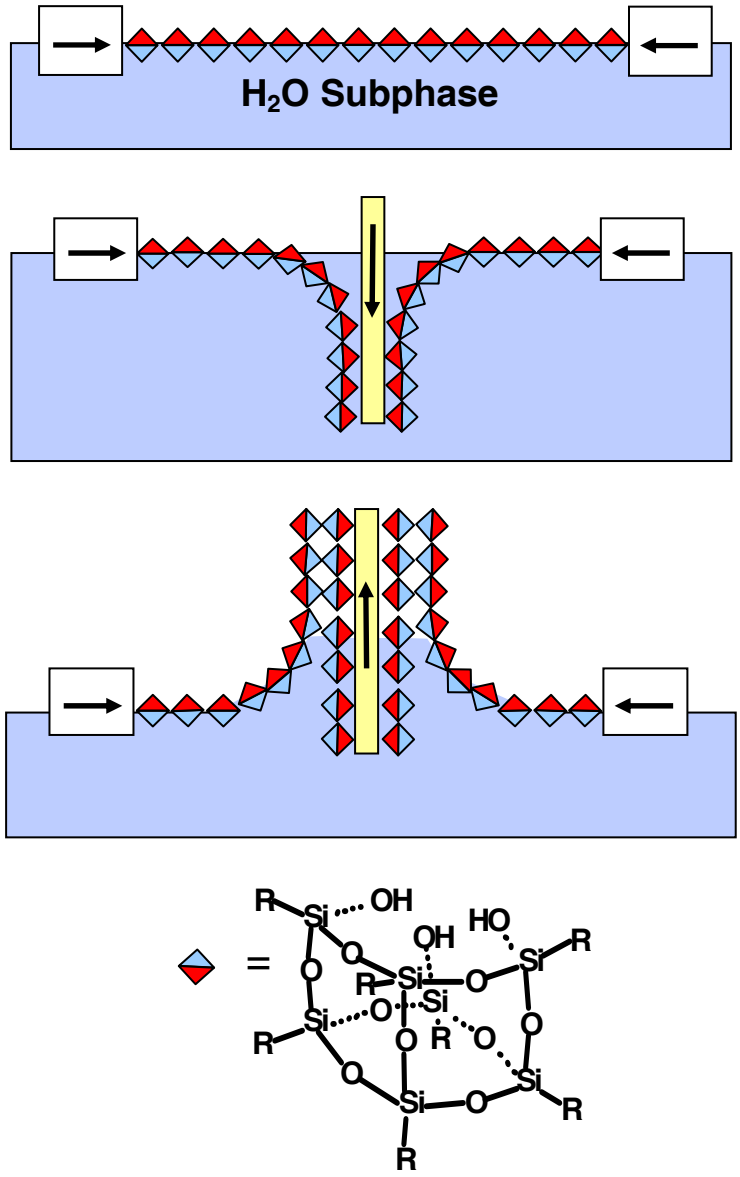

Figure 4.2 A schematic representation of Y-type Langmuir-Blodgett film preparation. The blue side of the square represents the hydrophilic Si-OH side of the POSS molecule.

initiate monolayer growth on the substrate. As the substrate is raised through the monolayer, hydrophilic interactions drive the formation of a bi-layer. Multilayers are formed from repeated raising and lowering of the substrate.[162] Z-type deposition creates films only as the substrate is passed from the water to air and x-type deposition builds multilayers as a substrate is passed from the air to the water.

LB-deposition offers an adequate means for creation of ordered multilayer films. Preparatory methods are highly sensitive to dust and vibrations, therefore to avoid contamination and subsequent seeding of surface defects, great care must be taken. Unlike SAMs, the monomolecular layers of the multilayer film are not chemisorbed to the substrate or neighboring layers. As a result, LB-films are, in comparison, more unstable and have been shown to disorder and deteriorate at elevated temperatures.[163] Nonetheless, Langmuir and LB-films have proven useful in the study of the interfacial chemistry of fatty-acids and other amphiphilic systems. The wide variety of possible structures is promising for the future design of thin-film devices and model systems.

4.1.2. Trisilanol-Phenyl Polyhedral Oligomeric Silsesquioxane LB-Films

Esker et al. have pioneered the use of POSS molecules in thin films prepared using Y-type Langmuir-Blodgett deposition.[142,164] The three silanol groups on the apex of the cubic structures, in conjunction with the hydrophobic organic coronae, drive the self assembly of molecules on a water interface. In turn, ordered films, such as that depicted in Figure 4.1, are created. A variety of surface analytical tools have been used to characterize the POSS films. Surface pressure (Π) versus area per molecule (A) isotherm results, shown in Figure 4.3, reveal that a uniform monolayer of POSS molecules forms on the water interface and has a collapse pressure near 12 mN/m and limiting area of 155 $Å^2$/molecule. Infrared spectroscopy confirms the ordered structure of multilayer LB-systems prepared at a surface pressure of ~10.5 mN/m. The spectra in Figure 4.4 are those of 20 layer POSS films prepared at varied surface pressures (8-10.5 mN/m). Utilizing a transfer pressure that is slightly lower than the collapse pressure ensures that transfer of disordered layers is avoided. A decrease in surface pressure

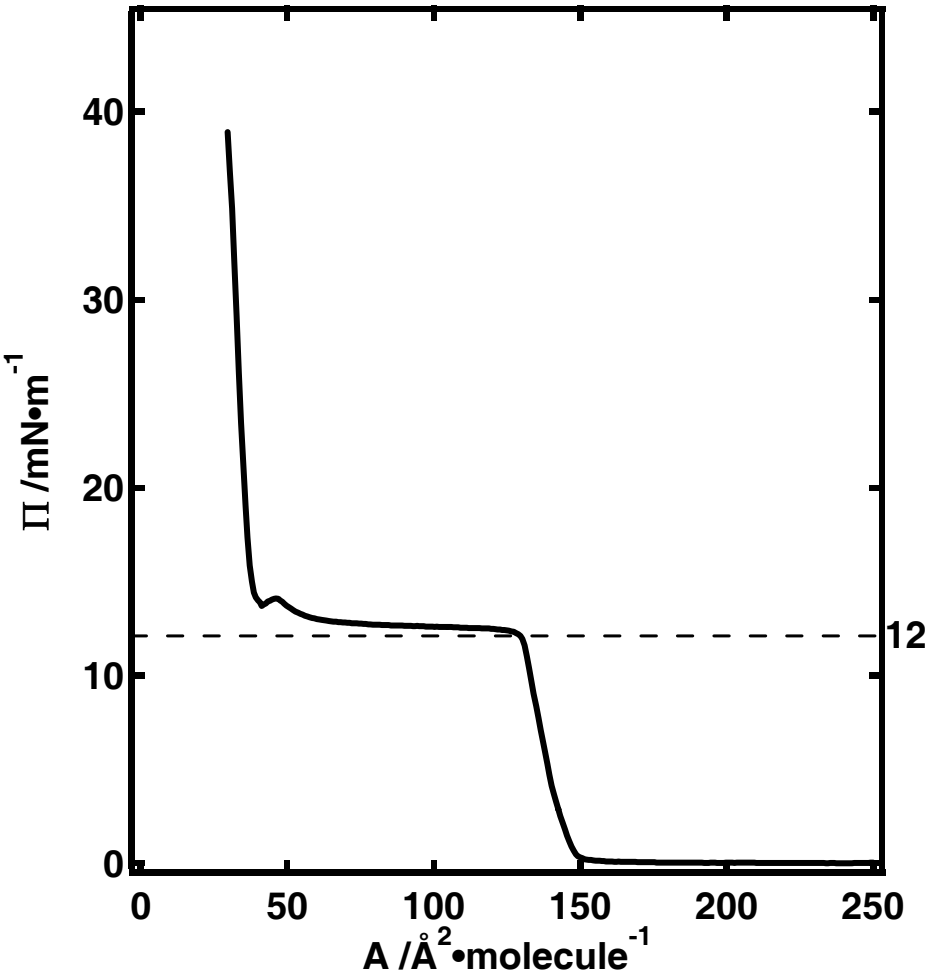

Figure 4.3 Π-A isotherm results reveal a collapse pressure of 12 mN/m and a limiting area of 155 Å^2/molecule.

during transfer, however, results in poor transfer of film layers. This is evidenced by the notable decrease in absorbance signal intensity for films prepared a surface pressure of >8.5 mN/m.

X-ray reflectivity (XRF) data obtained from films of 10, 20, 30, and 40 layers of POSS molecules, illustrated in Figure 4.5, reveals information about film thickness. A plot of the number of POSS layers versus the film thickness, as determined from the intermittent spacing of the interference fringes and Bragg's Law, suggests that the LB-films are uniformly ordered (Figure 4.6). Moreover, the decay of the interference fringes,

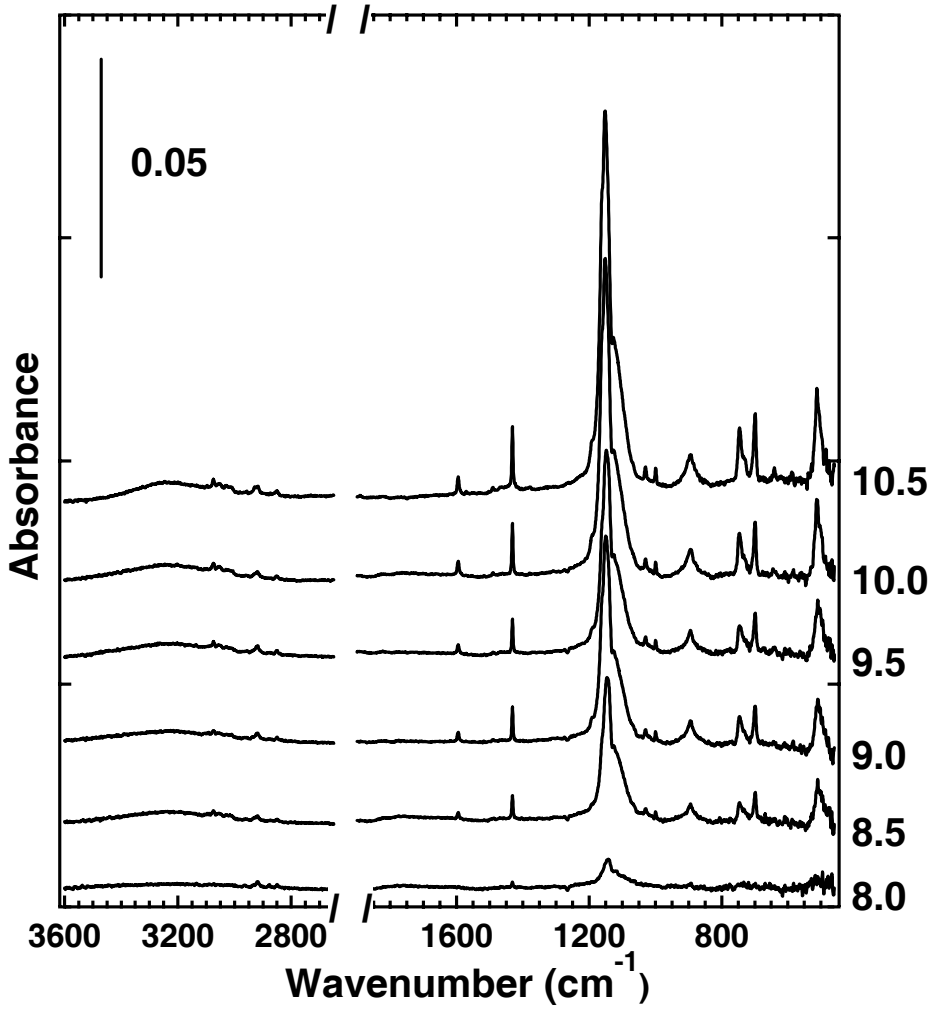

Figure 4.4 RAIR spectra of 20 layer POSS films prepared at varied surface pressures (8-10.5 mN/m). Ordered POSS LB-films are prepared at a surface pressure of ~10.5 mN/m.

as q, the wavevector, increases indicates that the surface roughness of these POSS films is less than 10 Å. POSS LB-films have proven useful in the study of chemical processes, as well as diffusive transport, and here are explored as a unique silicon-oxide system for the sequestering of organophosphonate CWA simulants.

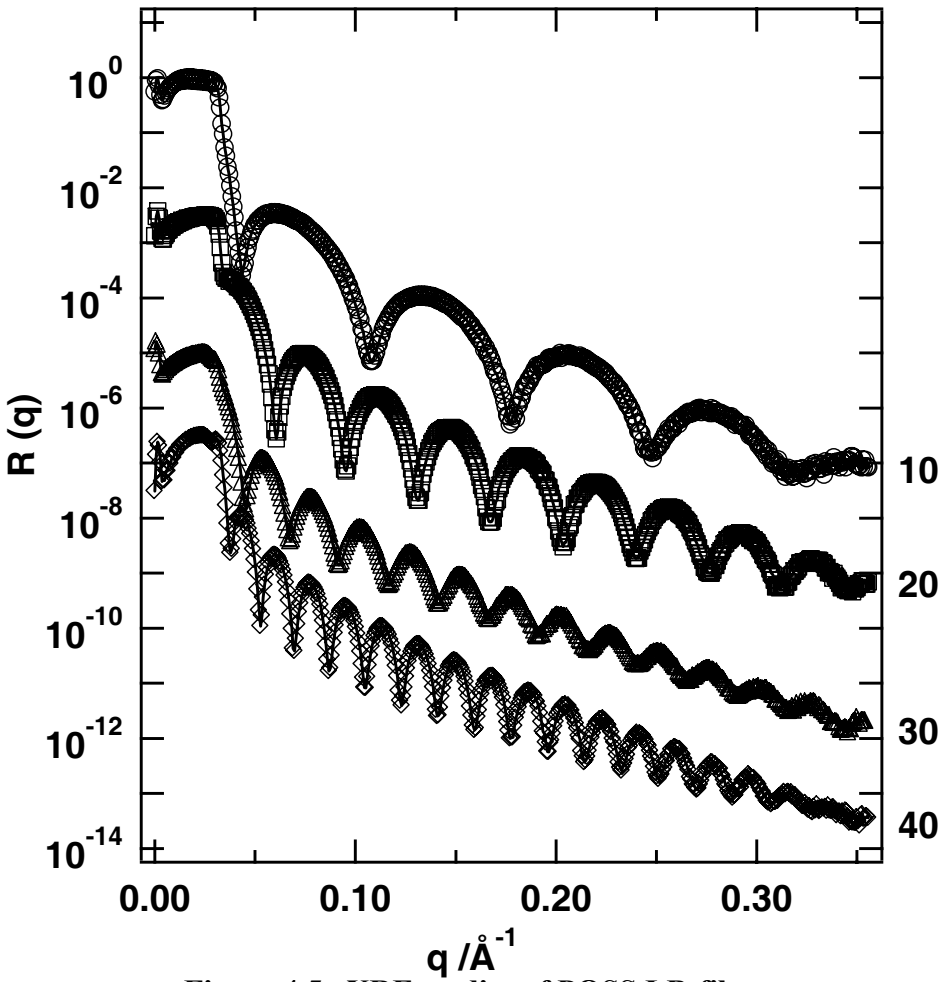

Figure 4.5 XRF studies of POSS LB-films.

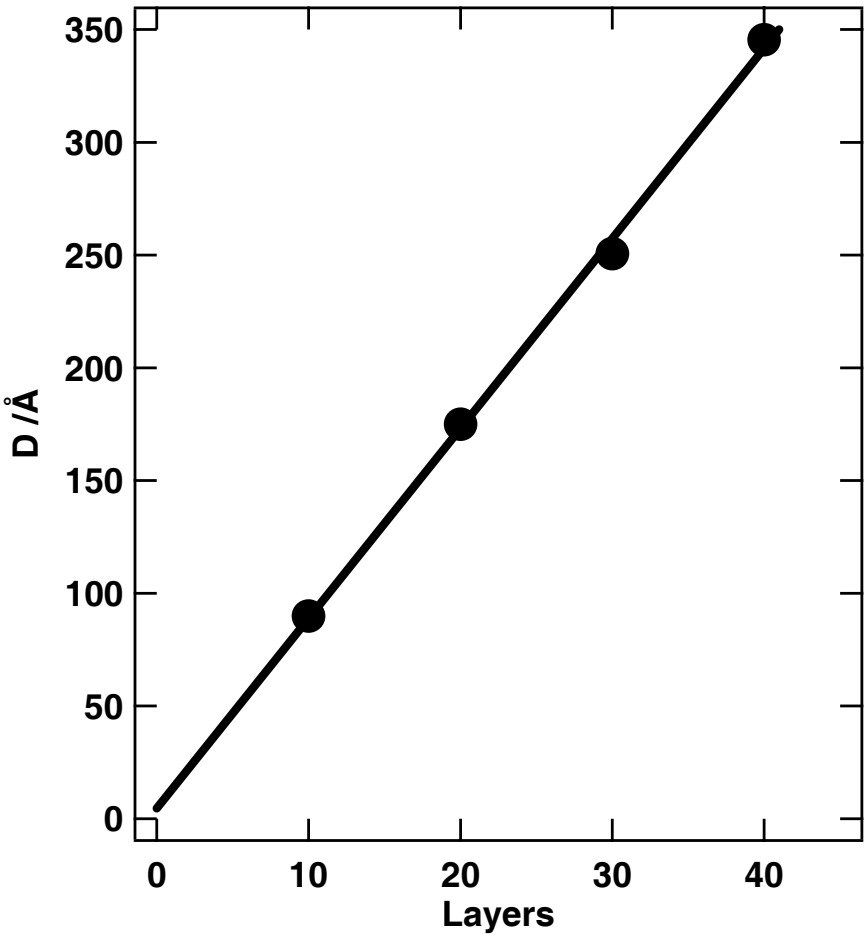

Figure 4.6 The linearity of a plot of the number of POSS layers in a film versus the film thickness implies a highly uniform LB-film.

4.2. Experimental Details

4.2.1. Materials

1-hexadecanethiol (92%), dimethyl methylphosphonate (97%) and trimethylphosphate (99+%) were obtained from Aldrich. Trisilanolphenyl-polyhedral oligomeric silsesquioxane (POSS) and trisilanolethyl-polyhedral oligomeric silsesquioxane (TEP) were obtained from Hybrid Plastics, Inc. All chemicals were used as received. The LB-films were created on hydrophobized gold-coated glass substrates prepared by evaporation of a 50 Å chromium adhesion layer, followed by a coating of

1000 Å of gold (Evaporated Metal Films Corp.).

4.2.2. Langmuir-Blodgett Film Deposition

Gold substrates (1" x 1" x 0.062" and 1 cm x 1 cm x 1 mm) were cleaned in a 3:7 mixture of H_2O_2 (30%):H_2SO_4 (concentrated) (*"piranha solution" is an oxidizing mixture that can be explosive when brought in contact with organic materials*) at room temperature for 1 hour, rinsed with copious amounts of deionized water (18.2 MΩ, Millipore, MilliQ Gradient A-10) and placed in a 1 mM ethanolic solution of 1-hexadecanethiol for approximately 18 h. The resulting alkanethiol SAM served as a hydrophobic surface for LB-film deposition and the underlying gold provided a reflective surface for RAIRS. The smaller gold substrates were used for XPS studies. Films were also prepared on mixed monolayer templates prepared from solutions with varying mole fractions (χ) of OH-terminated ($HS(CH_2)_{16}OH$) and CH_3-terminated ($HS(CH_2)_{15}CH_3$) alkanethiols.

Silicon wafers were used to prepare POSS LB-films for XPS studies. The wafers were initially cut to 1" x 1" sizes and cleaned for 2 hours in 28% NH_4OH:30% H_2O_2:Millipore water (1:1:5 ratio by volume). The substrates were then cleaned in a 3:7 mixture of H_2O_2 (30%):H_2SO_4 (concentrated). The silicon was hydrophobized using a buffered oxide etch (HF) and a 40% NH_4F solution (Doe and Ingalls, CMOS grade).

LB-films were prepared on a standard LB-trough (KSV 2000, KSV Instruments, Inc.) housed in a Plexiglas box held at 300 K. The clean trough was filled with ultra-pure water (18.2 MΩ, Millipore, MilliQ Gradient A-10), and a 0.5 mg/mL solution of POSS in chloroform was used to spread the film across the air-water interface.

POSS was spread to a pressure of 5-8 mN/m to eliminate the possibility of bi- or

multi-layer formation. Upon evaporation of the chloroform, the monolayer film was compressed to 10.5 mN/m and held constant at this pressure during film deposition. The hydrophobic substrate was raised and lowered at a rate of 10 mm/min, with an upper delay of 60 s and a lower delay of 15 s between layers.

After the desired number of layers was deposited, the freshly prepared films were stored in petri dishes at room temperature and pressure for further analysis. Control experiments revealed that placing the films in a vacuum for ~18 hours had no measurable affect on the results presented here. The POSS-coated silicon wafers were cleaved to approximately 1 cm x 1 cm prior to usage. A stream of ultra-pure N_2 was used to remove any particulate matter from the film surface preceding use.

4.2.3. Solution-Phase Preparation Methods

In an effort to create a surface structure that could be compared to the interfacial characteristics of ordered LB-films, POSS and TEP films were prepared using solution-phase routes. Clean Au substrates, as well as SAMs prepared from solutions with varying mole fractions (χ) of OH-terminated ($HS(CH_2)_{16}OH$) and CH_3-terminated ($HS(CH_2)_{15}CH_3$) alkanethiols, were immersed in 1 mM ethanolic solutions of the cubic silsesquioxane molecules. The exposure duration of the substrate in the silsesquioxane solution was determined to be independent of the film quality. Due to the weak interactions that drive the formation of the multilayer films, rinsing the sample substrates prior to analysis proved detrimental to the structure. Therefore, the solution-phase films were not rinsed prior to analysis, but were dried in a stream of ultra-pure N_2.

4.2.4. Characterization of LB-Films and Interactions with CWA Simulants

4.2.4.1. Reflection Absorption Infrared Spectroscopy

RAIRS measurements were performed using a Bruker IFS 66v/S spectrometer. Spectra were collected using p-polarized light at an incident angle of 86° and a liquid N_2 cooled MCT (mercury-cadmium-telluride) or a DTGS (deuterated-triglycine-sulphate) detector. Clean gold substrates were used as background references. Each spectrum was collected using a resolution of 2 cm^{-1} and is the average of 100 scans.

4.2.4.2. X-ray Photoelectron Spectroscopy

XPS was performed on a Perkin Elmer 5400 X-ray Photoelectron Spectrometer equipped with a monochromatized Mg(Kα) radiation source (1253.6 eV) and a position sensitive, multi-channel plate detector. Measurements were taken at a pressure of ~10^{-7} mbar and a take-off angle of 15° with respect to the surface normal. Binding energies are referenced to C (1s) at 284.8 eV. High resolution multiplex spectra were collected with an acquisition time of 8 minutes per region, a 1 mm x 3.5 mm spot size, and 300 W electron beam power.

4.2.4.3. Temperature Programmed Desorption Measurements

TPD measurements were performed in the UHV instrument described in Section 2.2.1. The DMMP-saturated POSS films were installed via a load-lock chamber and laser-aligned to place the normal in-line with the two collimating apertures of the Extrel mass spectrometer. The ionizer of the mass spectrometer is positioned 29 cm from the surface and views a 1 cm^2 spot size on the surface. The thermocouple was positioned at the face of the sample mount and a linear heating ramp of 0.1 K s^{-1} was employed. With no evidence of reaction products desorbing from the surface, the major fragments of

molecular DMMP, m/z 94, and molecular TMP, m/z 110, were monitored and used to determine the adsorption energy. TPD spectra were highly reproducible and showed a linear dependence of the peak intensity on the number of layers in the LB-films.

4.2.4.4. Uptake Coefficient Measurements

The uptake coefficient of DMMP on POSS was examined according to the King and Wells technique. Experiments were conducted in an ultra-high vacuum (UHV) chamber with a base pressure of 5 x 10^{-10} Torr, equipped with an Extrel mass spectrometer. At 303 K, DMMP is a liquid with a vapor pressure of 1.06 Torr. Molecular beams of DMMP were created by bubbling N_2 (~750 Torr) through a DMMP liquid reservoir held at 353 K. The resulting DMMP/N_2 vapor entered the first differential pumping stage (2.6 x 10^{-5} Torr) through a 0.05 mm diameter nozzle (General Valve). A 0.40 mm diameter conical skimmer located 6 mm from the nozzle collimated the beam before it entered a second differential pumping stage. The DMMP/N_2 beam then passed through a 1.5 mm collimating aperture, located in a third differentially-pumped chamber, before passing into the main UHV chamber through a 2.2 mm aperture. The beam strikes the surface with a spot size of 1 cm^2. Uptake measurements were recorded for a range of surface temperatures from 138 K to 298 K.

Using the King and Wells technique to measure uptake probability, a Teflon® flag was placed in the main UHV chamber to block the beam's path and prevent it from striking the surface. The partial pressure of DMMP/N_2 in the main chamber was measured with the mass spectrometer. The fraction of the incident beam that adsorbed on the surface was determined from the decrease in the partial pressure as the beam was allowed to strike the surface.

Adsorption energies were calculated according to equation 1:

$$\Re = \nu_n \cdot \theta^n \cdot e^{\frac{-E_a}{RT}} \quad (1)$$

where $\Re$ is the desorption rate of a species from a surface, ν_n is the preexponential factor and typically assumed to be 10^{-13} s^{-1},[84] n is the reaction order, θ is the coverage of adsorbates, E_a is the adsorption energy, R is the molar gas constant, T is the temperature. The data presented here describes zeroth order systems, thus E_a and ν_0 are assumed to be coverage independent and the slope of a plot of ln ($\Re$) versus $1/T$ reveals E_a.

4.2.5. CWA Simulant Exposure Studies

4.2.5.1. High-Vacuum Organophosphonate Vapor Exposure

Controlled exposure of the POSS LB-films to organophosphonate vapor was accomplished in the high vacuum system coupled to the RAIR spectrometer (Section 2.2.2.). The base pressure of the vacuum chamber was 10^{-6} Torr. Organophosphonate molecules were entrained in a beam of ultra-pure N_2 using the bubbler apparatus described in Section 2.2.1.1. During exposure the pressure rose to 10^{-2} Torr and interfacial interactions were monitored *in situ* with RAIRS.

4.2.5.2. Saturated Organophosphonate Vapor Sorption

Complete saturation of POSS films with DMMP was accomplished by placing the film in an atmosphere saturated with DMMP vapor. POSS films were placed in a 60 cm^3 vapor deposition chamber initially purged with N_2 and approximately 5 μL of the DMMP was introduced via pipette. The gas-phase concentration of the DMMP molecules was kept high by heating the chamber mildly to 308 K. RAIR studies revealed that the POSS

film saturated after 10 min of exposure under these conditions (Figure 4.16). After ten minutes, a film has been exposed to ~1 x10^{8} langmuirs of DMMP, where 1 langmuir is equivalent to 10^{-6} Torr · s.

4.3. Results and Discussion

4.3.1. Film Structure

4.3.1.1. Reflection Absorption Infrared Spectroscopy

4.3.1.1.1. Ordered POSS LB-Films

The RAIRS results presented here indicate that POSS can form a multilayer LB-film with a well-ordered structure. Further insights into the molecular structure and order of the films are revealed by the infrared spectra of Figures 4.7 and 4.8, which indicate the peak positions and the mode assignments of the primary transitions for the POSS films. The spectra are found to be highly reproducible for the range of multilayers studied. Furthermore, the POSS films are found to be reasonably stable at room temperature for weeks and can retain their well-ordered structure to temperatures above 100 °C. At higher temperatures, the loss of Si-O-H vibrational modes in the RAIRS data indicates that the open ends of the POSS molecules may cross-link or close, rendering the films inert (see Figure 4.10).

Figure 4.7 shows the high frequency region of the RAIR spectra for films containing 10, 20, 30 and 40 layers of POSS molecules. The broad Si-O-H mode at 3262 cm^{-1} is indicative of a high degree of hydrogen-bonding among the POSS molecules that form the highly-dense, well-ordered film. The shape and position of this peak are in sharp contrast to the free Si-O-H stretching mode exhibited on a silica surface containing only isolated hydroxyl groups, which occurs at 3747 cm^{-1}. The high energy region of the

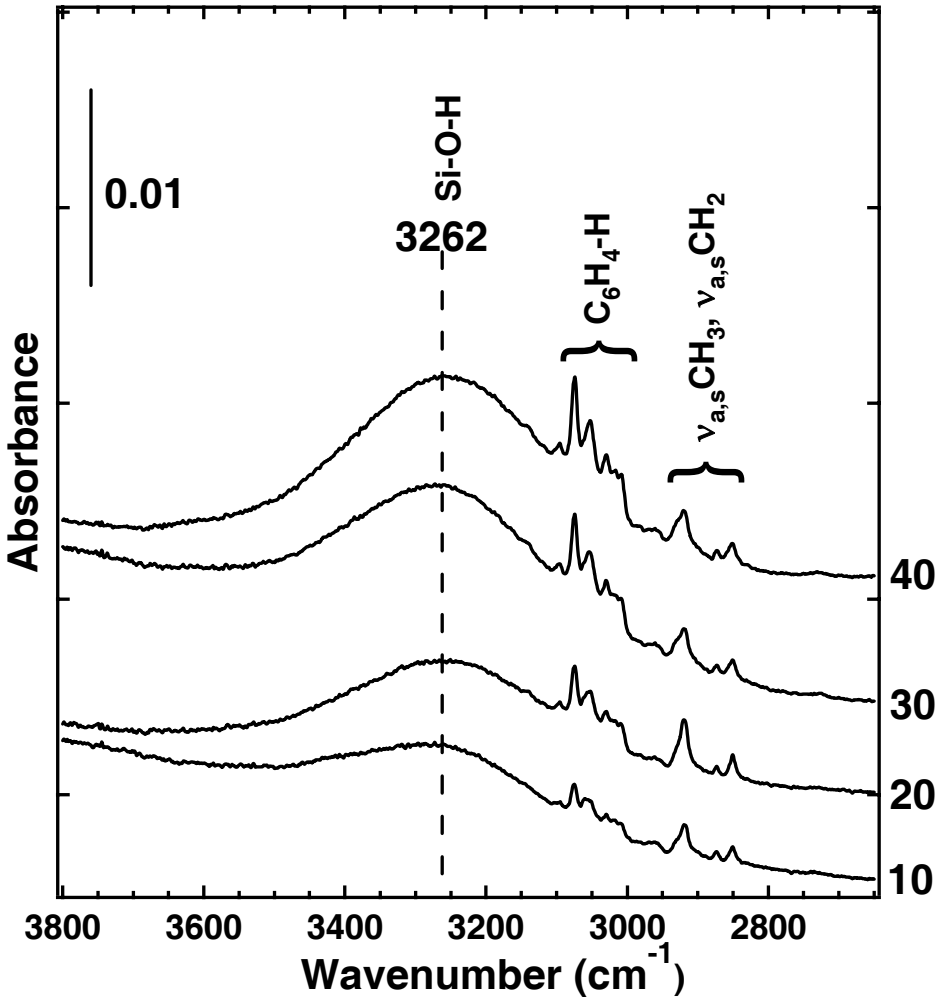

Figure 4.7 RAIR spectra of trisilanolphenyl-polyhedral oligomeric silsesquioxane (POSS) Langmuir-Blodgett films containing 10, 20, 30, and 40 layers. The films exhibit a high degree of hydrogen bonding as evidenced by the Si-O-H mode at 3262 cm^{-1}.

spectrum also contains peaks associated with the vibrational modes of the phenyl rings (2997-3110 cm^{-1}) and the underlying alkanethiol self-assembled monolayer (2835-2976 cm^{-1}). The CH_2 vibrational modes are unchanged after LB-film deposition, suggesting that the SAM structure is unaffected by the deposition of POSS molecules.

The low frequency modes, shown in Figure 4.8, confirm a high degree of hydrogen-bonding between the POSS molecules. Si-O-H modes for non-hydrogen-bonded groups have been reported at 863 and 768 cm^{-1}, RAIRS data of POSS films

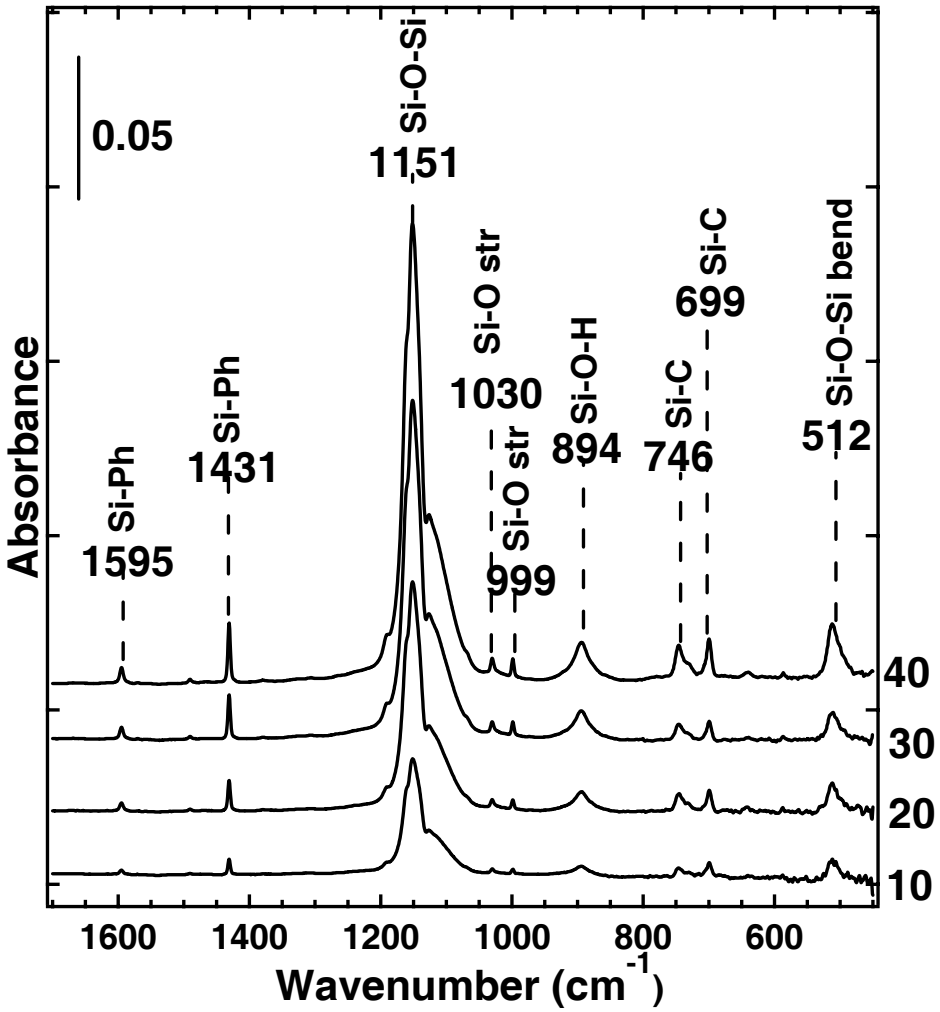

Figure 4.8 RAIR spectra of POSS Langmuir-Blodgett films containing 10, 20, 30, and 40 layers. The films exhibit a high degree of hydrogen bonding.

discussed here contains a broad Si-O-H stretch positioned at 894 cm^{-1}. This region of the spectrum further reveals a broad, intense Si-O-Si stretch at 1151 cm^{-1} and peaks at 1595, and 1431 cm^{-1} resulting from the phenyl modes. Peaks at 1030 and 999 cm^{-1} are likely associated with Si-O stretches of the polyhedral oligomeric silsesquioxane molecules, while an Si-O-Si bending mode is visible at 512 cm^{-1}.[165] Modes associated with Si-C vibrations are present at 746 and 699 cm^{-1}.[165]

The RAIRS data show that as the deposited number of layers increases from 10 to 40, the IR absorbance increases linearly. The integrated area of the peaks positioned at 894 and 1431 cm^{-1} are shown in Figure 4.9 and the integrated peak area of the major Si-O-Si mode at 1151 cm^{-1} is displayed in the inset. The linearity of these plots further confirms the high degree of order present in the POSS LB-films and is in accord with Beer's Law (equation 2),

$$\boldsymbol{A = \varepsilon bc} \tag{2}$$

where $\boldsymbol{A}$ is the absorbance ($log_{10}\ P_0 / P$), $\boldsymbol{\varepsilon}$ is the molar absorptivity, $\boldsymbol{b}$ is the path length, and $\boldsymbol{c}$ is the concentration of the analyte. Furthermore, the conformity with Beer's Law substantiates that the orientation of each bilayer adsorbed on the substrate is the same. If bilayer orientations were in fact different through out the multilayer film, surface selection rules would suggest that the system would not adhere to Beer's Law. The difference in slope for the modes displayed in Figure 4.9 is also accounted for by the variability of the molar absorptivity for the different infrared active modes and the surface selection rule that says only vibrations with a dipole component aligned perpendicular to the surface plane can interact with the incident IR light. Thus, the orientation of the dipole in molecular vibrations affects the absorption intensity, as well as the intrinsic molecular properties.

Control studies indicate that the ordered POSS multilayer systems are resistant to deterioration at elevated temperatures. The spectra presented in Figure 4.10 are those of a freshly prepared 36 layer POSS film (A), that has been sequentially heated to 370 K for 1.5 hours (B) and 440 K for 1 hour (C). These results demonstrate that upon heating to ~100 °C for 1.5 hours, the underlying SAM layer is decomposed and desorbed, as

evidenced by the loss of absorbance intensity of the C-H bands near 2900 cm^{-1}. Furthermore, a loss of hydrogen-bonded Si-OH intensity in the higher frequency regions of the spectrum and a loss of intensity of the Si-OH bending mode near 900 cm^{-1} suggests a loss of the trisilanol groups at the apices. It is likely that the "open" corner of the cage structure is closed due to crosslinking within the molecular unit or with adjacent molecules, resulting in a loss of water.

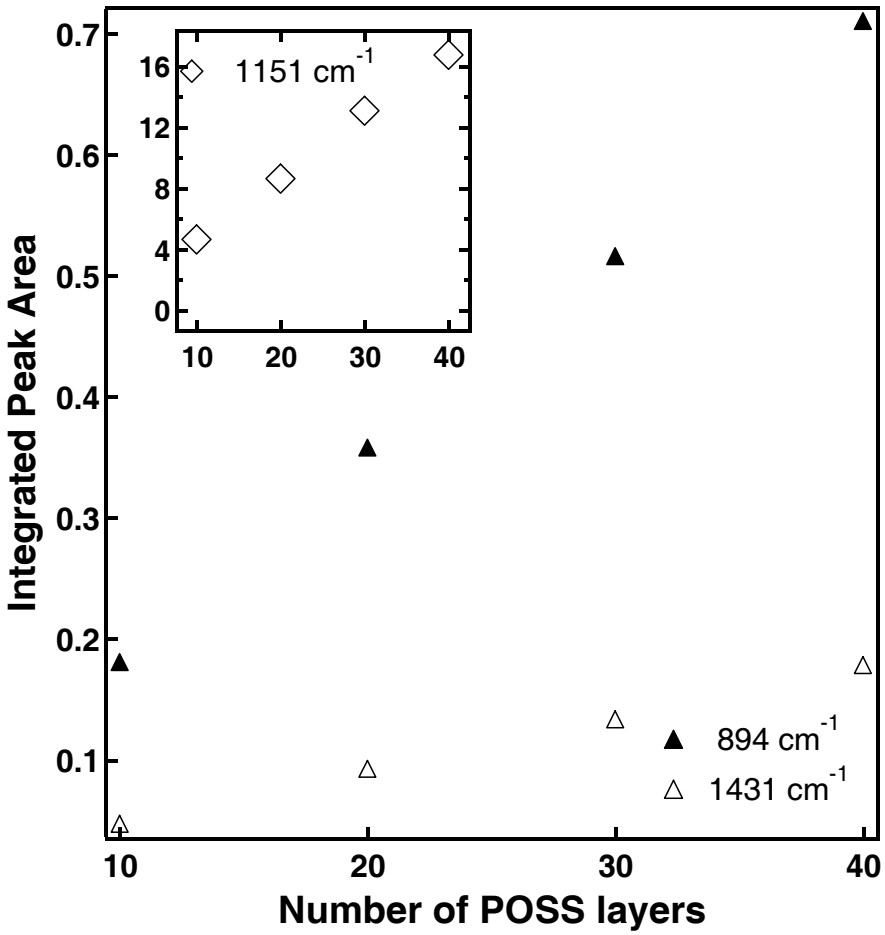

Figure 4.9 RAIRS peak integrations for major modes of the POSS films. The linearity suggests that the multilayer films are well-ordered.

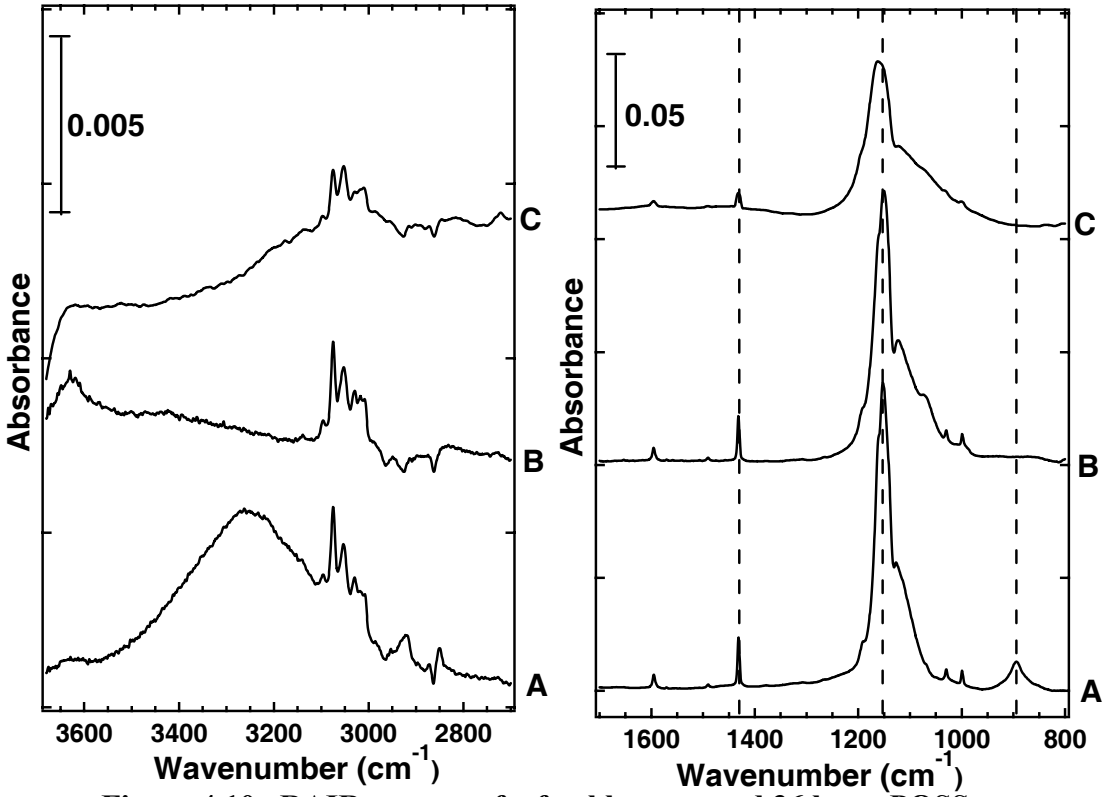

Figure 4.10 RAIR spectra of a freshly prepared 36 layer POSS LB-film (A), heated sequentially at 370 K for 1.5 hours (B) and at 440 K for 1 hour.

4.3.1.1.2. POSS LB-Films Prepared on Mixed Monolayer Templates

Multilayer POSS LB-films prepared on mixed monolayer templates suggest that, regardless of monolayer template structure, the POSS molecules may orient in such a way that a high degree of ordered is maintained despite potential losses of intermolecular attractions. The spectra in Figure 4.11 are obtained from 10 layer POSS films prepared from solutions with varied mole fractions (χ) of OH-terminated ($HS(CH_2)_{16}OH$) and CH_3-terminated ($HS(CH_2)_{15}CH_3$) alkanethiols. The characteristic peaks of ordered POSS LB-films, reported in Figure 4.7 and Figure 4.8, are present in the RAIR spectra of Figure 4.11. The spectra are nearly identical and any subtle differences in multilayer structure, as a result of the monolayer template, are not apparent.

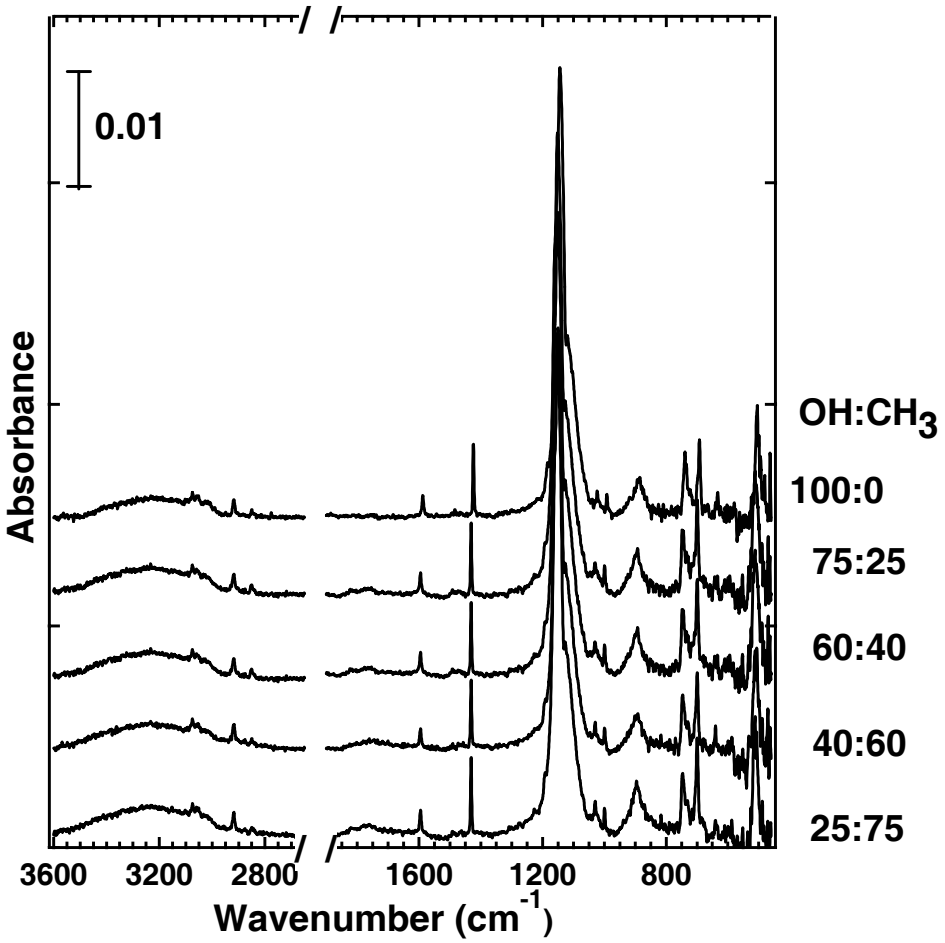

Figure 4.11 RAIR spectra of 10 layer POSS LB-Films prepared on mixed monolayer templates. The ratio of OH-terminated ($HS(CH_2)_{16}OH$) and CH_3-terminated ($HS(CH_2)_{15}CH_3$) alkanethiols in the template solution is indicated on the vertical axis.

4.3.1.1.3. POSS and TEP Films Prepared via Solution-Phase Routes

Spectra of POSS films, prepared on clean gold and a variety of mixed template monolayers with solution-phase deposition of the silsesquioxane molecules, are shown in Figure 4.12. Each of the spectra appears nearly identical, similar to spectral results obtained from POSS LB-films prepared on mixed monolayer templates. However, unlike the order implied by the spectra in Figure 4.11, the solution deposited films appear less well-ordered. The primary difference between the solution-deposited films and ordered POSS LB-films is the extent of hydrogen bonding interactions between the silanol groups

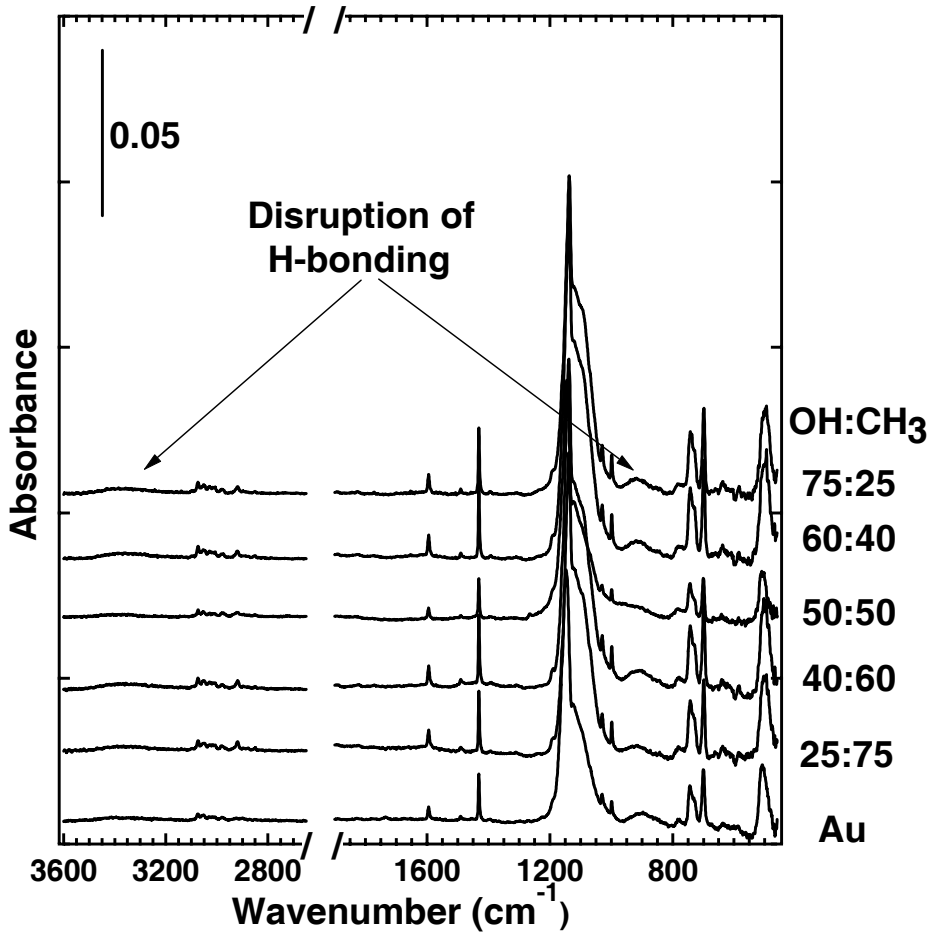

Figure 4.12 RAIR spectra of POSS films prepared on a clean Au substrate and mixed monolayer templates. The films were prepared via the solution-phase approach.

of the inorganic/organic hybrid molecules. A distinct loss in absorbance intensity of the hydrogen-bonded Si-O-H mode centered on 3262 cm^{-1} and a broadening of the Si-O-H bending mode at approximately 894 cm^{-1} support this assertion. In addition to the disruption of the intermolecular hydrogen-bonded network, the Si-O-Si backbone modes around 1151 cm^{-1} have broadened, suggesting a change in orientation of the cage-like structures.

Trisilanolethyl polyhedral oligomeric silsesquioxane (TEP) molecules do not offer sufficient hydrophobic/hydrophilic interactions for the successful creation of LB-films. The solution-phase preparatory methods are, however, successful for creating thin

films of the ethyl-functionalized silsesquioxane cage structures. The spectrum of a solution-deposited TEP film on a clean gold substrate is reported in Figure 4.13. The absorbance intensity is on the order of solution-deposited POSS films, and approximately equivalent to the intensities observed for 30 layer POSS LB-films. The notable features of the spectrum are the enhanced C-H asymmetric and symmetric stretching vibrations (2980-2860 cm^{-1}) and the deformations of the Si-C moieties (1490-1390 cm^{-1} and 1255 cm^{-1}).

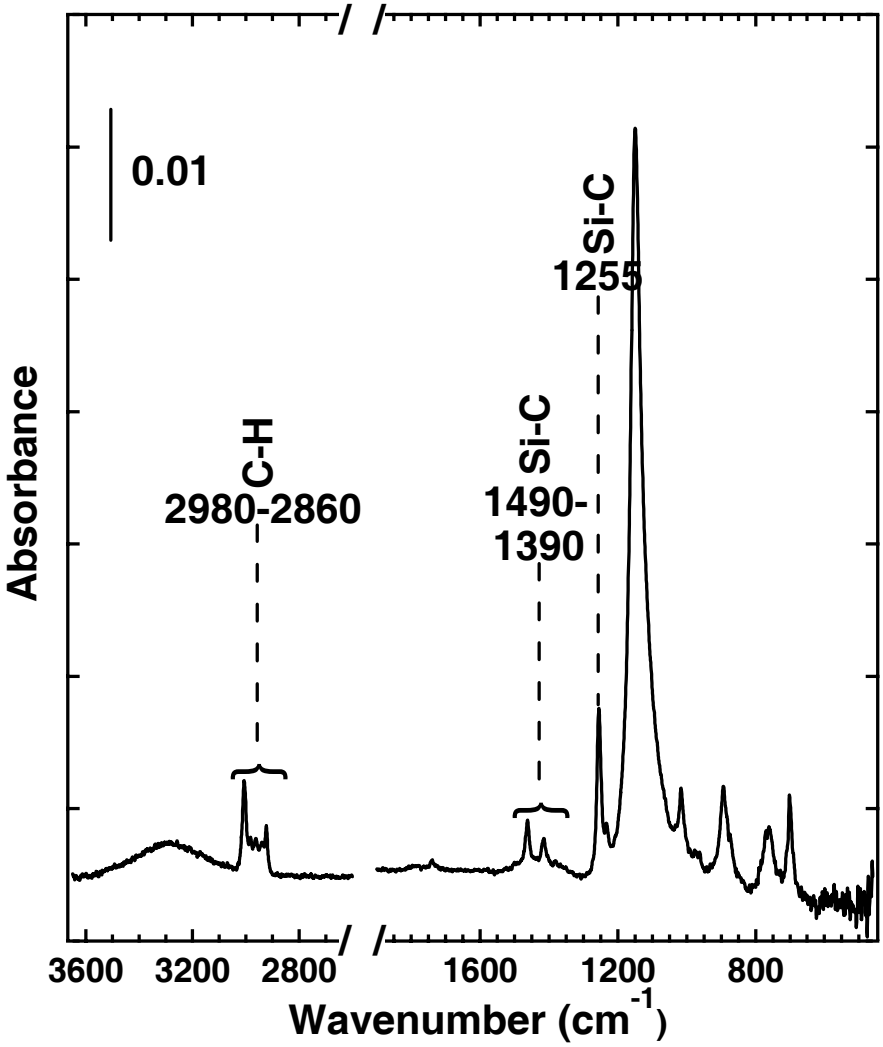

Figure 4.13 The RAIR spectrum of a TEP film prepared using solution deposition of the silsesquioxane molecules.

4.3.1.2. X-ray Photoelectron Spectroscopy

The elemental composition and bonding environment of a freshly-prepared POSS LB-film was assessed with XPS. Figure 4.14 shows the XP survey spectra of a 40 layer POSS film. The primary features of the survey spectra include signal from the silicon and oxygen atoms comprising the cubic-structure of the POSS molecules and the carbon atoms present in the phenyl ring substituents. Signal from the underlying silicon substrate also makes contributions to this spectrum.

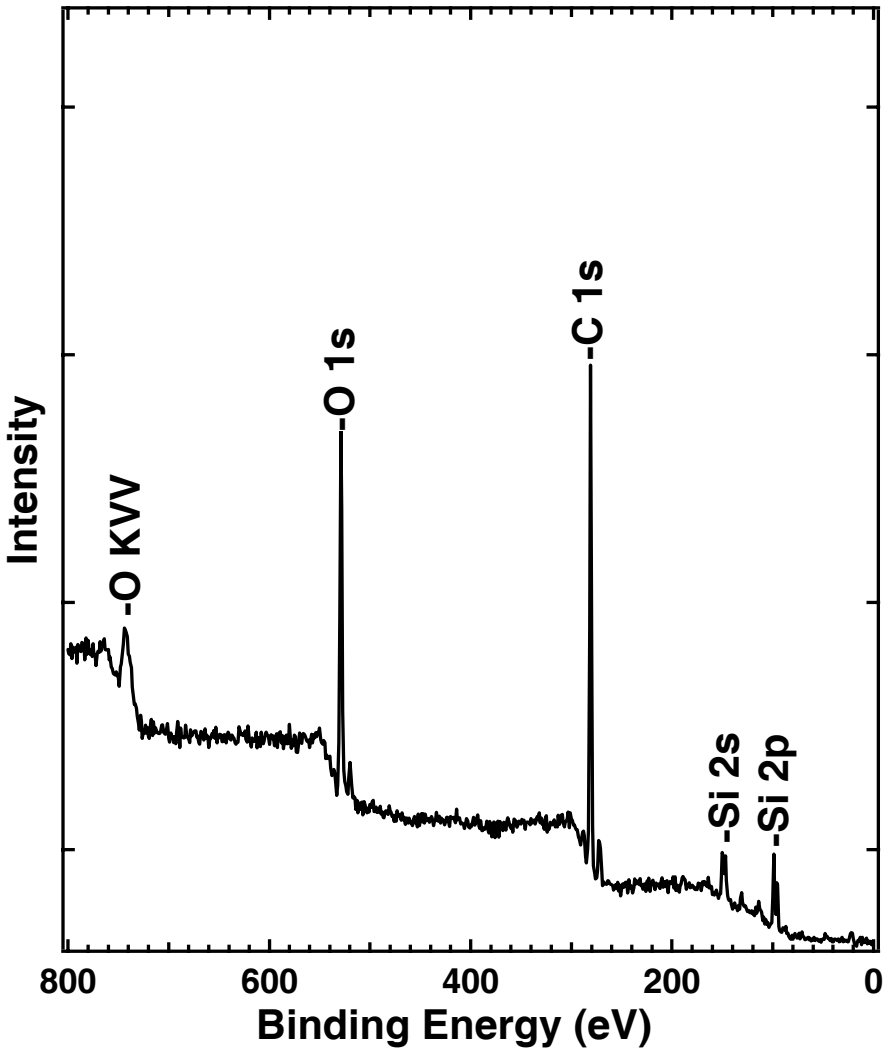

Figure 4.14 An XP survey spectrum of a freshly-prepared 40 layer POSS LB-film.

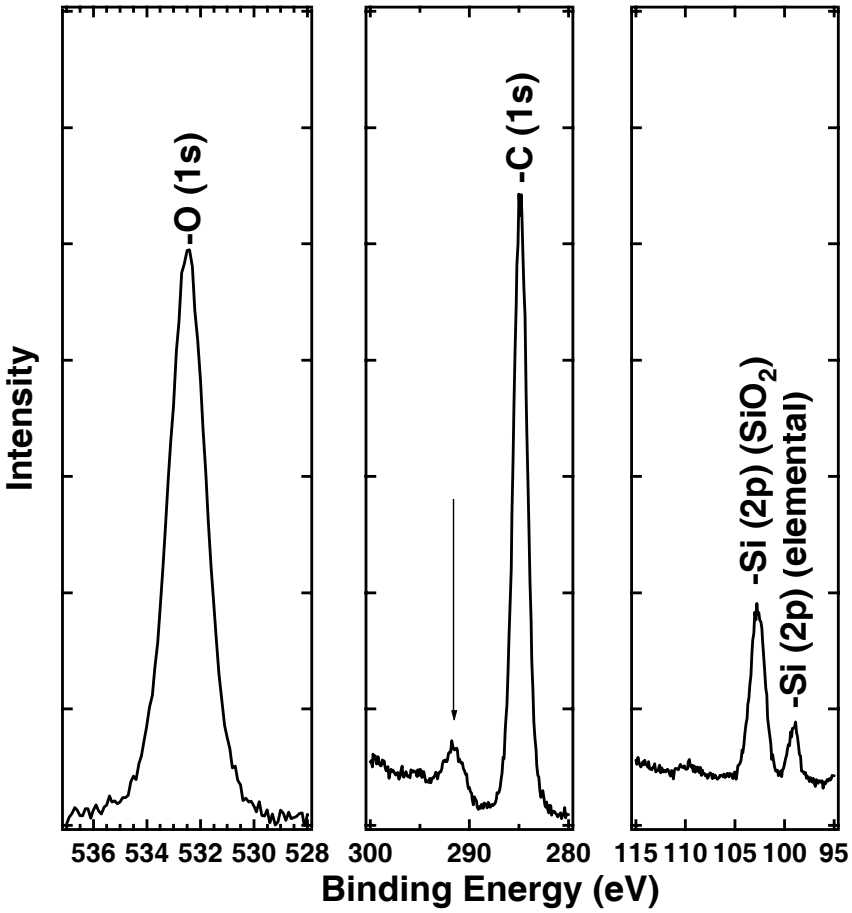

Figure 4.15 The high resolution O (1s), C (1s) and Si (2p) regions of the XP spectrum of a freshly-prepared 40 layer POSS LB-film.

Figure 4.15 shows the high resolution XP spectra of the O (1s), C (1s), and Si (2p) regions for a 40 layer freshly-prepared POSS LB-film. The oxygen component is comprised of signal from the oxygen atoms incorporated in the POSS molecules, as well as signal from any oxide formed on the silicon substrate. The main C (1s) component results from the phenyl rings of the film; these organic rings are also responsible for the shake-up intensity at slightly higher binding energies (indicated by arrow). The silicon-oxide component of the XP data arises from the cage structure of the silsesquioxane molecules. A small contribution from elemental silicon is attributed to the underlying substrate.

4.3.2. Exposure of Films to Non-Chlorinated CWA Simulant Molecules

4.3.2.1. Uptake of DMMP within POSS Films

Uptake coefficient measurements, conducted according to the King and Wells technique, indicate that the sticking probability of DMMP on POSS films is below the detection limits of the UHV instrument used in this study, $\lesssim 0.05$. Figure 4.16 shows the mass spectrometer signal for DMMP molecules reflecting from an inert surface and a freshly prepared POSS LB-film. These results are in agreement with RAIR spectra collected during organophosphonate exposure studies under high-vacuum conditions. No

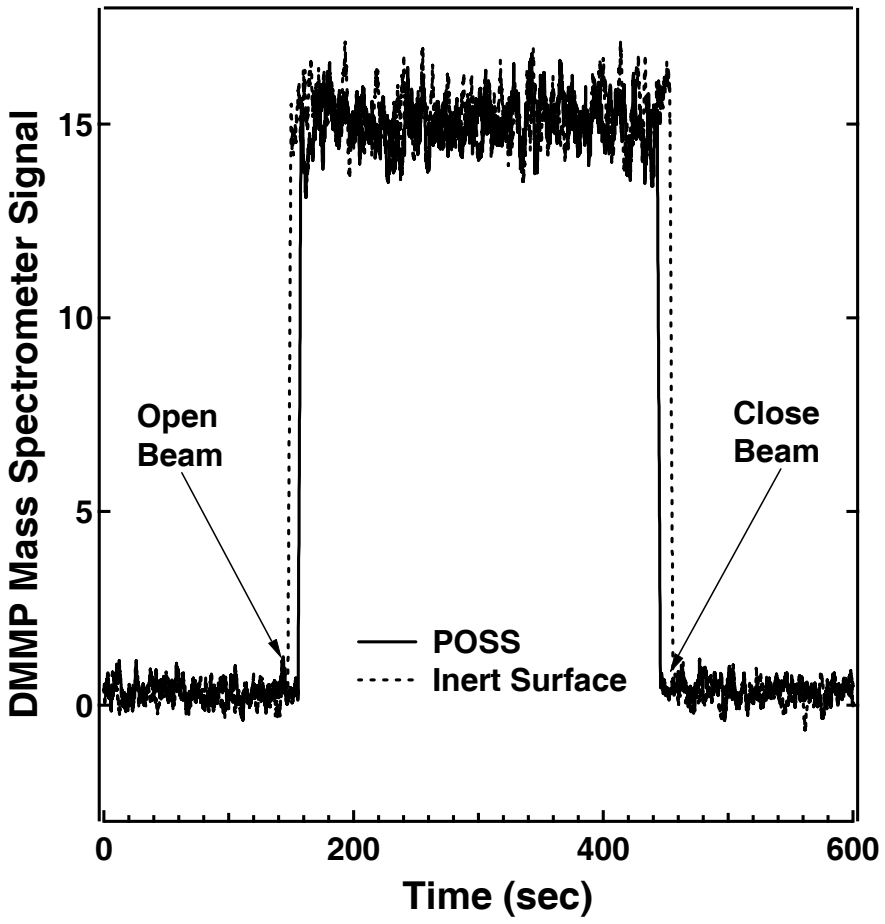

Figure 4.16 The uptake coefficient of DMMP on POSS LB-films is <0.05.

measurable uptake or interfacial interactions between organophosphonate molecules and POSS LB-films were recorded, even at very cold temperatures (138 K). The lack of significant interaction between DMMP and POSS films corroborates the work of Bertilsson and Crooks who have studied the interaction of organophosphonates on non-polar, non-hydrogen-bonding surfaces. Bertilsson and coworkers have evaluated the adsorption characteristics of DMMP on self-assembled monolayers with varying terminal groups. Their results show that organic SAMs with methyl terminal groups interact only very weakly with DMMP and adsorption at room temperature is limited. Crooks et al. also report that diisopropyl methylphosphonate (DIMP) interacts with CH_3-terminated SAMs through weak van der Waals forces. Similar to these results, the low uptake probability of DMMP within POSS is likely a consequence of the ordered, densely-packed, and hydrophobic nature of the outer surface of the POSS film. The outer surface of the film is comprised of phenyl groups bound to the rigid silicon-oxide cubic structure (see Figure 4.1). The hydrophobic quality of the surface is reflected by the 74 ± 1° static contact angle of water on a clean POSS film, which is in good agreement with the contact angle of water on SAMs comprised of aryl-terminated alkanethiols. The bulky phenyl groups impede the path of the organophosphonate molecules, limiting the interaction between the polar silanol groups and the impinging DMMP.

Despite a low uptake probability, under saturated vapor conditions organophosphonate molecules are capable of diffusing into and absorbing within the POSS films. RAIR studies, shown in Figure 4.17, reveal that in an environment saturated with DMMP, a 10 layer POSS LB-film saturates with organophosphonate molecules after approximately 10 minutes. The notable δ_s (P-CH_3) mode at 1313 cm^{-1} is designated by an arrow. This mode, in addition to other characteristic peaks associated with sorbed

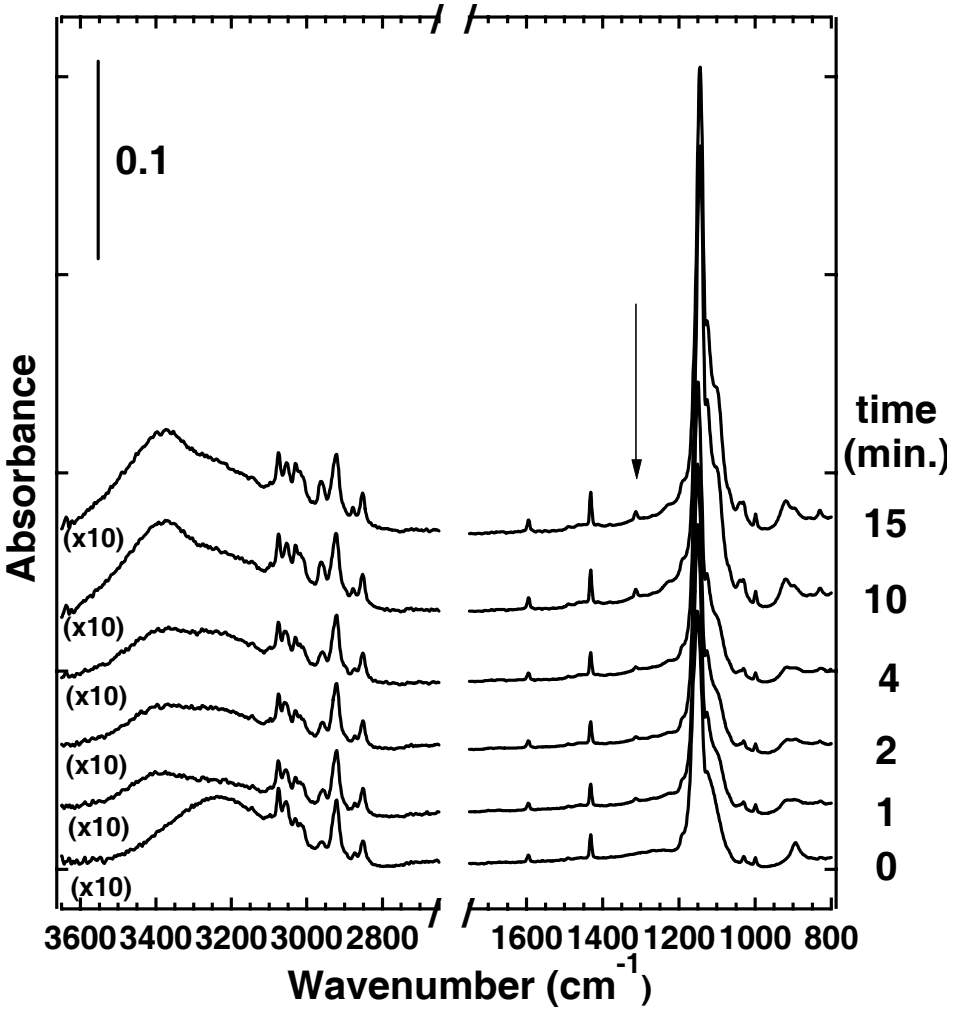

Figure 4.17 RAIR studies show that a 10 layer POSS LB-film is saturated with DMMP after 10 minutes of exposure in a saturated environment. The peaks associated with sorbed-DMMP do not increase in intensity after 10 minutes.

DMMP (3380 cm^{-1}, 919 cm^{-1}) do not increase in intensity after 10 minutes of exposure. The significant quantities of absorbed DMMP do not considerably disrupt the initial well-ordered film structure. Figure 4.18 shows the RAIR spectra of a clean 40-layer POSS film and a 40-layer film after saturation with DMMP molecules. The minor differences in the spectra are attributed to vibrational modes of the absorbed DMMP vapor. Figure 4.19 plots the RAIR integrated peak area of the P-CH_3 symmetric deformation mode, at 1313 cm^{-1}, for DMMP absorbed in multilayer POSS films. Measurements were made by exposing clean films with 10, 20, 30 and 40 layers of POSS molecules to saturated

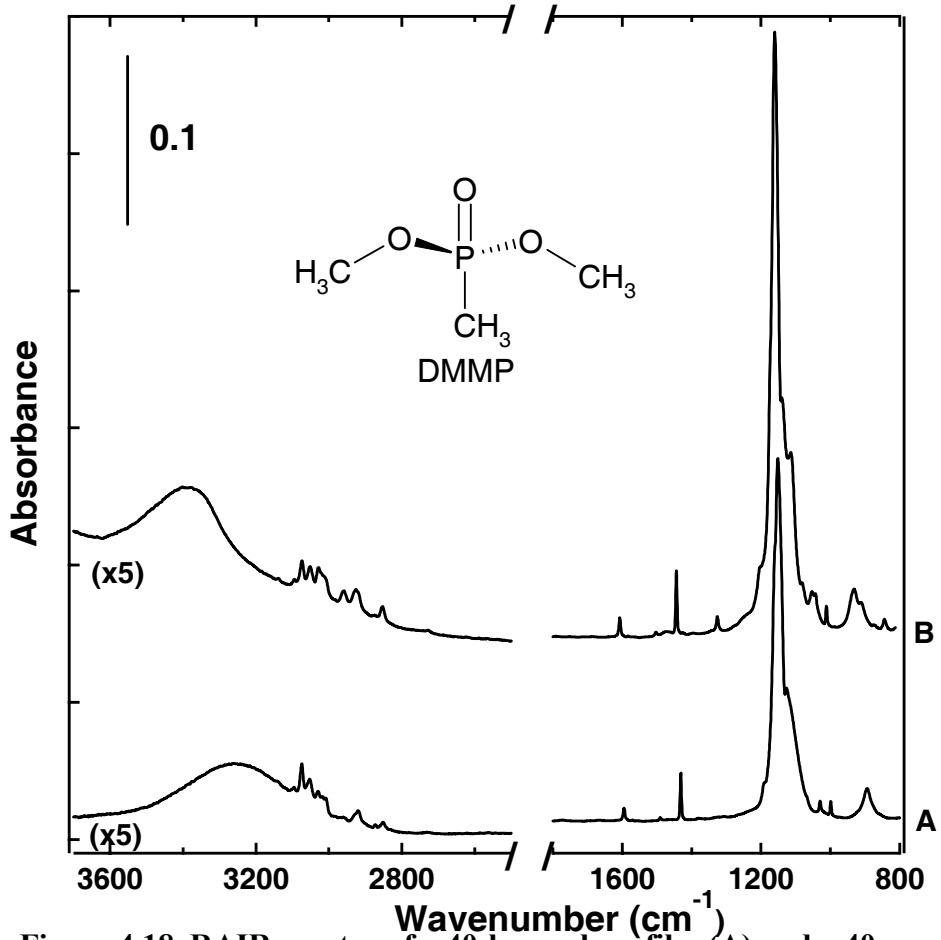

Figure 4.18 RAIR spectra of a 40-layer clean film (A) and a 40-layer DMMP-exposed film (B). Sorption of DMMP does not significantly alter the POSS film structure.

DMMP vapor. Figure 4.19 reveals that the absorbed amount of DMMP is directly proportional to the number of layers of POSS molecules comprising the LB-films.

The POSS films exhibit a high degree of stability both before and after exposure to organophosphonate molecules, as demonstrated by the spectra in Figure 4.20. Clean and DMMP-saturated films are resilient at room temperature in a sanitary environment and show no signs of decomposition, even after several weeks. However, upon heating the DMMP-saturated film to ~425 K, RAIR spectra show that the DMMP can be driven

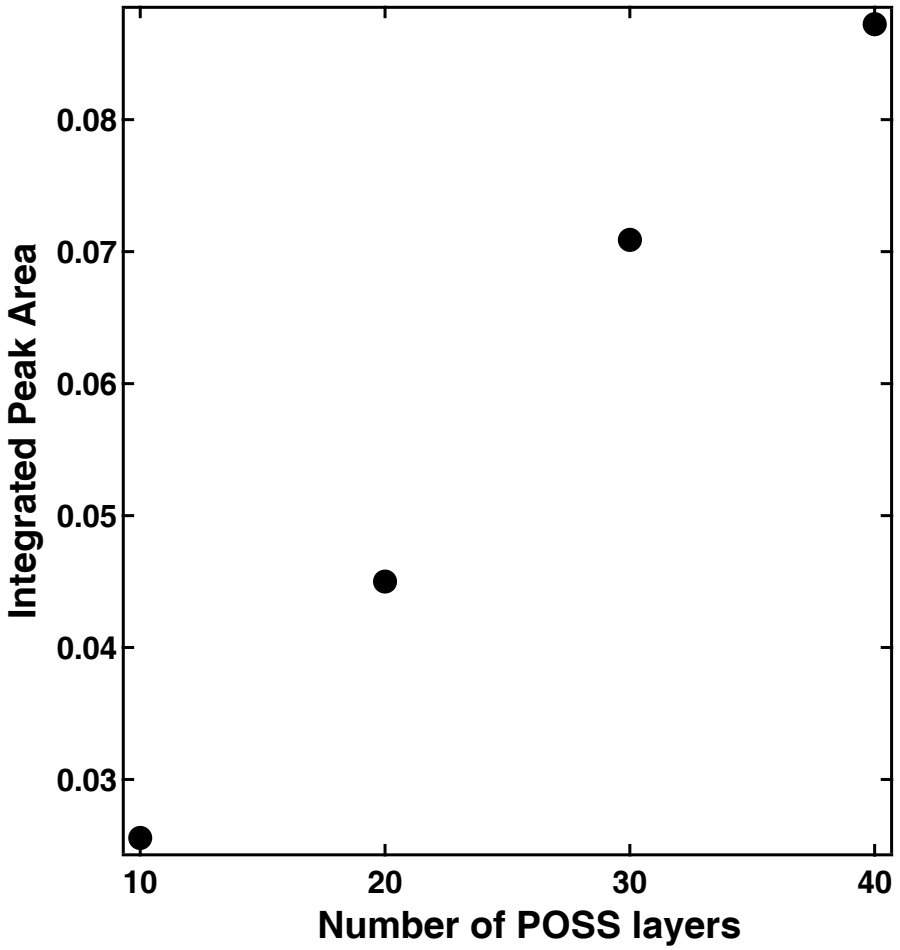

Figure 4.19 RAIR data of DMMP adsorbed within POSS films. The linearity of the integrated area of the δ_s (P-CH_3) mode (●) at 1313 cm^{-1} suggests that DMMP adsorbs into the multilayers of the POSS LB-film.

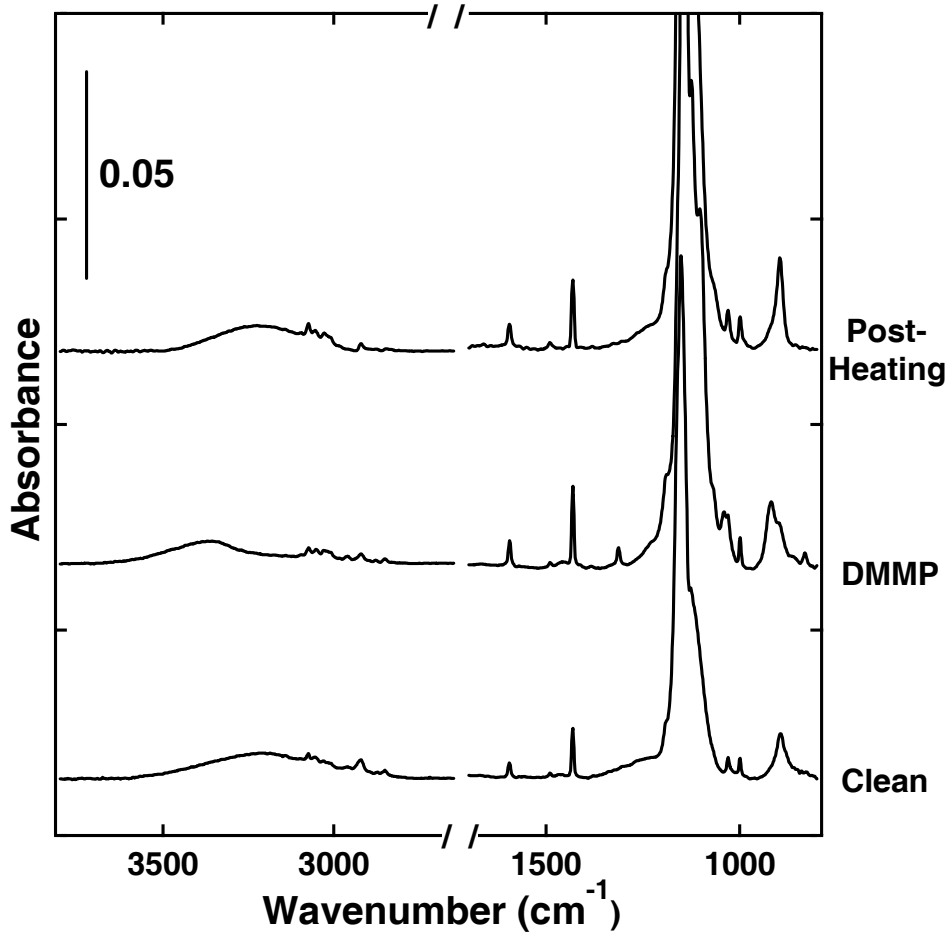

Figure 4.20 A POSS LB-film saturated with DMMP can be heated mildly (~425 K) to desorb the organophosphonate molecules. Subsequently, the initial film structure returns and the system can be used to sequester additional organophosphonates molecules.

off and the film returned to its initial structure. This is confirmed by the presence of sharp, well-defined peaks in the spectrum of the heat-treated film, which is indistinguishable from the clean film spectrum. Section 4.3.2.3. details the interaction of DMMP within the POSS films and presents the RAIR spectrum of gas phase DMMP.

4.3.2.2. Adsorption Energy of DMMP and TMP within POSS Films

TPD experiments were conducted to determine the adsorption energy of the DMMP and TMP molecules within the POSS film. The ions in the fragmentation pattern of molecular DMMP were observed concomitantly during the heating ramp, revealing desorption of intact DMMP from the POSS films. Expected ion signals from DMMP decomposition products, such as CH_3OH, were absent. Figure 4.21 shows the TPD trace for the most intense ion at m/z 94, which exhibits a peak temperature of 427 K. The leading edge of the trace gradually increases to a maximum and then abruptly decreases

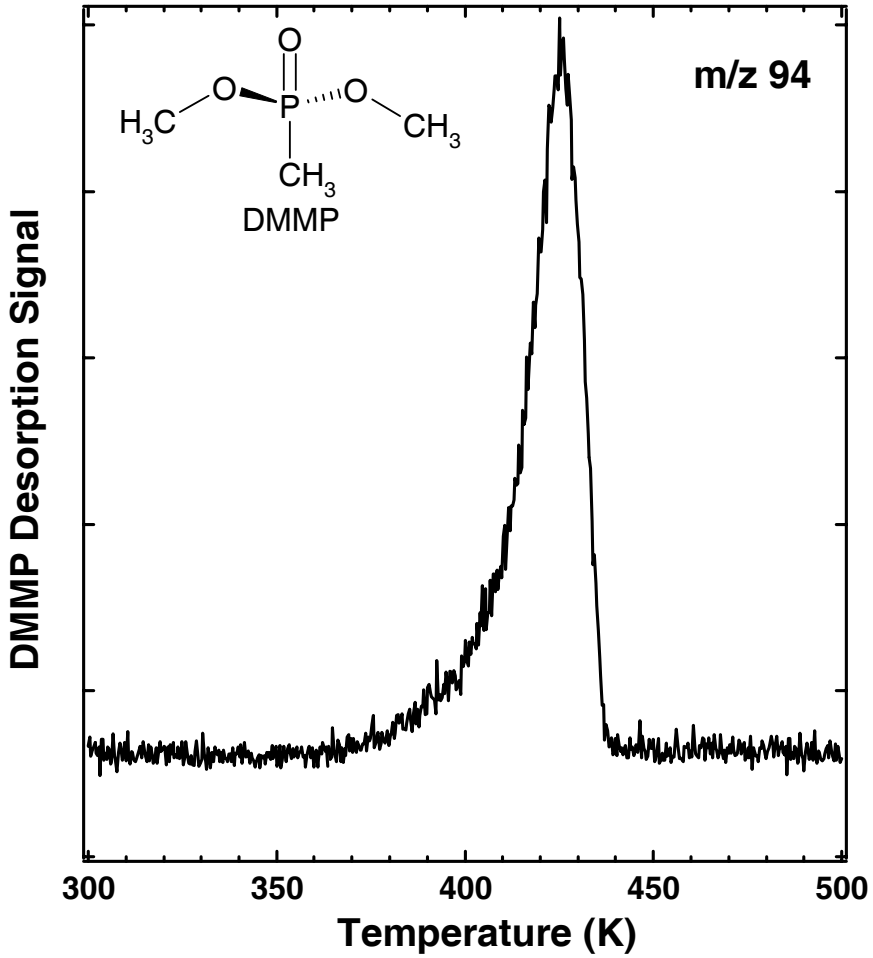

Figure 4.21 TPD of DMMP from a 40 layer POSS film. Shown is the trace of the m/z 94.

from the maximum to zero. Plotting the logarithm of rate of DMMP desorption against the reciprocal temperature reveals a linear relationship. This is consistent with zeroth order desorption kinetics, which are often observed for multilayer sublimation. Assuming a pre-exponential factor of 10^{13} s^{-1}, a value of 122 (±1.0) kJ/mol is predicted for the adsorption energy of DMMP within a POSS film. This value is consistent for LB-films ranging from 10 to 40 layers of POSS molecules. The observation of a single adsorption energy indicates that the interactions between the DMMP molecules and the silanol groups of the POSS films are similar throughout the entire film and are independent of the location of the sorption site with respect to the interface.

Analogous to DMMP, the ions from the fragmentation of TMP were observed simultaneously in the mass spectrometer during thermal ramps. Signal resulting from decomposition products was not present. Thus, TMP was determined to desorb molecularly. Figure 4.22 contains the mass spectrometer trace of the most intense ion at m/z 110. Assuming zeroth-order desorption kinetics and factoring in the temperature ramp and peak temperature, TMP was determined to have an adsorption energy of 138 kJ/mol. The slightly higher adsorption energy, as compared to DMMP, is likely a result of additional hydrogen-bonding interactions present between the TMP molecules and the silanols of the POSS film. Each TMP molecule contains one more methoxy moiety than a comparable DMMP molecule. This, in conjunction, with a somewhat different geometry may result in the stronger interaction between the TMP molecules and the apical silanols of the sorbent film.

Relative to the adsorption energy of DMMP on a variety of other surfaces, the interaction between DMMP (and TMP) and POSS films is strong. Values ranging from

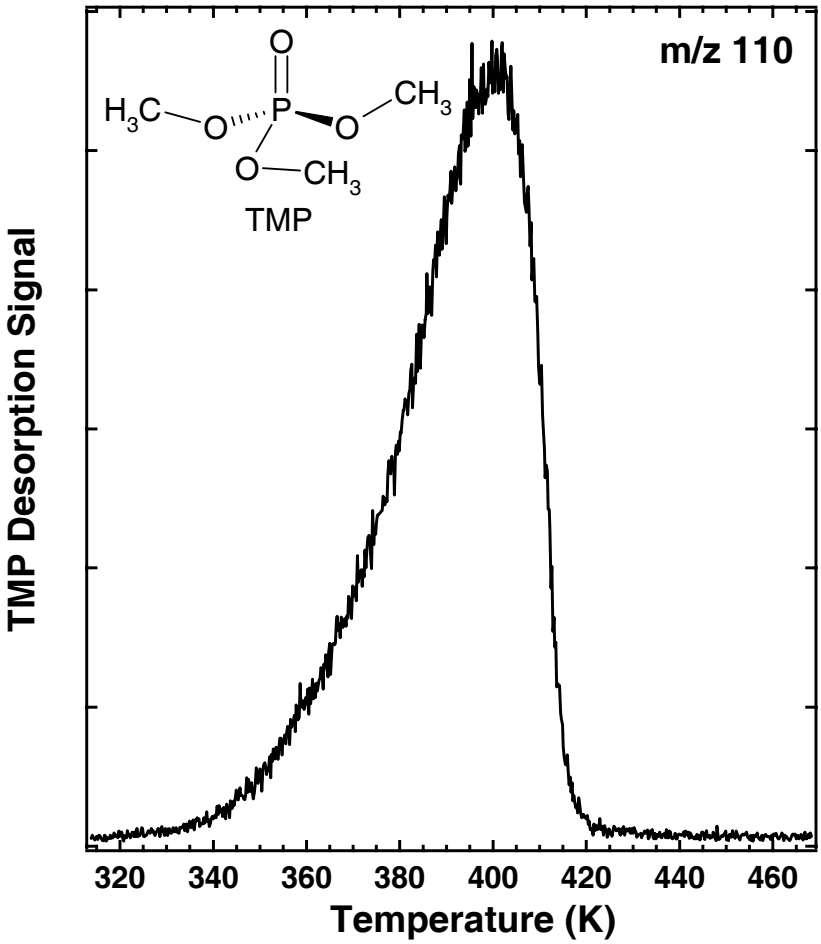

Figure 4.22 TPD of TMP from a 40 layer POSS film. Shown is the trace of the m/z 110.

49.3 to 59.4 kJ/mol have been reported for the adsorption energies of DMMP on functionalized organic self-assembled monolayers. Most relevant to the work presented here, Henderson et al. reported a value of 70.7 kJ/mol for the adsorption energy of DMMP on high surface area silica. The high adsorption energy of the DMMP within the POSS film is attributed primarily to the strength of the hydrogen-bonding interactions between the phosphoryl group of the DMMP molecule and the multiple silanol groups of the cage-like POSS molecules. Once the DMMP molecules become confined in the silicon-oxide cage structures, a significant amount of energy is required to drive the molecules from the film.

4.3.2.3. RAIRS Characterization of DMMP-saturated POSS Films

The RAIR spectrum resulting from a 40 layer POSS film exposed to DMMP is shown in Figures 4.23.B and 4.24.B For reference, the spectra of a clean 40 layer POSS

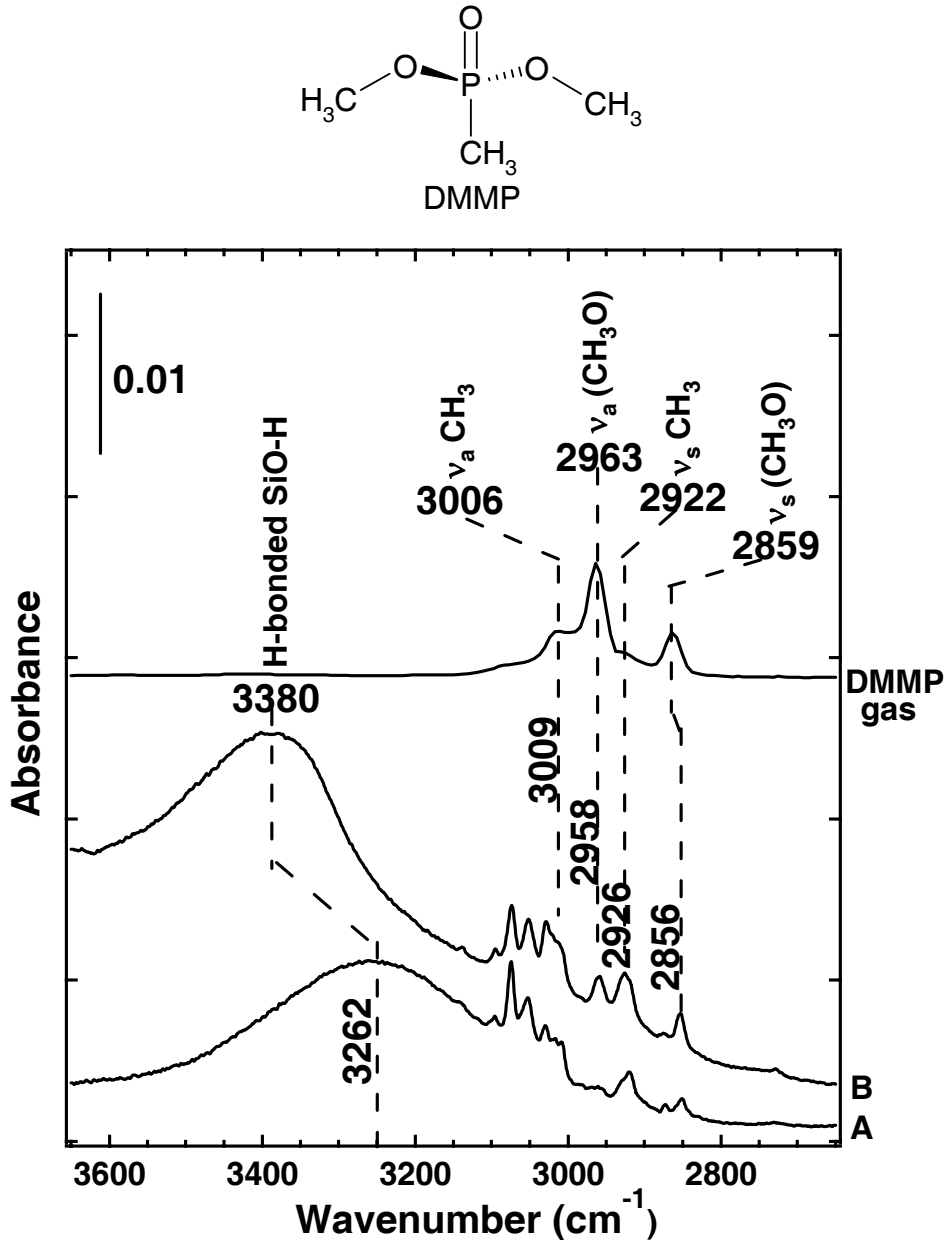

Figure 4.23 RAIR spectra of a 40-layer clean film (A), a 40-layer DMMP-exposed film (B), and gas-phase DMMP. The high frequency region of the spectrum shows a distinct shift in the hydrogen-bonded Si-OH mode to higher wavenumbers upon exposure to DMMP.

film (labeled A) and of DMMP vapor (labeled DMMP gas) are also included in Figures 4.23 and 4.24. Inspection of the high frequency modes in Figure 4.23 provides insight into the interaction between the DMMP molecules and the POSS film. The wavenumber of the SiO-H mode shifts from 3262 to 3380 cm^{-1} upon sorption of DMMP. This shift is indicative of a disruption of the hydrogen-bonding network between silanol groups within the original POSS film.[37] The perturbation is likely the result of the formation of

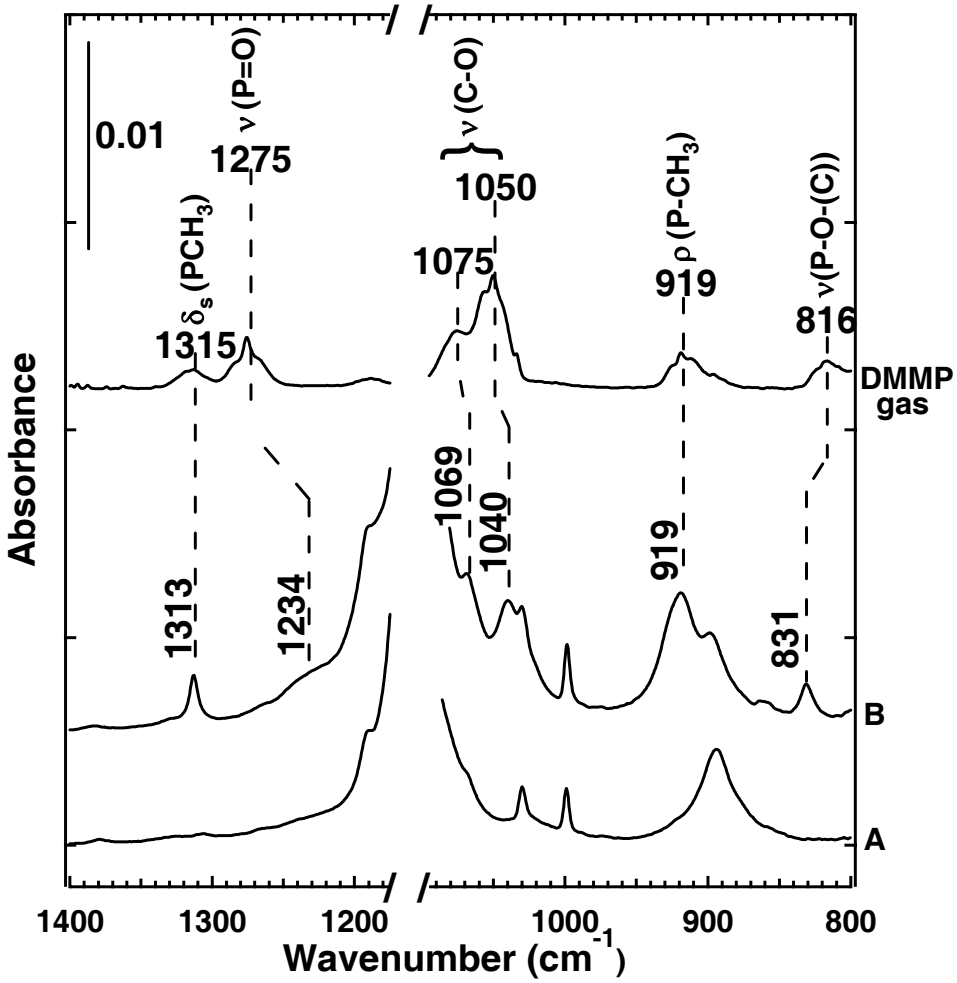

Figure 4.24 RAIR spectra of a 40-layer clean film (A), a 40-layer DMMP-exposed film (B), and gas-phase DMMP. Low-frequency modes indicate that the primary interaction between DMMP and POSS films is hydrogen-bonding through the phosphoryl group of the DMMP.

new hydrogen bonds between the silanol groups and the DMMP molecules. Figure 4.23 shows several peaks in the region of 2900-3100 cm^{-1}, due to vibrational modes of the phenyl rings of the POSS molecules. Figure 4.23.B reveals asymmetric and symmetric methoxy stretching modes of the absorbed DMMP molecules at 2958 and 2856 cm^{-1}, respectively. Each of these modes is shifted only slightly with respect to the gas-phase DMMP spectrum, indicating weak hydrogen-bonding interactions with the POSS film through the methoxy functional groups. The asymmetric methyl stretch appears at 3009 cm^{-1} for the surface bound species and the symmetric methyl stretch, which is red-shifted with respect to the gas-phase spectrum of DMMP, appears at 2926 cm^{-1}. Thus, only weak interactions occur between the methyl groups and the POSS film.

The low wavenumber IR data, shown in Figure 4.24, confirms weak interactions between the methoxy and methyl functional groups of the DMMP molecules and the silanol groups of the POSS films. The 1313 and 919 cm^{-1} absorptions due to the P-CH_3 symmetric deformation and rocking mode, respectively, are only slightly shifted from the corresponding gas-phase DMMP modes. Stretching frequencies at 1069 and 1040 cm^{-1} confirm a slight interaction through the methoxy moieties, as these (C-O) modes are red-shifted from 1075 and 1050 cm^{-1} in the gas-phase DMMP. A stronger interaction, however, appears to occur between the phosphoryl group of DMMP and the LB-film.

Inspection of the phosphoryl stretching band reveals a significant shift from 1275 cm^{-1} in the gas phase to a broad shoulder positioned at 1234 cm^{-1} in the DMMP-saturated POSS film. The significant change of the ν(P=O) stretching mode frequency on POSS LB-films and the absence of significant (O-CH_3) and (P-CH_3) peak shifts indicate that the hydrogen-bonding interaction between the phosphoryl functional group

and the silanol groups of the film is primarily responsible for the significant adsorption energy of DMMP. Upon exposure to DMMP, the perturbation of the silicon-oxide cage structures gives rise to the new Si-O frequency at 1100 cm^{-1}. This mode appears as a shoulder to the more intense Si-O-Si mode at 1151 cm^{-1}, which is also slightly shifted from the pre-exposure Si-O-Si mode at 1148 cm^{-1} (see Figure 4.18). Absorptions at 999 and 1030 cm^{-1}, assigned to Si-O stretching modes, are unchanged after exposure. In agreement with TPD data, the RAIR spectra show no evidence of DMMP decomposition within the film.

Work by Kanan and Tripp examining DMMP adsorbed onto silica suggests that the interactions occur primarily through hydrogen bonds between the methoxy groups of the organophosphonate molecules and the free hydroxyl groups on the silica surface. Their IR spectra show no change in the P-CH_3 modes and a 19 cm^{-1} shift of the P=O stretching mode of DMMP, which is much smaller than the shift observed for this mode when DMMP is adsorbed on other metal-oxide surfaces. The high-frequency methoxy modes reportedly did not change upon adsorption, however, the low-frequency modes at 1075 and 1049 cm^{-1} disappeared. To investigate this occurrence, White et al. examined the adsorption of methoxysilanes on silica surfaces and found identical behavior of the methoxy modes and the SiO-H stretching mode, which lead to their conclusion that DMMP is adsorbed on silica only through hydrogen bonds between the surface silanol groups and the two methoxy groups of DMMP. In contrast, the results presented here indicate strong interactions between the silanols of the POSS film and the *phosphoryl* groups of the DMMP molecules, while weaker interactions are observed between POSS molecules and the methoxy and methyl groups of the DMMP molecules.

The POSS molecules may provide a geometrically-optimal sorption site for impinging DMMP molecules. The hydrogen bonds initially present between the silanol groups at the corner of the POSS molecules are significantly disrupted upon DMMP sorption. The relative proximity of the silanol groups and the molecular structure of DMMP appear to result in a highly-favorable sorbent-sorbate system. It is expected that lone pairs of the P=O oxygen and the methoxy functional groups of the DMMP participate in newly-formed hydrogen-bonding interactions with the silanols of the POSS films, as depicted in Figure 4.25. The significant shift to lower wavenumbers of the P=O stretch and the shift of the hydrogen-bonded Si-OH mode to higher wavenumbers offers insight into the strength of the interaction between DMMP and the POSS film. Bertilsson et al. and Crooks et al. observed the surface adsorbed DMMP P=O mode in the range of 1208-1246 cm^{-1} on organic SAM systems, while Tripp and co-workers observed the same P=O stretch at 1256 cm^{-1} for DMMP adsorbed on silica. The large red shift observed for the P=O mode at 1234 cm^{-1} in the DMMP-POSS system discussed here indicates strong hydrogen bonds with the phosphoryl groups. The electron withdrawing nature of the phenyl rings likely renders the silanol groups slightly more acidic than those of a pure

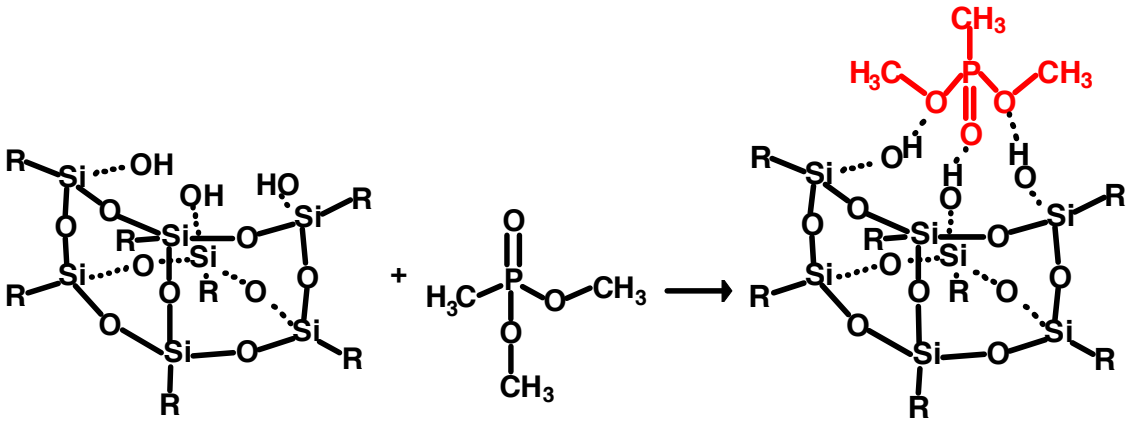

Figure 4.25 DMMP hydrogen bonds with the silanol groups of POSS molecules.

silica surface, allowing a stronger interaction to take place. The strength of the interaction leads to an adsorption energy of DMMP within a POSS film that is significantly higher than energies reported for DMMP adsorbed on high surface area silica and other polar surfaces.

4.3.2.4. RAIRS Characterization of TMP-saturated POSS Films

The RAIR spectrum resulting from a 40 layer POSS film exposed to TMP is shown in Figures 4.26.B and 4.27.B. For reference, the spectra of a clean 40 layer POSS film (labeled A) and of TMP vapor (labeled TMP gas) are also included in Figures 4.26 and 4.27. Duplicating DMMP-saturated POSS films, a striking characteristic of TMP saturated films is the dramatic shift of the hydrogen-bonded Si-OH mode from 3262 cm^{-1} to a higher frequency (3400 cm^{-1}). The disruption of the initial hydrogen-bonding network of the POSS molecules is a result of TMP forming new associations within the film. TMP likely forms strong hydrogen bonds with the surface silanol groups through three methoxy functional groups, as well as the phosphoryl moiety. The additional hydrogen-bonding interaction between TMP, as compared to DMMP (two methoxy groups, one phosphoryl group per molecule), is responsible for the larger shift (20 cm^{-1}). Figure 4.26 shows several peaks in the region of 2900-3100 cm^{-1}, due to vibrational modes of the phenyl rings of the POSS molecules. Figure 4.26.B reveals asymmetric and symmetric methoxy stretching modes of the absorbed TMP molecules at 2960 and 2852 cm^{-1}, respectively. Each of these modes is shifted only slightly with respect to the gas-phase TMP spectrum, indicating weak hydrogen-bonding interactions with the POSS film through the methoxy functional groups. The asymmetric methyl stretch appears at 3009 cm^{-1} for the surface bound species and the symmetric methyl stretch appears at

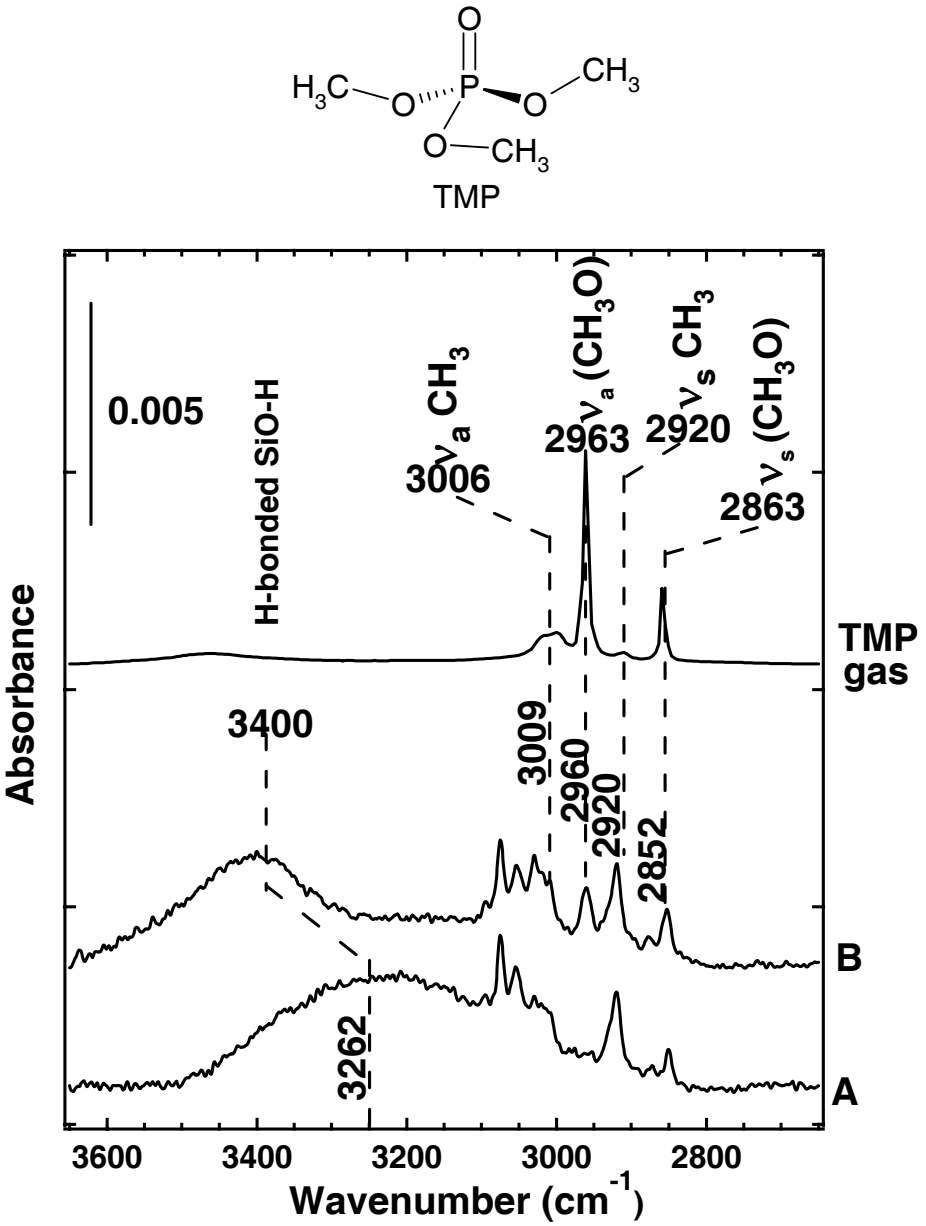

Figure 4.26 RAIR spectra of a 40-layer clean film (A), a 40-layer TMP-exposed film (B), and gas-phase TMP. The high frequency region of the spectrum shows a distinct shift in the hydrogen-bonded Si-OH mode to higher wavenumbers upon exposure to DMMP.

2920 cm^{-1}.

The low wavenumber IR data, shown in Figure 4.27, confirms weak interactions between the methoxy functional groups of the TMP molecules and the silanol groups of the POSS films. A stretching frequency at 1053 cm^{-1} confirms a slight interaction

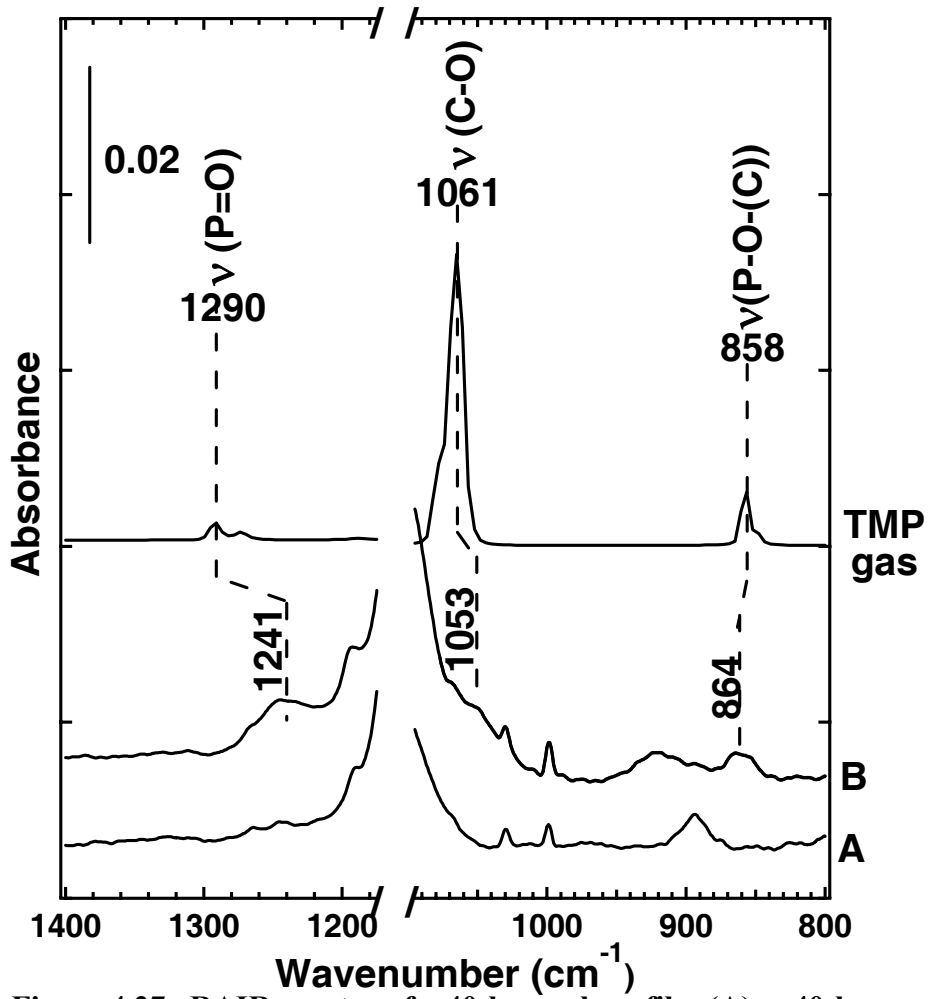

Figure 4.27 RAIR spectra of a 40-layer clean film (A), a 40-layer TMP-exposed film (B), and gas-phase TMP. Low Frequency modes indicate that the primary interaction between TMP and POSS films is hydrogen-bonding through the phosphoryl group of the DMMP.

through the methoxy moieties, as this (C-O) mode is red-shifted from 1061 cm^{-1} in the gas-phase TMP. A stronger interaction, however, appears to occur between the phosphoryl group of TMP and the LB-film. Inspection of the phosphoryl stretching band reveals a significant shift from 1290 cm^{-1} in the gas phase to a broad shoulder positioned at 1241 cm^{-1} in the TMP-saturated POSS film. The significant change of the ν(P=O) stretching mode frequency on POSS LB-films and the absence of significant (O-

CH_3) peak shift indicates that the hydrogen-bonding interaction between the phosphoryl functional group and the silanol groups of the film is primarily responsible for the significant adsorption energy of TMP. Upon exposure to TMP, the silicon-oxide cage structure is slightly perturbed, giving rise to a new Si-O frequency at 1100 cm^{-1}. This is consistent with the results obtained from DMMP-saturated films and suggests that upon organophosphonate saturation, the silicon-oxide cage structures may reorient to accommodate the sorbate molecules. In agreement with TPD data, the RAIR spectra show no evidence of TMP decomposition within the film.

4.3.2.5. XPS Characterization of DMMP- and TMP-saturated POSS Films

The elemental composition and bonding environment of freshly-prepared and phosphate-saturated POSS LB-films were assessed using XPS. Figure 4.28 shows the high resolution XP spectra of the O (1s), C (1s), and P (2p) regions for (A) freshly-prepared, (B) DMMP-saturated, and (C) TMP-saturated films. Other features of the spectra, not shown, include peaks resulting from the silicon atoms comprising the cubic-structure of the POSS molecules.

The O (1s) peak of the freshly-prepared POSS LB-film is present at 532.4 eV. This binding energy is consistent with O (1s) binding energies reported for pressed SiO_2 wafers. Upon exposure to DMMP or TMP, the oxygen component of the POSS-system broadens to contain a shoulder at approximately 531 eV (Spectrum B). The shoulder is attributed to oxygen atoms present in DMMP or TMP physisorbed within the POSS LB-film.

The C (1s) peak of the freshly-prepared POSS LB-film is centered at 284.8 eV with a satellite peak at 291.6 eV transpiring from the phenyl rings in the system. Upon

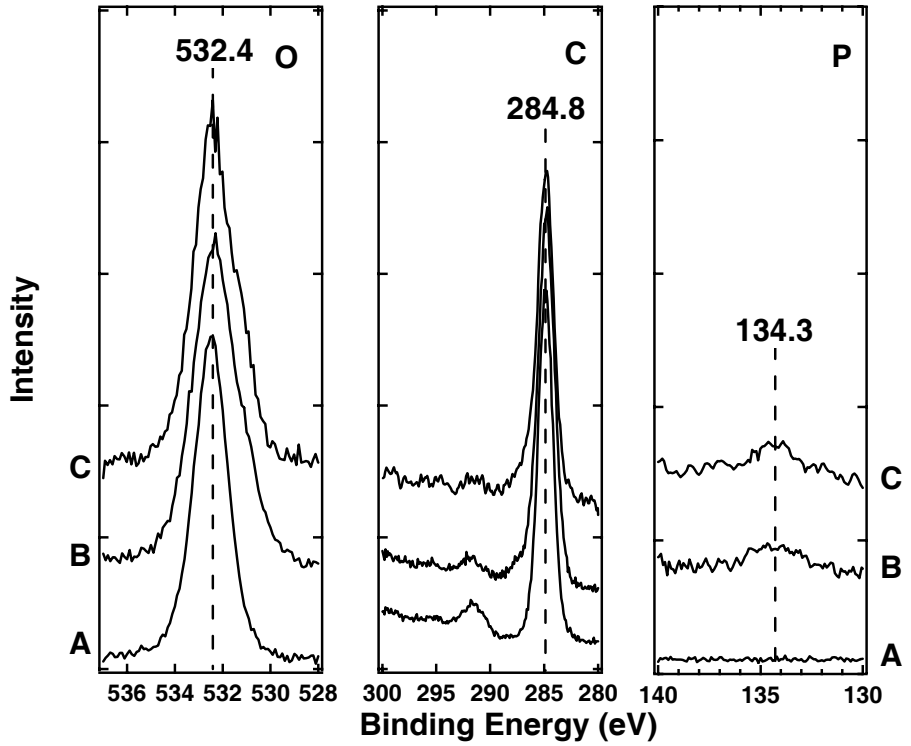

Figure 4.28 High resolution XP spectra of the O (1s), C (1s) and P (2p) regions of a freshly-prepared POSS LB film (A), a DMMP-saturated POSS LB-film (B) and a TMP-saturated POSS LB-film (C).

saturation with DMMP or TMP, a shoulder is evident at about 287.7 eV. This signal, at slightly higher binding energies, is consistent with carbon atoms that are neighboring electronegative atoms, such as the oxygen atoms in methoxy functional groups.

Figure 4.28 shows that, as expected, phosphorus was detected on the DMMP- and TMP-saturated POSS LB-films and not on the freshly-prepared film. DMMP molecules physisorbed within the POSS LB-film give rise to a binding energy of about 134.3 eV. This value is in good agreement with the binding energies of other published DMMP-sorbent systems and further substantiates that hydrogen-bonding interactions are responsible for the adsorption of DMMP molecules within POSS LB-films. Zhou et al. report that multilayers of DMMP molecularly adsorbed on titania surfaces, held at 120 K, have P (2p) binding energies of 135.4 and 134.9 eV, for condensed and molecularly

sorbed DMMP, respectively.

4.3.2.6. Exposure of Solution-Phase POSS Films to DMMP

The somewhat disordered structure present in the solution-deposited POSS films provides an opportunity to investigate film characteristics, such as packing density, that may affect the uptake coefficient of organophosphonate molecules. Exposure of the solution-phase films to controlled amounts of DMMP in the high vacuum chamber suggests that the disruption of the POSS film structure does not measurably affect the uptake characteristics. No evidence of DMMP uptake was observed in the *in situ* RAIR spectra. It is likely that the silsesquioxane molecules self-orient in such a way that hydrogen-bonding interactions with neighboring molecules are favored. This orientation may leave the more hydrophobic portions of the molecules at the interfacial regions and thus limit uptake, as in the case of POSS LB-films. Attempts at creating films possessing free, interfacial silanol groups were unsuccessful. When exposed to saturated DMMP vapor, the solution-deposited films absorbed the organophosphonate molecules. Resulting spectra were similar to those obtained from saturated POSS LB-films.

4.3.2.7. Exposure of Solution-Phase TEP Films to DMMP

RAIR studies indicate that, even in saturated-vapor conditions, DMMP molecules do not absorb within solution-deposited TEP films. It is likely that the ethyl groups on the apices of the silicon oxide cubic structures affect the reactive silanol sights in such a way that organophosphonates, such as DMMP, are not absorbed within the film. The nature of the TEP system may support the notion that the electron withdrawing nature of the phenyl rings within the POSS film may result in slightly acidic silanol protons. This characteristic may lead to the strong interactions with organophosphonate molecules.

4.4. Conclusions

The sorption of DMMP and TMP within a POSS LB-film was investigated by RAIRS, uptake coefficient and TPD measurements. Even at very cold temperatures, the uptake probability of DMMP on the ordered POSS films is very low. However, once the DMMP molecules penetrate the film, RAIR data indicate that the silanol groups of the POSS molecules interact with the phosphoryl and methoxy functional groups of the organophosphonate molecules, causing the multilayered film to become saturated with DMMP. The hydrogen-bonding interactions between the phosphoryl and the silanol groups are primarily responsible for the high stability of the saturated films at room temperature. Consequently, energies of 122 kJ/mol are required to drive the DMMP from the POSS films. Likewise, under saturated-vapor conditions POSS LB-films readily absorb TMP through strong hydrogen bonding interactions between the phosphoryl group and three methoxy groups present in the TMP molecules . Energies of 130 kJ/mol are necessary to drive the TMP molecules from the silsesquioxane films.

The absorption of DMMP and TMP within POSS films suggests a possible route to a prefiltering or preconcentrating scheme of organophosphonates. Low uptake probabilities limit the usefulness of this system in its present condition as a sensing strategy. If the sticking coefficient of CWA simulants on or within POSS films can be increased, the system may be more effective as a protective coating or sensor. Conceivably, freeing silanol groups from the strong hydrogen bonds with adjacent POSS molecules may render them available to impinging CWA simulants and subsequently increase the uptake. Disruption of film structure was insufficient in freeing Si-OH groups and increasing uptake of DMMP, however, POSS molecules may be incorporated in

polymer films that contain available adsorption sites for impinging molecules. Moreover, the molecular sorption of the DMMP and TMP molecules curbs the idea of a system capable of decomposition. DMMP and TMP, while frequently used as less-toxic simulants of more noxious phosphate derivatives, lack halogen atoms that are in part responsible for the reactive nature of nerve agents, such as sarin or soman. Exposure of POSS films to molecules that more closely mimic CWAs, such as methyl dichlorophosphate (MDCP) and trichlorophosphate (TCP), may offer a more realistic view of how CWAs may interact with POSS films.

Chapter 5
POSS Langmuir-Blodgett Films: Exposure to Methyl Dichlorophosphate and Trichlorophosphate

5.1. Introduction

The chemistry of organophosphonates on metal-oxide and organic thin films has received a great deal attention.[27,50] Fundamental understanding of the surface chemistry of phosphate derivatives may lead to the development of more efficient decontamination strategies,[8,11,15,24-26,28-36,43,166] sensing methodologies,[9,37-41] and protective coatings or barriers. Here, the decomposition of chlorinated phosphate molecules within a novel set of hybrid inorganic-organic films is described. Specifically, the following studies describe the interactions between trisilanol-phenyl polyhedral oligomeric silsesquioxane (POSS) Langmuir-Blodgett films and the chlorophosphates: methyl dichlorophosphate (MDCP) and trichlorophosphate (TCP).

Dimethyl methylphosphonate (DMMP) is frequently used as a less-toxic simulant of more noxious phosphate derivatives employed as chemical agents or pesticides. A number of studies have focused on the decomposition of DMMP on oxide surfaces at elevated temperatures,[8-11,26,29,33,40,62,63,75-77,167,168] while other systems are capable of decomposing organophosphonates at or below room temperature.[24,25,27,28,30-32,50,169-171] DMMP decomposition at room temperature or below has been observed over Rh, γ-Al_2O_3, Fe_2O_3, γ-Al_2O_3/FeO_x, TiO_2, and FeO_x/CeO_y/Al_2O_3 surfaces.[24,25,27,28,30-32,50,169-171] These mechanistic studies have proven helpful in the description of organophosphonate surface chemistry. DMMP is found to adsorb on surfaces through interactions with the phosphoryl oxygen at both Lewis and Brønsted surface acid sites.[25,74] Adsorption at Brønsted acid sites results in molecular interactions and evacuation at elevated

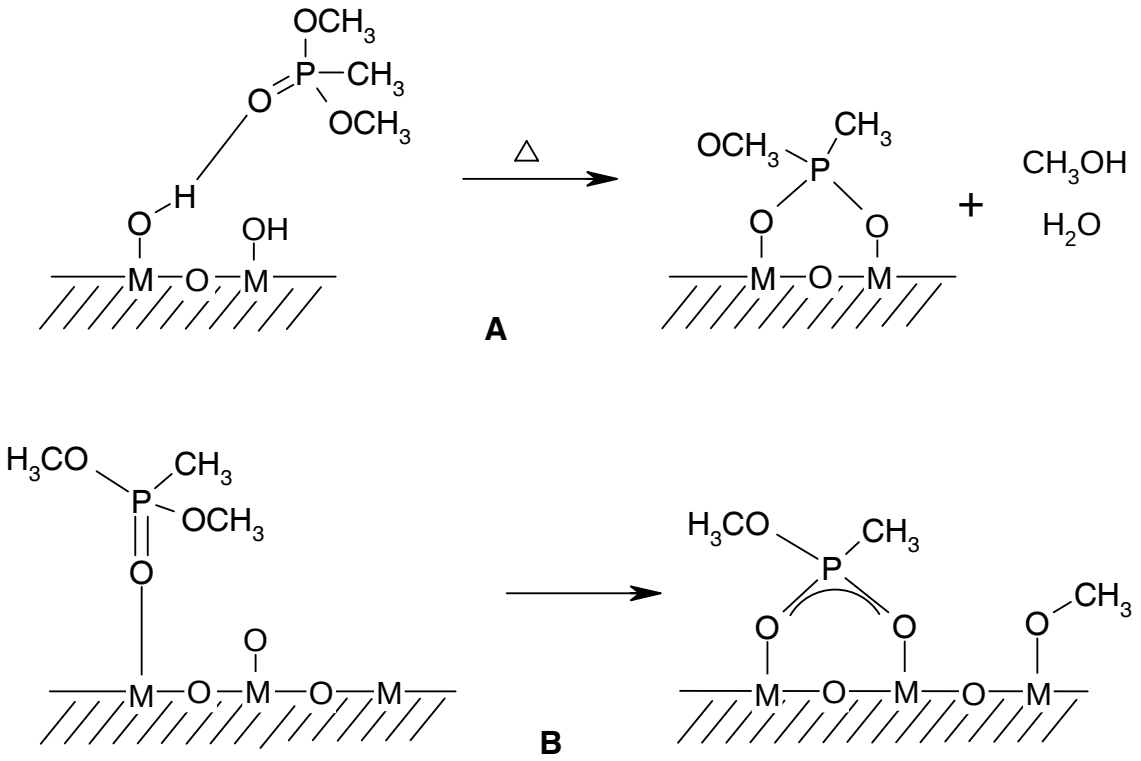

Figure 5.1 A subset of possible interaction pathways for DMMP on a metal oxide surface. Scheme A shows a decomposition route at a Brønsted acid site and scheme B shows a decomposition pathway at a Lewis acid site.

temperatures may lead to elimination of methoxy groups and result in surface bound phosphate residues. Adsorption at Lewis acid sites often leads to dissociation of the organophosphonate, resulting in surface bound phosphate residues and methanol.[25,74] Figure 5.1 depicts possible decomposition routes through interactions at both surface Brønsted and Lewis acid sites.

Despite this contribution to the understanding of organophosphonate surface chemistry, that of halogenated phosphate molecules has remained largely unexplored. Nerve agents such as sarin (GB or O-isopropyl methylphosphonofluoridate) and soman (GD or O-pinacolyl methylphosphonofluoridate), depicted in Figure 1.1 on page 1, contain fluorine atoms. The fluorine atoms can undergo rapid hydrolysis and are thus much more reactive than simulants such as DMMP. The appeal in studying actual agents

and halogenated phosphate simulants stems from this highly reactive nature and the degree to which their interfacial characteristics may differ from those of less toxic simulants. Kuiper et al. and Wagner and co-workers examined the uptake and reactivity of GB, GD, and VX (O-Ethyl S-2-diisopropylaminoethyl methyl phosphonothiolate) on MgO, Al_2O_3, and CaO.[34,172-174] GB and GD decomposed through hydrolysis reactions to generate chemisorbed phosphonate fragments. Theoretical studies by Michalkova et al. indicated that GB can physisorb on MgO through the formation of hydrogen-bonding, ion-dipole, and dipole-dipole interactions or chemisorb to unhydroxylated MgO fragments and decompose to yield HF.[175] Nadler et al. reported that diisopropyl fluorophosphate (DFP) readily hydrolyzes on Al_2O_3, but reacts more slowly on pre-wetted SiO_2 surfaces.[176] DFP formed strong molecular interactions with both SiO_2 and charcoal, but no signs of decomposition were observed.[176] Kanan et al. used MDCP and TCP as nerve agent simulants in their studies on SiO_2 thin films and WO_3.[37,39] Though no hydrolysis was observed on the silica surfaces, water in the WO_3 system led to the hydrolysis of MDCP and TCP, which yielded a range of phosphate derivatives.

Langmuir-Blodgett films of trisilanolphenyl-polyhedral oligomeric silsesquioxane (POSS) have proven to be strong sorbents of DMMP and TMP.[78] POSS films contain numerous silanol sites that are capable of hydrogen bonding with organophosphonates. The adsorbates are held very strongly within the silicon oxide-like films and have relatively high energies of adsorption (Section 4.3.2.2.). This study further investigates the POSS system by focusing on the chemical interactions between chlorinated phosphates, MDCP and TCP, and POSS LB-films. The idealized film, shown schematically in Figure 5.2 depicts the multilayer structure. The van der Waals

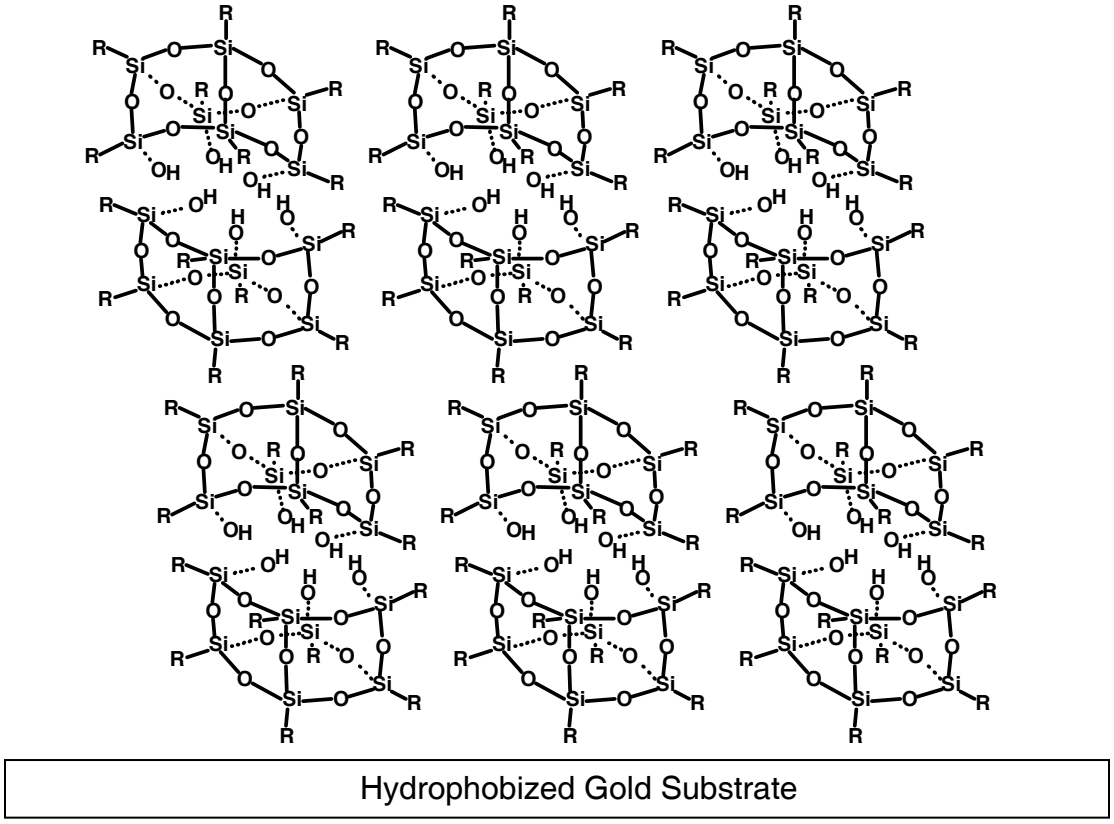

Figure 5.2 Multilayer POSS films created using Langmuir-Blodgett techniques. R represents a phenyl ring.

interactions between the hydrophobic phenyl rings and the hydrophobized substrate initiate the film formation, while hydrogen-bonding interactions between silanol groups and van der Waals forces between the phenyl rings sustain multilayer growth.[142] Here, the combination of a silicon oxide core and organic ring substituents provides a unique surface from which to study the chemistry of chlorinated phosphate molecules. It was hypothesized that the slightly acidic, highly-hydrogen bonding environment would provide a system capable of adsorbing and decomposing chlorophosphates. RAIRS, XPS, uptake coefficient measurements, TPD, and FAB-MS revealed that both MDCP and TCP undergo hydrolysis reactions with surface silanol sites. This reaction leads to POSS molecules that are corner capped by a phosphoryl functional group.

5.2. Experimental Details

5.2.1. Materials

1-hexadecanethiol (92%), dimethyl methylphosphonate (97%), methyl dichlorophosphate (97%), trichlorophosphate (99%), phosphoric acid (≥85%), and hydrochloric acid (≥99%) were purchased from Aldrich and trisilanolphenyl-polyhedral oligomeric silsesquioxane (POSS) was purchased from Hybrid Plastics, Inc. All chemicals were used as received. Glass substrates coated with a 50 Å chromium adhesion layer and a 1000 Å gold layer were purchased from Evaporated Metal Films, Corp.

5.2.2. Langmuir-Blodgett Film Deposition

LB-films were deposited on gold substrates (1" x 1" x .062") that provided a reflective surface for RAIRS studies. Smaller gold substrates (1 cm x 1 cm x 1 mm) were used for XPS studies. A 3:7 mixture of H_2O_2 (30%):H_2SO_4 (concentrated) was used to clean the gold substrates for one hour. (*"Piranha solution" is an oxidizing mixture that can be explosive when brought in contact with organic materials.)* The substrates were rinsed with copious amounts of deionized water (18.2 MΩ, Millipore, MilliQ Gradient A-10) and absolute ethanol and placed immediately in a 1 mM ethanolic solution of 1-hexadecanethiol for approximately 18 hours. The resulting hydrophobic self-assembled monolayer was rinsed with absolute ethanol and dried in a stream of N_2. The substrate was then affixed to a hydrophobized glass sample mount and used as a template for LB-film deposition.

In addition to gold substrates, silicon wafers were used to prepare POSS LB-films for XPS studies. The wafers were initially cut to 1" x 1" sizes and cleaned for 2 hours in

28% NH_4OH:30% H_2O_2:Millipore water (1:1:5 ratio by volume). The substrates were then cleaned in a 3:7 mixture of H_2O_2 (30%):H_2SO_4 (concentrated). The silicon was hydrophobized using a buffered oxide etch (HF) and a 40% NH_4F solution (Doe and Ingalls, CMOS grade).

POSS LB-films were prepared on a standard LB-trough (KSV 2000, KSV instruments, Inc.) housed in a Plexiglas box held at 300 K. The clean trough was filled with ultra-pure water (18.2 MΩ, Millipore, MilliQ Gradient A-10), and a 0.5 mg/mL solution of POSS in chloroform was used to spread the film across the air-water interface. The solution was spread to a pressure of 5-8 mN/m, well below the target value, to eliminate the formation of bi- or multi-layers. A compression rate of 10 mm/min was used to achieve the desired Π value of 10.5 mN/m and maximum barrier speeds of 10 mm/min were used to maintain constant Π. The dipper speed was held at 10 mm/min for both the downwards and upwards strokes with an upper delay of 60 s and a lower delay of 15 s. Using Y-type deposition, 10 dipping cycles created LB-films with 20 layers of POSS molecules. Further preparatory and film characterization details are described in Chapter 4.

5.2.3. Solution-Phase Preparation Methods

Solution-phase preparation methods were employed in effort to disorder the POSS film and potentially free some of the silanol groups from hydrogen bonding interactions with adjacent POSS molecules. SAMs prepared from solutions of OH-terminated ($HS(CH_2)_{16}OH$) alkanethiols, were immersed in 1 mM ethanolic solutions of the cubic silsesquioxane molecules. The extent of exposure of the substrate in the silsesquioxane solution was independent of the film quality. The films were not rinsed prior to use, but

were dried in a stream of ultra-pure N_2.

5.2.4. Characterization of LB-Films and Interactions with CWA Simulants

5.2.4.1. Reflection Absorption Infrared Spectroscopy

Reflection absorption infrared (RAIR) spectra were collected using a Bruker IFS 66v/S spectrometer with a resolution of 2 cm^{-1}. Spectra were collected using p-polarized light at an incident angle of 86° and a DTGS (deuterated-triglycine-sulphate) detector. Spectra were collected with a clean gold substrate as a background reference and are the average of 100 scans.

5.2.4.2. X-ray Photoelectron Spectroscopy

XPS was performed on a Perkin Elmer 5400 X-ray Photoelectron Spectrometer equipped with a monochromatized Mg(Kα) radiation source (1253.6 eV) and a position sensitive, multi-channel plate detector. Measurements were taken at a pressure of ~10^{-7} mbar and a take-off angle of 15° with respect to the surface normal. Binding energies are referenced to C (1s) at 284.8 eV. High resolution multiplex spectra were collected with an acquisition time of 8 minutes per region, a 1 mm x 3.5 mm spot size, and 300 W electron beam power.

5.2.4.3. Uptake Coefficient Measurements

Sorption of phosphate molecules on or within POSS LB-films was studied using the direct reflection technique of King and Wells.[82] Uptake measurements were performed in an ultra-high vacuum chamber with a base pressure of 5 x 10^{-10} Torr equipped with an Extrel mass spectrometer. Molecular beams were created by bubbling N_2 (~750 Torr) through a reservoir of the liquid phosphate held at 353 K. The phosphate/N_2 vapor passed through a 0.05 mm diameter nozzle (General Valve) and into

the first differential pumping stage (2.6 x 10^{-5} Torr). A 0.40 mm diameter conical skimmer located 6 mm from the nozzle further collimated the simulant/N_2 beam as it entered the second differentially-pumped chamber. The beam then passed through a 1.5 mm aperture, located in the third differentially-pumped stage and through a 2.2 mm collimating aperture before passing into the main UHV chamber, where it struck the sample surface with a 1 cm^2 spot size.

The POSS substrate was mounted on a stainless steel sample holder and introduced to the UHV chamber via a load-lock chamber. A liquid N_2 reservoir allowed cooling of the sample to ~140 K. A Teflon® flag in the main chamber was used to prevent the beam from hitting the surface until desired. The partial pressure of the adsorbing gas in the main chamber was measured with the mass spectrometer. The fraction of the incident molecular beam which adsorbed on the surface was established from the decrease in the partial pressure as the beam was allowed to strike the surface.[82] The sticking coefficient is dependant upon surface coverage and energy barriers to adsorption and is described by Equation 1 in Chapter 2.

5.2.4.4. Temperature Programmed Desorption Measurements

The UHV instrument used to conduct uptake coefficient measurements was also utilized in the collection of temperature programmed desorption data. POSS LB-films saturated with phosphate species were installed in the main UHV chamber and laser-aligned to place the surface normal in-line with the two collimating apertures of the Extrel mass spectrometer. The surface was positioned 29 cm from the ionizer of the detector, which viewed a 1 cm^2 spot size on the surface. The thermocouple was positioned at the face of the sample mount and a linear heating ramp of 0.1 K s^{-1} was

used to study the adsorption energy of phosphate derivatives and residues.

5.2.4.5. Fast Atom Bombardment Mass Spectrometry (FAB-MS)

Fast atom bombardment (FAB) is an extension of particle desorption methods, such as plasma desorption. In FAB, an analyte/matrix mixture is bombarded with a fast particle beam, such as an atom beam, depicted in Figure 5.3. As the atomic beam strikes the sample matrix, energy is transferred and the sample is disrupted, resulting in the emission of sputtered secondary ions that can be detected and analyzed with a mass spectrometer.

Mass spectra were recorded with a JMS-HX110 dual-focusing mass spectrometer (MS) (JEOL Co. Ltd., Tokyo, Japan) located in the analytical services center in the department of chemistry at Virginia Polytechnic Institute and State University. The MS

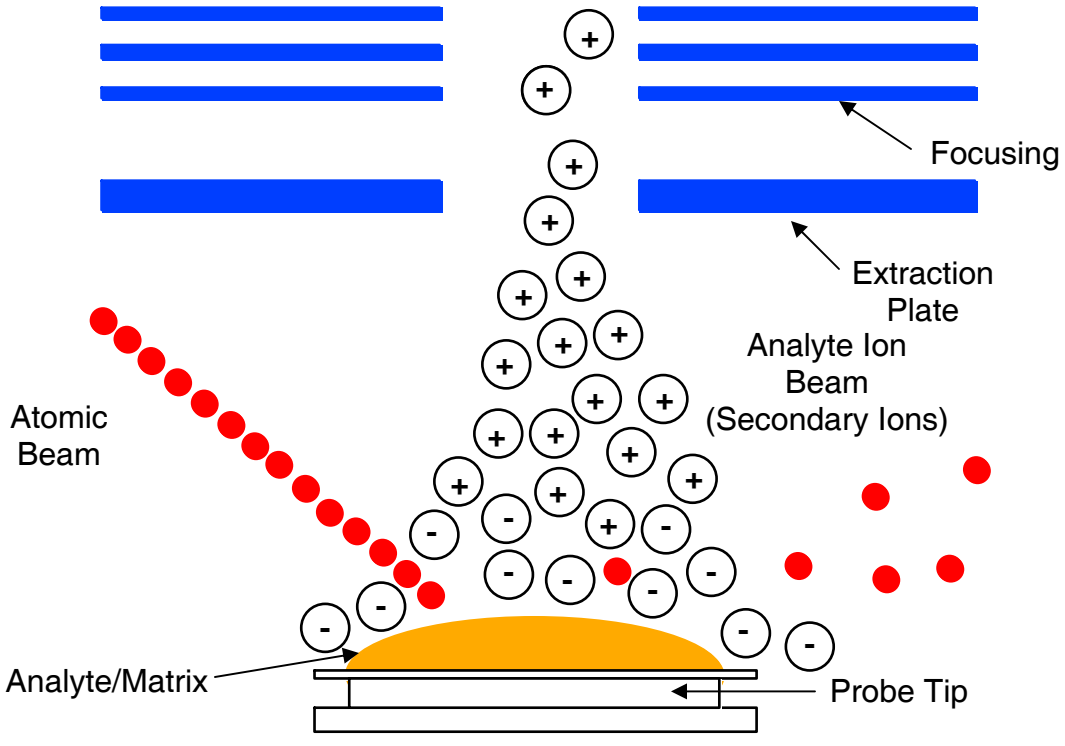

Figure 5.3 Representation of a fast atom bombardment (FAB) source.

is equipped with a xenon fast-atom bombardment (FAB) gun, with an ion acceleration voltage of 10 kV. The ionization mode was set to FAB-(+) with 3-nitrobenzyl alcohol as the matrix. Bulk samples of POSS were exposed to MDCP in the same manner as the POSS LB-films described below (Section 5.2.5.). Both unmodified POSS and MDCP-exposed POSS samples were analyzed by MS.

5.2.5. CWA Simulant Exposure Studies: Saturated Organophosphonate Vapor Sorption

Complete saturation of POSS LB-films by phosphate molecules was accomplished by placing a freshly prepared film into a 60 cm^3 N_2-purged vapor deposition chamber. Approximately 5μL of the desired sorbate was then placed adjacent to the surface sample. The vapor-phase concentration of the chlorinated phosphate molecules was augmented by heating the chamber slightly above room temperature (308 K). The chamber was allowed to remain at these conditions for at least ten minutes to ensure complete saturation of the LB-film. After ten minutes, a film has been exposed to ~1 $x10^8$ langmuirs of DMMP, where 1 langmuir is equivalent to 10^{-6} Torr · s. Upon saturation, the films were removed from the vapor deposition chamber and subjected to a N_2 purge prior to further analysis.

5.3. Results and Discussion

5.3.1. Exposure of Films to Chlorinated CWA Simulant Molecules

5.3.1.1. Uptake of MDCP within POSS Films

Investigation of the sticking probability of DMMP on POSS LB-films indicated that uptake is low ($\lesssim$0.05), even at surface temperatures of 140 K (see Section 4.3.2.1.).[78] The absence of considerable DMMP uptake in the UHV studies was attributed to the

densely-packed hydrophobic phenyl rings located at the film/vacuum interface.[78] This interpretation is in agreement with results presented by Bertilsson and Crooks, who reported similar interactions between organophosphate derivatives and non-polar non-hydrogen bonding surfaces.[14,17,19] To further assess the interactions of CWA simulants with POSS LB-films, the present study examines the uptake and reactivity of chlorinated phosphate derivatives that are expected to be more reactive than non-chlorinated phosphate species and in turn may be a better model for CWAs.

Like DMMP, results suggest that the sticking probability of MDCP on POSS LB-films is very low. The uptake coefficient was determined to be below the detection limits ($\lesssim$0.05) of our experimental design. RAIRS confirms low uptake of organophosphonates on solution deposited films, as well. The bulky phenyl substituents of the POSS LB-films appear to significantly limit the uptake of both non-chlorinated and chlorinated organophosphate compounds. However, upon prolonged exposure to high vapor pressure MDCP or TCP, POSS LB-films absorb substantial amounts of organophosphate molecules. However, unlike the DMMP molecules absorbed within the film, the chlorinated phosphate molecules significantly alter the structure of the POSS LB-film upon adsorption. Whereas DMMP adsorbs to the silanol groups of the POSS molecules through hydrogen-bonding interactions between the phosphoryl and methoxy functional groups,[78] MDCP and TCP appear to react with the POSS LB-film in such a way that the hydroxyl groups are completely removed.

5.3.1.2. RAIRS Characterization of MDCP- and TCP-saturated POSS Films

The infrared spectra of a freshly prepared 20-layer POSS LB-film are included in Figures 5.4.A and 5.5.A for reference. Spectra 5.4.B and 5.5.B are acquired from a 20-

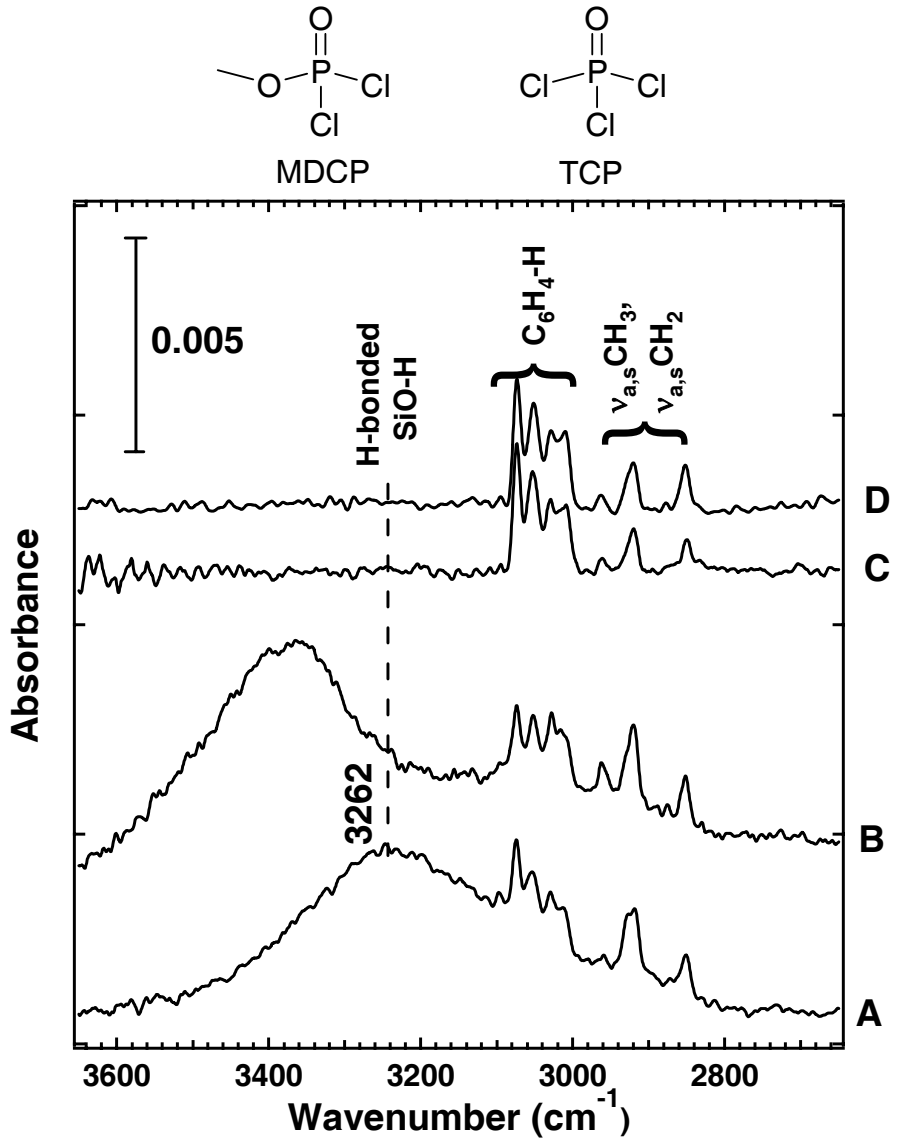

Figure 5.4 The RAIR spectrum of a freshly-prepared POSS LB-film (A) and the spectra of POSS LB-films saturated with DMMP (B), MDCP (C) , and TCP (D). Assessment of the SiO-H mode suggests that while DMMP is molecularly adsorbed within the film, the chlorinated phosphate molecules react with the hydroxyl groups of the POSS molecules.

layer POSS LB-film saturated with DMMP. Spectra of MDCP and TCP saturated 20-layer films are included as spectra C and D, respectively, in Figures 5.4 and 5.5. The peak positions are highly reproducible in both unmodified and saturated films and the intensity of peaks associated with the film structure and the absorbed or reacted

phosphate derivatives increases linearly with the number of layers of POSS molecules present in the film.[78]

The high frequency region of the infrared spectrum is shown in Figure 5.4. The infrared spectrum of a POSS-film reveals strong hydrogen-bonding interactions between the silanol groups of the film (Figure 5.4.A), as indicated by the broad, intense mode centered at 3262 cm^{-1}. As expected, the high frequency region of a freshly prepared film also includes a series of modes between 2800 and 3100 cm^{-1} attributed to vibrational modes of the phenyl rings and the underlying 1-hexadecanethiol self-assembled monolayer used in the preparation of the POSS LB-films.

The characterization of DMMP-saturated POSS LB-films is detailed in Chapter 4. In brief, Figure 5.4.B displays evidence that, upon DMMP diffusion and subsequent adsorption, the hydrogen-bonding network between the silanol groups of the POSS LB-film is disrupted, causing a shift in peak position to 3380 cm^{-1}. The absorbed organophosphonate molecules also give rise to surface bound methyl and methoxy groups which have vibrational modes at 3009 and 2926 and 2958 and 2856 cm^{-1}, respectively.

In contrast to the molecular adsorption of DMMP within the multilayered LB-films, both MDCP and TCP react with the silanol groups of the POSS molecules. Figures 5.4.C and 5.4.D show that upon exposure to MDCP or TCP vapor there is a complete loss of the hydrogen-bonded SiO-H mode. In addition, the predicted peaks associated with methoxy vibrational modes in the spectrum of a MDCP-saturated film at 2999 and 2968 cm^{-1} are absent.[37]

Figure 5.5 shows the low-energy region of the RAIR spectra of an unmodified

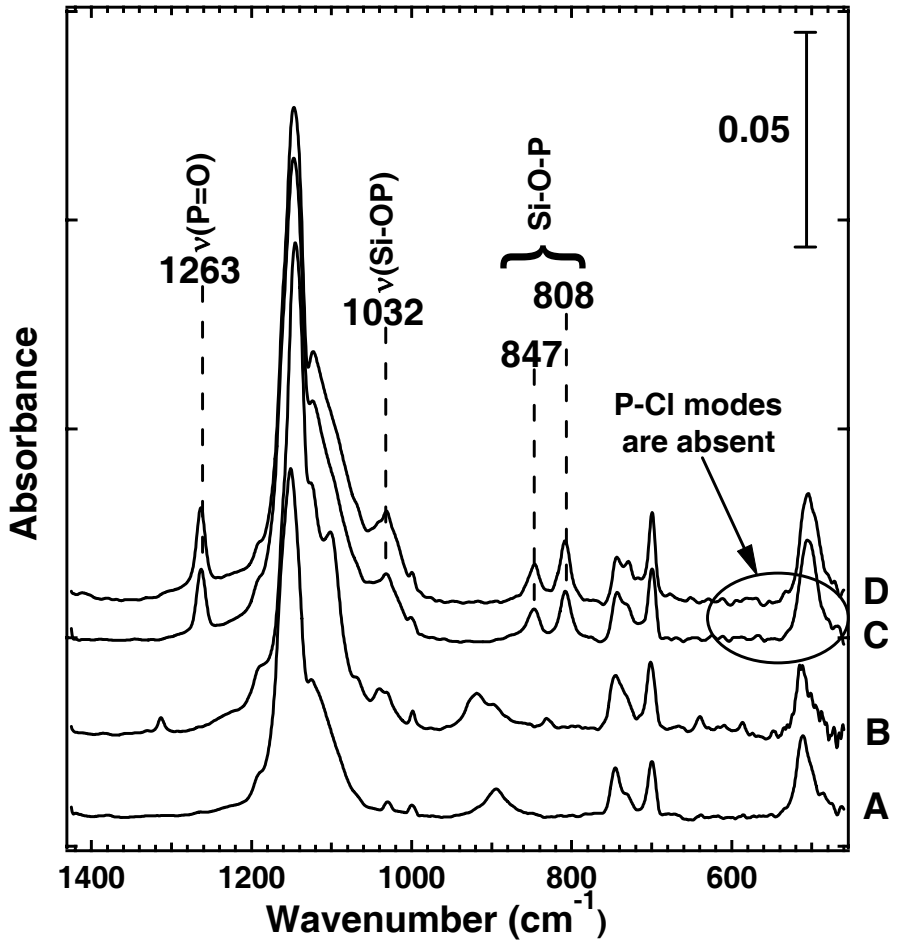

Figure 5.5 The RAIR spectrum of a freshly-prepared POSS LB-film (A) and the spectra of POSS LB-films saturated with DMMP (B), MDCP (C), and TCP (D). The presence of Si-O-P vibrational modes and the absence of P-Cl stretches denote a reaction between the chlorinated phosphate molecules and the POSS LB-films.

POSS LB-film (A) and POSS LB-films exposed to DMMP (B), MDCP (C) and TCP (D) vapor. The Si-O-Si vibrational mode of the POSS cages gives rise to the most intense peak, centered at 1150 cm^{-1} in the freshly-prepared film. Saturation with any of the three phosphate derivatives examined in this study causes this peak to shift several wavenumbers. This, in conjunction with new Si-O modes, present as prominent shoulders between 1100 and 1130 cm^{-1} in Figure 5.5.B, C, and D, supports the assertion that upon phosphate exposure, the silicon-oxide film structure is somewhat perturbed.

The phosphoryl stretching mode of DMMP absorbed within the POSS LB-film gives rise to a broad shoulder positioned at 1234 cm^{-1}, while the $\delta_s(P\text{-}CH_3)$ mode is apparent at 1313 cm^{-1}.[78] Examination of POSS LB-films saturated with the chlorinated phosphates reveals a sharp, intense peak at 1263 cm^{-1} in both spectra (Figure 5.5.C and 5.5.D), which is consistent with surface bound phosphoryl groups.[37] Vapor-phase MDCP and TCP give rise to $\nu(P{=}O)$ modes in this spectral region, at 1316 and 1321 cm^{-1}, respectively.[37] The nearly 60 cm^{-1} shift to lower energies of the $\nu(P{=}O)$ mode of chlorophosphates absorbed within POSS LB-films is significantly larger than that observed for the MDCP and TCP adsorbed on silica, which red-shift to 1291 and 1285 cm^{-1}, respectively.[37] Further inspection of the low-energy spectral region shows a new peak in both Figures 5.5.C and 5.5.D at 1032 cm^{-1}, attributed to an Si-O stretching vibration in Si-O-P linkages.[177,178] Bands at 808 and 847 cm^{-1} are likely associated with Si-O-P bending motions.[177-179] These modes are not present in the DMMP-saturated film system. DMMP diffuses into and physisorbs within the POSS LB-film at silanol sites via hydrogen-bonding interactions (Figure 5.5.B).[78] MDCP and TCP appear to diffuse into the POSS LB-film and undergo a hydrolysis reaction with silanol groups, leaving phosphate residues chemisorbed within the film. This interpretation is supported by the absence of P-Cl stretching modes, as well as the notable absence of methoxy vibrational modes in the MDCP-POSS system (Figures 5.4.C and 5.5.C). The new modes associated with surface bound phosphoryl functional groups persist when films are heated to temperatures of 450 K.

Kanan et al. reported vibrational modes of adsorbed TMP, DMMP, MDCP and TCP on thin films of silica and investigated the desorption of these phosphate species at

elevated temperatures.[37] Based upon their results, it was concluded that each of the molecules undergoes hydrogen-bonding interactions with surface Si-OH groups. The strength of the interaction was attributed to the number and type of hydrogen-bonds formed between the adsorbate molecules and the silica surface. Their work indicated that the TCP was only weakly held on the surface through one hydrogen bond and was completely removed by evacuation at room temperature. MDCP was held more strongly on the silica surface than TCP. Hydrogen-bonds between the surface Si-OH functional groups and the P=O and the O-CH_3 groups of MDCP were responsible for the strength of the interactions. Furthermore, MDCP molecules could be removed by evacuation at 428 K. In their studies, IR spectra indicated that the P-Cl bonds remained intact and no decomposition of the phosphate molecules occurred. In sharp contrast, in the experiments discussed here, the RAIR spectra of MDCP and TCP saturated-POSS systems are effectively identical. The P-Cl modes are absent and phosphoryl functional groups appear to be incorporated in the POSS molecules, generating Si-O-P vibrations and a dramatically shifted ν(P=O) mode. Moreover, on a macroscopic level, adsorption of MDCP and TCP results in a change in the optical reflectivity of the film. The clean film initially appears a metallic gold color due to the substrate. Upon adsorption of phosphate molecules, the film has a milky white appearance. Further insight into the resulting structure of the reacted film was provided by XPS and FAB-MS measurements.

5.3.1.3. XPS Characterization of MDCP- and TCP-saturated POSS Films

The elemental composition and bonding environment of freshly-prepared and phosphate-saturated POSS LB-films were assessed using XPS. Figure 5.6 shows the high resolution XP spectra of the O (1s), Cl (2p), and P (2p) regions for freshly-prepared (A),

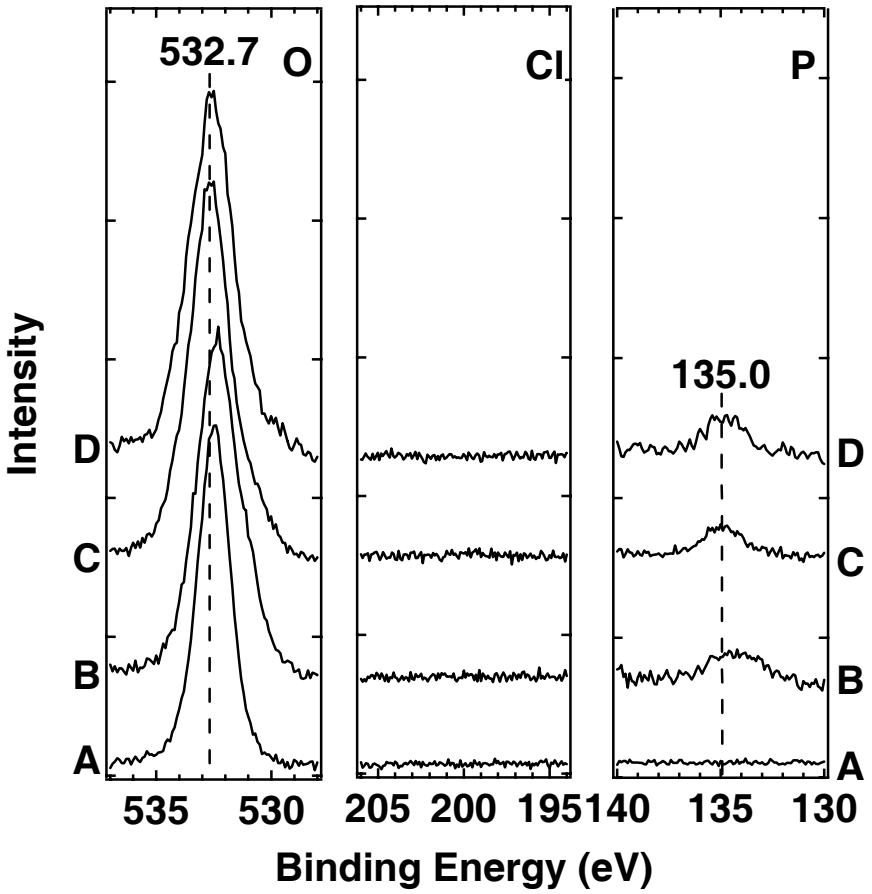

Figure 5.6 High resolution XP spectra of the O (1s), Cl (2p), and P (2p) regions of (A) a freshly-prepared POSS LB-film, (B) a DMMP-saturated POSS LB-film, (C) a MDCP-saturated POSS LB-film, and (D) a TCP-saturated POSS LB-film.

DMMP-saturated (B), MDCP-saturated (C), and TCP-saturated films (D). Other features of the spectra include peaks resulting from the silicon atoms comprising the cubic-structure of the POSS molecules and the carbon atoms present in the phenyl ring substituents and organophosphate molecules.

The O (1s) peak of the freshly-prepared POSS LB-film is present at 532.4 eV. This binding energy is consistent with O (1s) binding energies reported for pressed SiO_2 wafers.[180] Upon exposure to DMMP, the oxygen component of the POSS-system broadens to contain a shoulder at approximately 531 eV (Spectrum B). The shoulder is

attributed to oxygen atoms present in DMMP physisorbed within the POSS LB-film. MDCP- and TCP-exposure causes an overall broadening of the O (1s) peak and an increase to higher binding energies. The peak position at 532.7 eV for both the MDCP-POSS and TCP-POSS systems indicates that the oxygen atoms are present in a more strongly oxidizing environment than those oxygen atoms present in the DMMP-POSS system.[181]

The lack of XPS signal intensity between 195 and 205 eV indicates that chlorine atoms are absent in each of the films examined. This result is in agreement with RAIR data, where no indication of P-Cl stretching modes was observed. Chlorine was not expected in the spectra of freshly-prepared or DMMP-saturated POSS LB-films. The absence of chlorine in the MDCP-exposed and TCP-exposed films gives further credence to the proposed reaction occurring between chlorinated-phosphate species and silanol groups of the POSS molecules.

Figure 5.6 shows that, as expected, phosphorus was detected on the DMMP-, MDCP-, and TCP-saturated POSS LB-films and not on the freshly-prepared film. DMMP molecules physisorbed within the POSS LB-film give rise to a binding energy of about 134.3 eV. This value is in good agreement with the binding energies of other published DMMP-sorbent systems and further substantiates that hydrogen-bonding interactions are responsible for the adsorption of DMMP molecules within POSS LB-films. Zhou et al. report that multilayers of DMMP molecularly adsorbed on titania surfaces, held at 120 K, have P (2p) binding energies of 135.4 and 134.9 eV, for condensed and molecularly sorbed DMMP, respectively.[75] Hegde et al. report a P (2p) binding energy of 134.5 eV for monolayers of DMMP held on Rh (100) surfaces through

bonds with the lone electron pairs of the phosphoryl oxygen atom.[27]

MDCP- and TCP-saturated POSS LB-films exhibited a P (2p) binding energy of 135.0 eV. A P (2p) binding energy slightly higher than that observed for surface bound DMMP indicates a more positive oxidation state for MDCP or TCP within the POSS film. In combination with RAIR spectra and the notable absence of chlorine in the XP spectra, this is consistent with the chlorinated phosphates undergoing a hydrolysis reaction, eliminating silanol functional groups, and leaving a phosphoryl species effectively capping the trisilanol-corner of the POSS molecules to yield Si-O-P=O groups.

5.3.1.4. Temperature Programmed Desorption Studies

TPD experiments were conducted on POSS LB-films that were saturated with MDCP or TCP, as described above. The ions in the fragmentation pattern of molecular chlorophosphates were not observed during the heating ramp to 578 K, nor were predicted hydrolysis products including HCl and CH_3OH. Thus, the data showed no evidence of molecular MDCP, molecular TCP or decomposition products desorbing from the surface during the TPD measurements. It is likely that the lifetime of non-covalently bound reaction products within the LB-film structure is very short. Therefore, upon transfer of the substrate from the vapor deposition chamber to the UHV instrument, the brief duration of these reaction products within the film precludes direct observation by TPD.

5.3.1.5. FAB-MS Characterization of Bulk POSS and MDCP-exposed Bulk POSS

Bulk POSS and MDCP-exposed bulk POSS samples were subjected to FAB-MS to better characterize the reaction between the chlorinated phosphate species and the

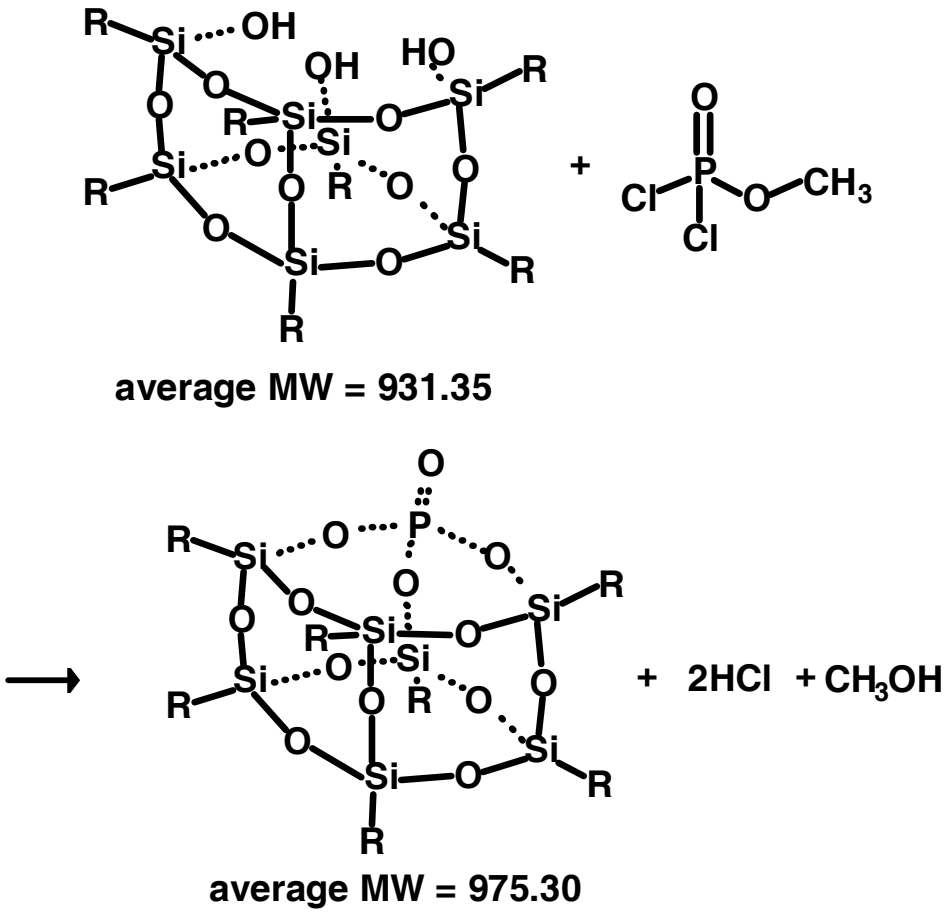

Figure 5.7 FAB-MS results indicate that MDCP reacts with the silanol groups of the POSS molecules, leaving a silicon oxide cage structure capped with a phosphoryl functional group.

POSS molecules. Similar analyses were conducted on POSS molecules and reaction products initially present in an LB-film structure. The pre-and post-exposure POSS LB-films were sonicated in several milliliters of ethanol and the resulting POSS solution was analyzed by FAB-MS. The signal from the ethanolic solutions, however, was insufficient. Thus, the results presented here were obtained from bulk POSS samples. A parent ion was observed at *m/z* 931.0852 ($M + H^+$) for the bulk POSS sample (mass expected for $C_{42}H_{38}O_{12}Si_7$ is 931.0827 amu). MDCP-exposed bulk POSS gave rise to a new ion peak at *m/z* 975.0355 ($M + H^+$). This peak is consistent with a corner-capping reaction that leaves a phosphoryl residue bound to a POSS molecule in bulk reactions, as

shown in Figure 5.7.

5.3.2. Hydrolysis of Chlorinated Phosphates within POSS Films

The reaction between MDCP or TCP and POSS LB-films is consistent with the reaction observed between halogenated phosphate molecules and various metal-oxide surfaces. The room temperature hydrolysis of sarin over MgO and γ-Al_2O_3 was first reported by Kuiper et al.[173] Wagner et al. further examined the interactions between GB and GD with MgO and Al_2O_3 surfaces.[16,34] The nerve agents were shown to readily decompose via hydrolysis reactions at room temperature to generate phosphonate species chemisorbed on both MgO and Al_2O_3 surfaces.

Kanan et al. have shown that upon exposure to WO_3 powders at room temperature, MDCP rapidly undergoes hydrolysis. Water vapor in the system was concluded to play an important role in the production of gas-phase HCl and CH_3Cl.[39] In addition, gas chromatography-mass spectrometry (GC-MS) analysis revealed phosphate derivatives including $(CH_3O)PO(OH)Cl$, $(CH_3O)PO(OH)_2$, and $PO(OH)_3$.[39] MDCP was reported to initially interact with the surface through the phosphoryl group and subsequent hydrolysis reactions generated a range of phosphate residues chemisorbed to the surface. Not unexpectedly, elevated temperatures induced further decomposition by driving the methoxy groups from the surface.[39] The results presented here suggest that similar reactions occur between MDCP or TCP and POSS LB-films. Upon exposure and diffusion into the film, the chlorinated phosphate molecules appear to readily hydrolyze to yield surface bound phosphoryl groups. Rather than a range of absorbed hydrolysis products, the parent MDCP and TCP molecules appear to react and saturate all, or very nearly all, available sorption sites within a POSS LB-film.

In contrast to previous studies on thin films of silica,[37] POSS LB-films provide a unique silicon-oxide environment that is capable of decomposing chemical warfare agent simulants at room temperature. The POSS molecules supply surface Brønsted acid sites that can readily participate in acid catalyzed hydrolysis of chlorinated phosphate molecules. It is expected that the substitution reaction involves the nucleophilic addition of the OH group to the phosphate species and is followed by the elimination of the chlorine leaving group coupled with a proton transfer, which results in the production of HCl. Similar arguments can be made for the elimination of the methoxy groups of MDCP. Control experiments, exposing freshly prepared POSS films to HCl and phosphoric acid, revealed that expected hydrolysis products of MDCP and TCP were not absorbed within the silicon oxide cage-like structures, even under saturated vapor conditions. This is in contrast to literature reports of the decomposition products of organophosphonates adsorbing to MgO, Al_2O_3, and WO_3 surfaces.

In their work on silica, Kanan et al. report only weak interactions between MDCP and TCP and SiO_2 thin films.[37] In contrast, a highly-favorable interaction between POSS and MDCP or TCP is likely a result of the steric conformation of the silanol groups within the POSS molecules and the molecular structure of chlorinated phosphates. The phenyl rings of the POSS molecules seem to provide slightly acidic hydroxyl groups that interact very strongly with both non-chlorinated and chlorinated phosphate molecules. Isobaric measurements conducted by the Esker Research Group at Virginia Polytechnic Institute and State University suggest that the pKa of POSS is ~6-7. A red-shift in the ν(P=O) mode when incorporated within the POSS LB-film, the appearance of Si-O-P vibrational modes, and the persistence of these modes at elevated temperatures suggests

that the slightly acidic hydroxyl groups catalyze the hydrolysis of the chlorinated phosphate molecules. This reaction generates highly stable surface bound phosphate residues.

5.3.3. The Role of Water Co-Absorbed within POSS Films

As described by Oliveira et al.,[182] the presence of co-absorbed water on or within thin films is highly relevant and can dramatically affect film properties, such as electrical response. Although many reports have detailed the negative affects of humidity on sample response reproducibility, the presence of co-adsorbed water can be harnessed for beneficial applications. As illustration, the development of sensitive taste sensors[183] and the efficient doping of polyaniline LB-films have been attributed to water adsorbed at the system-gas interfaces.[182]

To investigate the influence of water co-absorbed within the POSS LB-film structures on the adsorption of organophosphonate species, deuterium oxide exposure studies were conducted. A freshly prepared POSS LB-film was exposed to an environment saturated with D_2O vapor for 2.5 hours at room temperature. Figure 5.8 shows the high frequency region of a spectrum obtained from a clean POSS film (A), as well as that generated by a post D_2O exposed POSS film (B). Spectra C and D, discussed below, are those resulting from the deuterated film being sequentially exposed to DMMP and MDCP, respectively. In addition to the previously reported hydrogen-bonded Si-O-H mode at 3262 cm^{-1}, D_2O exposure results in a new mode at 2388 cm^{-1}, which is attributed to the hydrogen-bonded D-O-D stretching mode of D_2O absorbed molecularly within the film. This broad absorption feature may also contain contributions from hydrogen-bonded Si-O-D functionalities.[184] However, if exchange occurs it does not

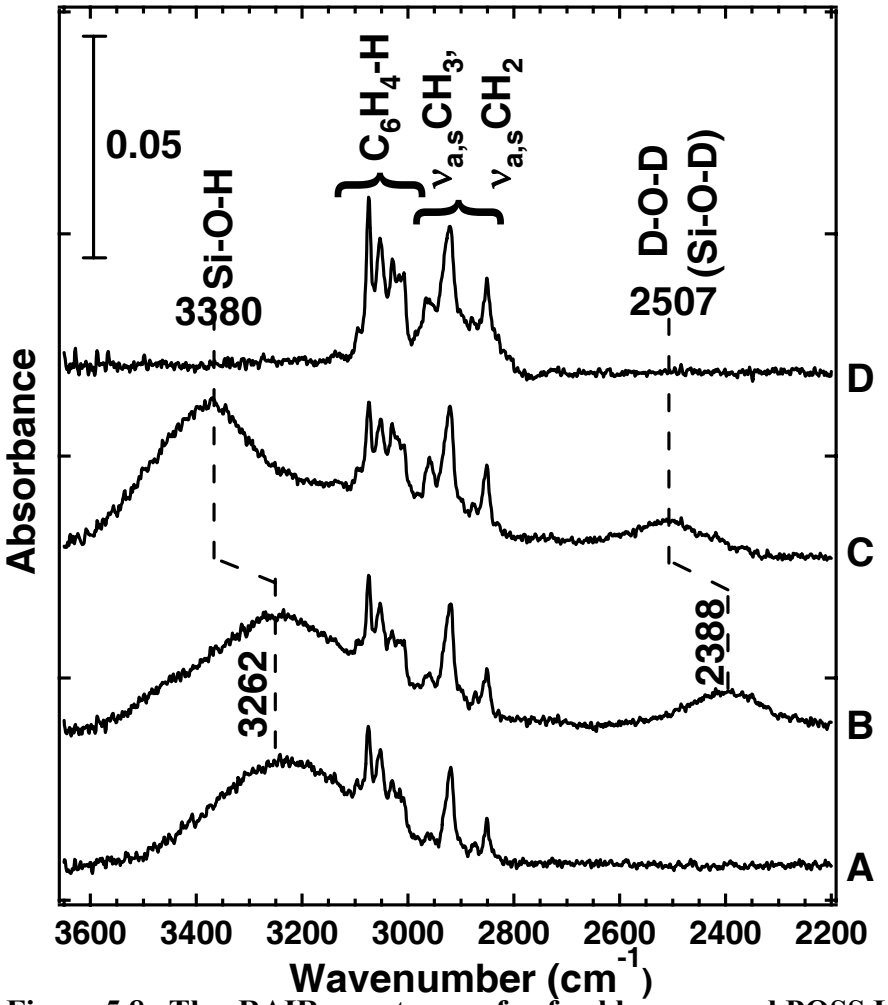

Figure 5.8 The RAIR spectrum of a freshly-prepared POSS LB-film (A) and the spectra of a POSS LB-film exposed sequentially to D_2O (B), then DMMP (C) , and finally MDCP (D).

appear to be complete, as the absorption at 3262 cm^{-1} persists after D_2O exposure. Comparison of spectra A and B reveals a slight decrease in the intensity of this mode. This suggests that the broad feature initially contains contributions from both hydrogen-bonded silanol stretches and possibly hydrogen-bonded O-H stretches arising from absorbed water. Therefore, D_2O molecules are able to diffuse into the film and exchange with the absorbed water molecules, leaving Si-O-H functional groups intact. Surprisingly, the overwhelming majority of these silanol groups do not undergo exchange, even after extended periods of D_2O exposure (18 hours). Thus, the strong

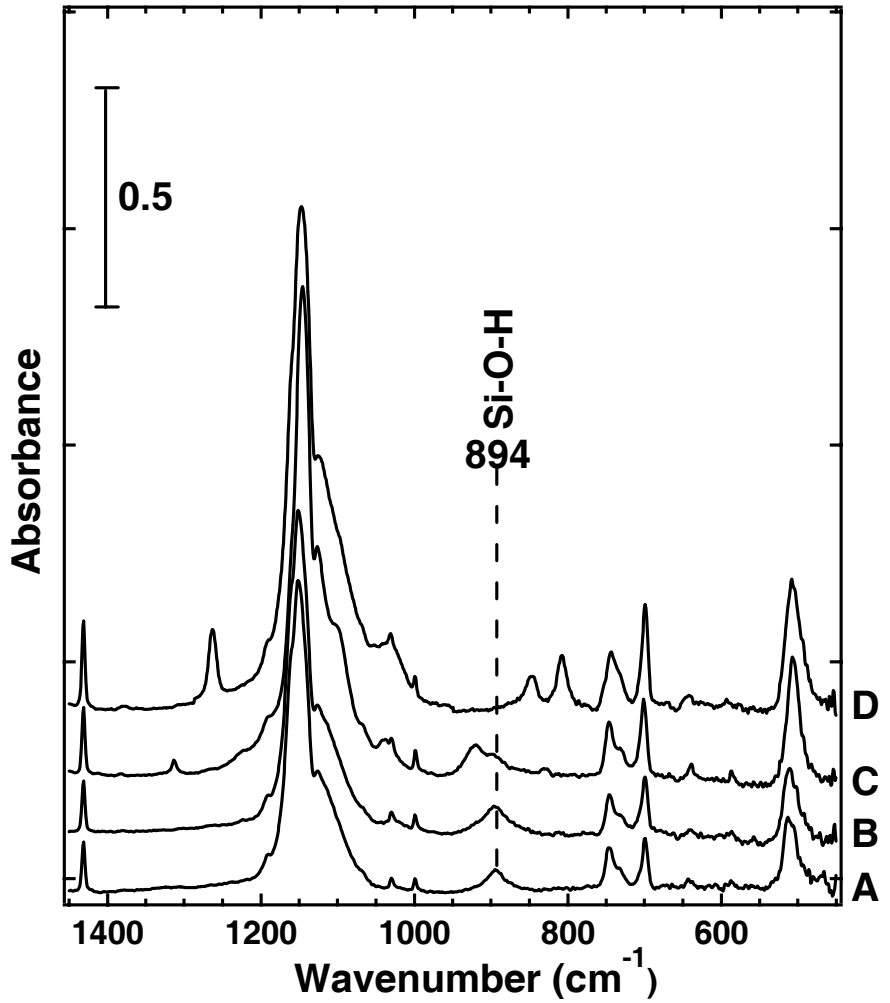

Figure 5.9 The low frequency region of the RAIR spectra of a freshly-prepared POSS LB-film (A) exposed sequentially to D_2O (B), then DMMP (C) , and finally MDCP (D).

hydrogen bonding interactions between neighboring Si-O-H groups render an H-D exchange unfavorable. The possibility of exchange at film defect sites, however, cannot be eliminated.

Inspection of the lower frequency region of these spectra in Figure 5.9.A and 5.9.B shows no spectral changes attributed to the diffusion and adsorption of D_2O within the POSS film structure. The Si-O-H stretching mode persists and any signal attributed to Si-O-D stretching vibrations is not observed. This supports the hypothesis that few, if any, silanol functionalities undergo H-D exchange.

The reverse exchange of OD for OH groups is not rapid. At room temperature and under ambient humidity, the D_2O exposed film was removed from the deposition chamber and transferred to the RAIR spectrometer for analysis. Even after this interval and exposure to background water in the spectrometer, the signal at 2388 cm^{-1} was present and did not deteriorate over the analysis period. The rapid exchange between sorbed water and D_2O occurs in a saturated environment, but the reverse exchange does not readily occur with atmospheric water.

Immediately after RAIRS analysis, the deuterated POSS LB-film was placed in a deposition chamber that was saturated with DMMP vapor. The film was allowed to remain in the saturated environment at 308 K for at least 10 minutes and was then examined by RAIR spectroscopy. The resulting spectrum is presented in Figure 5.8.C and 5.9.C. Saturation of the deuterated film with DMMP, as in the case of a freshly-prepared POSS film, results in the dramatic shift of the hydrogen-bonded Si-O-H mode from 3262 cm^{-1} to 3380 cm^{-1}. This is a result of newly formed hydrogen bonding interactions between the organophosphonate molecules and the surface silanol sites. In addition, there is a notable shift of the D-O-D peak from 2388 cm^{-1} to 2507 cm^{-1}. The shift of this mode to higher energies implies that D_2O, and therefore water, plays a role in the adsorption channel of DMMP within the POSS LB-films. In addition, there is a slight loss in absorbance intensity of the peak at 2507 cm^{-1}, as compared to the band at 2388 cm^{-1}. This decrease indicates that some of the DMMP appears to displace D_2O molecules, though there is not a complete replacement. It is likely that coincident interactions between co-absorbed water (D_2O) and DMMP and surface silanols and DMMP result in relatively high energies of adsorption as compared to analogous

systems.

In an effort to characterize the nature of the interactions between chlorinated phosphate species and the POSS LB-films, the D_2O/DMMP saturated film was subsequently exposed to a saturated environment of MDCP molecules at a slightly elevated temperature for 10 minutes. The RAIRS data obtained from this film is presented in Figures 5.8.D and 5.9.D and is nearly identical to that presented in Figure 5.4.C and 5.5.C. The spectrum reveals that the MDCP molecules diffuse in the multilayered POSS system, displace the initially sorbed DMMP molecules and undergo the hydrolysis reaction, as detailed above. Thus, while it is apparent that the presence of co-absorbed water may be beneficial for the adsorption of non-chlorinated organophosphonates within the POSS LB-films, the chlorinated species appear to displace pre-absorbed species and undergo decomposition reactions with surface silanol groups. It is expected that the chlorinated phosphate molecules also undergo hydrolysis reactions with co-absorbed water, however, as indicated previously, expected reaction products, such as phosphoric acid and HCl, did not remain within the film structure. If any vapor-phase hydrolysis products do absorb within the POSS LB-film, they are quickly displaced by the more reactive chlorinated phosphate molecules. The reaction products diffuse away from the system and are not detected by the RAIR studies presented here.

The ultimate role of water in the adsorption of organophosphonates and chlorophosphates within POSS LB-films is uncertain. RAIRS studies confirm the presence of water within the film structure and indicate that only some of the water is displaced when the film is exposed to DMMP. Therefore, it is difficult to determine the

necessity of water in the adsorption mechanism. The film deposition techniques result in the incorporation of water within the film and make the creation of a dry film unfeasible. Heating a POSS LB-film to drive water from the surface results in the elimination of silanol groups and closing of the silicon oxide cage structure, resulting in an inert film (Section 4.3.1.1.1). As discussed above, the concurrent interactions between organophosphonates and co-absorbed water (D_2O) and surface silanols likely result in strong sorbate-sorbent interactions. Chlorophosphates, in contrast, appear to displace pre-absorbed organophosphonates and readily undergo hydrolysis with surface silanols and likely co-absorbed water.

5.4. Conclusions

This study has examined the uptake and reactivity of chlorinated phosphate derivatives within trisilanolphenyl-polyhedral oligomeric silsesquioxane Langmuir-Blodgett films. Despite a low uptake coefficient the POSS LB-films are found to react with chlorophosphates and saturate with the phosphoryl residues. The structure of the POSS molecules likely provides a sterically favorable adsorption site and the slightly acidic hydroxyl groups readily undergo hydrolysis reactions with chlorinated phosphate molecules. RAIRS, XPS, and FAB-MS indicate that upon adsorption, subsequent substitution and elimination reactions produce surface bound phosphoryl groups. The chemisorbed phosphoryl residues are very strongly held within the LB-film and are not removed at 450 K.

The experimental results reported here positively demonstrate that POSS LB-films are capable of sequestering and decomposing halogenated CWA simulant molecules at room temperature. MDCP and TCP are similar to nerve agents in that they

both possess phosphoryl and organic functional groups, as well as halogen atoms (see Figures 1.1 and 1.2). Therefore, the results reported for the decomposition of MDCP and TCP within POSS LB-films may be indicative of the behavior of nerve agents (i.e. GB or GD) within a POSS system. Reports in the literature indicate that GB, GD, and VX decompose on MgO, Al_2O_3, and CaO through hydrolysis reactions to generate chemisorbed phosphate residues.[34,172-174] Similarly, the nature of the POSS films is such that chlorophosphates readily decompose upon adsorption to yield bound phosphoryl residues. The reactivity of CWAs and simulants within POSS films may be useful in the development of sensors and other self decontaminating materials. Complexities arise with respect to the uptake probabilities of organophosphonates and chlorophosphates on POSS films; however, if this issue can be addressed, POSS could be integrated into a CWA detection scheme. Reactive nerve agent molecules could be selectively extracted from a stream of gas and using analytical tools, such as infrared spectroscopy and mass spectrometry, the resulting bound residues and desorbing products could be identified. Furthermore, the change in optical reflectivity, though not a conclusive result, could prove useful as a first indication that harmful chemicals may be present.

Chapter 6
Conclusions and Future Work

6.1. Conclusions

A primary objective of the research presented here was the design and synthesis of model urethane-containing surfaces. The fundamental goal of this project was to create well-ordered self assembled monolayers (SAMs) that contained controlled concentrations of intrachain carbamate linkages at specified positions within the thin film. The data presented in Chapter 3 reveal that isocyanate chemistry can be used to create SAMs that have the general structure: $Au/S\text{-}(CH_2)_{16}O(C{=}O)NH(CH_2)_{n\text{-}1}CH_3$. Reflection absorption infrared spectroscopy (RAIRS), contact angle goniometry, and x-ray photoelectron spectroscopy (XPS) were the analytical tools used to characterize the organic thin films. The data indicate that vapor-phase isocyanate reactions, in conjunction with well-ordered hydroxyl-terminated template monolayers, yielded well-ordered organic thin films that contained intrachain hydrogen bonding functional groups. This study represents the first reported case of hydrogen bonding groups being placed within films while a high degree of order was maintained. The novel carbamate SAMs have been used to explore energy exchange pathways[185] and acid-base surface chemistry, as well as serving as a model for urethane chemical agent resistive coatings (CARC) used by the military.

Urethane-based CARC and similar paints are used in effort to limit the uptake of harmful CWAs. Exposure of the carbamate SAMs to both non-chlorinated and chlorinated organophosphonates resulted in no measurable uptake of the CWA simulant molecules. The result suggests that the coatings used by the military may in fact be beneficial in terms of personnel and equipment protection from exposure to CWAs.

In addition to modeling CARC surfaces, a goal of this research was to design a new set of nanostructured silicon oxide based surfaces capable of sequestering and decomposing organophosphonate molecules. Previous studies in the literature, described in Chapter 1, have focused primarily on the uptake and reactivity of CWA simulants on organic thin films and metal oxide powders and films. The studies reported in Chapters 4 and 5 present a detailed description of the interactions between non-chlorinated and chlorinated organophosphonate molecules with trisilanol-phenyl polyhedral oligomeric silsesquioxane (POSS) Langmuir-Blodgett films. These surfaces are comprised of molecules that contain a silicon oxide inorganic core that is surrounded by an organic corona of phenyl rings. RAIRS, XPS, temperature programmed desorption (TPD), uptake coefficient measurements, and fast atom bombardment mass spectrometry (FAB-MS) were used to probe the uptake and reaction characteristics of CWA simulants with the silicon oxide system.

Uptake measurements revealed that DMMP has a very low sticking probability on or within the POSS LB-films. Spectroscopy data, however, confirm that non-chlorinated organophosphonate species, specifically dimethyl methylphosphonate (DMMP) and trimethylphosphate (TMP), absorb molecularly within the POSS LB-films under saturated vapor conditions. DMMP and TMP are held strongly within the film through a network of hydrogen bonding interactions with adjacent silanol groups. Methyl dichlorophosphate (MDCP), like DMMP, was determined to have a very low uptake probability. Under saturated vapor conditions, chlorinated phosphates (MDCP and trichlorophosphate (TCP)) were shown to undergo hydrolysis reactions with the silanol groups of the POSS molecules and likely with water co-absorbed within the film. This

reaction resulted in POSS molecules corner capped with phosphoryl residues, as observed directly with FAB-MS. Due to the low uptake coefficient, direct observation of desorbing reaction products, like the expected HCl and methanol, was not viable.

6.2. Future Work

The high degree of hydrogen bonding present in the ordered structure of POSS LB-films is not amenable to organophosphonate uptake at low fluxes. However, exposure of bulk POSS samples to saturated environments of organophosphonates may offer additional information about reaction products. Bulk POSS samples contain the silicon oxide cubic structures in a randomized environment. Conceivably more silanol groups would be available for interaction with impinging CWA simulants. In order to further investigate the interfacial properties of CWA simulant and POSS molecules, namely direct observation of decomposition products of the MDCP and TCP hydrolysis reactions, experiments back-filling and saturating a closed system with organophosphonate molecules may be useful. This experimental design would mimic the saturated vapor conditions present in the vapor deposition chambers discussed in Sections 4.2.5.2. and 5.2.4.

Back-filling analytical chambers with highly reactive chlorophosphates may be damaging to the integrity of a UHV system. A more acceptable approach for back-filling a system with organophosphonates and exposing bulk samples would be utilizing a gas vacuum manifold to deliver DMMP to a diffuse reflectance infrared spectroscopy (DRIFTS) cell through tubing connected to a manifold. As reported by Mitchell and co-workers, DRIFTS can be used to follow *in situ* reactions between metal oxides and organophosphonates.[29] Extension of this technique to monitor the interactions between

POSS and organophosphonates may prove useful. Difficulties of such back-filling exposure studies arise because of competitive interactions with system water. In addition, monitoring reactions with DRIFTS can be difficult when the background pressures of CWA simulant molecules are fluctuating. It may become necessary to introduce a flux of organophosphonate molecules to the reaction cell, evacuate the cell and subsequently examine POSS/organophosphonate interactions with IR spectroscopy. Nonetheless, these types of experiments may be useful to further characterize the decomposition of chlorophosphates absorbed within POSS systems.

Force microscopy measurements, using atomic force microscopy (AFM) and scanning tunneling microscopy (STM), may also provide an interesting description of the topography of POSS films. A systematic study of film structure, both prior and subsequent to organophosphonate species, may generate new and interesting information regarding film degradation upon reaction with CWA simulants.

As a further extension of the body of literature reporting on the interfacial characteristics of organophosphonates on organic and metal oxide films, preliminary work in the Esker Research Group as incorporated metal ions, such as Cu^{2+}, within the POSS multilayered PB-films. Exposure of metal ion functionalized POSS films to organophosphonates may reveal very interesting chemistry. Crooks et al. reported that metal ion functionalized SAMs were capable of adsorbing multilayers of DIMP. This reported result is encouraging that the metal ion-POSS system may be superior in the sequestering of CWA simulants.

Investigators hoping to develop technology for the simultaneous detection of CWA simulants and high explosives (HEs), such as trinitrotoluene (TNT) and hexahydro-

1,3,5-trinitro-s-triazine (RDX), are faced with the requisite of examining highly polar species in conjunction with neutral species. Thorough insight into the chemical nature of parent species and their primary decomposition products is necessary for development of an efficient, effective and selective extraction strategy. Future research may investigate the fundamental chemical interactions of CWA simulants and HEs with novel POSS molecules, in an effort to develop solid phase extraction (SPE) techniques that are uniquely designed to preconcentrate two very different classes of molecules. Altering the hydrophobic organic functional groups will allow for the concurrent targeting and pre-concentration of the neutral HE molecules. This in turn will tailor the hydrophilic character of the POSS species and will provide a selective means by which the CWA simulant species can be concentrated and in turn chromatographically separated. This research will introduce novel extraction systems that are capable of recovering both highly polar and neutral species and can be directly applied to the concurrent investigation of CWA simulants and HEs.

The contribution of the hybrid inorganic organic POSS system to the field of CWA protection, detection and decontamination is noteworthy. POSS presents a tailorable silicon oxide system that has proven useful in adsorption and decomposition of CWA simulants. The chemistry of this system may prove useful in future development of CWA resistant coatings, sensors, and self-decontaminating films.

References

(1) Tusarova, I.; Halamek, E.; Kobliha, Z. *Enzyme and Microbial Technology* **1999**, *25*, 400-403.

(2) Smart, J. K. In *Medical Aspects of Chemical and Biological Warfare*; Sidell, F. R., Takafuji, E. T., Franz, D. R., Eds.; Borden Institute: Washington, D. C., 1997, pp 9-86.

(3) Yang, Y. C.; Baker, J. A.; Ward, J. R. *Chemical Reviews* **1992**, *92*, 1729-1743.

(4) Ward, J. R.; Yang, Y. C.; Wilson, R. B.; Burrows, W. D.; Ackerman, L. L. *Bioorganic Chemistry* **1988**, *16*, 12-16.

(5) Yang, Y. C.; Szafraniec, L. L.; Beaudry, W. T.; Rohrbaugh, D. K. *Journal of the American Chemical Society* **1990**, *112*, 6621-6627.

(6) Amos, D.; Leake, B. *Journal of Hazardous Materials* **1994**, *39*, 107-117.

(7) David, M. D.; Seiber, J. N. *Environmental Pollution* **1999**, *105*, 121-128.

(8) Li, Y. X.; Klabunde, K. J. *Langmuir* **1991**, *7*, 1388-1393.

(9) Lin, S. T.; Klabunde, K. J. *Langmuir* **1985**, *1*, 600-605.

(10) Li, Y. X.; Schlup, J. R.; Klabunde, K. J. *Langmuir* **1991**, *7*, 1394-1399.

(11) Li, Y. X.; Koper, O.; Atteya, M.; Klabunde, K. J. *Chemistry of Materials* **1992**, *4*, 323-330.

(12) Nieves, I.; Klabunde, K. J. *Journal of Materials Chemistry and Physics* **1988**, *18*, 485-498.

(13) Hoq, M. F.; Nieves, I.; Klabunde, K. J. *Journal of Catalysis* **1990**, *123*, 349-363.

(14) Crooks, R. M.; Yang, H. C.; McEllistrem, L. J.; Thomas, R. C.; Ricco, A. J. *Faraday Discussions* **1997**, *107*, 285-305.

(15) Zhanpeisov, N. U.; Zhidomirov, G. M.; Yudanov, I. V.; Klabunde, K. J. *Journal of Physical Chemistry* **1994**, *98*, 10032-10035.

(16) Wagner, G. W.; Bartram, P. W.; Koper, O.; Klabunde, K. J. *Journal of Physical Chemistry B* **1999**, *103*, 3225-3228.

(17) Bertilsson, L.; Engquist, I.; Liedberg, B. *Journal of Physical Chemistry B* **1997**, *101*, 6021-6027.

(18) Hughes, R. C.; Ricco, A. J.; Butler, M. A.; Pfeifer, K. B. *Applied Biochemistry and Biotechnology* **1993**, *41*, 77-85.

(19) Bertilsson, L.; Potje-Kamloth, K.; Liess, H.; Engquist, I.; Liedberg, B. *Journal of Physical Chemistry B* **1998**, *102*, 1260-1269.

(20) Levitsky, I.; Krivoshlykov, S. G.; Grate, J. W. *Analytical Chemistry* **2001**, *73*, 3441-3448.

(21) Simonson, D. L.; Houser, E. J.; Stepnowski, J. L.; Pu, L.; McGill, R. A. *Polymeric Matericals Science and Engineering* **2003**, *89*, 866-867.

(22) Houser, E. J.; Simonson, D. L.; Stepnowski, J. L.; Ross, S. K.; Stepnowski, S. V., III; McGill, R. A. *Polymer Preprints* **2004**, *45*, 541-542.

(23) Bertilsson, L.; Potje-Kamloth, K.; Liess, H. D.; Liedberg, B. *Langmuir* **1999**, *15*, 1128-1135.

(24) Henderson, M. A.; Jin, T.; White, J. M. *Journal of Physcial Chemistry* **1986**, *90*, 4607-4611.

(25) Templeton, M. K.; Weinberg, W. H. *Journal of the American Chemical Society* **1985**, *107*, 774-779.

(26) Henderson, M. A.; White, J. M. *Journal of the American Chemicl Society* **1988**, *110*, 6939-6947.

(27) Hegde, R. I.; Greenlief, C. M.; White, J. M. *Journal of Physcial Chemistry* **1985**, *89*, 2886-2891.

(28) Aurian-Blajeni, B.; Boucher, M. M. *Langmuir* **1989**, *5*, 170-174.

(29) Mitchell, M. B.; Sheinker, V. N.; Mintz, E. A. *Journal of Physical Chemistry B* **1997**, *101*, 11192-11203.

(30) Tesfai, T. M.; Sheinker, V. N.; Mitchell, M. B. *Journal of Physical Chemistry B* **1998**, *102*, 7299-7302.

(31) Rusu, C. N.; Yates, J. T., Jr. *Journal of Physical Chemistry B* **2000**, *104*, 12292-12298.

(32) Sheinker, V. N.; Mitchell, M. B. *Chemistry of Materials* **2002**, *14*, 1257-1268.

(33) Cao, L.; Segal, S. R.; Suib, S. L.; Tang, X.; Satyapal, S. *Journal of Catalysis* **2000**, *194*, 61-70.

(34) Wagner, G. W.; Procell, L. R.; O'Connor, R. J.; Munavalli, S.; Carnes, C. L.; Kapoor, P. N.; Klabunde, K. J. *Journal of the American Chemical Society* **2001**, *123*, 1636-1644.

(35) Decker, S. P.; Klabunde, J. S.; Khalel, A.; Klabunde, K. J. *Environmental Science and Technology* **2002**, *36*, 762-768.

(36) Panayotov, D.; Kondratyuk, P.; Yates, J. T., Jr. *Langmuir* **2004**, *20*, 3674-3678.

(37) Kanan, S. M.; Tripp, C. P. *Langmuir* **2001**, *17*, 2213-2218.

(38) Oh, S. W.; Kim, Y. H.; Yoo, D. J.; Oh, S. M.; Park, S. J. *Sensors and Actuators B* **1993**, *13-14*, 400-403.

(39) Kanan, S. M.; Lu, Z.; Tripp, C. P. *Journal of Physical Chemistry B* **2002**, *106*, 9576-9580.

(40) Kim, C. S.; Lad, R. J.; Tripp, C. P. *Sensors and Actuators B* **2001**, *76*, 442-448.

(41) Kanan, S. M.; Tripp, C. P. *Langmuir* **2002**, *18*, 722-728.

(42) Hegde, R. I.; White, J. M. *Journal of Physical Chemistry* **1986**, *90*, 2159-2163.

(43) Hegde, R. I.; White, J. M. *Applied Surface Science* **1987**, *28*, 1-10.

(44) Feng, S. X.; Lunney, P.; Wargo *Journal of Coatings Technology* **1999**, *71*, 143-149.

(45) Ginic-Markovic, M.; Choudhury, N. R.; Matisons, J. G.; Williams, D. R. G. *Journal of Thermal Analysis and Calorimetry* **2000**, *59*, 409-424.

(46) Jacobs, P. B.; Yu, P. C. *Journal of Coatings Technology* **1993**, *65*, 45-50.

(47) Mierisch, A. M.; Yuan, J.; Kelly, R. G.; Taylor, S. R. *Jounal of the Electrochemical Society* **1999**, *146*, 4449-4454.

(48) Garton, D. J.; Minton, T. K.; Alagia, M.; Balucani, N.; Casavecchia, P.; Volpi, G. G. *Faraday Discussions* **1997**, *108*, 387-399.

(49) Zhang, J.; Minton, T. K. *High Performance Polymers* **2001**, *13*, S467-S481.

(50) Ekerdt, J. G.; Klabunde, K. J.; Shapley, J. R.; White, J. M.; Yates, J. T. *Journal of Physical Chemistry* **1988**, *92*, 6182-6188.

(51) Ulman, A. *Chemical Reviews* **1996**, *96*, 1533-1554.

(52) Chechik, V.; Stirling, C. J. M. *Langmuir* **1998**, *14*, 99-105.

(53) Dubois, L. H.; Zegarski, B. R.; Nuzzo, R. G. *Journal of the American Chemical Society* **1990**, *112*, 570-579.

(54) Chailapakul, O.; Sun, L.; Xu, C. J.; Crooks, R. M. *Journal of the American Chemical Society* **1993**, *115*, 12459-12467.

(55) Mrksich, M.; Whitesides, G. M. *Annul Review of Biophysics and Biomolecular Structure* **1996**, *25*, 55-78.

(56) Okahata, Y.; Matsuura, K.; Ito, K.; Ebara, Y. *Langmuir* **1996**, *12*, 1023-1026.

(57) Shuler, S. F.; Davis, G. M.; Morris, J. R. *Journal of Chemical Physics* **2002**, *116*, 9147-9150.

(58) Sun, L.; Crooks, R. M.; Ricco, A. J. *Langmuir* **1993**, *9*, 1775-1780.

(59) Kwok, C. S.; Mourad, P. D.; Crum, L. A.; Ratner, B. D. *Biomacromolecules* **2000**, *1*, 139-148.

(60) Kohli, P.; Blanchard, G. J. *Langmuir* **2000**, *16*, 4655-4661.

(61) Persson, H. H. J.; Caseri, W. R.; Suter, U. W. *Langmuir* **2001**, *17*, 3643-3650.

(62) Guo, X.; Yoshinobu, J.; Yates, J. T., Jr. *Journal of Physical Chemistry* **1990**, *94*, 6839-6842.

(63) Smentkowski, V. S.; Hagans, P.; Yates, J. T. *Journal of Physical Chemistry* **1988**, *92*, 6351-6357.

(64) Xu, C.; Goodman, D. W. *Chemical Physics Letters* **1997**, *265*, 341-346.

(65) Yates, J. T. *Experimental Innovations In Surface Science*; Springer-Verlag: New York, 1998.

(66) Zhou, X. L.; Cowin, J. P. *Journal of Physical Chemistry* **1996**, *100*, 1055-1065.

(67) Yang, Y. C. *Accounts of Chemical Research* **1999**, *32*, 109-115.

(68) Yang, Y. C.; Szafraniec, L. L.; Beaudry, W. T.; Rohrbaugh, D. K.; Procell, L. R.; Samuel, J. B. *Journal of Organic Chemistry* **1996**, *61*, 8407-8413.

(69) Xu, C. J.; Sun, L.; Kepley, L. J.; Crooks, R. M.; Ricco, A. J. *Analytical Chemistry* **1993**, *65*, 2102-2107.

(70) Hewett, K. B.; Anderson, L. C.; Rosynek, M. P.; Lunsford, J. H. *Journal of the American Chemical Society* **1996**, *118*, 6992-6997.

(71) Wu, M. C.; Estrada, C. A.; Corneille, J. S.; Goodman, D. W. *Journal of Chemical Physics* **1992**, *96*, 3892-3900.

(72) Stirniman, M. J.; Huang, C.; Smith, R. S.; Joyce, S. A.; Kay, B. D. *Journal of Chemical Physics* **1996**, *105*, 1295-1298.

(73) Mars, P.; van Krevelen, D. W. *Chemical Engineering Science* **1954**, *3*, 41-59.

(74) Templeton, M. K.; Weinberg, W. H. *Jornal of the American Chemical Society* **1985**, *107*, 97-108.

(75) Zhou, J.; Varazo, K.; Reddic, J. E.; Myrick, M. L.; Chen, D. A. *Analytica Chimica Acta* **2003**, *496*, 289-300.

(76) Zhou, J.; Ma, S.; Kang, Y. C.; Chen, D. A. *Journal of Physical Chemistry B* **2004**, *108*, 11633-11644.

(77) Ma, S.; Zhou, J.; Kang, Y. C.; Reddic, J. E.; Chen, D. A. *Langmuir* **2004**, *20*, 9686-9694.

(78) Ferguson-McPherson, M. K.; Low, E. R.; Esker, A. R.; Morris, J. R. *Journal of Physical Chemistry B* **2005**, *To be submitted.*

(79) Ferguson-McPherson, M. K.; Low, E. R.; Esker, A. R.; Morris, J. R. *Journal of the American Chemical Society* **2005**, *To be submitted.*

(80) Davis, G. M. In *Chemistry*; Virginia Polytechnic Institute and State University: Blacksburg, VA, 2003, p 65.

(81) Shuler, S. F. In *Chemistry*; Virginia Polytechnic Institute and State University: Blacksburg, 2002.

(82) King, D. A.; Wells, M. G. *Surface Science* **1972**, *29*, 454.

(83) Valbusa, U. In *Atomic and Molecular Beam Methods*; Scoles, G., Ed.; Oxford University Press: New York, 1992; Vol. 2, pp 327-339.

(84) Redhead, P. A. *Vacuum* **1962**, *12*, 203-211.

(85) Yates, J. T., Jr. In *Methods of Experimental Physics*; Park, R. L., Lagally, M. G., Eds.; Academic Press, Inc.: Orlando, 1985; Vol. 22, pp 425-464.

(86) Greenler, R. G. *Journal of Chemical Physics* **1969**, *50*, 1963-1968.

(87) Greenler, R. G. *Journal of Chemical Physics* **1966**, *44*, 310.

(88) Schmidt, J.; Laitenberger, P.; Palmer, R. E. *Review of Scientific Instruments* **1998**, *69*, 313-314.

(89) Laibinis, P. E.; Whitesides, G. M.; Allara, D. L.; Tao, Y. T.; Parikh, A. N.; Nuzzo, R. G. *Journal of the American Chemical Society* **1991**, *113*, 7152-7167.

(90) Nuzzo, R. G.; Dubois, L. H.; Allara, D. L. *Journal of the American Chemical Society* **1990**, *112*, 558.

(91) Nuzzo, R. G.; Fusco, F. A.; Allara, D. L. *Journal of the American Chemical Society* **1987**, *109*, 2358-2368.

(92) Whitesides, G. M.; Laibinis, P. E. *Langmuir* **1990**, *6*, 87-96.

(93) Holman, M. W.; Liu, R.; Adams, D. M. *Journal of the American Chemical Society* **2003**, *125*, 12649-12654.

(94) Zamborini, F. P.; Crooks, R. M. *Langmuir* **1998**, *14*, 3279-3286.

(95) Li, D. Q.; Ratner, M. A.; Marks, T. J.; Zhang, C. H.; Yang, J.; Wong, G. K. J. *Journal of the American Chemical Society* **1990**, *112*, 7389-7390.

(96) Hickman, J. J.; Ofer, D.; Laibinis, P. E.; Whitesides, G. M.; Wrighton, M. S. *Science* **1991**, *252*, 688-691.

(97) Kumar, A.; Abbott, N. L.; Biebuyck, H. A.; Kim, E.; Whitesides, G. M. *Accounts of Chemical Research* **1995**, *28*, 219-226.

(98) Schomburg, K. C.; McCarley, R. L. *Langmuir* **2001**, *17*, 1983-1992.

(99) Kim, H.; Jang, J. *Polymer* **2000**, *41*, 6553-6561.

(100) Phadtare, S.; D'Britto, V.; Pundle, A.; Prabhune, A.; Sastry, M. *Biotechnology Progess* **2003**, *20*, 156-161.

(101) Fiegland, L. R.; McCorn Saint Fleur, M.; Morris, J. R. *Langmuir* **2005**, *21*, 2660-2661.

(102) Ferguson, M. K.; Low, E. R.; Morris, J. R. *Langmuir* **2004**, *20*, 3319-3323.

(103) Headquarters, D. o. A. In *Army Adoption of Chemical Agent Resistive Coating*, 1983.

(104) Office, o. t. S. G. *Textbook of Military Medicine - Occupational Health, the Soldier and the Industrial Base*, 1993; Vol. Part III, Volume 2.

(105) Rostker, B. "Environmental Exposure Report: Chemical Agent Resistant Coating (CARC)," United States Department of Defense, 2000.

(106) Ogawa, H.; Chihara, T.; Taya, K. *Journal of the American Chemical Society* **1985**, *107*.

(107) Schlotter, N. E.; Porter, M. D.; Bright, T. B.; Allara, D. L. *Chemical Physics Letters* **1986**, *132*, 93-98.

(108) Porter, M. D.; Bright, T. B.; Allara, D. L.; Chidsey, C. E. D. *Journal of the American Chemical Society* **1987**, *109*, 3559-3568.

(109) Bain, C. D.; Troughton, E. B.; Tao, Y.; Evall, J.; Whitesides, G. M.; Nuzzo, R. G. *Journal of the American Chemical Society* **1989**, *111*, 321-335.

(110) Nuzzo, R. G.; Allara, D. L. *Journal of the American Chemical Society* **1983**, *105*, 4481-4483.

(111) Yan, L.; Marzolin, C.; Terfort, A.; Whitesides, G. M. *Langmuir* **1997**, *13*, 6704-6712.

(112) Sabapathy, R. C.; Crooks, R. M. *Langmuir* **2000**, *16*, 1777.

(113) Sabapathy, R. C.; Crooks, R. M. *Langmuir* **2000**, *16*, 7783-7788.

(114) Ulman, A.; Tillman, N. *Langmuir* **1989**, *5*, 1418-1420.

(115) Tam-Chang, S.; Biebuyck, H. A.; Whitesides, G. M.; Jeon, N.; Nuzzo, R. G. *Langmuir* **1995**, *11*, 4371-4382.

(116) Clegg, R. S.; Hutchinson, J. E. *Langmuir* **1996**, *12*, 5239-5327.

(117) Lewis, P. A.; Smith, R. K.; Kelly, K. F.; Bumm, L. A.; Reed, S. M.; Clegg, R. S.; Gunderson, J. D.; Hutchison, J. E.; Weiss, P. S. *Journal of Physical Chemistry B* **2001**, *105*, 10630-10636.

(118) Smith, R. K.; Reed, S. M.; Lewis, P. A.; Monnell, J. D.; Clegg, R. S.; Kelly, K. F.; Bumm, L. A.; Hutchison, J. E.; Weiss, P. S. *Journal of Physical Chemistry B.* **2001**, *105*, 1119-1122.

(119) Valiokas, R.; Ostblom, M.; Svedhem, S.; Svensson, S. C. T.; Liedberg, B. *Journal of Physical Chemistry B* **2002**, *106*, 10401-10409.

(120) Clegg, R. S.; Hutchinson, J. E. *Journal of the American Chemical Society* **1999**, *121*, 5319-5327.

(121) Allerhand, A.; Schleyer, P. v. R. *Journal of the American Chemical Society* **1963**, *85*, 1715-1723.

(122) Sprik, M.; Delamarche, E.; Michel, B.; Rothlisberger, U.; Klein, M. L.; Wolf, H.; Ringsdorf, H. *Langmuir* **1994**, *10*, 4116-4130.

(123) Bertilsson, L.; Liedberg, B. *Langmuir* **1993**, *9*, 141-149.

(124) Hutt, D. A.; Leggett, G. J. *Langmuir* **1997**, *13*, 2740-2748.

(125) Bain, C. D.; Whitesides, G. M. *Journal of the American Chemical Society* **1989**, *111*, 7164-7175.

(126) Bain, C. D.; Evall, J.; Whitesides, G. M. *Journal of the American Chemical Society* **1989**, *111*, 7155-7164.

(127) Bain, C. D.; Biebuyck, H. A.; Whitesides, G. M. *Langmuir* **1989**, *5*, 723-727.

(128) Stovbun, E. V.; Kuzaev, A. I.; Baturin, S. M. *Polymer Science, Ser. A* **1996**, *38*, 691-695.

(129) Han, Q.; Urban, M. W. *Journal of Applied Polymer Science* **2001**, *81*, 2045-2054.

(130) Bellamy, L. J. *The Infrared Spectra of Complex Molecules*; John Wiley and Sons: New York, 1975.

(131) Wu, Y.; Murayama, K.; Ozaki, Y. *Journal of Physical Chemistry B.* **2001**, *105*, 6251-6259.

(132) Vigano, C.; Smeyers, M.; Raussens, V.; Scheirlinckx, F.; Ruysschaert, J. M.; Goormaghtigh, E. *Biopolymers* **2004**, *74*, 19-26.

(133) Bain, C. D.; Whitesides, G. M. *Journal of the American Chemical Society* **1988**, *110*, 3665-3666.

(134) Engquist, I.; Lestelius, M.; Liedberg, B. *Langmuir* **1997**, *13*, 4003-4012.

(135) Liedberg, B.; Wirde, M.; Tao, Y.-T.; Tengvall, P.; Gelius, U. *Langmuir* **1997**, *13*, 5329-5334.

(136) Weiß, J.; Himmel, H.-J.; Fischer, R. A.; Wöll, C. *Chemical Vapor Deposition* **1998**, *4*, 17-21.

(137) Fisher, G. L.; Walker, A. V.; Hooper, A. E.; Tighe, T. B.; Bahnck, K. B.; Skriba, H. T.; Reinard, M. D.; Haynie, B. C.; Opila, R. L.; Winograd, N.; Allara, D. L. *Journal of the American Chemical Society* **2002**, *124*, 5528-5541.

(138) Schwab, J. J.; Lichtenhan, J. D. *Applied Organometallic Chemistry* **1998**, *12*, 707-713.

(139) Cassagneau, T.; Caruso, F. *Journal of the American Chemical Society* **2002**, *124*, 8172-8180.

(140) Jeoung, E.; Carroll, J. B.; Rotello, V. M. *Chemical Communications* **2002**, *14*, 1510-1511.

(141) Carroll, J. B.; Waddon, A. J.; Nakade, H.; Rotello, V. M. *Macromolecules* **2003**, *36*, 6289-6291.

(142) Esker, A. R.; Vastine, B. A.; Deng, J.; Ferguson, M. K.; Morris, J. R.; Satija, S. K.; Viers, B. D. *Polymer Preprints* **2005**, *45*, 644-645.

(143) Feher, F. J.; Newman, D. A.; Walzer, J. F. *Journal of the American Chemical Society* **1989**, *111*, 1741-1748.

(144) Mantz, R. A.; Jones, P. F.; Chaffee, K. P.; Lichtenhan, J. D.; Gilman, J. W.; Ismail, I. M. K.; Burmeister, M. J. *Chemistry of Materials* **1996**, *8*, 1250-1259.

(145) Brunsvold, A. L.; Minton, T. K.; Gouzman, I.; Grossman, E.; Gonzalez, R. *High Performance Polymers* **2004**, *16*, 303-318.

(146) Hoflund, G. B.; Gonzalez, R. I.; Phillips, S. H. *Journal of Adhesion Science and Technology* **2001**, *15*, 1199-1211.

(147) Honig, E. P.; Hengst, J. H. T.; Den Engelsen, D. *Journal of Colloid and Interface Science* **1973**, *45*, 92-102.

(148) Alexander, A. E.; Schulmann, J. H. *Proceedings of the Royal Society A* **1937**, *161*, 115-127.

(149) Gaines, G. L., Jr. *Nature* **1982**, *298*, 544-545.

(150) Naselli, C.; Rabe, J. P.; Rabolt, J. F.; Swalen, J. D. *Thin Solid Films* **1985**, *134*, 173-178.

(151) Stewart, F. H. C. *Australian Journal of Chemistry* **1961**, *14*, 57-63.

(152) Ruaudel-Teixier, A.; Vandevyver, M.; Barraud, A. *Molecular Crystals and Liquid Crystals* **1985**, *120*, 319-322.

(153) Kuhn, H. *Pure and Applied Chemistry* **1981**, *53*, 2105-2122.

(154) Kuhn, H. *Pure and Applied Chemistry* **1979**, *51*, 341-352.

(155) Gaines, G. L., Jr. *Advances in Chemistry Series* **1975**, *144*, 338-346.

(156) Cemel, A.; Fort, T., Jr.; Lando, J. B. *Journal of Polymer Science, Polymer Chemistry Edition* **1972**, *10*, 2061-2083.

(157) Tieke, B.; Graf, H. J.; Wegner, G.; Naegele, B.; Ringsdorf, H.; Banerjie, A.; Day, D.; Lando, J. B. *Colloid and Polymer Science* **1977**, *255*, 521-531.

(158) Lukes, P. J.; Petty, M. C.; Yarwood, J. *Langmuir* **1992**, *8*, 3043-3050.

(159) Williams, G.; Bryce, M. R.; Petty, M. C. *Molecular Crystals and Liquid Crystals Science and Technology, Section A* **1993**, *229*, 83-90.

(160) Petty, M. C. *Langmuir-Blodgett films: an introduction*; Cambridge University Press: New York, 1996.

(161) O'Leary, T. J.; Levin, I. W. *Journal of Physical Chemistry* **1984**, *88*, 1790-1796.

(162) Robert, G. *Langmuir-Blodgett Films*; Plenum: New York, 1990.

(163) Naselli, C.; Rabolt, J. F.; Swalen, J. D. *Journal of Chemical Physics* **1985**, *82*, 2136-2140.

(164) Esker, A. R.; Dawson, K. J.; Huffer, S. M.; Karabiyik, U.; Deng, J.; Viers, B. D.; Ferguson-McPherson, M. K.; Morris, J. R.; Mao, M.; Ducker, W. A.; Satija, S. K. *Polymer Preprints* **2005**.

(165) Arkhireeva, A.; Hay, J. N. *Journal of Materials Chemistry and Physics* **2003**, *13*, 3122-3127.

(166) Wagner, G. W.; Bartram, P. W. *Langmuir* **1999**, *15*, 8113-8118.

(167) Graven, W. M.; Weller, S. W.; Peters, D. L. *I. E. C. Proc. Des. Dev.* **1966**, *5*, 183-189.

(168) Lee, K. Y.; Houalla, M.; Hercules, D. M.; Hall, W. K. *Journal of Catalysis* **1994**, *145*, 223-231.

(169) Davies, P. R.; Newton, N. G. *Applied Surface Science* **2001**, *181*, 296-306.

(170) Mitchell, M. B.; Sheinker, V. N.; Cox, W. W., Jr.; Gatimu, E. N.; Tesfamichael, A. B. *Journal of Physical Chemistry B* **2004**, *108*, 1634-1645.

(171) Mitchell, M. B.; Sheinker, V. N.; Tesfamichael, A. B.; Gatimu, E. N.; Nunley, M. *Journal of Physical Chemistry B* **2003**, *107*, 580-586.

(172) Wagner, G. W.; Bartram, P. W. *Journal of Molecular Catalysis* **1999**, *144*, 419-424.

(173) Kuiper, A. E. T.; van Bokhoven, J. J. G. M.; Medema, J. *Journal of Catalysis* **1976**, *43*, 154-167.

(174) Wagner, G. W.; Koper, O. B.; Lucas, E.; Decker, S.; Klabunde, K. J. *J. Phys. Chem.B* **2000**, *104*, 5118-5123.

(175) Michalkova, A.; Ilchenko, M.; Gorb, L.; Leszcynski, J. *Journal of Physical Chemistry B* **2004**, *108*, 5294-5303.

(176) Nadler, M. P.; Nissan, R. A.; Hollins, R. A. *Applied Spectroscopy* **1988**, *42*, 634-642.

(177) Chakraborty, I. N.; Condrate, R. A., Snr. *Physics and Chemistry of Glasses* **1985**, *26*, 68-73.

(178) Niida, H.; Takahashi, M.; Uchino, T.; Yoko, T. *Journal of Non-Crystalline Solids* **2002**, *306*, 292-299.

(179) Lockyear, M. W. G.; Holland, D.; Dupree, R. *Physics and Chemistry of Glasses* **1995**, *36*, 22-30.

(180) Barr, T. L. *Applications of Surface Science* **1983**, *15*, 1-35.

(181) Wagner, C. D.; Riggs, W. M.; Davis, L. E.; Moulder, J. F. *Handbook of X-ray Photoelectron Spectroscopy*; Perkin-Elmer: Eden Prairie, MN, 1979.

(182) Oliveira, O. N., Jr.; Riul, A., Jr.; Leite, V. B. P. *Brazilian Journal of Physics* **2004**, *34*, 73-83.

(183) Ferreira, M.; Riul, A., Jr.; Wohnrath, K.; Fonseca, F. J.; Oliveira, O. N., Jr.; Mattoso, L. H. C. *Analytical Chemistry* **2003**, *75*, 953-955.

(184) Ignatyev, I. S.; Partal, F.; González, J. J. L.; Sundius, T. *Spectrochimica Acta Part A* **2004**, *60*, 1169-1178.

(185) Ferguson, M. K.; Lohr, J. R.; Day, B. S.; Morris, J. R. *Physical Review Letters* **2004**, *92*, 073201-073201-073201-073204.

Vita

Melinda Kay McPherson was born on July 21, 1978, in Coldwater, Michigan, United States of America, to Jack and Kathleen Ferguson. After growing up in Coldwater with her sister, Sarah, and graduating at the top of her class from Coldwater High School in 1996, Melinda attended Michigan State University to study chemistry and forensic science. She received her Bachelor of Arts degree in chemistry in May 2000 and her Master of Science degree in criminal justice, with a specialization in forensic science, 2001. In the fall of 2001, Melinda began her graduate studies in analytical chemistry at Virginia Polytechnic Institute and State University. On June 19th, 2004, Melinda was married to Joshua Paul McPherson. Upon completion of graduate studies in Blacksburg in the Summer of 2005, the couple plans to live happily ever after.